TECHNISCHE UNIVERSITÄT MÜNCHEN

Fachgebiet Molekulare Katalyse

Cyclopentadienyl Molybdenum(II) Carbonyl Alkene Epoxidation Precatalysts

Synthesis, Catalysis, Kinetics and Mechanisms

Nidhi Grover

Vollständiger Abdruck der von der Fakultät für Chemie der Technischen Universität München zur Erlangung der akademischen Grades eines

Doktors der Naturwissenschaften

genehmigten Dissertation.

Vorsitzender: Univ.-Prof. Dr. K. Köhler

Prüfer der Dissertation: 1. Univ.-Prof. Dr. F. E. Kühn

2. Univ.-Prof. Dr. K.-O. Hinrichsen

Die Dissertation wurde am 4. Dezember 2013 bei der Technischen Universität München eingereicht und durch die Fakultät für Chemie am 8. Januar 2014 angenommen.

Die vorliegende Arbeit entstand in der Zeit von Oktober 2010 bis Dezember 2013 am Anorganisch-Chemischen Institut, Fachgebiet Molekulare Katalyse, der Technischen Universität München.

I am grateful to my academic supervisor

Prof. Dr. Fritz E. Kühn

for giving me the opportunity to work in his research group,
his patience, support and encouragement.

I am humbled by his trust and confidence in me and my work.

For my mother

– ever inspiring and loving,

in her strength and compassion,

steadfast of both word and action.

Earnestness is the path of immortality, thoughtlessness the path of death. Those who are in earnest do not die, those who are thoughtless are as if dead already.

- On Earnestness, Dhammapada

All created things perish, all created things are grief and pain, all forms are unreal – he who knows and sees this, becomes passive in pain; this is the way to purity.

- The Way, Dhammapada

There is no suffering for him who has finished his journey and abandoned grief, who has freed himself on all sides, and thrown off all fetters.

- The Venerable, Dhammapada

Acknowledgements

Foremost, I am grateful to **Prof. Dr. Fritz E. Kühn** for giving me the opportunity to work in his research group. I also acknowledge **Dr. Mirza Cokoja** for proof-reading manuscripts, **Dr. Alexander Pöthig** for X-ray crystallographic data, and **Dr. Markus Drees** for his support with TUM Graduate School and contribution to all theoretical work presented in this thesis.

Next, I wish to convey my gratitude towards **Frau Irmgard Grötsch**, **Frau Roswitha Kaufmann**, **Frau Renate Schuhbauer-Gerl**, **Frau Ulla Hifinger** and **Frau Nora Boerschel** for their help with bureaucratic work; **Dr. Gabi Raudaschl-Sieber** for solid-state NMR measurements; **Frau Georgeta Krutsch**, **Herr Jürgen Kudermann** and **Frau Maria Weindl** for their dedicated assistance with numerous, miscellaneous NMR experiments and TGA-MS. **Frau Ulrike Ammari**, **Frau Petra Ankenbauer** and **Frau Bircan Dilki** of the microanalysis team as well as **Frau Rodica Dumitrescu** of mass spectrometry lab, **Herr Thomas Schröferl** of the GC-MS lab and **Herr Martin Schellerer** for chemical distribution and management, I am grateful to you as well.

I would also like to mention the following people (in no particular biased order) – chica **Valentina**, **Daniel**(ssesses), tiny **Amylia, Bill** (Gates), **Bo**(bo(bo)) and **Su**; **Typhene**, **Antoine** and **Tina** – in whom I have found and grown to admire a very positive and re-affirming strength of character. Thank you for sharing the various odd little things with me.

Last, but the most important people of all who have supported me from afar. **Shipra**, **Tanishq**, **Mehar**, **Sakshi**, **Surbhi**, **Bhavika**, **Siddharth** and **Nikhil**, I thank you for always being totally *bindas* about my choices and who I am.

Abbreviations

°	Degree
δ	chemical shift, units ppm
°C	degree centigrade
Å	Angstrom
ATR-FTIR	Attentuated Total Reflection – Fourier Transform Infra-red
Ar	aromatic group
bpy	2,2'-bipyridyl
Bz	benzyl, $-CH_2C_6H_5$
CCDC	Cambridge Crystallographic Data Centre
CIF	Crystallographic Information File
Cp	cyclopentadienyl, C_5H_5
Cp*	pentamethylcyclopentadienyl, $C_5(CH_3)_5$
CP MAS NMR	Cross Polarization Magic Angle Spinning NMR
d	doublet (NMR)
DCM	Dichloromethane
DFT	Density Functional Theory
DMF	N,N'-dimethylformamide
DMSO	Dimethylsulfoxide
EI	Electron Ionisation
Et	ethyl, $-CH_2CH_3$
Et_2O	Diethylether
EtOH	Ethanol
FAB	Fast Atom Bombardment
GC-FID	Gas Chromatography – Flame Ionization Detector
HFB	Hexafluorobenzene
HFIP	Hexafluoroisopropanol
Hz	Hertz
Im	Imidazolyl
IR	Infra-red (spectroscopy)
J	coupling constant, units Hertz
m	Meta
m	Multiplet
Me	methyl, $-CH_3$
Mes	mesityl, 2,4,6-trimethylbenzyl

MHz	Megahertz
mL	Millilitre
m.p.	melting point
MS	Mass Spectrometry
MTO	methyltrioxorhenium, CH_3ReO_3
NHC	N-heterocyclic carbene
NMR	Nuclear Magnetic Resonance (spectroscopy)
o	Ortho
p	Para
Ph	phenyl, $-C_6H_5$
phen	1,10-phenanthrolinyl
ppm	parts per million
q	Quartet
r.t.	room temperature
R	any alkyl or aryl group
RTIL	room temperature ionic liquid
s	singlet (NMR), strong (IR)
t	triplet
t-BuOH	*tert*-butanol
TBHP	*tert*-butylhydroperoxide
THF	tetrahydrofuran
TGA-DSC	Thermogravimetric Analysis Differential Scanning Calorimetry
TOF	Turnover Frequency
TON	Turnover Number
XRD	X-ray Diffraction

Table of Contents

Acknowledgements i

Abbreviations iii

I. Organomolybdenum Oxides 1

1 Introduction 3

1.1 Molybdenum (VI) Complexes for Catalytic Olefin Epoxidation 3

1.2 Cyclopentadienyl Molybdenum Complexes as Epoxidation Catalysts 4

1.2.1 Synthesis 4

1.2.2 Catalytic Performance 6

1.2.3 State of the Art 13

1.2.3.1 Kinetics 13

1.2.3.2 Mechanisms 15

1.3 Conclusions and Scope 16

1.4 References 17

1.5 Additional References (Figure 1.2) 20

2 Objectives 27

II. Synthesis and Catalysis 29

3 Cyclopentadienyl Imidazo[1,5-*a*]pyridine-3-ylidene Molybdenum Complexes and their Application as Olefin Epoxidation Precatalysts 31

3.1 Introduction 31

3.2 Experimental 33

3.2.1 Methods and Materials 33

3.2.2 Synthesis and Characterization of Complexes **2** and **3** 33

3.2.3 Catalytic Epoxidation 34

3.3 Results and Discussion 35

3.3.1 Synthesis and Characterization of **2** and **3** 35

3.3.2 X-ray Crystal Analysis for Complexes **2** and **3** 38

3.3.3 Application in Epoxidation Catalysis 42
3.3.3.1 Optimisation of Temperature 42
3.3.3.2 Choice of Solvent 43
3.3.3.3 Optimal Catalyst Concentration 43
3.3.3.4 Epoxidation of Other Olefin Substrates and Recyclability in RTIL 45
3.3.4 Structure-Activity Relationship 46
3.4 Conclusion 47
3.5 References 48
3.6 Supporting Information 51

4 Cyclopentadienyl Molybdenum Alkylester Complexes as Catalyst Precursors for Olefin Epoxidation 57

4.1 Introduction 57
4.2 Experimental 59
4.2.1 Methods and Materials 59
4.2.2 X-ray Crystallography 59
4.2.3 General procedure for synthesis of **1-5** 60
4.2.4 Epoxidation catalysis 61
4.3 Results and Discussion 62
4.3.1 Synthesis and characterization of complexes **1-5** 62
4.3.2 NMR spectroscopy 63
4.3.3 Vibrational spectroscopy 64
4.3.4 Thermogravimetry and Mass Spectrometry 64
4.3.5 Single crystal X-ray diffraction 65
4.3.6 Epoxidation Catalysis 67
4.3.7 Catalytic Activity (TOFs) and ^{95}Mo NMR Chemical Shift 70
4.4 Conclusion 72
4.5 References 72
4.6 Supporting Information 75

III. Kinetics and Mechanisms 95

5 A Kinetic Study of Catalytic Olefin Epoxidation with [CpMo(CO)$_3$(η^1-CH$_2$COOR)] Precatalysts using NMR 97

5.1 Introduction 97
5.2 Experimental 99
5.3 Results and Discussion 100
  5.3.1 Catalytic Epoxidation of cis-Cyclooctene 100
  5.3.2 Effect of Varying Reaction Conditions 104
    5.3.2.1 Effect of Temperature 104
    5.3.2.2 Effect of Oxidant Concentration 106
    5.3.2.3 Effect of Precatalyst Concentration 107
    5.3.2.4 Effect of Substrate Concentration 108
  5.3.3 Epoxidation with [CpMo(CO)$_3$R] complexes 109
5.4 Conclusion 110
5.5 References 111
5.6 Supporting Information 113

6 Oxidation of [CpMo(CO)$_3$R*] Pre-catalysts with *tert*-Butyl Hydroperoxide 115

6.1 Introduction 115
6.2 Experimental 117
6.3 Results and Discussion 118
  6.3.1 Oxidation of the Pre-catalyst 118
  6.3.2 Pre-catalyst Oxidation under Varying Reaction Conditions 122
    6.3.2.1 Effect of Oxidant Concentration 122
    6.3.2.2 Effect of Pre-catalyst Concentration 124
    6.3.2.3 Effect of Temperature 125
  6.3.3 Nature of the Precipitate 125
  6.3.4 Nature of the Intermediate Species **A** and **B** 126
  6.3.5 Scheme for Oxidative Transformations 133
6.4 Conclusion 135
6.5 References 135
6.6 Supporting Information 138

7 Theoretical Concepts and Experimental Insights − Catalysis with [CpMo(CO)$_3$R] Complexes 145

7.1 Introduction 145

7.2 Experimental 145

7.3 Results and Discussion 146

7.3.1 Theoretical Study: Mo(IV) Mono-oxo Complex, its Stability and Catalytic Potential 146

7.3.2 Kinetic Isotope Effect 147

7.3.3 Effect of additives HFIP and ^{t}BuOH on catalytic epoxidation 148

7.4 Conclusion 149

7.5 References 150

8 The Fluorinated Complex [CpMo(CO)$_3$CF$_3$] and its Unexpected Catalytic Activity 153

8.1 Introduction 153

8.1.1 Background 153

8.1.2 The Expected and Unexpected Catalytic Activity of Pre-catalyst **2** 156

8.2 The ‘Bottom-Up’ Approach 157

8.2.1 Synthesis and Stability of the Pre-catalysts 158

8.2.2 Comparison of Spectroscopic and Structural Data of **1** and **2** 160

8.2.3 Reaction of **1** and **2** with TBHP 163

8.2.4 Differences in Reactivity of Dioxo and Oxo-peroxo Complexes 163

8.2.5 Comparison of Oxo-Peroxo Complexes 166

8.2.6 Activity in Fluorinated Solvents 169

8.3 The ‘Top-Down’ Approach 171

8.3.1 An Explanation from Reaction Kinetics 171

8.3.2 A Consideration of Reaction Mechanisms 172

8.4 Conclusion 173

8.5 References 174

9 Summary 179

IV. Index 183

I. Organomolybdenum Oxides

1 Introduction

Catalysis is a cornerstone of technological achievement in the 20th and 21st centuries. Organometallic transition metal catalysts have transformed industrial production of bulk and fine chemicals as well as organic syntheses. Often the choice of the transition metal complex to be utilised for catalysis is limited by its synthesis, which must be easy, high yielding and economical. Consequently in the last decade, efforts have been directed towards facile syntheses of high oxidation state molybdenum complexes and then screening them for catalytic activity in oxidation reactions. It is not unusual to choose molybdenum over other transition elements for such purposes. It is a relatively cheap metal, exhibits low toxicity and is also an essential element for both plants and animals.[1] Oxidation states ranging from –II to +VI are found in its various coordination compounds and the coordination number can range between 4 and 8, resulting in rich stereochemical diversity. It forms compounds with both inorganic and organic ligands, preferring O, S, F and Cl donor ligands. Bi- and poly-nuclear compounds that contain either bridging oxide and chloride ligands or Mo−Mo bonds are also well–known.[2]

1.1 Molybdenum (VI) Complexes for Catalytic Olefin Epoxidation

Olefin epoxidation with peroxides (and hydroperoxides) as oxidants catalyzed by molybdenum complexes has been extensively studied in literature.[3–7] The main structural classes include dioxo complexes of the type $[MoO_2R_2L]$,[3] oxo bisperoxo complexes $[Mo(O_2)_2(O)L]$,[7] trioxide $LMoO_3$ type [8,9] (L = usually N-donor base such as 1,1'-bipyridine (bpy), 1,10-phenanthroline (phen), pyrazolylpyridine (pzpy), R = alkyl, halide) and half-sandwich $[CpMo(O)_2R]$ complexes.[10,11] This is primarily motivated by the high demand for epoxides which are valuable industrial intermediates that undergo ring opening reactions with suitable reagents to give desired mono-functional or bi-functional products.[12]

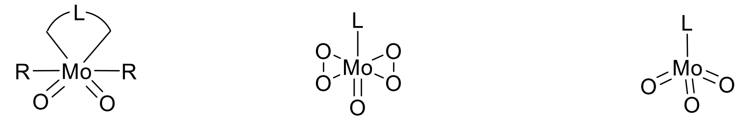

R = Cl, Br, CH_3
L = Bidentate N base ligand
e.g. bipy, phen, pzpy

L = N-donor
Lewis base
ligands

L = Tp/Tp*; tridentate
Anionic, Mo(VI)
Heterogeneous
organic/inorganic hybrid
materials based on MoO_3

Figure 1.1. Illustration of different structural classes of molybdenum oxo complexes studied for epoxidation catalysis.

In this work, organomolybdenum compounds of the type $[CpMo(CO)_3R]$ (Cp = C_5H_5, R = alkyl, halide etc.) are the focal point of study. These compounds have been extensively applied as catalysts for the epoxidation of unfunctionalized olefins. The synthesis, catalytic performance, kinetics and mechanisms of CpMo–based catalysts are discussed in the following sections.

1.2 Cyclopentadienyl Molybdenum Complexes as Epoxidation Catalysts

1.2.1 Synthesis

The first complex of the general formula η^5-Cp$^{\neq}$MoO$_2$X (X = halide) synthesized in 1963 by Cousins and Green, CpMoO$_2$Cl **1a** (Figure 1.2) was obtained in very low yields *via* an unspecific pathway and several other species such as mono-oxo and dimeric complexes were also formed.[13] Synthetic chemistry for **1a** and **1b** was further explored by Green et al.[14,15] but neither of these complexes was investigated as a catalyst for olefin epoxidation, possibly due to difficulties encountered in synthesis and stability. After a long gap period, in 1988, Faller and Ma reported the synthesis of complex Cp*MoO$_2$Cl, **2a**.[16,17] Bergman and Trost reported a modified synthesis of **2a** in 1991 and for the first time, studied this representative example of CpMo complexes for successful catalytic olefin epoxidation with various olefin substrates and hydroperoxide oxidants.[18]

Kühn, Romão et al. reported a general and straightforward one-step synthesis of [(η^5-C$_5$R$_5$)MoO$_2$Cl] (R = H **1**, Me **2**, CH$_2$Ph (Bz) **4**) from their corresponding parent carbonyl compounds [(η^5-C$_5$R$_5$)Mo(CO)$_3$Cl] **5a**-**7** when treated with 10 equiv. of hydroperoxide oxidant *tert*-butylhydroperoxide (TBHP) solution in *n*-decane.[19] Since this publication, a number of structurally diverse CpMo carbonyl complexes have been synthesized and applied for catalytic conversion of unfunctionalized alkenes to their epoxides (Figure 1.2).[10] The use of tricarbonyl precursors is preferred over direct use of the respective oxo-complexes dioxo [CpMoO$_2$R] and oxo-peroxo [CpMo(O)(O$_2$)R] because these precatalysts are more stable to air and moisture, easier to handle, and can be stored for long periods of time. Loss in yield on isolating the oxides can also be prevented if *in situ* oxidation is carried out.[19] Aforementioned catalytically active oxo complexes can be easily obtained on treatment of these precatalysts with TBHP, which is also the oxidant for the epoxidation reaction.

The aforementioned tricarbonyl precursors are usually prepared by treating sodium cyclopentadienide[20] with Mo(CO)$_6$ in dry THF to obtain Na[CpMo(CO)$_3$] salt. On subsequent reaction with a desired alkyl (RX) or aryl halide, complexes of the type [CpMo(CO)$_3$R] can be obtained in good yields.[21] This method is an improvement over reduction of Mo−Mo dimer [Cp$_2$Mo$_2$(CO)$_6$] with Na amalgam and subsequent reaction with the suitable R group precursor. Synthesis of Cp* analogues (and complexes that have an unsymmetrical substitution pattern on Cp ring) follows much of the same synthetic route, except that Cp*Li salt is often used.

Complexes such as **14**, **19−24** with an *ansa* bridge, and **30−40** with N-heterocyclic carbene side chain ligands are synthesized by alternative methods. Eilbracht reported the synthesis of several molybdenum *ansa* compounds from the Mo(CO)$_3$L$_3$ precursor (L = CH$_3$CN, THF) and spiro-annulated compounds spiro[4.4]hepta-1,3-diene and spiro[4.4]nona-1,3-diene to give [Mo(η^5-C$_5$H$_4$CH$_2$-η^1-CH$_2$)(CO)$_3$] **14a** and [Mo(η^5-C$_5$H$_4$(CH$_2$)$_3$-η^1-CH$_2$)(CO)$_3$] **21** respectively.[22] Later, Royo et al. also explored the synthetic chemistry of *ansa* bridged cyclopentadienyl molybdenum complexes.[23] Molybdenum and tungsten *ansa* complexes with a cycloalkyl unit as *ansa* bridge [24] i.e. M{η^5-C$_5$H$_4$[CH(CH$_2$)$_{n+2}$]-η^1-CH}(CO)$_3$, (M = Mo **23a-d**, W **24a-d**; n = 1-4) have been synthesized in better yields and more pure than synthesis from the [M(CO)$_3$(NCMe)$_3$] precursors[25,26] by reacting the respective spiro-bicyclic dienes with [M(CO)$_3$(Me$_3$tach)], (M = Mo, W; Me$_3$tach = 1,3,5-trimethyl-1,3,5-

triazacyclohexane). NHC complexes **34-38** have been prepared from [CpMo(CO)$_3$Br] and respective silver carbenes formed *in situ* on refluxing in toluene for 40 min.[27] The ionic complex [CpMo(CO)$_2$(IMes)(CH$_3$CN)][BF$_4$] **39**, IMes = 1,3-bis-(2,4,6-trimethylphenyl)-imidazol-2-ylidene is prepared by treating **38** with AgBF$_4$ in CH$_3$CN.[27]

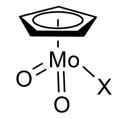

X = Cl **1a**
X = Br **1b**

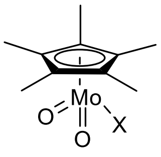

X = Cl **2a**
X = Br **2b**

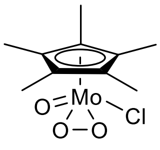

3

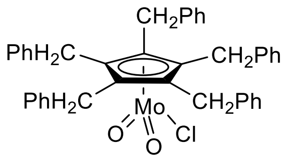
CH2Ph
PhH2C
CH2Ph
PhH2C
CH2Ph
Mo
O
O
Cl

4

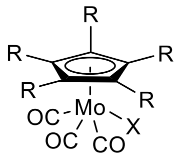
R
R
R
R
R
OC
Mo
X
OC
CO

X = Cl : R = H **5a**, CH$_3$ **6**, CH$_2$Ph **7**
X = Br : R = H **5b**

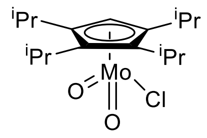
iPr
iPr
iPr
iPr
Mo
O
O
Cl

8

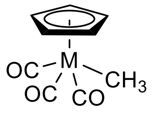
OC
M
CH3
OC
CO

M = Mo **9a**
W **9b**

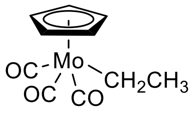
OC
Mo
CH2CH3
OC
CO

10

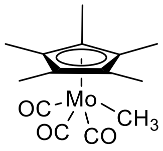
OC
Mo
CH3
OC
CO

11

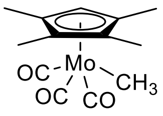
OC
Mo
CH3
OC
CO

12

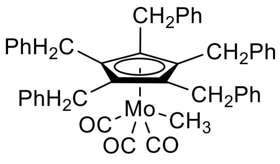
CH2Ph
PhH2C
CH2Ph
PhH2C
CH2Ph
OC
Mo
CH3
OC
CO

13

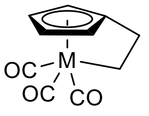

M = Mo **14a**
W **14b**

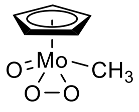

15

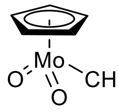

16

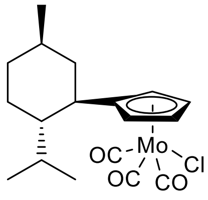
OC
Mo
Cl
OC
CO

17

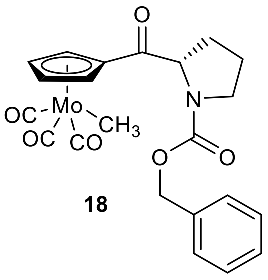
O
N
OC
Mo
CH3
OC
CO
O
O

18

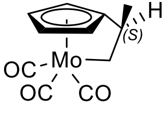
Ph
H
(S)
OC
Mo
OC
CO

19

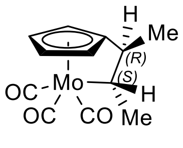
H
Me
(R)
(S)
H
OC
Mo
OC
CO
Me

20

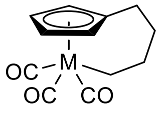

M = Mo **21**
W **22**

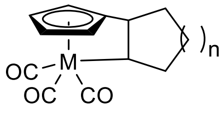

M = Mo **23**, W **24**

n = 1, **23a, 24a**
n = 2, **23b, 24b**
n = 3, **23c, 24c**
n = 4, **23d, 24d**

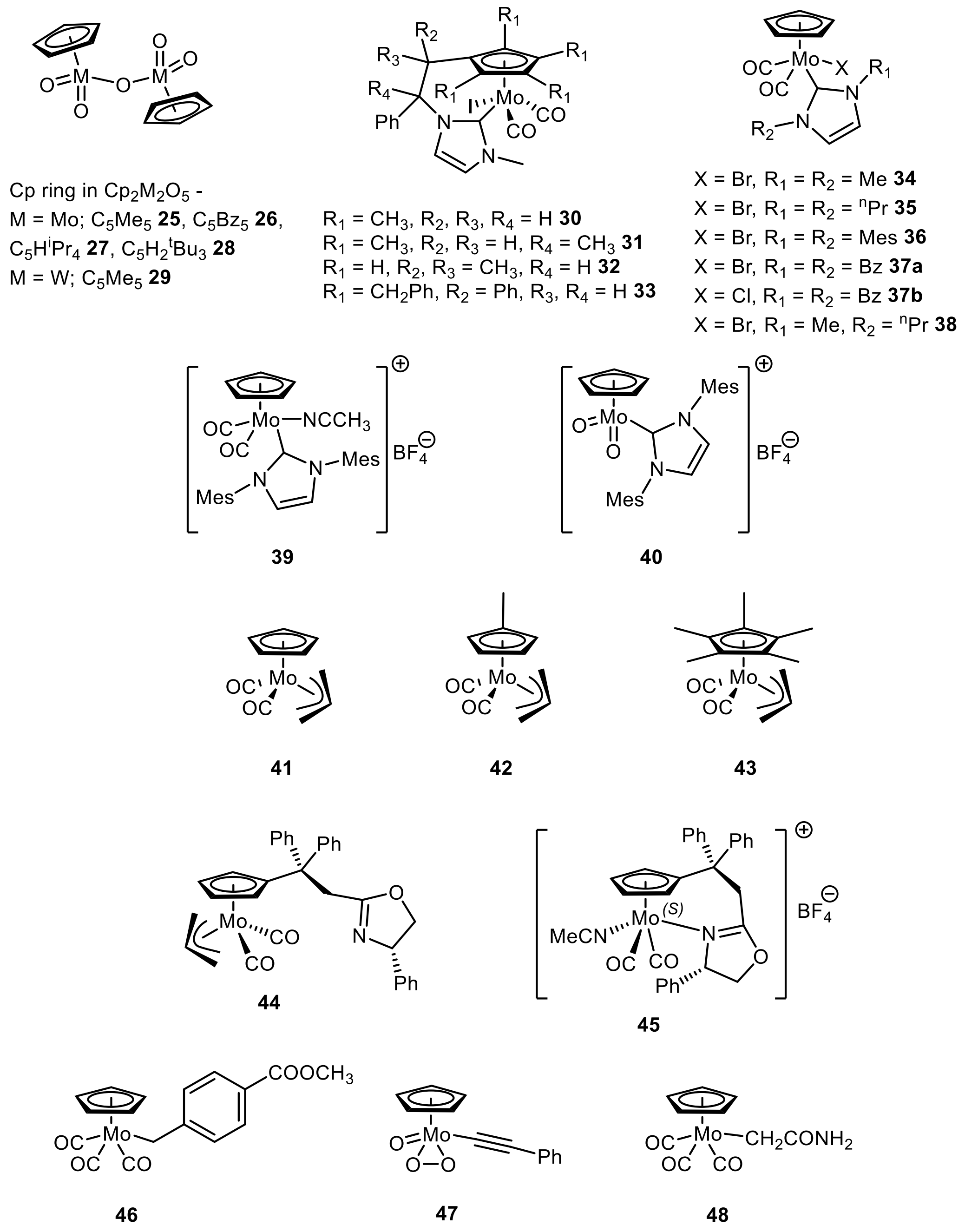
Cp ring in Cp2M2O5 -
M = Mo; C5Me5 25, C5Bz5 26, C5HiPr4 27, C5H2tBu3 28
M = W; C5Me5 29
R1 = CH3, R2, R3, R4 = H 30
R1 = CH3, R2, R3 = H, R4 = CH3 31
R1 = H, R2, R3 = CH3, R4 = H 32
R1 = CH2Ph, R2 = Ph, R3, R4 = H 33
X = Br, R1 = R2 = Me 34
X = Br, R1 = R2 = nPr 35
X = Br, R1 = R2 = Mes 36
X = Br, R1 = R2 = Bz 37a
X = Cl, R1 = R2 = Bz 37b
X = Br, R1 = Me, R2 = nPr 38
39
40
41
42
43
44
45
46
47
48

Figure 1.2 A literature compilation of CpMo complexes applied for homogeneous olefin epoxidation till date. See additional references.

1.2.2 Catalytic Performance

The catalytic performance of the various CpMo complexes is compiled in Tables 1.1–1.9 and has been previously compared in detail.[10] Generally, substrates *cis*-cyclooctene, 1-octene, cyclohexene, *cis*- and *trans*-stilbene, styrene, *trans*-β-methylstyrene and propylene are studied for epoxidation with such precatalysts. Epoxidation of terpenes such as α-pinene, dl-limonene and camphene has also been investigated.[28] Catalytic reactions are often performed in organic solvents, and usually at 55 °C using substrate:oxidant ratio = 1:1.5 or 1:2. The oxidant of choice is TBHP (in n-decane) although some complexes have been shown to be active for epoxidation with aqueous TBHP, H_2O_2 and cumylhydroperoxide as well. In most cases, the catalytic reaction is initiated by addition of the oxidant to the (pre)catalyst-substrate mixture in the absence or presence of additional co-solvent (organic solvent, H_2O or room temperature ionic liquid (RTIL)).

Trost and Bergman first showed that in the absence of olefinic substrates, **2a** and *tert*-butyl hydroperoxide (TBHP) react to give the peroxo complex $Cp^*Mo(O_2)OCl$, **3**, which is inactive in catalytic olefin epoxidation with TBHP,[18] an observation that was later confirmed by Roesky et al.[29] The nonreactive peroxo complex **3** was also formed when H_2O_2 and Ph_3COOH were used in the epoxidation reactions with **2a** and therefore, for catalysis, use of these reagents as oxidants was disregarded. It was concluded that the η^2-peroxo complex **3** was not an active species during the epoxidation reaction of olefins with **2a** and that its formation was a side reaction that limits the usefulness of the catalyst.

Table 1.1. Catalytic olefin epoxidation with complexes $Cp^{\neq}MO_2X$ and $Cp^{\neq}M(CO)_3X$ (M = Mo, W) at 55 °C with TBHP (5.5 M in *n*-decane).

Entry	Catalyst	Ref.	Substrate	Catalyst: Substrate:Oxidant	Conversion [%]		TOF (h^{-1})	Solvent
					at 4 h	at 24 h		
1.	**1a**	19	*cis*-cyclooctene	0.01:1:2	100	100	1200	-
2.		30		0.01:1:2	100[a]	100	-	$CHCl_3$[g]
3.	**1b**	27	See entry 20					
4.	**2a**[d]	19	*cis*-cyclooctene	0.01:1:2	*ca.* 55	-	800	-
5.		30		0.01:1:2	64	64	-	$CHCl_3$[g]
6.		30		0.01:1:2[c]	37	-	-	$CHCl_3$
7.	**4**	19	*cis*-cyclooctene	0.01:1:2	100	100	1200	-
8.		19		0.001:1:2	66	80	4000	-
9.		19		0.0001:1:2	32	48	20000	-
10.		30		0.01:1:2	100[a]	100	-	$CHCl_3$[g]
11.		19	Styrene	0.01:1:2	75	*ca.* 82	-	-
12.		19	1-octene	0.01:1:2	< 10	< 15	-	-
13.	**5a**	19	*cis*-cyclooctene	0.01:1:2	-	-	1300	-
14.		31	*cis*-cyclooctene	0.02:1:2	100	-	-	-
15.		31	*trans*-2-octene	0.02:1:2	*ca.* 70	-	-	-
16.		31	1-octene	0.02:1:2	15	-	-	-
17.		31	Cyclododecene	0.02:1:2	*ca.* 85	-	-	-
18.		31	*(R)*-(+)-Limonene	0.02:1:2	100[b]	-	-	-
19.		31	α-pinene	0.02:1:2	*ca.* 45	-	-	-
20.	**5b**	27	*cis*-cyclooctene	0.001:1:2	-	-	2040	-
21.	**8**	30	*cis*-cyclooctene	0.01:1:2	67	85		$CHCl_3$[g]
22.	**9a**	32	*cis*-cyclooctene	0.01:1:2	95	100	820	-
23.		32		0.01:1:2	100	100	960[e]	-

24.		32		0.001:1:2	quant.	quant.	6000	-
25.	**9b**	32	*cis*-cyclooctene	0.01:1:2	15	30	60	-
26.		32		0.01:1:2	62	100	240[f]	-
27.	**10**	32	*cis*-cyclooctene	0.01:1:2	94	100	230	-
28.	**11**	32	*cis*-cyclooctene	0.01:1:2	68	100	270	-
29.	**12**	32	*cis*-cyclooctene	0.01:1:2	75	100	150	-
30.	**13**	30	*cis*-cyclooctene	0.01:1:2	82[b]	-	-	$CHCl_3$[g]

[a] At 3.5 h; [b] At 0.5 h; [c] Aqueous 70% TBHP; [d] Also see Table 1; [e] At 75 °C; [f] At 90 °C; [g] Dry solvent

Despite the use of chiral catalysts such as **17−20** and **45**, efficient asymmetric epoxidation catalysis has not been possible so far with CpMo precatalysts. The highest enantiomeric excess is only 19% on epoxidation of *trans*-β-methylstyrene with **17**. To the best of our knowledge, a satisfactory explanation for poor asymmetric induction is not available in literature from published kinetic and mechanistic models.

Table 1.2. Catalytic olefin epoxidation with **17** and TBHP oxidant (catalyst:substrate:oxidant = 0.01:1:2) at 55 °C in $CHCl_3$ solvent. Ref. 33

Entry	Substrate	Conversion [%][a]		Epoxide Yield [%]		*ee*[a,d] [%]
		at 4 h	at 24 h	at 4 h	at 24 h	
1.	*cis*-cyclooctene	100	100	100	100	-
2.	*trans*-β-methylstyrene	34	84	34[b]	84[b]	19
3.	Styrene	27	68	<5[c]	<5[c]	-

[a] Determined by GC analysis; [b] Determined by NMR; [c] Ring opening of the styrene epoxide to phenylethane-1,2-diol; [d] Epoxide *ee* of the RR isomer.

Table 1.3. Catalytic epoxidation of various substrates with *ansa* complexes with TBHP in the ratio catalyst:substrate:oxidant = 0.01:1:2.

Entry	Catalyst	Ref.	Substrate	Yield[%]			TOF	Temp.
				at 0.5 h	at 4 h	at 24 h	(h^{-1})	(°C)
1.	**14a**	32,35	*cis*-cyclooctene	-	92	100	250	55
2.		24		95	quant.	-	900	r.t.[b]
3.		24		72	94	-	3700[c]	r.t.[b]
4.		24		2	6	-	1700[d]	r.t.[b]
5.	**14b**	32	*cis*-cyclooctene	-	10	35	25	55
6.		24		22[a]	75	-	240	55[b]
7.		25,32		-	41	90	110	90
8.		24		6[a]	46	-	90	r.t.[b]
9.	**19**	35	*cis*-cyclooctene	-	*ca.* 85	-	-	55
10.		35	*trans*-β-methylstyrene	-	66	-	-	55
11.	**20**	35	*cis*-cyclooctene	-	*ca.* 90	-	-	55
12.		35	*trans*-β-methylstyrene	-	50	-	-	55

13.	**21**	25	*cis*-cyclooctene	-	*ca.* 98	-	-	55
14.	**22**	25	*cis*-cyclooctene	-	60	-	-	90
15.	**23a**	26	*cis*-cyclooctene	100[a]	quant.	-	750	r.t.[b]
16.		26	*cis*-cyclooctene	30[a]	100	-	3650[c]	r.t.[b]
17.		24	*cis*-cyclooctene	82	quant.	-	11800[c]	r.t.[b]
18.		26	1-octene	-	*ca.* 45	-	40	r.t.[b]
19.		26	*cis*-stilbene	-	35	75	140	r.t.[b]
20.		24	*cis*-cyclooctene	95	quant.	-	900	r.t.[b]
21.	**24a**	24,26	*cis*-cyclooctene	15[a]	67	-	230	r.t.[b]
22.		24	*cis*-cyclooctene	7[a]	23	-	10	55[b]
23.	**23b**	24	*cis*-cyclooctene	95	quant.	-	970	r.t.[b]
24.	**24b**	24	*cis*-cyclooctene	5[a]	21	-	-	r.t.[b]
25.		24	*cis*-cyclooctene	44[a]	59	-	400	55[b]
26.	**23c**	24	*cis*-cyclooctene	96	quant.	-	790	r.t.[b]
27.	**24c**	24	*cis*-cyclooctene	20[a]	44	-	40	r.t.[b]
28.		24	*cis*-cyclooctene	37[a]	63	-	18	55[b]
29.	**23d**	24	*cis*-cyclooctene	30	quant.	-	750	r.t.[b]
30.	**24d**	24	*cis*-cyclooctene	11[a]	36	-	30	r.t.[b]
31.		24	*cis*-cyclooctene	31[a]	57	-	200	55[b]

[a] After 1.5 h; [b] Solvent CH_2Cl_2; [c] catalyst:substrate:oxidant = 0.001:1:2; [d] catalyst:substrate:oxidant = 0.0001:1:2.

Alkyl *ansa* bridged complexes **14**, **19−24** (Table 1.3) show the highest TOFs in *cis*-cyclooctene epoxidation at room temperature (11800 h^{-1} with **23a** in solvent CH_2Cl_2 using catalyst:substrate:oxidant = 0.001:1:2) when compared to other complexes discussed in this chapter (excluding complexes presented in Chapter 3). *Ansa*-bridged NHC complexes **30-33** (Table 1.5) on the other hand show poor conversion of substrate cyclooctene to its epoxide.[34]

Another important subclass of CpMo (and CpW) olefin epoxidation catalysts are μ-oxo bridged dimers **25−29**.[30] Compared to the mononuclear species, all the bimetallic complexes investigated achieve similar or better conversions with the exception of the C_5Bz_5 derivative **26**, which performed the least satisfactorily. On the other hand, after 24 h, complex **27** was found to outperform all the catalysts tested, excluding the monomeric species **1a** and **4**. Recently, Poli et al. have reported catalytic epoxidation of *cis*-cyclooctene with tungsten(VI) and molybdenum(VI) binuclear complexes $Cp^*_2M_2O_5$ (M = Mo **25**, W **29**) where 30% aqueous H_2O_2 was used as the oxidant.[36] Kühn et al. had earlier reported the detrimental effect of water on the (η^5-C_5Bz_5)MoO_2Cl catalytic system when very low catalyst concentrations are employed for the epoxidation reaction[19] but Poli and co-workers suggest as evidence from computational studies that presence of water is not wholly undesirable. These authors have also previously determined the existence of the species $[(Cp^*)MoO_2(H_2O)_n]^+$ and $[(Cp^*)MoO_3]^-$ in aqueous solutions formed by self-ionization of the binuclear complex $Cp^*_2Mo_2O_5$ and postulated that the cationic species might be catalytically active.[37] From recent theoretical mechanistic[36] and kinetic studies,[38] epoxidation reaction with Cp^*MO_2Cl catalyst (as a model for the binuclear metal complex, M = Mo, W) and H_2O_2 oxidant; the authors conclude that the presence of an H_2O molecule drives the energy profile to significant energetic stabilization, and in particular lowers the relative barrier height of the H_2O_2 activation step.

A few recent reports in literature describe the use of *N*-heterocyclic carbene coordinated CpMo complexes as catalysts for alkene epoxidation. Royo et al. have reported successful epoxidation catalysis with complexes of the type η^5-$Cp^x[CR_2R_3CR_4Ph$-η^1-$NHC^{Me}]Mo(CO)_2I$ (Cp^x = C_5H_4, C_5Me_4, $C_5(CH_2Ph)_4$; R_2, R_3, R_4 = H, CH_3, Ph; **30-33**).[34] These carbonyl precatalysts were tested for catalysis of *cis*-cyclooctene at 55 °C using catalyst:substrate:TBHP ratio 0.01:1:3 and $CHCl_3$ as the solvent. The authors reported an increased stability of such Cp-functionalized NHC molybdenum complexes compared to complexes of the type $Cp^{\neq}Mo(CO)_3X$ (X = halide, alkyl) and $Mo(\eta^5$-$C_5H_4(CH_2)_x$-η^1-$CH_2)(CO)_3$ (x = 1, 3) *ansa* complexes. The catalytic epoxidation reaction with these complexes performed under air was found to proceed relatively slowly with a large induction period.

Table 1.4. Catalytic olefin epoxidation with complexes $[Cp^{\neq}MO_2]_2O$ (M = Mo, W) at 55 °C with TBHP (5.5 M in *n*-decane). Ref. 30.

Entry	Catalyst	Substrate	Catalyst: Substrate: Oxidant	Conversion [%] at 4 h	at 24 h	TOF (h^{-1})	Solvent
1.	**25**	*cis*-cyclooctene	0.01:1:2	55.5	87	-	dry $CHCl_3$
2.			0.01:1:2[a]	27	-	-	$CHCl_3$
3.	**25a**	*cis*-cyclooctene	0.01:1:2	-	90	-	dry $CHCl_3$
4.	**26**	*cis*-cyclooctene	0.01:1:2	-	70	-	dry $CHCl_3$
5.	**27**	*cis*-cyclooctene	0.01:1:2	74.5	99.9	-	dry $CHCl_3$
6.	**27a**	*cis*-cyclooctene	0.01:1:2	-	100	-	dry $CHCl_3$
7.	**28**	*cis*-cyclooctene	0.01:1:2	72	79	-	dry $CHCl_3$
8.	**28a**	*cis*-cyclooctene	0.01:1:2	-	76.4	-	dry $CHCl_3$

[a] 70% (aqueous) TBHP.

Table 1.5. Catalytic epoxidation of *cis*-cyclooctene with *N*-heterocyclic carbene ligated cyclopentadienyl molybdenum complexes **30**-**39** at 55 °C with TBHP oxidant.

Entry	Catalyst	Ref.	Catalyst:Substrate:Oxidant	Yield(%) of cyclooctene epoxide at 8 h	at 24 h	Solvent
1.	**30**	34	0.01:1:3	19	25[a]	$CHCl_3$
2.	**32**	34	0.01:1:3	5	11[a]	$CHCl_3$
3.	**33**	34	0.01:1:3	51	91[a]	$CHCl_3$
4.	**34**	27	0.01:1:2	5[b]	15[b]	-
5.	**35**	27	0.01:1:2	10[b]	20[b]	-
6.	**36**	27	0.01:1:2	25[b]	42[b]	-
7.	**37a**	27	0.01:1:2	8[b]	12[b]	-
8.	**37b**	27	0.01:1:2	22[b]	27[b]	-

9.	**38**	[27]	0.01:1:2	10[b]	15[b]	-
10.	**39**	[27]	0.01:1:2	97[b]	100	-

[a] Yield at 20 h; [b] Approximate data

Zhao et al. have also recently reported the synthesis and characterization of a series of NHC cyclopentadienyl molybdenum complexes of the type $CpMo(CO)_2(NHC)X$ (X = Cl, Br) **34-38**.[27] Poor catalytic activity was observed with complexes **34-38** when employed in ratio 0.01:1:2 of catalyst:substrate:TBHP for cyclooctene epoxidation although these activities were still better than those obtained with *ansa*-bridged complexes $[(Cp^xCR_2R_3R_4Ph\text{-}NHC^{Me})Mo(CO)_2I$ ($Cp^x = C_5H_4$, C_5Me_4, $C_5(CH_2Ph)_4$; R_2, R_3, R_4 = H, CH_3, Ph; **30-33**).[34]

Table 1.6. Catalytic epoxidation of various substrates with complexes **41**-**43** at 55 °C. TBHP (in *n*-decane) employed as the oxidant unless stated otherwise. Catalyst:substrate:oxidant = 0.01:1:2. Ref. 39.

Entry	Catalyst	Substrate	Oxidant	Solvent	Conversion %		Selectivity %		TOF[a]
					6 h	24 h	6h	24h	(h^{-1})
1.	**41**	*cis*-cyclooctene	TBHP	-	99	100	100	100	310
2.			TBHP	DCE	100	100	100	100	361
3.			TBHP (aq.)	-	80	99	100	100	97
4.			H_2O_2 (aq.)	-	11	27	100	100	<1
5.		1-octene	TBHP	DCE	35	51	100	100	6
6.		*trans*-2-octene	TBHP	DCE	74	89	100	100	81
7.		Cyclododecene	TBHP	DCE	86	92	100	100	188
8.		*(R)*-(+)-Limonene	TBHP	DCE	98	100	100	100	289[b]
9.	**42**	*cis*-cyclooctene	TBHP	-	94	98	100	100	307
10.	**43**	*cis*-cyclooctene	TBHP	-	50	84	93	96	32

[a] TOF calculated at *ca.* 10 min of the reaction; [b] Sum of selectivities to 1,2-epoxy-*p*-menth-8-ene and 1,2-8,9-diepoxy-*p*-menthane.

Cyclopentadienyl molybdenum dicarbonyl complexes with η^3-allyl ligands $Cp''Mo(CO)_2(\eta^3\text{-}C_3H_5)$ (Cp'' = $\eta^5\text{-}C_5H_5$ **41**, $\eta^5\text{-}C_5H_4Me$ **42**, $\eta^5\text{-}C_5Me_5$ **43**) have been the subject of investigation as catalyst precursors for olefin epoxidation by Gonçalves et al.[39] Complexes **41-43** used as catalyst precursors for *cis*-cyclooctene epoxidation with TBHP (in *n*-decane at 55 °C, under atmospheric pressure) without a co-solvent and show conversions of 84-100% at 24 h (catalyst:substrate:oxidant = 0.01:1:2).

A few recent reports in literature outline the successful use of H_2O_2 with cyclopentadienyl molybdenum catalysts. $[CpMo(CO)_3(C{\equiv}CPh)]$ (precatalyst of oxo peroxo complex **47**) has been employed for selective *cis*-dihydroxylation of olefins,[42] *N*-oxidation of aromatic amines to nitroso compounds,[43] and selective oxidation of aromatic primary alcohols to aldehydes.[44] H_2O_2 oxidant with $[Cp^{\neq}Mo(CO)_3Cl]$ ($Cp^{\neq}$ = Cp, Cp*) precatalyst is successful for transformation of sulfides to sulfoxides or sulfones.[45] Catalytic epoxidation of cyclohexene with the tricarbonyl analogue of **47** has also been studied (Table 1.9).

Table 1.7. Olefin epoxidation catalyzed by **44** and **45** with catalyst:substrate:oxidant ratio 1:100:200. Ref. 40

Entry	Catalyst	Substrate	Oxidant	Temp. [°C]	Solvent	Time	Yield [%]	ee [%]
1.	**44**	*cis*-cyclooctene	TBHP	55	$CHCl_3$	45 min	96	-
2.	**44**	*(R)*-limonene	TBHP	55	$CHCl_3$	1 h	100	50:50[d]
3.	**44**	*trans*-β-methylstyrene	TBHP	r.t.	$CHCl_3$	16 h	58	≤ 5%
4.	**44**	*cis*-cyclooctene	H_2O_2[a]	70	CH_3CN	20 h	77	-
5.	**45**	*cis*-cyclooctene	TBHP	55	$CHCl_3$	30 min	98	-
6.	**45**[b,c]	*cis*-cyclooctene	TBHP	55	$CHCl_3$	-	90	-
7.	**45**	*(R)*-limonene	TBHP	55	$CHCl_3$	1 h	100	60:40[d]
8.	**45**	*trans*-β-methylstyrene	TBHP	r.t.	$CHCl_3$	16 h	14	≤ 5%
9.	**45**	*cis*-cyclooctene	H_2O_2	70	CH_3CN	11 h	92	-
10.	**45**	*cis*-cyclooctene	H_2O_2	55	CH_3CN	20 h	9	-
11.	**5a**	*cis*-cyclooctene	H_2O_2	70	CH_3CN	10 h	92	-
12.	**5a**	*cis*-cyclooctene	H_2O_2	55	CH_3CN	20 h	8	-

[a] H_2O_2 (30% in H_2O) was used as oxidant; [b] catalyst amount 0.2 mol%; [c] TOF at 5 min = 5421 mol mol_{cat}^{-1} h^{-1}; [d] *cis/trans* epoxide ratio.

Table 1.8. *Cis*-cyclooctene epoxidation with complex **46** at 55 °C with different oxidants in different solvents using catalyst:substrate:oxidant = 1:100:150. Ref. 41.

Entry	Oxidant	Solvents	Yield [%] at 6 h	Yield [%] at 24 h
1.	TBHP (decane)	no cosolvent	100[a]	–
2.	TBHP (aqueous)	no cosolvent	80	95
3.		H_2O/n-hexane	53	80
4.		glycerol/n-hexane	3	10
5.		ionic liquid[b]/n-hexane	5	9
6.	H_2O_2	H_2O/n-hexane	8	78

[a] At 3 h; [b] 1-butyl-3-methylimidazolium chloride.

Precatalyst $[CpMo(CO)_3(CH_2CONH_2)]$ **48** has also been used for cyclooctene epoxidation. Yield of the epoxide is 100 % after 24 h when the reaction is carried out at 55 °C using TBHP (decane) as oxidant without additional co-solvent and the TOF calculated after 10 min is 247 h^{-1}.[47]

Table 1.9. Oxidation of cyclohexene using [CpMo(CO)$_3$(C≡CPh)] catalyst (precursor for **47**).[a] Ref. 46.

Entry	Oxidant	Solvent	Conversion%	Time (h)	Selectivity %		
					Epoxide	Diol	Others
1.	TBHP	$C_2H_4Cl_2$	53	12	79.2	14.4[b]	6.4
2.	H_2O_2 (50%)	^{t}BuOH	95	9	–	91[c]	9

[a] Reaction conditions: cyclohexene (0.02 mol), catalyst (0.01 mmol), oxidants H_2O_2 (0.04 mol) and TBHP (0.02 mol) at 80 °C; [b] *trans*-Diol; [c] *cis*-Diol.

1.2.3 State of the Art

1.2.3.1 Kinetics

Often the reaction progress kinetic profile of catalytic epoxidation using [CpMo(CO)$_3$R] precursors is a sigmoidal curve. This implies an initial ‘induction’ period of slower substrate conversion. The current accepted explanation is that the metal precursor must transform into the active oxo complex during this slow phase. The reaction proceeds slowly since a sufficient amount of the active catalyst must be made available. This is followed by a steep curve in the conversion *vs.* time plot – the ‘fast’ phase. TOFs of the catalytic reaction are often calculated from the slope in this phase. This is followed by a transitional decrease in rate and eventual plateau phase which suggests catalytic deactivation.

Epoxidation reactions performed at 55 °C on the other hand show time-dependent curves with relatively high initial rates of the reaction, indicative of first order kinetics. There is no distinctly observable induction period and decrease in reaction rate at later stages of the reaction is understood to be a consequence of catalyst deactivation, either due to complex decomposition or due to competing coordination of the by-product *tert*-butanol to Mo centre in place of the oxidant TBHP, as already studied for isoelectronic complexes MoO$_2$X$_2$L (X = Cl, Br, Me; L = bidentate Lewis base). [48–50]

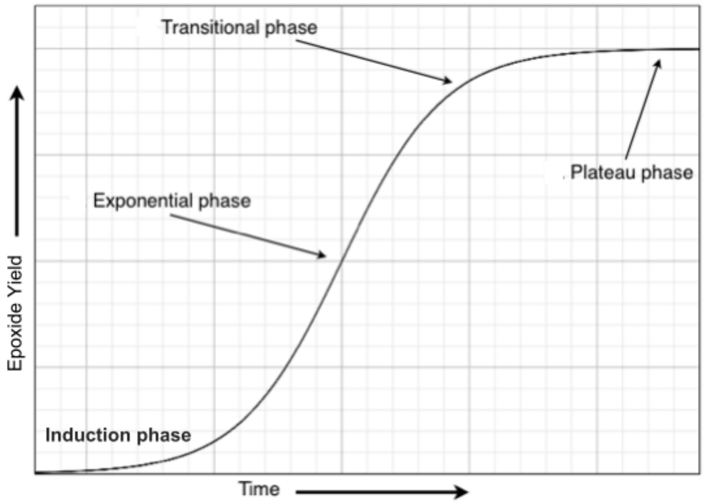

Figure 1.3. The kinetic stages of a typical olefin epoxidation reaction using [CpMo(CO)$_3$R] precatalyst with TBHP.

Although the technique of oxidation of Mo carbonyl complexes with TBHP has been widely utilized in the last 10 years for the synthesis of numerous Mo homogeneous catalysts and heterogeneous materials, several important aspects of this chemistry remain unexplained, such as –

a) How do inactive CpMo(II) carbonyl precatalysts transform to catalytically active CpMo(VI) oxo complexes? For the epoxidation of some substrates, the conversion−time curves do not follow ideal sigmoidal behaviour. Therefore, how and what oxidative transformations take place in the 'induction phase' of epoxidation reaction when TBHP is added to the catalyst and substrate reaction mixture?

b) Which catalytic species – dioxo [CpMo(O)$_2$R] or oxo-peroxo [CpMo(O)(O$_2$)R] (or perhaps an entirely different Mo complex or intermediate?) is responsible for the 'fast' phase of the catalysis reaction? What are the reasons for the difference in catalytic performance of dioxo and oxo-peroxo complexes?

c) What is the influence of the side chain ligand R on oxidative decarbonylation reaction and catalytic epoxidation reaction mechanism?

d) What processes or transformations result in catalyst deactivation or apparent slow phase at later stages of the epoxidation reaction?

e) Why is oxidative decarbonylation of some carbonyl complexes exothermic?

f) What are the fundamental reasons for the difference in epoxidation reaction rates with various olefin substrates – *cis*-cyclooctene (cyclic alkene), 1-octene (terminal alkene), stilbene (sterically hindered alkene) etc.

g) Despite several rational catalyst design attempts for the purpose of asymmetric catalysis, why do chiral CpMo complexes give poor enantiomeric excess on epoxidation of prochiral alkenes?

h) Does a generic mode of activation of carbonyl Mo complexes exist when such compounds are treated with TBHP? Can such knowledge be derived and used for design of catalysts that utilize H_2O_2 for epoxidation catalysis without deactivation of the catalyst or poor epoxide yields?

i) Is the oxidative transformation of CpMo(II) precatalysts to CpMo(VI) oxo complexes with TBHP efficient? Are the oxidized complexes stable for long periods of time and easily re-usable or recycled?

j) How does the presence of trace impurities or additives affect the reaction progress and mechanisms of catalytic epoxidation?

k) What is the nature of the precipitate observed to have formed during epoxidation with some CpMo precatalysts? How and why does the precipitate form and what might be possible ways to prevent its formation?

In the following chapters of this work, attempts have been made to explain some of these observations. Although a thorough and detailed model for epoxidation reaction is not yet available, the insights are valuable for understanding and explaining the aforementioned experimental observations.

1.2.3.2 Mechanisms

The mechanism of olefin epoxidation with dioxomolybdenum(VI) catalysts MoO$_2$X$_2$L (X = halide, CH$_3$; L = bidentate ligand) [48–50] and Mo oxo bisperoxo complexes [7,51–53] has been widely studied. However, the identity of the catalytically active species formed with [CpMo(CO)$_3$R] precursors and mechanism of catalysis is still a subject of current research. The widely accepted kinetic and mechanistic models for oxygen transfer to olefins with Mo-peroxo species (Figure 1.4) and Mo-oxo species (Figure 1.5) are illustrated below.

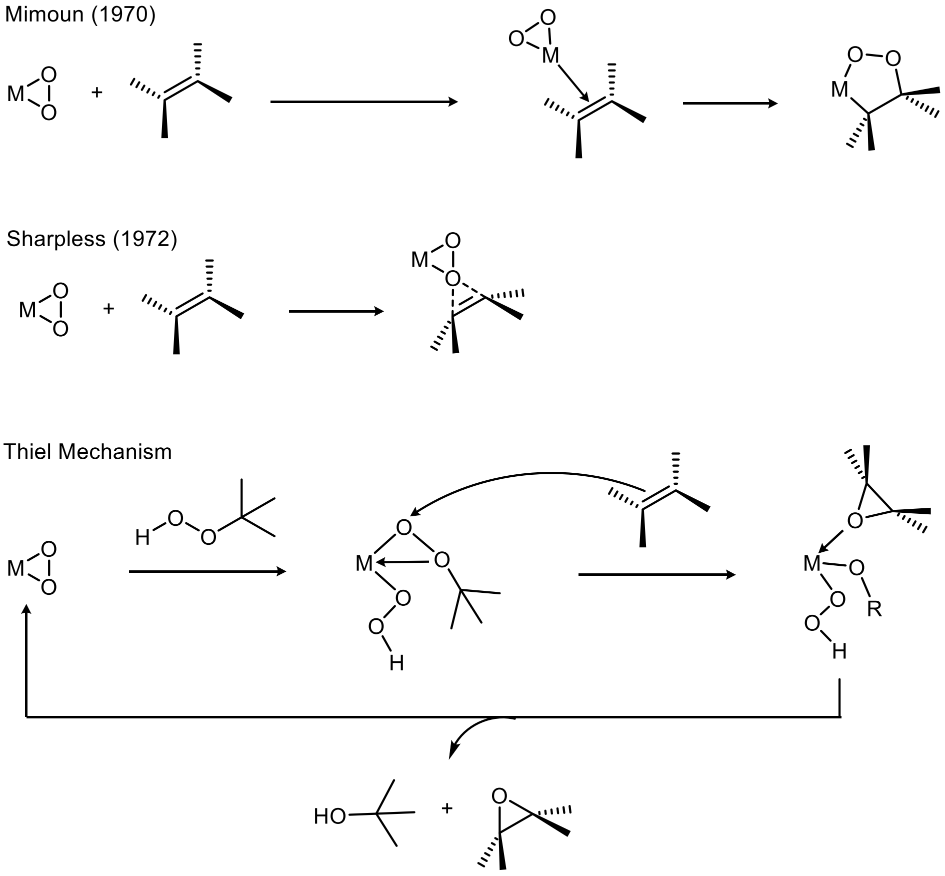

Figure 1.4. Mechanisms proposed for olefin epoxidation with Mo-peroxo compounds.

In the mechanisms involving TBHP oxidant, the oxo or peroxo ligand acts as a temporary repository of the proton.[46,54–57] Thus the oxidant is activated by coordination to Mo, and becomes susceptible to nucleophilic attack by the olefin at the electrophilic oxygen atom of the intermediate complex. The Thiel mechanism is reasoned for TBHP, but can also be operative for H$_2$O$_2$. In this mechanism, the principle is identical to that of the Sharpless mechanism, whereby an exogenous attack of the olefin takes place at the electrophilic oxygen atom without coordination at the metal centre.

In the mechanism proposed by Calhorda et al.[55] the oxido ligand (Mo=O) is the hydrogen depository and the alkylperoxido moiety ($-O^{\alpha}O^{\beta}R$) bonds with Mo, to give the intermediate [CpMo(OH)(OOR)L] (R = Me for calculation model, L = side chain ligand). This intermediate is stabilized by H-bonding between hydroxide proton and O$^{\beta}$ of alkylperoxido group.[54,55] Subsequently, olefin insertion similar to Mimoun mechanism has been proposed.

Poli et al. in contrast have proposed an asymmetrical η^2-coordination of the alkylperoxido intermediate, i.e. interaction between Mo and O^{β} takes place.[54] This interaction is critical for the activation of the O^{α} atom toward an exogenous nucleophilic attack by the olefin substrate, leading to significantly lower activation barriers for the oxygen atom transfer to the olefin compared to the Calhorda mechanism.[54]

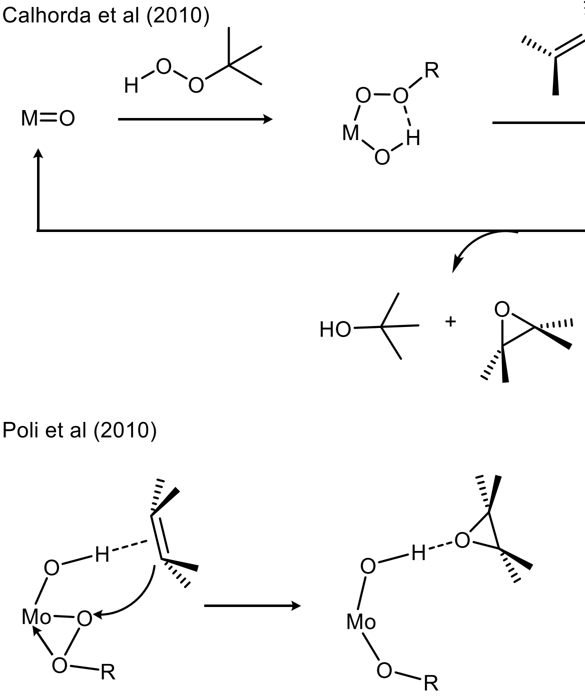
Calhorda et al (2010)

Poli et al (2010)

Figure 1.5. Mechanisms proposed in literature for olefin epoxidation with Mo-oxo compounds.

Rational catalyst design is possible based on the knowledge of generic modes of activation, induction, reactivity and deactivation; for which an understanding of the mechanism of hydroperoxide activation with the transition metal in epoxidation reactions is crucial.[53,58–61] In this regard, with $Cp^{\neq}Mo(CO)_3X$ (X = halide, alkyl) complexes, several groups have proposed models from comprehensive kinetic and DFT studies, but a consensus on the nature and identity of the catalytically active species studied is yet to be reached.[36,54,55,62,63] From these studies it may be concluded that catalysis with different cyclopentadienyl ligated molybdenum complexes follows slightly different mechanisms of activation of the hydroperoxide and oxygen transfer or insertion into the olefin. Competing reaction pathways may exist which are probably dependent on the ligand environment of the metal centre including the type of substitution present on the Cp ring. It may be worthwhile to invest effort into resolving the debate presented by reported theoretical studies and experimental kinetic data.

1.3 Conclusions and Scope

A high turnover frequency (TOF) with a low mol% catalyst ratio; regio- and stereoselectivity, high yield or enantiomeric excess (*ee*) are desirable attributes in any catalytic reaction. As may be concluded from the present literature, Cp ligated dioxomolybdenum(VI) complexes are in general more active in epoxidation catalysis than related $MoO_2X_2L_2$ complexes and even rival the catalytic activity reported for methyltrioxidorhenium (MTO).[64] Nevertheless, these complexes still suffer from limited applicability; for instance they show generally poor activity with unfunctionalized olefins, and efficient catalysis with them is largely dependent on the use of TBHP instead of more environmentally benign H_2O_2 oxidant. It is therefore worthwhile to investigate if use of H_2O_2 with CpMo complexes is feasible, which would further the advantages of these catalysts. Since asymmetric epoxidation catalysis has not developed to a satisfactory extent with Mo-based organomolybdenum compounds, there is a need to understand why asymmetric induction fails. Strategies towards achieving this end have included modification of the Cp ligand by chiral substituents[33,65] or including chiral centres on the *ansa* bridge[35] or even different NHCs coordinated to the cyclopentadienyl fragment.[34] Parameters to be considered for this purpose are facile syntheses, stability, good catalytic activities and chiral induction ability for versatile applicability of such potential catalysts. Epoxidation in alternative solvents such as room temperature ionic liquids [66–68] and microwave heating[69] has also been reported, in an effort to extend the applicability of these complexes with sustainability in mind. In this context, heterogeneous catalytic applications with CpMo complexes are also a worthwhile study.

1.4 References

[1] http://www.imoa.info/HSE/environmental_data/molybdenum_in_biology.php, (Accessed on 18 November, 2013).

[2] http://www.imoa.info/molybdenum/molybdenum_properties.php, (Accessed on 18 November, 2013).

[3] F.E. Kühn, A.M. Santos, M. Abrantes, Chem. Rev. 106 (2006) 2455–2475.

[4] F.E. Kühn, J. Zhao, W.A. Herrmann, Tetrahedron: Asymmetry. 16 (2005) 3469–3479.

[5] F.E. Kühn, A.M. Santos, W.A. Herrmann, Dalton Trans. (2005) 2483–2491.

[6] K.R. Jain, W.A. Herrmann, F.E. Kühn, Coord. Chem. Rev. 252 (2008) 556–568.

[7] M. Amini, M.M. Haghdoost, M. Bagherzadeh, Coord. Chem. Rev. 257 (2013) 1093–1121.

[8] E. da Palma Carreiro, A.J. Burke, J. Mol. Catal. A. Chem. 249 (2006) 123–128.

[9] E. da Palma Carreiro, C. Monteiro, Y. Guo, A.J. Burke, A.I. Rodrigues, J. Mol. Catal. A. Chem. 260 (2006) 295–298.

[10] N. Grover, F.E. Kühn, Curr. Org. Chem. 16 (2012) 16–32.

[11] C. Müller, N. Grover, M. Cokoja, F.E. Kühn, Homogeneous Catalytic Olefin Epoxidation with Molybdenum Complexes, in: Adv. Inorg. Chem. Vol. 65, 2013: pp. 33–83.

[12] R.H. Holm, Chem. Rev. 87 (1987) 1401–1449.

[13] M. Cousins, M.L.H. Green, J. Chem. Soc. (1963) 889–894.

[14] M. Cousins, M.L.H. Green, J. Chem. Soc. (1964) 1567–1572.

[15] M. Cousins, M.L.H. Green, J. Chem. Soc. A. Inorg. Phys. Theor. (1969) 16–19.

[16] J.W. Faller, Y. Ma, J. Organomet. Chem. 340 (1988) 59–69.

[17] J.W. Faller, Y. Ma, J. Organomet. Chem. 368 (1989) 45–56.

[18] M.K. Trost, R.G. Bergman, Organometallics 10 (1991) 1172–1178.

[19] M. Abrantes, A.M. Santos, J. Mink, F.E. Kühn, C.C. Romão, Organometallics 22 (2003) 2112–2118.

[20] T.K. Panda, M.T. Gamer, P.W. Roesky, Organometallics. 22 (2003) 877–878.

[21] T.S. Piper, G. Wilkinson, J. Inorg. Nucl. Chem. 3 (1956) 104–124.

[22] P. Eilbracht, Chem. Ber. 109 (1976) 1429–1435.

[23] F. Amor, P. Royo, T.P. Spaniol, J. Okuda, J. Organomet. Chem. 604 (2000) 126–131.

[24] A. Capapé, A. Raith, E. Herdtweck, M. Cokoja, F.E. Kühn, Adv. Synth. Catal. 352 (2010) 547–556.

[25] J. Zhao, K.R. Jain, E. Herdtweck, F.E. Kühn, Dalton Trans. (2007) 5567–5571.

[26] A. Capapé, A. Raith, F.E. Kühn, Adv. Synth. Catal. 351 (2009) 66–70.

[27] S. Li, C.W. Kee, K. Huang, T.S.A. Hor, J. Zhao, Organometallics. 29 (2010) 1924–1933.

[28] S.A. Hauser, M. Cokoja, F.E. Kühn, Catal. Sci. Technol. 3 (2013) 552–561.

[29] D. Chakraborty, M. Bhattacharjee, R. Krätzner, R. Siefken, H.W. Roesky, I. Uson, H.-G. Schmidt, Organometallics. 18 (1999) 106–108.

[30] A.M. Martins, C.C. Romão, M. Abrantes, M.C. Azevedo, J. Cui, A.R. Dias, M. T. Duarte, M. A. Lemos, T. Lourenço, R. Poli, Organometallics. 24 (2005) 2582–2589.

[31] A.A. Valente, J.D. Seixas, I.S. Gonçalves, M. Abrantes, M. Pillinger, C.C. Romão, Catal. Lett. 101 (2005) 127–130.

[32] J. Zhao, A.M. Santos, E. Herdtweck, F.E. Kühn, J. Mol. Catal. A. Chem. 222 (2004) 265–271.

[33] M. Abrantes, A. Sakthivel, C.C. Romão, F.E. Kühn, J. Organomet. Chem. 691 (2006) 3137–3145.

[34] V.V.K.M. Kandepi, A.P. da Costa, E. Peris, B. Royo, Organometallics. (2009) 4544–4549.

[35] J. Zhao, E. Herdtweck, F.E. Kühn, J. Organomet. Chem. 691 (2006) 2199–2206.

[36] C. Dinoi, M. Ciclosi, E. Manoury, L. Maron, L. Perrin, R. Poli, Chem. Eur. J. 16 (2010) 9572–9584.

[37] R. Poli, Chem. Eur. J. 10 (2004) 332–341.

[38] P. Sözen-Aktaş, E. Manoury, F. Demirhan, R. Poli, Eur. J. Inorg. Chem. 2013 (2013) 2728–2735.

[39] P. Neves, C.C.L. Pereira, F.A.A. Paz, S. Gago, M. Pillinger, C.M. Silva, A. A. Valente, C. C. Romão, I. S. Gonçalves, J. Organomet. Chem. 695 (2010) 2311–2319.

[40] P.M. Reis, C.A. Gamelas, J.A. Brito, N. Saffon, M. Gómez, B. Royo, Eur. J. Inorg. Chem. (2011) 666–673.

[41] A.C. Gomes, S.M. Bruno, C. Tomé, A.A. Valente, M. Pillinger, M. Abrantes, I. S. Gonçalves, J. Organomet. Chem. 730 (2013) 116–122.

[42] A. V Biradar, B.R. Sathe, S.B. Umbarkar, M.K. Dongare, J. Mol. Catal. A. Chem. 285 (2008) 111–119.

[43] A. V Biradar, T. V Kotbagi, M.K. Dongare, S.B. Umbarkar, Tet. Lett. 49 (2008) 3616–3619.

[44] A. V Biradar, M.K. Dongare, S.B. Umbarkar, Tet. Lett. 50 (2009) 2885–2888.

[45] C.A. Gamelas, T. Lourenço, A.P. da Costa, A.L. Simplicio, B. Royo, C.C. Romão, Tet. Lett. 49 (2008) 4708–4712.

[46] P. Chandra, S.L. Pandhare, S.B. Umbarkar, M.K. Dongare, K. Vanka, Chem. Eur. J. 19 (2013) 2030–2040.

[47] S.S. Braga, S. Gago, J.D. Seixas, A.A. Valente, M. Pillinger, T.M. Santos, I. S. Gonçalves, C.C. Romão, Inorg. Chim. Acta. 359 (2006) 4757–4764.

[48] F. E. Kühn, M. Groarke, E. Bencze, E. Herdtweck, A. Prazeres, A.M. Santos, M. J. Calhorda; C. C. Romão; I. S. Gonçalves; A. D. Lopes; M. Pillinger, Chem. Eur. J. 8 (2002) 2370–2383.

[49] A.M. Al-Ajlouni, A.A. Valente, C.D. Nunes, M. Pillinger, A.M. Santos, J. Zhao, C. C. Romão; I. S. Gonçalves; F. E. Kühn Eur. J. Inorg. Chem. (2005) 1716–1723.

[50] L.F. Veiros, F.E. Kühn, P.J. Costa, C.C. Romão, M.J. Calhorda, Dalton Trans. (2006) 1383–1389.

[51] D. V Deubel, G. Frenking, P. Gisdakis, W.A. Herrmann, N. Rösch, J. Sundermeyer, Acc. Chem. Res. 37 (2004) 645–652.

[52] I. V Yudanov, C. Di Valentin, P. Gisdakis, N. Rösch, J. Mol. Catal. A. Chem. 158 (2000) 189–197.

[53] W.R. Thiel, J. Eppinger, Chem. Eur. J. 3 (1997) 696–705.

[54] A. Comas-Vives, A. Lledós, R. Poli, Chem. Eur. J. 16 (2010) 2147–2158.

[55] P.J. Costa, M. José Calhorda, F.E. Kühn, Organometallics. 29 (2010) 303–311.

[56] J. Morlot, N. Uyttebroeck, D. Agustin, R. Poli, ChemCatChem. 5 (2013) 601–611.

[57] M. Drees, S.A. Hauser, M. Cokoja, F.E. Kühn, J. Organomet. Chem. (2013) DOI 10.1016/j.jorganchem.2013.05.004.

[58] H. Mimoun, I.S. de Roch, L. Sajus, Tetrahedron. 26 (1970) 37–50.

[59] A.O. Chong, K.B. Sharpless, J. Org. Chem. 42 (1977) 1587–1590.

[60] W.R. Thiel, T. Priermeier, Angew. Chem. Int. Ed. Engl. 34 (1995) 1737–1738.

[61] W.R. Thiel, J. Mol. Catal. A Chem. 117 (1997) 449–454.

[62] M. Pratt, J.B. Harper, S.B. Colbran, Dalton Trans. (2007) 2746–2748.

[63] A.M. Al-Ajlouni, D. Veljanovski, A. Capapé, J. Zhao, E. Herdtweck, M.J. Calhorda, F.E. Kühn, Organometallics. 28 (2009) 639–645.

[64] M.C.A. van Vliet, I.W.C.E. Arends, R.A. Sheldon, Chem. Comm. (1999) 821–822.

[65] M. Abrantes, F.A.A. Paz, A.A. Valente, C.C.L. Pereira, S. Gago, A.E. Rodrigues, J. Klinowski, M. Pillinger, I.S. Gonçalves, J. Organomet. Chem. 694 (2009) 1826–1833.

[66] L. Graser, D. Betz, M. Cokoja, F.E. Kühn, Curr. Inorg. Chem. 1 (2011) 166–181.

[67] D. Betz, W.A. Herrmann, F.E. Kühn, J. Organomet. Chem. 694 (2009) 3320–3324.

[68] D. Betz, A. Raith, M. Cokoja, F.E. Kühn, ChemSusChem. 3 (2010) 559–562.

[69] M. Abrantes, P. Neves, M.M. Antunes, S. Gago, F.A. Almeida Paz, A.E. Rodrigues, M. Pillinger, I. S. Gonçalves, C. M. Silva, A. A. Valente, J. Mol. Catal. A. Chem. 320 (2010) 19–26.

[70] S. Li, Z. Wang, T.S.A. Hor, J. Zhao, Dalton Trans. 41 (2012) 1454–1456.

1.5 Additional References (Figure 1.2)

Complex(es)	Reference(s)	Complex(es)	Reference(s)
1a	13−15,19,30,31	**16**	63
1b	27	**17**	33
2a	16−19,30	**18**	65
2b	15,27	**19, 20**	35
3	18,29	**21**	22,25
4	19,30	**22**	25
5a	19,31	**23, 24**	24,26
5b	27	**25–29**	30,36
6	19	**30–33**	34
7	19	**34–38**	27
8	30	**39, 40**	27,70
9−12	32	**41–43**	39
13	30	**44, 45**	40
14a	22,24,32,35	**46**	41
14b	24,25,32	**47**	42−44,46
15	32	**48**	47

2 Objectives

The aim of this thesis is to gain an understanding of the generic modes of induction, reactivity and deactivation of [CpMo(CO)$_3$R] precatalysts in the olefin epoxidation reaction. Until now, there are only a few instances where spectroscopic and/or structural features adequately explain trends in catalytic activity.[1−3] Despite a fundamental understanding of how different ligand environments may exert their stereoelectronic influence on the metal centre, a correlation with catalytic performance is difficult to derive from kinetic[4,5] and mechanistic models[6−8] published in the last decade.

Therefore in **Part II** of this work, an attempt has been made to determine the relevant parameters − ^{95}Mo chemical shifts, IR absorption frequencies, relevant bond lengths and angles − and their trends, that may be correlated with catalytic activity or turnover frequencies. The concept of more Lewis acidity of Mo being responsible for higher catalytic epoxidation activity has been challenged. In **Chapter 3**, synthesis and characterization of two novel imidazo-[1,5-*a*]-pyridyl-3-ylidine carbene CpMo complexes is described. N-heterocyclic carbene ligands are strong σ-donors and therefore, from present understanding of structure-activity relationships with Mo-based organometallic epoxidation catalysts, expected to exhibit poor catalytic activity on account of decreased Lewis acidity of the metal centre. To contrast and compare, in **Chapter 4** alkylester complexes that are either substituted or unsubstituted at the α-carbon have been synthesized. The alkylester side chain exerts a net –I (inductive) effect and serves as a potential route for introducing chirality in the catalyst. It is expected that the more Lewis acidic metal centre in these complexes should exhibit better catalytic activity in comparison to complex [CpMo(CO)$_3$(CH$_3$)], for example, in which the methyl side chain is a simple σ-donating ligand.

The task of studying *in situ* processes is inherently complicated. Challenges and unexplained experimental observations include – highly exothermic oxidative decarbonylation which ‘blurs’ kinetic information about the induction phase and formation of a precipitate that challenges the notion of catalyst robustness. Furthermore, for some CpMo complexes the two oxidative transformations take place at such a high rate that even sophisticated reaction progress monitoring methods (such as *in situ* IR, UV-Vis and kinetic NMR) are limited in their capacity to provide in-depth information. While it is evident that an outline of molecular catalyst design principles would be of immense help to extend the scope of CpMo chemistry, it is not sufficient to merely synthesize such CpMo complexes and determine their structure-activity relationships. It is also important to evaluate the kinetic behaviour of the two nearly simultaneously occurring oxidation reactions individually and to determine whether there are commonalities within a structural class and what implications these bear for molecular catalyst design.

With these intentions, the work in **Part III** has been undertaken to treat both *in situ* oxidative transformations separately and also study their effect on each other. Alkylester complexes (discussed in **Chapter 4**) and other examples from literature were chosen for this purpose and the results are presented in **Chapters 5 and 6**. The kinetic and mechanistic studies in these chapters assess the induction phase behaviour under varying reaction conditions and the subsequent mechanistic implications. **Chapter 7** presents a summary of theoretical studies of the oxidation reactions of [CpMo(CO)$_3$R] precatalysts and other relevant work.

The catalytic activity of a fluorinated molybdenum complex [CpMo(CO)$_3$CF$_3$] has been described in literature.[8,9] In this work, a contradiction is again apparent to the widely accepted concept of a more Lewis acidic Mo centre being a better catalyst for epoxidation. Based on the results of previous chapters, the reasons for unexpected catalytic performance of this complex are discussed in **Chapter 8**.

References

[1] J. Zhao, E. Herdtweck, F.E. Kühn, J. Organomet. Chem. 691 (2006) 2199–2206.

[2] J. Zhao, A.M. Santos, E. Herdtweck, F.E. Kühn, J. Mol. Catal. A: Chem. 222 (2004) 265–271.

[3] J. Zhao, K.R. Jain, E. Herdtweck, F.E. Kühn, Dalton Trans. (2007) 5567–5571.

[4] M. Pratt, J.B. Harper, S.B. Colbran, Dalton Trans. (2007) 2746–2748.

[5] A.M. Al-Ajlouni, D. Veljanovski, A. Capapé, J. Zhao, E. Herdtweck, M.J. Calhorda, F.E. Kühn, Organometallics 28 (2009) 639–645.

[6] C. Dinoi, M. Ciclosi, E. Manoury, L. Maron, L. Perrin, R. Poli, Chem. Eur. J. 16 (2010) 9572–84.

[7] P.J. Costa, M.J. Calhorda, F.E. Kühn, Organometallics. 29 (2010) 303–311.

[8] M. Drees, S.A. Hauser, M. Cokoja, F.E. Kühn, J. Organomet. Chem. (2013) DOI 10.1016/j.jorganchem.2013.05.004.

[9] S.A. Hauser, M. Cokoja, M. Drees, F.E. Kühn, J. Mol. Catal. A: Chem. 363-364 (2012) 237–244.

II. Synthesis and Catalysis

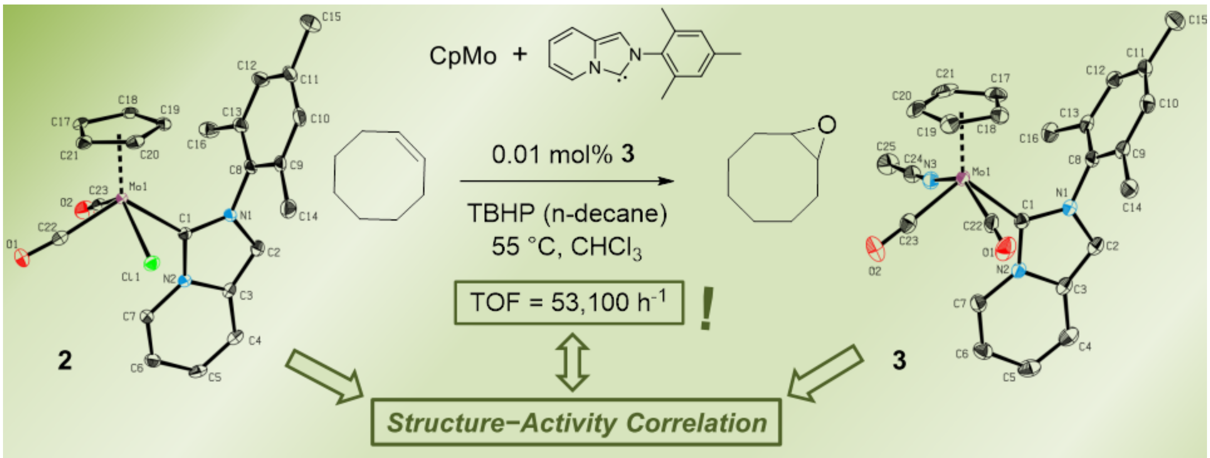
CpMo +
0.01 mol% 3
TBHP (n-decane)
55 °C, CHCl$_3$
TOF = 53,100 h^{-1}
!
2
3
Structure–Activity Correlation

- ➢ CpMo dicarbonyl complexes with imidazo-[1,5-*a*]-pyridyl-3-ylidene ligands have been synthesized.
- ➢ Highest TOFs of all known CpMo complexes in olefin epoxidation with TBHP are achieved.
- ➢ Crystal structures of these complexes are reported and discussed.
- ➢ Spectroscopic and structural data are discussed to identify structure-activity relationships.

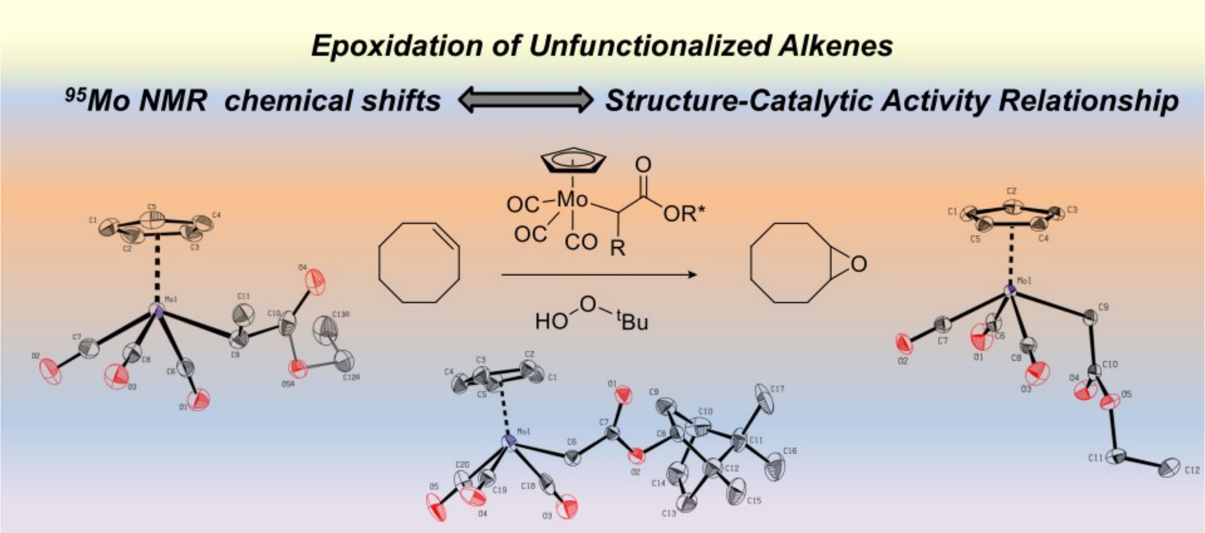
Epoxidation of Unfunctionalized Alkenes
^{95}Mo NMR chemical shifts
Structure-Catalytic Activity Relationship
OC–Mo
OC
CO
R
O
OR*
HO–O–^{t}Bu
O

- ➢ [CpMo(CO)$_3$R] complexes containing alkylester side chains R have been synthesized.
- ➢ These complexes have been applied in the epoxidation of unfunctionalized alkenes with TBHP oxidant.
- ➢ Structure-catalytic activity relationship has been discussed by comparing ^{95}Mo NMR chemical shifts.

3 Cyclopentadienyl Imidazo[1,5-*a*]pyridine-3-ylidene Molybdenum Complexes and their Application as Olefin Epoxidation Precatalysts

Note: The experimental work (synthesis, characterization and catalysis) presented in this Chapter has been performed by M.Sc. A. Schmidt and has been submitted as a part of a master thesis. The author of this doctoral thesis has contributed to the collaborative work by initiating the study, providing technical know-how and proof-reading of master thesis work. Prior text has been extensively re-written by the author for this Chapter. In addition, the author also contributes to an original and in-depth interpretation of experimental results in the Results and Discussion section.

The work presented in this chapter will be submitted for publication.

Abstract

A novel cyclopentadienyl molybdenum complex [CpMo(ImPyMes)$(CO)_2$Cl] (**2**) containing 2-mesitylimidazo[1,5-*a*]pyridyl (ImPyMes, **1**) NHC ligand has been prepared *via* silver carbene transmetallation route in 90% yield. On treatment of **2** with $AgBF_4$ in CH_3CN, ionic complex [CpMo(ImPyMes)$(CO)_2$(NCMe)][BF_4] (**3**), is obtained in 87% yield. Complexes **2** and **3** have been fully characterized using spectroscopic techniques and their crystal structures are presented. The single crystal X-ray structures of imidazo[1,5-*a*]pyridine-3-ylidene molybdenum complexes **2** and **3** are the first examples reported. These complexes are highly active precatalysts in olefin epoxidation with *tert*-butylhydroperoxide (TBHP) as oxidant at room temperature and at 55 °C. Turnover frequencies (TOFs) achieved for epoxidation of *cis*-cyclooctene in chloroform are 40,900 h^{-1} with 0.005 mol% of **2** and 53,100 h^{-1} with 0.01 mol% of **3**. Remarkably, even at such low catalyst concentrations, quantitative substrate conversion with high selectivity takes place. Epoxidation of more challenging substrates such as 1-octene, *cis*-stilbene and *trans*-β-methylstyrene also results in good conversion to their respective epoxides. Complex **2** can be successfully reused for epoxidation in room temperature ionic liquid [OMIM]NTf_2 for at least 10 runs without loss in activity.

3.1 Introduction

In the last decade, several η^5-cyclopentadienyl (C_5H_5 or Cp) molybdenum complexes of the type [CpMo$(CO)_3$R] having different side chain ligands, R = alkyl, halide, *ansa*-bridged etc.; have been applied as precatalysts for epoxidation of unfunctionalized olefins with *tert*-butylhydroperoxide (TBHP) as oxidant.[1-11] Catalytic activity of these complexes has been shown to depend on the nature of substitution on the Cp ring,[12,13] and the *ansa* bridge ring strain.[9,10] Varying the side chain ligands R and studying their stereoelectronic influence on turnover frequencies (TOFs) is another method to study structure-catalytic activity trends.

During the last two decades neutral 2e^- σ-donor *N*-heterocyclic carbene (NHC) ligands[14,15] have gained prominence as ligands in catalysts of a great variety of transition metals.[16–18] As spectator ligands they often lead to better stability under oxidative conditions and are an interesting alternative to phosphine ligands, offering multiple opportunities in modulating stereoelectronic properties.[19] The first Mo(VI) and W(VI) NHC complexes were described in the mid 1990's,[20] with several additional examples of Mo(NHC) complexes reported in the following years.[21−26]

Recently, Royo et al. have reported *ansa*-bridged imidazolylidene CpMo complexes with the general formula of η^5-$C_5R_4[CR_2CRPh$-η^1-$NHC^{Me}]Mo(CO)_2I$ (R = H, alkyl; e.g. complex **A**) (Figure 3.1).[27] A series of neutral CpMo imidazolylidene complexes $[CpMo(CO)_2(NHC)X]$ (X = halide, e.g. complex **B**) has been reported and applied as olefin epoxidation precatalysts by Hor et al.[28] These complexes display poor catalytic activities for epoxidation reactions with model olefin substrates. On treating the neutral complex **B** with $AgBF_4$ in CH_3CN, the ionic complex $[CpMo(CO)_2(IMes)(CH_3CN)][BF_4]$ (**C**) is obtained which demonstrates a higher catalytic activity − 0.1 mol% of **C** for epoxidation of *cis*-cyclooctene at 55 °C with TBHP (decane) has TOF = 3420 h^{-1}.[28] Another novel triazolylidene NHC molybdenum complex **D**, $[CpMo(CO)_2(L)Cl]$, L = 1-methyl-2-phenyl-4-tolyl-1,2,3-triazol-5-ylidenyl has been recently reported.[29] The triazolylidene based Mo-catalyst has been applied as a precatalyst for epoxidation and shows better catalytic activity in ionic liquids than in conventional solvents. Similar to complex **A**, *ansa*-bridged complexes **E** and **F** with different substitution pattern of Cp ring have also been synthesized.[27]

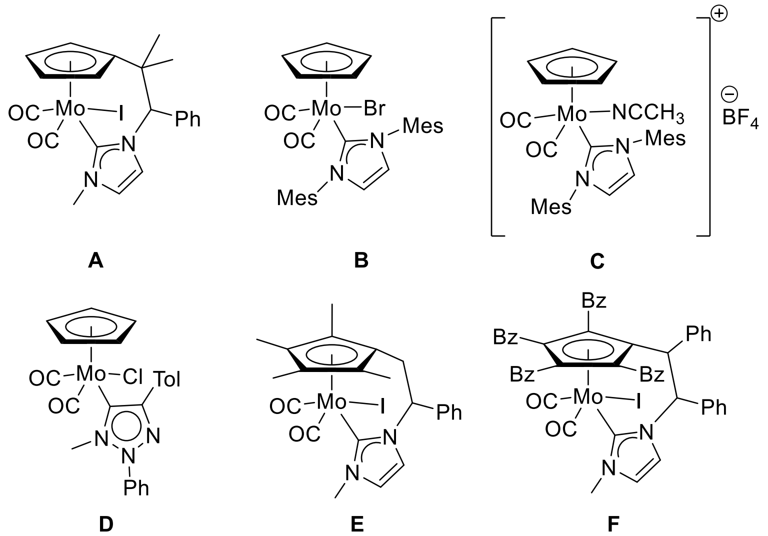

Figure 3.1. Literature known CpMo(NHC)-complexes **A**,[27] **B** and **C**,[28] **D**,[29] **E** and **F**.[27]

Being strong σ-donors, the NHC ligands are expected to increase the electron density at the Mo centre, and thus reduce its Lewis acidity significantly unless good π acceptor ligands such as CO are present. Therefore, based on the widely accepted mechanisms of catalytic epoxidation,[30−33] poor catalytic activity of the CpMo(NHC) oxo complexes might be anticipated.[28,34] Indeed, complexes **A**, **B**, **D** and **E** show very poor conversions of *cis*-cyclooctene to its epoxide.[27,29] Yet, complexes **C** and **F** are exceptions and show good catalytic activities.[27,28]

Regardless of the allegedly poor catalytic activity, the study of CpMo(NHC) complexes is interesting. Appropriate NHC ligand geometries can be conceived for efficient stereoselective catalytic transformations. Compared to the Mo(VI) NHC complex $[MoO_2Cl(IMe)_3]Cl$,[20] the cyclopentadienyl complexes show improved stability. Furthermore, NHC ligands can stabilize the high oxidation state

Mo(VI) and thus, if both stability under oxidative conditions and increased Lewis acidity of the metal are ensured, an increased catalytic activity of CpMo(NHC) complexes might be expected.

Imidazo[1,5-*a*]pyridine-3-ylidene (ImPy) ligands are strong heteroaromatic σ-donors and sterically more demanding than 1,3-disubstituted imidazolylidenes.[35] The bicyclic structure of ImPy-ligands facilitates a unique stereoelectronic environment and the metal coordination sphere can be easily influenced by varying substituents on the aromatic ring.[35–37] Several transition metal complexes of Rh,[38–40] Ir[36,39] and Pd[36,40] with these ligands have been synthesized and applied as catalysts for allylic substitution,[40] Suzuki-Miyaura[36] and other cross-coupling reactions.[37] To the best of our knowledge, no molybdenum complex with these ligands has been reported.

In this work the syntheses, characterization and crystal structures of the complexes [CpMo(ImPyMes)(CO)$_2$Cl] (**2**) and [CpMo(ImPyMes)(CO)$_2$(NCCH$_3$)][BF$_4$] (**3**) is reported, where ImPyMes = 2-mesitylimidazo[1,5-*a*]pyridyl-3-ylidene. Reaction conditions have been optimised for the use of these complexes in epoxidation of unfunctionalized olefins. Furthermore, the available spectroscopic and structural data for complexes **2**, **3** and **A**–**F** have been compared in order to identify possible structure-catalytic activity trends.

3.2 Experimental

3.2.1 Methods and Materials

All preparations and manipulations were performed using standard Schlenk techniques under an argon atmosphere. All reagents were purchased from commercial sources and used without further purification. All solvents were dried with the MBraun MB SPS 800 purification system and stored under argon over molecular sieves. Chromatographic separations were performed using silica gel (40-63 µm). All catalytic reactions were carried out under laboratory atmosphere. NMR spectra were recorded with a Bruker Avance DPX 400 or a Bruker Avance III 400 spectrometer at a temperature of 298 K. The spectra were referenced to the residual ^{1}H and ^{13}C{^{1}H} signals of the solvents in parts per million (ppm). Abbreviations for NMR multiplicities are: singlet (s), doublet (d), triplet (t), quartet (q), multiplet (m). Coupling constants *J* are given in Hz. The IR spectra were recorded on a Varian ATR-FTIR instrument. Elemental analyses were carried out by the microanalytical laboratory of the Technical University of Munich. FAB mass spectra were obtained with a Finnigan MAT 90 spectrometer. Catalytic runs were monitored by GC methods on a Varian CP-3800 gas chromatograph. 2-Mesitylimidazo[1,5-*a*]pyridinium chloride **1** was prepared according to a known procedure.[35]

*3.2.2 Synthesis and Characterization of Complexes **2** and **3***

[CpMo(CO)$_2$Cl(ImPyMes)] **(2)** 2-Mesitylimidazo[1,5-*a*]pyridinium chloride (ImPyMes), **1** (0.400 g, 1.5 mmol, 1.0 equiv.) and silver(I)-oxide (0.170 g, 0.7 mmol, 0.5 equiv.) were suspended in dry dichloromethane (20 mL). The reaction mixture was stirred at room temperature under exclusion of light for 16 h. The suspension was filtered through celite and dried under reduced pressure to give a pale yellow solid. The solid was dissolved in dry toluene (25 mL) and CpMo(CO)$_3$Cl (0.253 g, 0.9 mmol, 0.6 equiv.) was added. The solution was heated to reflux under exclusion of light for 1 h. The dark red solution was concentrated under reduced pressure and the residue was purified by column chromatography (gradient elution with hexane:ethyl acetate = 2:1). The eluting pink band was collected and concentrated under reduced pressure to give the product as a pink solid (0.395 g, 90%). ^{1}H NMR (400 MHz, CDCl$_3$): δ (ppm) = 8.21 (d, $^3J_{HH}$ = 7.5 Hz, 1H, o-CH_{Py}), 7.32 (d, $^3J_{HH}$ = 9.2 Hz, 1H, m-CH_{Py}), 7.25 (s, 1H, NCCHN), 7.11 (s, 1H, m-CH_{Mes}), 7.07 (s, 1H, m-CH_{Mes}), 6.92 (dd, $^3J_{HH}$ = 9.1, 6.5 Hz, 1H, p-CH_{Py}), 6.65 (t, $^3J_{HH}$ = 7.0 Hz, 1H, m-CH_{Py}), 4.94 (s, 5H, CH_{Cp}), 2.43 (s, 3H, p-CH_3), 1.98 (s, 6H, o-CH_3). ^{13}C NMR (101 MHz, CDCl$_3$): δ (ppm) = 257.4 (CO), 252.2 (CO), 179.6 ($C_{carbene}$), 140.4, 138.0, 137.2, 135.5, 133.4, 130.7, 129.3, 129.1, 123.4, 117.0, 113.4, 113.2, 95.2 (CH$_{Cp}$), 21.3 (p-CH$_3$), 18.2 (o-CH$_3$), 17.8 (o-CH$_3$). ^{95}Mo NMR (26 MHz, CDCl$_3$): δ (ppm) = -513. IR (solid): v (cm^{-1}) = 1943 (CO), 1834 (CO). MS (FAB) m/z (%): 455.1 [M-Cl]$^+$. EA: Calcd for $C_{23}H_{21}ClMoN_2O_2$ (%): C, 56.51; H, 4.33; N, 5.73. Found: C, 56.49; H, 4.41; N, 5.71.

[CpMo(CO)$_2$(NCCH$_3$)(ImPyMes)][BF$_4$] **(3)** Complex **2** (0.488 g, 1.0 mmol, 1.0 equiv.) was dissolved in dry acetonitrile (25 mL) and AgBF$_4$ (0.389 g, 2.0 mmol, 2.0 equiv.) was added to the pink solution. The mixture was stirred at room temperature for 1 h to afford a red suspension which was filtered through celite. Volatiles were removed under reduced pressure. The red residue was purified by recrystallisation from acetonitrile and diethyl ether to obtain the product as red crystals (0.504 g, 87%). ^{1}H NMR (400 MHz, CD$_3$CN): δ (ppm) = 8.07 (d, $^3J_{HH}$ = 7.6 Hz, 1H, o-CH_{Py}), 7.72 (s, 1H, NCCHN), 7.61 (d, $^3J_{HH}$ = 9.3 Hz, 1H, m-CH_{Py}), 7.20 (s, 1H, m-CH_{Mes}), 7.18 (s, 1H, m-CH_{Mes}), 7.11 (dd, $^3J_{HH}$ = 9.2, 6.5 Hz, 1H, p-CH_{Py}), 6.91 (t, $^3J_{HH}$ = 6.9 Hz, 1H, m-CH_{Py}), 5.12 (s, 5H, CH_{Cp}), 2.42 (s, 3H, p-CH_3), 2.10 (s, 3H, o-CH_3), 1.96 (s, 3H, NCCH_3), 1.81 (s, 3H, o-CH_3). ^{13}C NMR (101 MHz, CD$_3$CN): δ (ppm) = 250.8 (CO), 248.7 (CO), 171.7 ($C_{carbene}$), 141.8, 138.1, 136.9, 136.5, 134.9, 130.3, 130.1, 129.1, 124.3, 119.4, 117.6, 116.0, 95.7 (CH$_{Cp}$), 21.2 (p-CH$_3$), 17.7 (o-CH$_3$), 17.5 (o-CH$_3$). ^{95}Mo NMR (26 MHz, CD$_3$CN): δ (ppm) = -643. ^{11}B NMR (128 MHz, CD$_3$CN): δ (ppm) = -1.18. ^{19}F NMR (377 MHz, CD$_3$CN): δ (ppm) = -151.68 (^{10}BF$_4^-$), -151.73 (^{11}BF$_4^-$). IR (solid): v (cm^{-1}) = 1969 (CO), 1860 (CO), 1047 (BF$_4^-$). MS (FAB) m/z (%): 455.1 [M-NCCH$_3$]$^+$. EA: Calcd for $C_{25}H_{24}BF_4MoN_3O_2$ (%): C, 51.66; H, 4.16; N, 7.23. Found: C, 50.41; H, 4.18; N, 7.06.

3.2.3 Catalytic Epoxidation

For *cis*-cyclooctene: Substrate (1.10 g, 10 mmol) and the catalyst [0.1 mol%, 10 µmol (or: 1 mol%, 0.05 mol%, 0.01 mol%, 0.005 mol%)] were added to the reaction vessel. The catalyses were carried out neat, in an organic solvent, e.g. CHCl$_3$ (5 mL) or in RTIL [OMIM]NTf$_2$ (0.5 mL) at 55°C or at room temperature. The reaction was initiated by adding the oxidant TBHP (3.64 mL, 5.5 M in *n*-decane). For other substrates: Olefin [1-octene (112 mg), *cis*-stilbene (180 mg) or *trans*-β-methylstyrene (118 mg); 1 mmol], 1,2-dichloroethane (99 mg, 1 mmol, internal standard) and the catalyst (0.1 mol%, 1 µmol) were dissolved in CDCl$_3$ (0.5 mL). The reaction was carried out in a NMR tube at 55 °C and initiated by adding TBHP (364 µL, 5.5 M in *n*-decane).

The kinetic course of the epoxidation of *cis*-cyclooctene was monitored by GC-MS. Samples (0.2 mL) were withdrawn at specific time intervals, treated with activated MnO$_2$ to decompose excess TBHP, filtered through a short column of MgSO$_4$ to remove water and diluted with isopropanol (0.3 mL). After filtration, a mixture of indane and *p*-xylene (4 mg/mL) in isopropanol was added as an external standard and the solution was injected into a GC column. The conversion of *cis*-cyclooctene and the formation of cyclooctene epoxide were calculated from calibration curves (r^2 = 0.999). For catalysis in

RTIL [OMIM]NTf$_2$, a sample was taken after 24 h and treated as described above. For subsequent recycling runs, the organic phase was separated from the reaction vessel and *t*BuOH was removed from the remaining ionic liquid phase under reduced pressure. After overnight drying, the next batch of *cis*-cyclooctene (1.10 g, 10 mmol) and TBHP (3.64 mL, 5.5 M in *n*-decane), were added at 55 °C. The course of the reaction in case of the other substrates (1-octene, *cis*-stilbene and *trans*-β-methylstyrene) was monitored by ^{1}H-NMR analysis at specific time intervals. The conversion of the olefins and the yields of epoxides were calculated according to integral peak of the internal standard 1,2-dichloroethane.

3.3 Results and Discussion

*3.3.1 Synthesis and Characterization of **2** and **3***

The ligand precursor 2-mesitylimidazo[1,5-*a*]pyridinium chloride **1** was synthesized according to a literature procedure[35] *via* a three-component coupling reaction between picolinaldehyde, formalin and 2,4,6-trimethylaniline (

Scheme 3.1). Subsequently, the reaction of Ag-carbene of **1** (prepared *in situ*) with [CpMo(CO)$_3$Cl] in dry toluene by a modified literature procedure,[28] gave complex **2** in a reproducible yield of 90%.

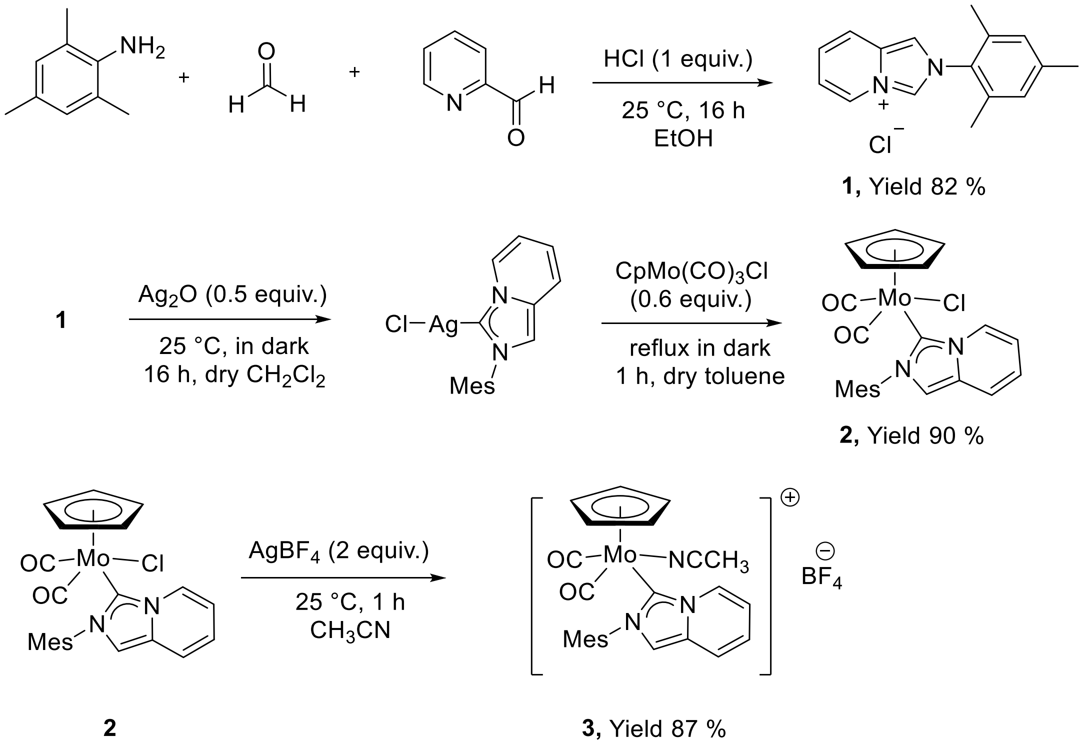
NH2
O
H
H
N
H
O
HCl (1 equiv.)
25 °C, 16 h
EtOH
N
N
+
Cl⁻
1
Ag2O (0.5 equiv.)
25 °C, in dark
16 h, dry CH2Cl2
Cl–Ag
N
N
Mes
CpMo(CO)3Cl
(0.6 equiv.)
reflux in dark
1 h, dry toluene
OC–Mo–Cl
OC
N
N
Mes
AgBF4 (2 equiv.)
25 °C, 1 h
CH3CN
OC–Mo–NCCH3
OC
N
N
Mes
⊕
⊖
BF4

1, Yield 82 %

2, Yield 90 %

2

3, Yield 87 %

Scheme 3.1. Synthesis of cyclopentadienyl molybdenum imidazo[1,5-*a*]pyridine-3-ylidene N-heterocyclic carbene containing complexes **2** and **3**.

Complex **2** is a pink solid, air- and moisture-stable and can be easily stored and handled under laboratory atmosphere. It is well soluble in polar and non-polar solvents such as methanol, acetonitrile, chloroform, THF, toluene, and benzene but poorly soluble in hexane and pentane. The ionic imidazo[1,5-*a*]pyridine-3-ylidene molybdenum complex **3** is also prepared by modifying a literature procedure.[28] Complex **2** was reacted with $AgBF_4$ in acetonitrile and after removal of AgCl over celite, careful vacuum evaporation of the volatiles gave a red residue. Recrystallization of the residue from acetonitrile and diethylether resulted in red crystals of complex **3** in excellent yields of 87%.

Complex **3** exhibits lower air- and moisture stability than **2** but can be easily handled under laboratory atmosphere for a few hours. It is well soluble in polar solvents such as methanol and acetonitrile, less soluble in chloroform and insoluble in other solvents. In ^1H NMR, the Cp-signal for $[CpMo(CO)_3Cl]$ shifts upfield from 5.66 ppm to 4.94 ppm in **2**. Formation of a Mo-carbene bond is confirmed by ^{13}C NMR spectroscopy by the appearance of the characteristic carbene signal at 179.6 ppm. The formation of the new complex $[CpMo(CO)_2(ImPyMes)Cl]$ is further verified by the two terminal carbonyl signals at 252.2 and 257.4 ppm.[26,41] Formation of complex **3** is similarly confirmed by NMR. The signal for Cp ligand shifts downfield from 4.94 ppm of **2** (in $CDCl_3$) to 5.12 ppm (in CD_3CN) in ^1H NMR while the carbene signal shifts upfield from 179.6 in **2** to 171.7 ppm in ^{13}C NMR for complex **3**. The chemical shift for the terminal carbonyl groups appear at 248.7 and 250.8 ppm. ^{11}B and ^{19}F NMR shifts confirm the existence of BF_4^- as the counter anion. Additionally, the appearance of a signal in ^1H NMR at 1.96 ppm, elemental analysis and MS data indicate that one acetonitrile molecule coordinates to molybdenum, as observed for complex **C**.[28]

Table 3.1. Selected spectral data for complexes discussed in this work.[a]

Complex	NMR Shifts (ppm)				IR	Reference
	^1H	^{13}C		Solvent	ν(CO) (cm^{-1})	
	Cp	Cp	Mo-carbene			
CpCl	5.6	95.6	–	C_6D_6	2043, 1931	This work
2	4.9	95.2	179.6	$CDCl_3$	1943, 1834	This work
3	5.1	95.7	171.7	CD_3CN	1969, 1860	This work
A	5.9-5.2	87.1-83.0	186.3	CD_2Cl_2	1945, 1851	27
B	4.7	94.7	189.7	$CDCl_3$	1956, 1860	28
C	4.9	95.5	183.9	CD_3CN	1953, 1870	28
D	5.1	96.5	185.8	CD_2Cl_2	1943, 1848	29
E	7.5-7.1	116.9	187	CD_2Cl_2	1933, 1834	27
F[b]	–	120.9-102.2	186.5, 184.6	CD_2Cl_2	1941, 1883sh, 1860, 1819sh	27
[Cp]⁺	5.9	–	–	CD_2Cl_2	2076, 1997	44
[Cp']⁺	5.9, 5.7	–	–	CD_2Cl_2	2072, 1988	45

[a] $[CpMo(CO)_3Cl]$ abbreviated as CpCl, $[CpMo(CO)_3(CH_3CN)]BF_4$ as $[Cp]^+$ and complex $[Cp'Mo(CO)_3(CH_3CN)]BF_4$ as $[Cp']^+$, where Cp' = C_5H_4Me. [b] The two ^{95}Mo NMR signals, four CO IR bands reported correspond to the two diasteromers.

^{95}Mo NMR signal shifts downfield from -836 ppm in $[CpMo(CO)_3Cl]$[42] to -513 ppm in **2** (Figure 3.2). For the cationic complex **3**, the chemical shift appears more upfield at -643 ppm compared to **2**. The ^{95}Mo shifts for **2** and **3** are both downfield when compared to the shifts for the *ansa*-NHC complexes

A, E and **F**.[27] In accordance with conventional trends,[12,43] these ^{95}Mo chemical shifts suggest a lower electron density at the metal centre and accordingly, higher Lewis-acidity of the metal when compared to [CpMo(CO)$_3$Cl] and **A**.

The IR spectrum shows a strong shift of ca. 100 cm^{-1} to lower stretching frequencies of terminal carbonyl groups from [CpMo(CO)$_3$Cl] to **2**. This supports strong σ-donating character of the NHC ligand that makes the metal electron rich and consequently results in more π-backbonding to CO. Thus, the interpretations regarding electron density at the metal from ^{95}Mo NMR data and IR ν(CO) absorptions are seemingly at odds. Compared to known complexes **A**–**D**[27–29] (Table 3.1), imidazo[1,5-*a*]pyridyl-3-ylidene of **2** is a stronger σ-donor than triazolylidene[29] (**D**: 1848 and 1944 cm^{-1}) and the *ansa*-NHC-ligand (**A**: 1851 and 1945 cm^{-1}).[27] This ligand is an even stronger σ-donor than the imidazolylidene ligand in complex **B** (1860 and 1956 cm^{-1}).[28] The CO bands in **3** are shifted to 1860 cm^{-1} and 1969 cm^{-1} which indicates that in the cationic complex there is lesser *π*-backbonding compared to the neutral complex **2**. This is also in contrast to the conclusion of ^{95}Mo NMR shifts trend which would conventionally indicate a relatively higher electron density of Mo in **3** compared to **2**.At this point in the discussion, it is important to note that only ^{95}Mo shifts of closely related compounds are comparable and even small changes in structure and electronic situation influence the ^{95}Mo shift.[43,46] Considering tricarbonyl complexes [CpMo(CO)$_3$CH$_3$] (-1736 ppm) and [CpMo(CO)$_3$Cl] (-836 ppm), it is conventional to assume that due to electron withdrawing -Cl group, the ^{95}Mo signal shifts downfield (lesser electron density) compared to the simple σ-donor -CH$_3$ group. However, ^{95}Mo chemical shifts for the dicarbonyl CpMo(NHC) complexes follow a different trend. Royo et al. have studied complexes **A**, **E** and **F** which have a different substitution pattern on Cp ring.[27] The metal centre in **F** having tetrabenzyl(ansa) NHC ligand is more electron rich than **E** (tetramethyl substituted). Thus, the order of decreasing electron density at metal is **2** > **3** ≈ **F** ≈ **E** > **A**. Following this order, the trend in IR absorption frequencies of CO group **2** < **3** can also be explained. For other complexes the differences in ν(CO) are marginal and a trend is not clear.

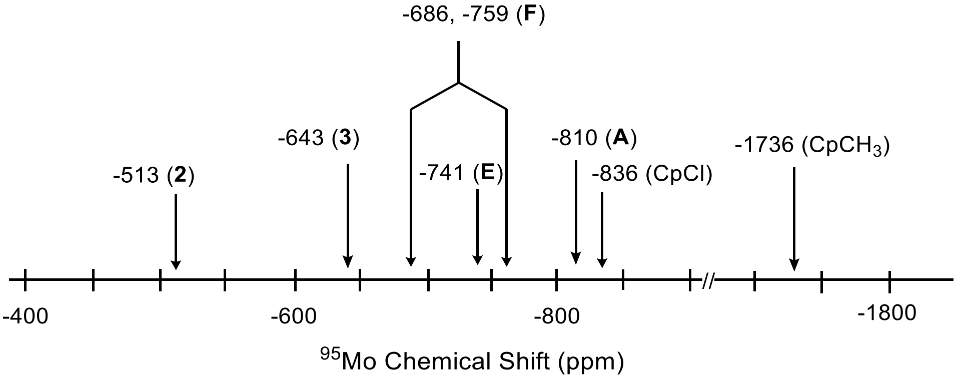

Figure 3.2. ^{95}Mo NMR chemical shifts for CpMo(NHC) complexes discussed in this chapter.

The ^{95}Mo chemical shifts for complexes **2** and **3** in comparison to **A**, **E** and **F**, show a normal halogen dependence (negative chemical shift change),[47] i.e. shielding of the ^{95}Mo nucleus follows the order **2** (X = Cl) > **A**, **E**, **F** (X = I). Kubicki et al. have shown that the metal centre is less shielded in dicarbonyl compounds [CpMo(CO)$_2$] relative to [CpMo(CO)$_3$] complexes.[42] This relationship also explains the broad range of chemical shifts observed for [CpMo(CO)$_2$(NHC)Cl] complexes **2**, **3** and **A−F** (which appear more downfield) and that of [CpMo(CO)$_3$R] complexes, where R = Cl or CH$_3$.

It is important to note, that the ^{95}Mo NMR shift is affected by both the p- and d-electron populations of the metal.[48] Some charge delocalization over the heteroaromatic imidazo[1,5-*a*]pyridyl ligand in complexes **2** and **3** is possible, which shields the central metal atom and therefore causes a decrease in the chemical shift. This is evident in the *difference* in magnitude of the downfield shifts for **2** (-513 ppm), especially when compared to the other NHC complexes (~680 ppm to ~800 ppm) as shown in Figure 3.1. Assuming that the NHC ligands lie lower in the spectrochemical series (strong σ-donors but poor π*-acceptors) compared to CO ligand (both strong σ-donor and π-acceptor), the strong downfield shift in ^{95}Mo NMR for these complexes may also be attributed to the fact that replacing a CO group with a ligand lower in the spectrochemical series causes de-shielding of the molybdenum nucleus.[49]

The structural parameters: Mo-CO bond lengths and *trans* angles C$_t$-Mo-L and CO-Mo-L (C$_t$ is the centroid of Cp ring, L = CO, Cl, Br, NCCH$_3$ or NHC) are also useful for comparing the stereoelectronic influence of the NHC ligand, as discussed in the next section. TG-MS-analysis indicates the high stability of **2** at ambient temperature and decomposition occurs at 241.5 °C by loss of a CO group, relating to a MS-signal with 28 m/z.

3.3.2 X-ray Crystal Analysis for Complexes **2** and **3**

Single crystals of **2** were obtained by diffusion of hexane into a solution of the complex in ethyl acetate and of **3** by diffusion of diethyl ether into a solution of the complex in acetonitrile. The molecular structures of the complexes are depicted in Figure 3.3 and Figure 3.4. Detailed crystallographic information is presented in the Supporting Information (SI). Selected structural parameters for these complexes have been compared with that of similar complexes in Table 3.2.

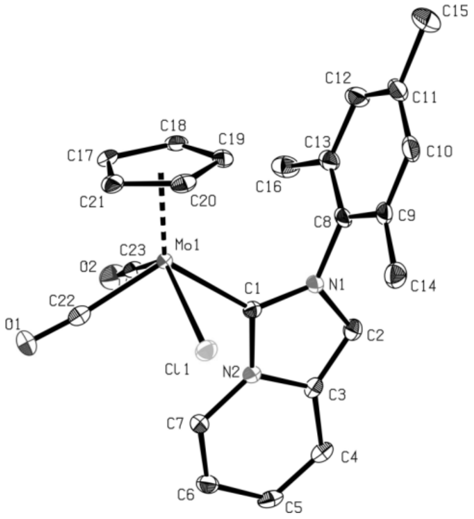

Figure 3.3. ORTEP view of the single crystal X-ray structure of compound **2**. Thermal ellipsoids are drawn at the 50 % probability level. Hydrogen atoms are omitted for clarity.

Compared to complex [CpMo(CO)$_3$Cl], in **2** one CO ligand is replaced by the imidazo[1,5-*a*]pyridyl-3-ylidine ligand. Thus the loss of a π-acceptor ligand and addition of the strong σ-donor NHC ligand requires the redistribution of increased electron density among the ligands. Thus there is increased back-donation to CO ligands, which is reflected in the shorter Mo-C1 and Mo-C2 distances compared to these bond lengths in [CpMo(CO)$_3$Cl], see Table 3.3. We might consider the bond distances Mo-C1 and Mo-C3 as indicative of the *trans* influence of CO *vs.* NHC ligands. While the decrease in Mo-C1 from 2.014 Å in [CpMo(CO)$_3$Cl] to 1.956 Å in **2** is partly due to increased backbonding, it may also arise from the *trans* influence of the NHC ligand, its magnitude for NHC being less than that for CO. The increase in Mo-C3 in **2** of ~ 0.2 Å can be attributed to larger *trans* influence of CO when a poor π-acceptor such as the carbene ligand is present.

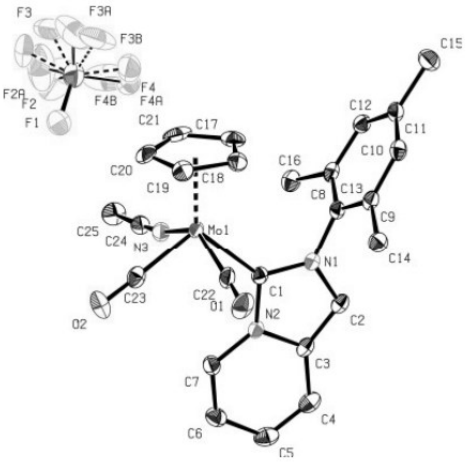

Figure 3.4. ORTEP view of the single crystal X-ray structure of compound **3**. Thermal ellipsoids are drawn at the 50 % probability level. Hydrogen atoms are omitted for clarity.

A comparison of the neutral complexes **2** and **B** is also worthwhile. The Mo-CO distances of **2** (1.961(2) and 1.956(2) Å) are slightly longer than for **B** (1.939(5) and 1.932(4) Å). This is unusual since the carbene ligand generated from **1** is a stronger σ-donor than the imidazolidene ligand. Therefore, due to increased π-backbonding shorter Mo-C1 and Mo-C2 distances are expected for these two complexes. However, the structural *trans* influence of the halide ligands (Cl$^-$ *vs.* Br$^-$) must be considered.[28] Consequently, Mo-NHC (Mo-C3), Mo-Cp$_{centroid}$ (Mo-C$_t$) and Mo-X distances are all slightly elongated for **B** (X = Br) in comparison to **2** (X = Cl).

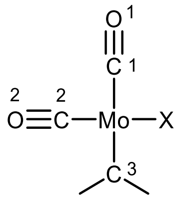

X	Complexes
Cl	**2, D**
Br	**B**
N (from CH$_3$CN)	**3, C**

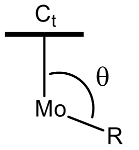

R = CO, NCCH$_3$, Cl or Br

Figure 3.5. Atom renumbering scheme in the distorted square planar analogy for basal ligands of the piano stool X-ray crystal structures for comparison of precatalysts **2**, **3**, **B**, **C** and **D**. *Trans* angles θ refer to C$_t$-Mo-R, where C$_t$ = Cp centroid.

An opposite relationship is true for the cationic complexes **3** and **C**, where bond distances Mo-C1 and Mo-C2 are shorter for **3**. Here instead of the *trans* effect of the halide, the stereoelectronic differences between the two NHC ligands (imidazo[1,5-*a*]pyridine-3-ylidene for **3** and imidazol-2-ylidene for **C**) are likely to be more relevant.

Table 3.2. Selected bond lengths [Å] and bond angles (°) of complexes [CpMo(CO)$_3$Cl] (abbreviated as CpCl),[50] **2**, **3**, **B**,[28] **C**,[28] **D**[29] and [Cp'Mo(CO)$_3$(CH$_3$CN)]BF$_4$ (abbreviated as [Cp']$^+$) where Cp' = C$_5$H$_4$Me.[45] X = Cl, Br or N. C1 is *trans* to carbene carbon C3, C2 is *trans* to the heteroatom X.

Parameter	CpCl	2	B	[Cp']$^+$	3	C	D
Bond Lengths							
Mo-C1	2.014(2)	1.956(2)	1.932(4)	2.029	1.941(3)	1.947(3)	1.945(4)
Mo-C2	1.980(2)	1.961(2)	1.939(5)	2.001	1.985(3)	1.996(3)	1.965(4)
Mo-C3	2.008(2)	2.227(2)	2.244(3)	2.017	2.222(2)	2.249(3)	2.221(4)
Mo-X	2.5030(6)	2.5389(5)	2.6704(6)	2.151	2.1770(2)	2.172(2)	2.519(1)
Mo-C$_t$	1.988	2.015	2.040	1.974	2.003	2.009	2.017
Bond Angles							
C1-Mo-X	78.15(7)	82.43(6)	83.8(1)	81.25	84.72(8)	81.0(1)	81.5(1)
C2-Mo-X	134.49(7)	131.85(6)	145.6(2)	139.14	141.12(9)	140.3(1)	136.3(1)
C3-Mo-X	77.86(7)	78.58(5)	80.11(7)	76.72	79.05(7)	82.7(1)	79.40(9)
C1-Mo-C3	111.84(1)	115.60(8)	107.2(1)	112.78	109.18	110.3(1)	113.3(2)
C1-Mo-C2	78.15(10)	74.67(9)	76.7(2)	78.19	75.55(9)	76.0(1)	77.4(2)
C2-Mo-C3	75.80(10)	74.36(8)	79.1(2)	79.31	76.43(9)	75.8(1)	74.6(2)
Trans angles							
C$_t$-Mo-C1 (θ_1)	124.05	116.19	119.97	123.86	119.52	119.81	120.72
C$_t$-Mo-C2 (θ_2)	112.93	116.36	108.21	110.25	110.32	111.07	114.14
C$_t$-Mo-C3 (θ_3)	124.11	128.07	132.74	123.36	131.09	129.63	125.98
C$_t$-Mo-X (θ_4)	112.55	111.72	106.01	110.55	108.55	108.40	109.55

The Mo-CO bond lengths of the neutral complex **2** are shorter than the ones of the ionic complexes **3** (1.985(3) and 1.941(3) Å) and **C** (1.996(3) and 1.947(3) Å), which hints at more π-backbonding. The differences in the Mo-C$_{carbene}$ bond distances are only marginal. Complexes **2** and **3** have comparable bond lengths − 2.227(2) and 2.222(2) Å respectively, to **D** (2.221(4) Å) and slightly shorter ones to **B** (2.244(3) Å) and **C** (2.249(3) Å). All L-Mo-L (L = basal ligands CO, Cl, NHC and NCCH$_3$) acute bond angles range between 74.36(8) and 82.43(6)° for **2** and between 75.55(9) and 84.72(8)° for **3**, similar to related compounds.[27,28]

Similar to [CpMo(CO)$_3$Cl], complexes **2** and **3** are four-legged piano-stool structures, which show distortions in the basal ligands. In this pseudo square pyramidal geometry, the *trans* angle C$_t$-Mo-L (designated as θ[51,52] or α[53]) is an informative parameter for quantifying distortion from the ideal geometry and understanding the effects of angular *trans* influence. It has been shown that the two ligands with larger values of θ are mutually *trans* to each other, as are the pair of ligands, which have the smallest angles. This is easily observed for [CpMo(CO)$_3$Cl] and complexes **3** and **B**−**D** in values of angles (θ_1, θ_3), and (θ_2, θ_4). Curiously, there is not much difference in the angles (θ_1, θ_2) for the two *cis* CO ligands in **2** (≈ 116°).

It is worthwhile to note the 'direction' of distortion in the angles $\theta_1 - \theta_4$ to determine whether these structural deviations occur along the Berry pseudorotation coordinate.[52–54] As summarized in Table 3.2, in contrast to the similar values of (θ_1, θ_3) in [CpMo(CO)$_3$Cl], for all CpMo(NHC) complexes, the angle θ_1 decreases while θ_3 increases which indicates an unsymmetrical distortion. The set of angles (θ_2, θ_4) on the other hand, show a simultaneous decrease towards smaller angles; *except* in **2** and triazolylidine complex **D**. In this case, θ_2 increases from 112.93° in [CpMo(CO)$_3$Cl] to 116.36° and 114.14° in **2** and **D** respectively. The angle θ_4 instead decreases from 112.55° in [CpMo(CO)$_3$Cl] to 111.72° (**2**) and 109.55° (**D**). For complexes **B**, **3** and **C**, the set of ligands X and CO *trans* to X (C2) show unidirectional distortions. In these complexes both angles (θ_2, θ_4) decrease in comparison to these angles for [CpMo(CO)$_3$Cl], decrease in θ_4 being slightly larger than in θ_2 on account of the stronger σ interaction as discussed above.

Ideally, to understand the effect of replacing a CO group with NHC ligand, differences in ν(CO), ^{95}Mo chemical shifts and structural data should only be compared between electronically and structurally similar complexes. For this reason, a comparison between [CpMo(CO)$_3$Cl] is successful for complexes **2** and **B**, but for cationic complexes **3** and **C**, previously reported complexes [CpMo(CO)$_3$(CH$_3$CN)](BF$_4$)[44] and [Cp'Mo(CO)$_3$(CH$_3$CN)](BF$_4$)[45] (Cp' = C$_5$H$_4$Me) are more appropriate.

A comparison of structural data available for the [Cp'Mo(CO)$_3$(CH$_3$CN)]BF$_4$ complex (abbreviated as **[Cp']$^+$** for simplicity) and cationic NHC complexes **3** and **C** indicates that the differences in bond lengths and acute bond angles are marginal, but follow the same trends as discussed for [CpMo(CO)$_3$Cl] and **2**. *Trans* angles (θ_1, θ_3) and (θ_2, θ_4) distort along the Berry pseudo-rotation coordinate for complexes **3** and **C** compared to **[Cp']$^+$**, which is a more accurate comparison than with [CpMo(CO)$_3$Cl]. The ideal *trans* angles in pseudo-square pyramidal and trigonal bipyramidal geometry are 120° and, 108° and 130° respectively.[54] The data summarized in Table 3.2 illustrates both, the expected stereochemical non rigidity and fluxionality of non-*ansa* CpMo(NHC) complexes and structures that are intermediate between ideal geometries. Such distortions in structure are, nevertheless, an inadequate explanation for the differences in reactivity of the various CpMo(NHC) complexes with TBHP and ligand electronic effects must be taken into account as well (see Section 3.4).

Strong σ-bonding ligands or σ-/π- donors such as halides prefer to be coordinated to the metal with a small C$_t$-Mo-L angle to maximise the covalent σ interaction, as evident in the smaller values of θ_4 compared to $\theta_1 - \theta_3$ for all complexes.[53] Furthermore, the θ angles for CO or similarly good π-acceptor ligands are often found to be large.[53] In the case of CpMo(NHC) complexes discussed here, θ_1 is one such *trans* angle.

The π-acceptor ability of a ligand may also be indicated by its *trans* angle. An evaluation of structural data has shown that phosphines experience the angular *trans* influence, i.e. larger values of θ when they are located *trans* to a CO group.[52] Considering both the isolobal analogy between phosphines and NHC ligands,[55,56] and the recent reports which show that the NHC ligands may also behave as π*-acceptors,[19,57–61] a closer look at the large θ_3 values is warranted. From θ_3 = 124.11° for

CO ligand in [CpMo(CO)$_3$Cl], this angle increases to 128.07° for **2** and is in fact, higher for all other examples – **B**, cationic complexes **3** and **C**, as well the triazolylidene complex **D**. At this point, we do not attempt a rigorous proof of π*-acceptor ability of the imidazo[1,5-*a*]-pyridine-3-ylidine ligand (although, since back donation occurs to an antibonding orbital of NHC ligand, this might also be responsible for the longer Mo-C3 bond lengths). Here we have merely considered that the ^{95}Mo NMR data (discussed in the previous section) and the *trans* angle θ_3 are parameters that hint at this ability of the NHC ligands in these CpMo complexes.

Similar to complexes **2** and **B**, there is a decrease of ~ 100 cm^{-1} in ν(CO) on substitution of one CO of **[Cp']$^+$** with imidazo[1,5-*a*]pyridine-3-ylidene in **3** and **C**, with the conclusion that this ligand is a strong σ-donor compared to the CO group (see Table 3.1).

3.3.3 Application in Epoxidation Catalysis

The catalytic potential of complexes **2** and **3** as precatalysts in the olefin epoxidation of various unfunctionalized olefins was investigated with *tert*-butylhydroperoxide (*n*-decane) as the oxidant. Control experiments showed that no epoxide forms with TBHP without either **2** or **3**. No diol formation is observed in any catalytic reaction. For optimisation of reaction conditions, **2** was employed for the epoxidation of model substrate *cis*-cyclooctene with TBHP (5.5 M in *n*-decane) as the oxidant. Reaction progress was followed by GC-MS and plotted as conversion *vs.* time graphs. TOFs were determined at the steepest part of these plots.

3.3.3.1 Optimisation of Temperature

Epoxidation at room temperature with 0.1 mol% catalyst loading proceeds with an induction period of about 20 minutes for **2** and about 10 minutes for **3** (Figure 3.6). In this period, oxidative decarbonylation of the precatalysts occurs and is indicated by evolution of gases (which are in good likelihood CO and CO$_2$ [62]) and a rapid colour change from pink or red to colourless. All further catalysis experiments were conducted at 55 °C to avoid the induction period and for the sake of comparison with other catalysts reported in literature. Compound **3** is in general, more active than **2** in epoxidation of *cis*-cyclooctene, both at room temperature and at 55 °C.

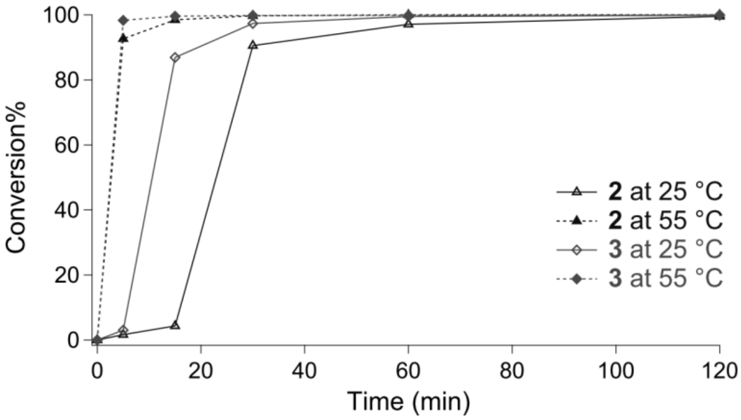

Figure 3.6. Kinetic profile of *cis*-cyclooctene epoxidation with precatalysts **2** and **3** (0.1 mol%) in CHCl$_3$ at 25 °C and 55 °C using TBHP (catalyst:substrate:oxidant = 1:1000:2000).

3.3.3.2 Choice of Solvent

Several solvents were tested for epoxidation of *cis*-cyclooctene at 55 °C with 0.1 mol% of **2**. Epoxidation in polar solvents such as methanol, tetrahydrofuran and acetonitrile gives lower conversions in comparison with chlorinated and non-polar solvents (Figure 3.7). This is due to the coordinating ability of these solvents, as the solvent can compete with the oxidant for coordination to the metal centre. Epoxidation of *cis*-cyclooctene in RTIL is slower compared to homogenous one-phase catalysis; this might be reasoned to mass transfer limitations of the biphasic system. The best conversions are in obtained toluene, dodecane, chloroform and without additional co-solvent (neat). All subsequent experiments were carried out in $CHCl_3$ or neat.

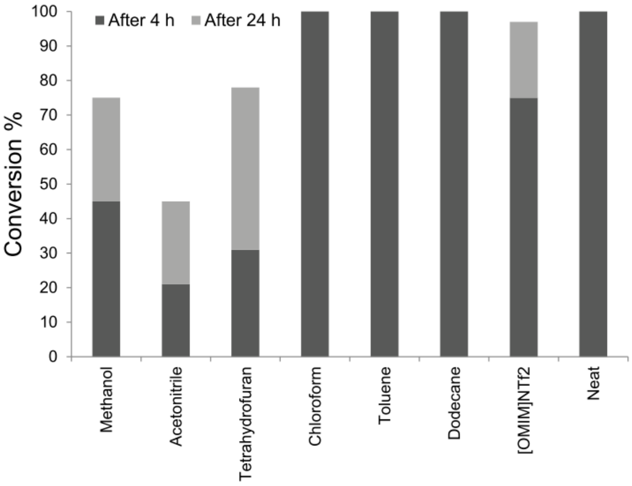

Figure 3.7. Conversions of *cis*-cyclooctene epoxidation with **2** (0.1 mol%) using TBHP (in *n*-decane) as oxidant at 55 °C in different solvents (catalyst:substrate:oxidant = 1:1000:2000).

3.3.3.3 Optimal Catalyst Concentration

With different concentrations of **2** and **3**, epoxidation of cyclooctene was studied at 55 °C either in chloroform or without solvent. The kinetic profiles are shown in Figure 3.8 and Figure 3.9; the resulting TOFs and conversions after 24 h are given in Table 3.3.

Precatalyst **2** exhibits extremely high TOFs and even at low catalyst loadings (0.005 mol%) conversion of cyclooctene to its epoxide is 97% in chloroform and 87% in the absence of a co-solvent after 24 h. Interestingly, at 0.01 mol% catalyst loading an induction period that lasts about 5 min is observed, and at lesser catalyst concentration of 0.005 mol% it lasts for 15 min (Figure 3.8). It is expected that a smaller concentration of the precatalyst would be converted into the active species faster because of presence of a larger concentration of TBHP. The longer induction phase can be explained by a higher dilution at lower concentration of the catalyst resulting in its slower diffusion. The effect of dilution is only partly responsible for the induction period, because even when reactions are performed in the absence of any additional co-solvent, the slow phase is still observed. These observations imply that the precatalyst is converted into the catalytically active species in the induction phase, which is most likely a dioxo complex similar to that derived from **C**.[34]

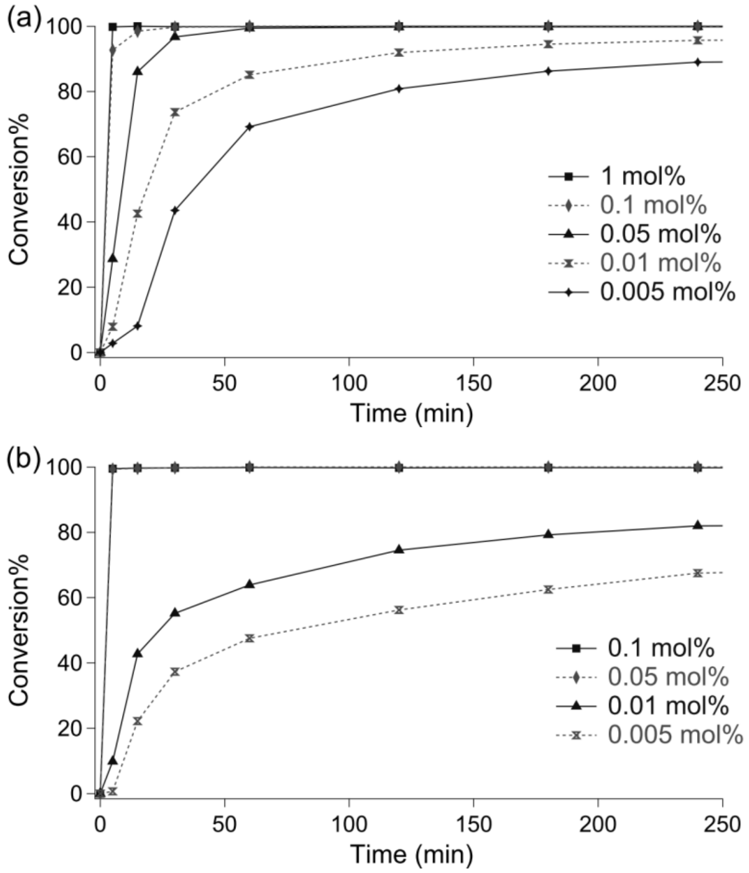

Figure 3.8. Kinetic profile of *cis*-cyclooctene epoxidation with different concentrations of precatalyst **2** at 55 °C using TBHP (substrate:oxidant = 1:2) (a) in $CHCl_3$ solvent, (b) without additional co-solvent.

Table 3.3. Catalytic activities in terms of TOFs [h^{-1}] and conversions [%] (after 24 h) of *cis*-cyclooctene epoxidation with different concentrations [mol%] of **2** and **3** using TBHP (in *n*-decane) as oxidant at 55 °C, neat or in $CHCl_3$ (substrate:oxidant = 1:2).

Solvent	Precatalyst		**2**		**3**	
	Catalyst load	TOF$_{5\ \text{min}}$	TOF$_{\text{max}}$	Conversion	TOF$_{5\ \text{min}}$	Conversion
$CHCl_3$	1	1200	1200	100	–	–
	0.1	11100	11100	100	11800	100
	0.05	6900	6900	100	22300	100
	0.01	2000	18500	99	53100	99
	0.005	1900	40900	97	45800	99
neat/ *n*-decane	0.1	12000	12000	100	–	–
	0.05	23800	23800	100	–	–
	0.01	4700	25800	93	–	–
	0.005	2300	30000	87	–	–

Another noteworthy aspect is that the reactions with a catalyst concentration of 0.1 and 0.05 mol% occur at higher reaction rates in the absence of a solvent and quantitative conversion is achieved after 5 min. In contrast, epoxidation with 0.01 and 0.005 mol% catalyst loads proceeds slower in the absence of a co-solvent. The slower reaction rate could be reasoned by a product inhibition due to the competitive coordination of the by-product *tert*-butanol[30] as described for polar solvents (e.g. methanol). The amount of the active catalyst present is smaller, yet because the same volume of *tert*-butanol is formed, competitive inhibition reduces reaction rate.

For subsequent experiments, 0.1 mol% of **2** in $CHCl_3$ was used. Under these conditions, a TOF of 11,100 h^{-1} is achieved after 5 min with 100% conversion within 30 min. Even a low catalyst loading of 0.01 mol% or 0.005 mol% is sufficient, since 100% conversion can be reached after 24 h and TOF of 40,900 h^{-1} is achieved.

The optimal catalyst concentration of **3** was similarly determined in $CHCl_3$ at 55 °C. Figure 3.9 illustrates the kinetics of the epoxidation reaction and the TOFs are summarized in Table 3.3. All epoxidation reactions at different catalyst loadings of **3** surpass the activities achieved with catalyst **2**. TOFs between 11,800 and 53,100 h^{-1} and conversions of 100% after 30 min at higher concentrations (0.1 mol% and 0.05 mol %) and after 24 h with lower catalyst concentrations (0.01 mol% and 0.005 mol %) can be attained. No perceptible induction period is seen with complex **3**.

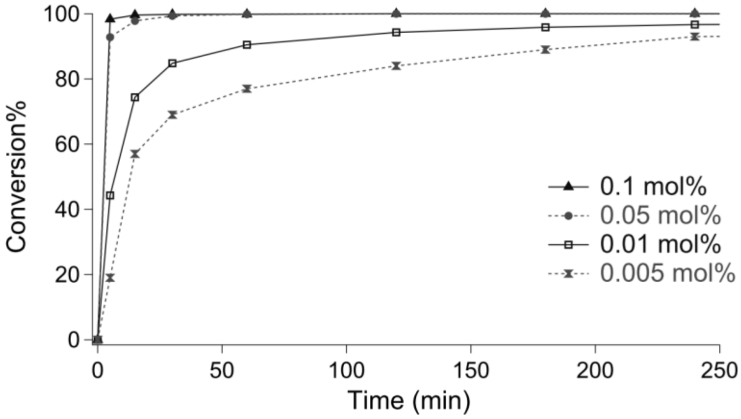

Figure 3.9. Kinetic profile of *cis*-cyclooctene epoxidation with different concentrations of precatalyst **3** in $CHCl_3$ at 55 °C using TBHP (substrate:oxidant = 1:2).

3.3.3.4 Epoxidation of Other Olefin Substrates and Recyclability in RTIL

Complex **2** was applied for the epoxidation of more challenging substrates such as 1-octene, *cis*-stilbene and *trans*-*β*-methylstyrene, and remarkable conversions for these olefins were observed with a catalyst loading of 0.1 mol% in $CDCl_3$ at 55 °C Table 3.4). All catalytic reactions proceed without significant formation of byproducts.

Table 3.4. Conversions of different olefin substrates with **2** (0.1 mol%) to their epoxides using TBHP as oxidant at 55 °C in $CDCl_3$ (catalyst:substrate:oxidant = 1:1000:2000).

Substrate	Conversion [%] after 4 h	Conversion [%] after 24 h
1-octene	66	75
cis-stilbene	82	100
trans-β-methylstyrene	87	100

Catalytic epoxidation of *cis*-cyclooctene in RTIL [OMIM]NTf$_2$ (OMIM = 1-octyl-3-methylimidazolium) with 0.1 mol% of **2** at 55 °C was carried out. Conversion after 24 h is 97% in the biphasic catalytic system, yet substantially slower with a TOF of 2,400 h^{-1} when compared to homogeneous epoxidation. This is most likely due to phase transfer limitations. The upper phase consists of the substrate and *n*-decane, while the lower phase contains the ionic liquid and catalyst. TBHP is partially soluble in both phases. Even though reaction times for quantitative conversion are longer, use of ionic liquids is advantageous because their low volatility, high thermal stability and polarity, facilitates catalyst recycling and product separation.[11,63] Additionally, recycling experiments were undertaken to test the stability of the precatalyst **2** and accordingly of the catalytically active species under oxidative conditions. The active Mo catalyst could be recycled for 10 catalytic runs; approximately 100% conversion was obtained for each run after 24 h (see Supporting Information, Table 3.5). In contrast to the triazolylidene based molybdenum complex,[29] complex **2** shows excellent performance in recycling experiments. Therefore, this observation hints at the higher stability of **2** compared to literature known molybdenum NHC catalysts.[28]

3.3.4 Structure-Activity Relationship

The cycloalkyl *ansa* bridged complex [Mo{η^5-$C_5H_4(CH(CH_2)_3)$-η^1-CH}$(CO)_3$],[9] outperforms all previously reported CpMo-catalysts with the highest reported TOFs being 11,800 h^{-1} in the organic solvent dichloromethane[10] and 44,000 h^{-1} in the room temperature ionic liquid (RTIL) [BMIM]NTf$_2$ for the epoxidation of *cis*-cyclooctene.[11] With 0.005 mol% of **2**, a TOF of 40,900 h^{-1} in the epoxidation of cyclooctene at 55 °C is achieved, which is the highest TOF for CpMo-NHC-complexes so far. This TOF is even higher than for most other neutral carbonyl complexes of the type [CpMo$(CO)_3$X] (X = alkyl, halide).[8,12,13,62] Epoxidation of *cis*-cyclooctene with **3** in $CHCl_3$ at 55 °C results in an even higher activity with TOFs up to 53,100 h^{-1} at a catalyst loading of 0.01 mol%. To the best of our knowledge, this is the highest TOF achieved to date with any CpMo derived catalyst.

With such remarkable TOFs, it is interesting to consider the unique stereoelectronic features of **2** and **3** described in previous sections. Complexes **A**, **B**, **D** and **E** perform poorly as epoxidation precatalysts under identical conditions.[27−29] The cationic complex **C** displays a TOF of 3420 h^{-1} in the epoxidation of *cis*-cyclooctene,[28] which is significantly lower than the activity of the structurally similar cationic complex **3**.

One reason for the higher activities of **2** and **3** might be the faster rate of oxidative decarbonylation for these complexes, compared to examples illustrated in Figure 3.1, which show longer induction periods. Since the catalytically active species is formed faster, the epoxidation reaction is also facile. It is important to consider that the neutral complex **2** and cationic species **3** might react with TBHP and substrate following somewhat different mechanisms. In complex **3**, the hydroperoxide or olefin can promote the de-coordination of labile solvent molecule CH_3CN which might contribute to its higher reactivity compared to **2**.

In the previous sections, the analytical data for complexes **2, 3** and **A−F** have been discussed. However, a correlation between ^{95}Mo shifts, IR absorption frequencies, structural parameters, the relative σ-donor (and π*-acceptor) ability of the NHC ligands and the catalytic activity of these complexes is neither straightforward nor easy to derive. In-depth information about the transformation of Mo(II) precatalysts to Mo(VI) oxo complexes with TBHP oxidant is not available, and the mechanisms of catalytic epoxidation are still a matter of debate.[31,32,64] In order to overcome these limitations, it is important to outline the parameters that might prove relevant for determining the stability and reactivity of these complexes.

In Section 3.3.2, distortions in the pseudo square pyramidal geometry in the structures of CpMo(NHC) complexes are discussed. These distortions and thus the fluxionality of the organometallic complex[54,65–67] can exert subtle influences on the oxidative decarbonylation process, although a rigorous proof for this statement is beyond the scope of the present work.

Hoffmann et al. have previously described the frontier orbital interactions occurring when photochemical induced decarbonylation of [CpMo$(CO)_3$R] complexes and subsequent reaction with a base takes place.[51] Generally, oxidative decarbonylation of the [CpMo$(CO)_3$R] precatalysts with TBHP occurs quite fast and all three CO groups are lost. However, the slower decarbonylation reactions of **A**, **B**, **D** and **E** (and thus lower TOFs) can be explained to be a consequence of the rate limiting step involving initial loss of one CO group as described for photo-induced decarbonylation by Barnett et al.[68] Ligand stereoelectronic effects and the apparent stereochemical rigidity of the organometallic molecule can negatively influence this rate, if there is a hindrance to attaining the appropriate 'electronic situation' or geometry for reaction with TBHP.

Oxidative decarbonylation of [CpMo$(CO)_3$R] complexes with TBHP and related mechanisms of alkene epoxidation with similar complexes are discussed in Chapter 6, which provides further insight into these issues.

3.4 Conclusion

Novel CpMo complexes with 2-mesitylimidazo[1,5-*a*]pyridine-3-ylidene ligand have been synthesized in excellent yields by silver carbene transmetallation route for **2** and by substitution reaction for **3**. Compounds **2** and **3** have been completely characterised by spectroscopic techniques, microanalysis and X-ray crystallography. These complexes have been successfully applied as precatalysts for catalytic epoxidation of unfunctionalized olefins with TBHP (in n-decane) as oxidant. Both catalysts outperform previously reported molybdenum epoxidation precatalysts in terms of catalytic activity. Even at low catalyst concentrations (0.005 mol%) quantitative conversion of *cis*-cyclooctene was obtained after 24 h and TOFs up to 40,900 h^{-1} for **2** and up to 53,100 h^{-1} for **3** can be reached. With more challenging substrates such as 1-octene, *cis*-stilbene and *trans*-*β*-methylstyrene, complex **2** delivers good epoxide yields with high selectivity. In addition, the neutral complex **2** can be recycled in RTIL [OMIM]NTf_2 for at least 10 subsequent runs without any loss in activity, indicating high stability of the active catalyst. The outstanding catalytic activity of precatalysts **2** and **3** in comparison to closely related CpMo(NHC) complexes has been studied by considering their structural and spectroscopic data. A discussion of the unusual ^{95}Mo chemical shifts, IR *v*(CO) stretching frequencies and *trans* bond angles is presented in an attempt to explain the high catalytic epoxidation activity.

3.5 References

[1] N. Grover, F.E. Kühn, Curr. Org. Chem. 16 (2012) 16–32.

[2] J. Zhao, A. Sakthivel, A.M. Santos, F.E. Kühn, Inorg. Chim. Acta. 358 (2005) 4201–4207.

[3] C. Freund, M. Abrantes, F.E. Kühn, J. Organomet. Chem. 691 (2006) 3718–3729.

[4] M. Abrantes, A. Sakthivel, C.C. Romão, F.E. Kühn, J. Organomet. Chem. 691 (2006) 3137–3145.

[5] J. Zhao, K.R. Jain, E. Herdtweck, F.E. Kühn, Dalton Trans. (2007) 5567–5571.

[6] A. Raith, P. Altmann, M. Cokoja, W.A. Herrmann, F.E. Kühn, Coord. Chem. Rev. 254 (2010) 608–634.

[7] M. Abrantes, F.A.A. Paz, A.A. Valente, C.C.L. Pereira, S. Gago, A.E. Rodrigues, J. Klinowski, M. Pillinger, I.S. Gonçalves, J. Organomet. Chem. 694 (2009) 1826–1833.

[8] S.A. Hauser, M. Cokoja, M. Drees, F.E. Kühn, J. Mol. Catal. A: Chem. 363-364 (2012) 237–244.

[9] A. Capapé, A. Raith, F.E. Kühn, Adv. Synth. Catal. 351 (2009) 66–70.

[10] A. Capapé, A. Raith, E. Herdtweck, M. Cokoja, F.E. Kühn, Adv. Synth. Catal. 352 (2010) 547–556.

[11] D. Betz, A. Raith, M. Cokoja, F.E. Kühn, ChemSusChem. 3 (2010) 559–562.

[12] M. Abrantes, A.M. Santos, J. Mink, F.E. Kühn, C.C. Romão, Organometallics. 22 (2003) 2112–2118.

[13] J. Zhao, A.M. Santos, E. Herdtweck, F.E. Kühn, J. Mol. Catal. A: Chem. 222 (2004) 265–271.

[14] K. Öfele, J. Organomet. Chem. 12 (1968) 42–43.

[15] H.-W. Wanzlick, H.-J. Schönherr, Angew. Chem. Int. Ed. 7 (1968) 141–142.

[16] F. Glorius, N-Heterocyclic Carbenes in Transition Metal Catalysis, Springer-Verlag: Berlin/Heidelberg, 2007.

[17] S.P. Nolan, N-Heterocyclic Carbenes in Synthesis, Wiley-VCH, New York, 2006.

[18] W.A. Herrmann, Angew. Chem. Int. Ed. 41 (2002) 1290–1309.

[19] H. Jacobsen, A. Correa, A. Poater, C. Costabile, L. Cavallo, Coord. Chem. Rev. 253 (2009) 687–703.

[20] W.A. Herrmann, G.M. Lobmaier, M. Elison, J. Organomet. Chem. 520 (1996) 231–234.

[21] K. Ogata, Y. Yamaguchi, T. Kashiwabara, T. Ito, J. Organomet. Chem. 690 (2005) 5701–5709.

[22] Y. Yamaguchi, T. Kashiwabara, K. Ogata, Y. Miura, Y. Nakamura, K. Kobayashi, T. Ito, Chem. Comm. (2004) 2160–2161.

[23] E. Mas-Marzá, P.M. Reis, E. Peris, B. Royo, J. Organomet. Chem. 691 (2006) 2708–2712.

[24] V. V. Krishna Mohan Kandepi, J.M.S. Cardoso, B. Royo, Catal. Lett. 136 (2010) 222–227.

[25] V.K. Dioumaev, D.J. Szalda, J. Hanson, J.A. Franz, R.M. Bullock, Chem. Comm. (2003) 1670–1671.

[26] F. Wu, V.K. Dioumaev, D.J. Szalda, J. Hanson, R.M. Bullock, Organometallics. 26 (2007) 5079–5090.

[27] V.V.K.M. Kandepi, A.P. da Costa, E. Peris, B. Royo, Organometallics. (2009) 4544–4549.

[28] S. Li, C.W. Kee, K. Huang, T.S.A. Hor, J. Zhao, Organometallics. 29 (2010) 1924–1933.

[29] L. Schaper, L. Graser, X. Wei, R. Zhong, K. Öfele, A. Pöthig, M. Cokoja, Bettina Bechlars, W. A. Herrmann, F. E. Inorg. Chem. 52 (2013) 6142–6152.

[30] A.M. Al-Ajlouni, A.A. Valente, C.D. Nunes, M. Pillinger, A.M. Santos, J. Zhao, C.C. Romão, I.S. Gonçalves, F.E. Kühn, Eur. J. Inorg. Chem. (2005) 1716–1723.

[31] A.M. Al-Ajlouni, D. Veljanovski, A. Capapé, J. Zhao, E. Herdtweck, M.J. Calhorda, F.E. Kühn, Organometallics 28 (2009) 639–645.

[32] A. Comas-Vives, A. Lledós, R. Poli, Chem. Eur. J. 16 (2010) 2147–2158.

[33] M.J. Calhorda, P. Jorge, Curr. Org. Chem. 16 (2012) 65–72.

[34] S. Li, Z. Wang, T.S.A. Hor, J. Zhao, Dalton Trans. 41 (2012) 1454–1456.

[35] J.T. Hutt, Z.D. Aron, Org. Lett. 13 (2011) 5256–5259.

[36] C. Burstein, C.W. Lehmann, F. Glorius, Tetrahedron. 61 (2005) 6207–6217.

[37] S. Würtz, F. Glorius, Acc. Chem. Res. 41 (2008) 1523–1533.

[38] A. Fürstner, M. Alcarazo, H. Krause, C.W. Lehmann, J. Am. Chem. Soc. 129 (2007) 12676–12677.

[39] M. Alcarazo, S.J. Roseblade, A.R. Cowley, R. Fernandez, J.M. Brown, J.M. Lassaletta, J. Am. Chem. Soc. 2 (2005) 3290–3291.

[40] S.J. Roseblade, A. Ros, D. Monge, M. Alcarazo, E. Álvarez, J.M. Lassaletta, R. Fernández, Organometallics 26 (2007) 2570–2578.

[41] M.D. Bala, D.C. Levendis, N.J. Coville, J. Organomet. Chem. 691 (2006) 1919–1926.

[42] J.-Y. Le Gall, M.M. Kubicki, F.Y. Petillon, J. Organomet. Chem. 221 (1981) 287–290.

[43] M. Minelli, J. Enemark, R.T.C. Brownlee, M.J. O'Connor, A.G. Wedd, Coord. Chem. Rev. 68 (1985) 169–278.

[44] W. Beck, K. Schloter, Z. Naturforsch. B. 33 (1978) 1214–1222.

[45] T. Munisamy, S.L. Gipson, A. Franken, Inorg. Chim. Acta. 363 (2010) 20–24.

[46] C.G. Young, M. Minelli, J.H. Enemark, G. Miessler, N. Janietz, H. Kauermann, J. Wachter, Polyhedron 5 (1986) 407–413.

[47] M. Minelli, K. Yamanouchi, J.H. Enemark, P. Subramanian, B.B. Kaul, J.T. Spence, Inorg. Chem. 111 (1984) 2554–2556.

[48] H. Teruel, A. Sierralta, Polyhedron. 15 (1996) 2215–2221.

[49] E.C. Alyea, A. Somogyvari, Trans. Met. Chem. 12 (1987) 310–314.

[50] A.O. Ogweno, M.O. Onani, Acta Crystallogr. Sect. E, Struct. Rep. Online. 68 (2012) m364.

[51] P. Kubacek, R. Hoffmann, Z. Havlas, Organometallics. 1 (1982) 180–188.

[52] R. Poli, Organometallics. 9 (1990) 1892–1900.

[53] Z. Lin, M.B. Hall, Organometallics. 12 (1993) 19–23.

[54] J.M. Smith, N.J. Coville, Organometallics. 15 (1996) 3388–3392.

[55] K. Öfele, W.A. Herrmann, D. Mihalios, M. Elison, E. Herdtweck, W. Scherer, J. Mink, J. Organomet. Chem. 459 (1993) 177–184.

[56] R.H. Crabtree, J. Organomet. Chem. 690 (2005) 5451–5457.

[57] D.M. Khramov, V.M. Lynch, C.W. Bielawski, Organometallics. 26 (2007) 6042–6049.

[58] A. Comas-Vives, J.N. Harvey, Eur. J. Inorg. Chem. 2011 (2011) 5025–5035.

[59] S. Díez-González, S.P. Nolan, Coord. Chem. Rev. 251 (2007) 874–883.

[60] M. Alcarazo, T. Stork, A. Anoop, W. Thiel, A. Fürstner, Angew. Chem. Int. Ed. Engl. 49 (2010) 2542–2546.

[61] R. Tonner, G. Heydenrych, G. Frenking, Chem. Asian J. 2 (2007) 1555–1567.

[62] A.A. Valente, J.D. Seixas, I.S. Gonçalves, M. Abrantes, M. Pillinger, C.C. Romão, Catal. Lett. 101 (2005) 127–130.

[63] J.A. Brito, S. Ladeira, E. Teuma, B. Royo, M. Gómez, Appl. Catal. A. Gen. 398 (2011) 88–95.

[64] M. Drees, S.A. Hauser, M. Cokoja, F.E. Kühn, J. Organomet. Chem. (2013) DOI 10.1016/j.jorganchem.2013.05.004.

[65] G. Davidson, E.M. Riley, J. Organomet. Chem. 51 (1973) 297–306.

[66] J.W. Faller, A.S. Anderson, C.-C. Chen, J. Chem. Soc. D. Chem. Commun. 13 (1969) 719–720.

[67] E. Pfeiffer, K. Vrieze, J.A. McCleverty, J. Organomet. Chem. 174 (1979) 183–189.

[68] D.G. Alway, K.W. Barnett, Inorg. Chem. 19 (1980) 1533–1543.

3.6 Supporting Information

1. Analytical data for [CpMo(ImPyMes)$(CO)_2$Cl] **2**

^{1}H, ^{13}C and ^{95}Mo NMR

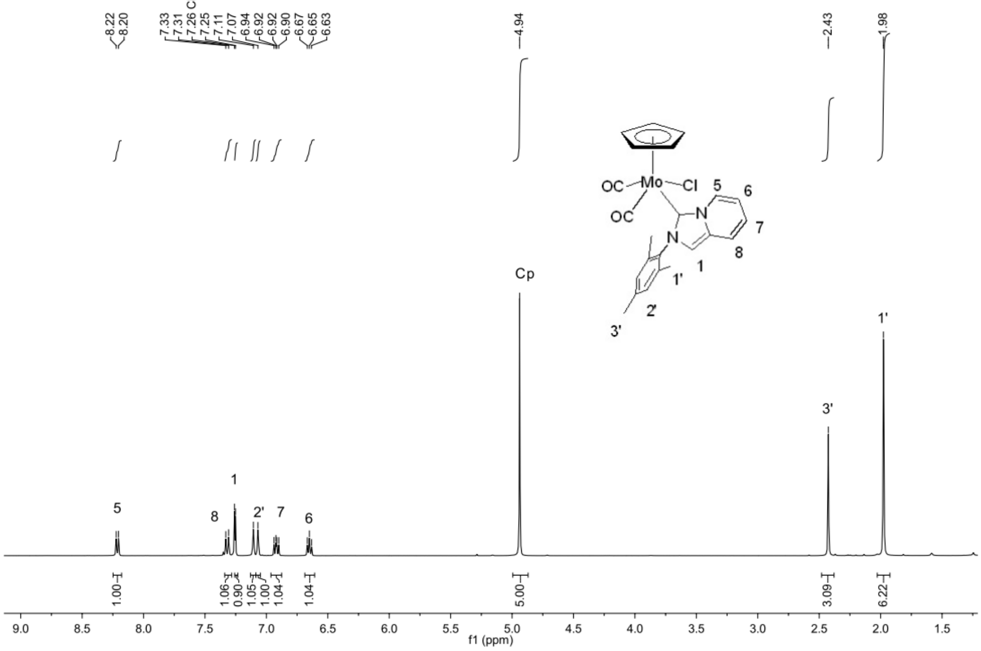

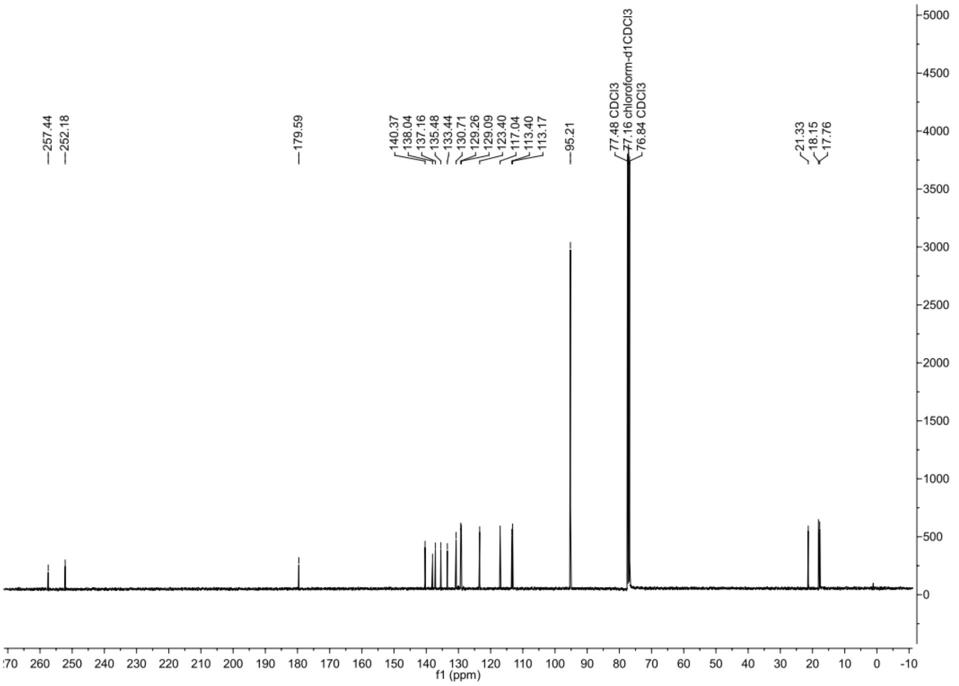

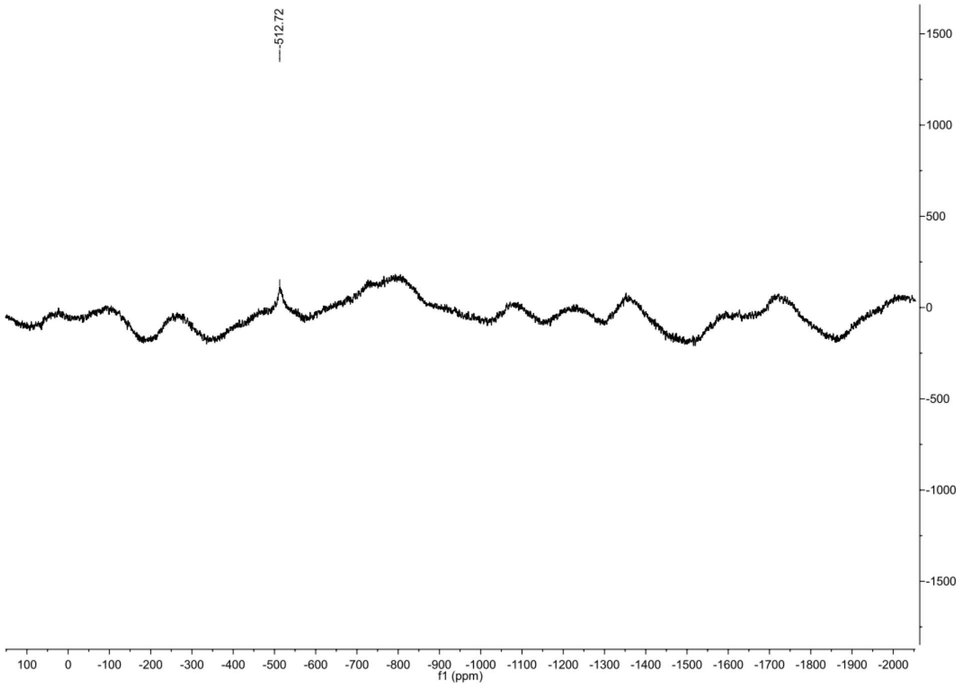

2. Analytical Data for [CpMo(ImPyMes)(CO)$_2$(NCCH$_3$)][BF$_4$] **3**

^{1}H, ^{13}C, ^{11}B, ^{19}F, ^{95}Mo NMR

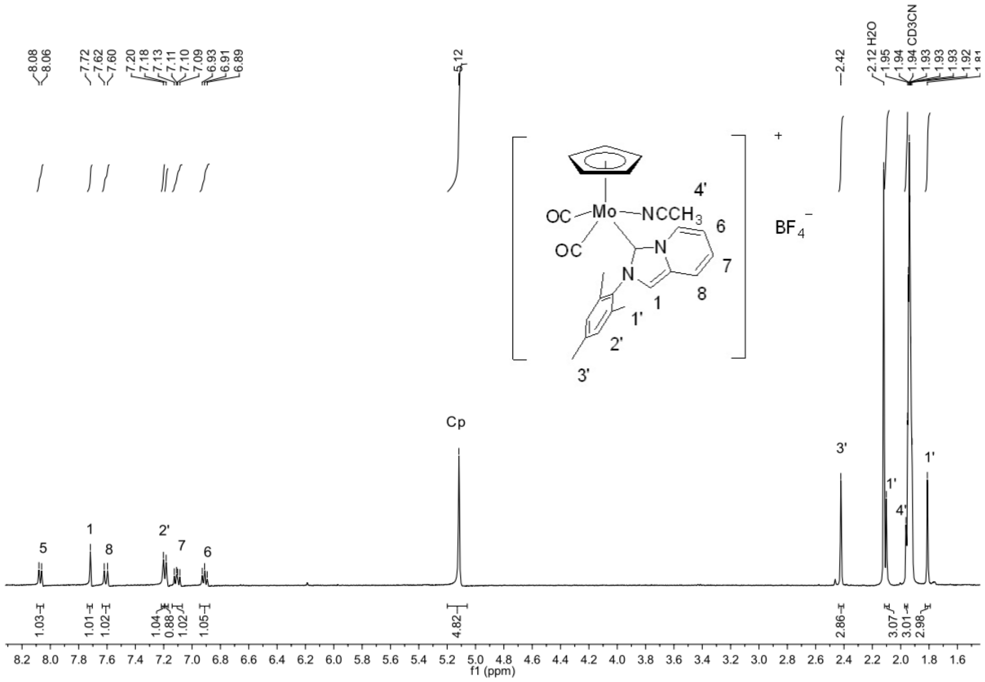

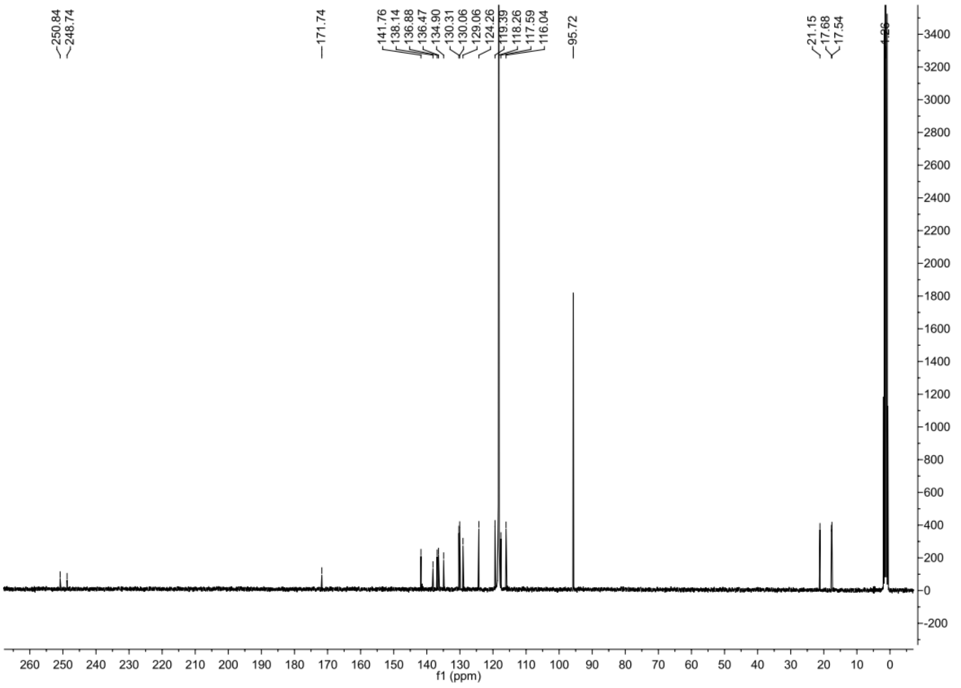
250.84
248.74
171.74
141.76
138.14
136.88
136.47
134.90
130.31
130.06
129.06
124.26
119.39
118.26
117.59
116.04
95.72
21.15
17.68
17.54
1.26
f1 (ppm)
260 250 240 230 220 210 200 190 180 170 160 150 140 130 120 110 100 90 80 70 60 50 40 30 20 10 0
3400 3200 3000 2800 2600 2400 2200 2000 1800 1600 1400 1200 1000 800 600 400 200 0 -200

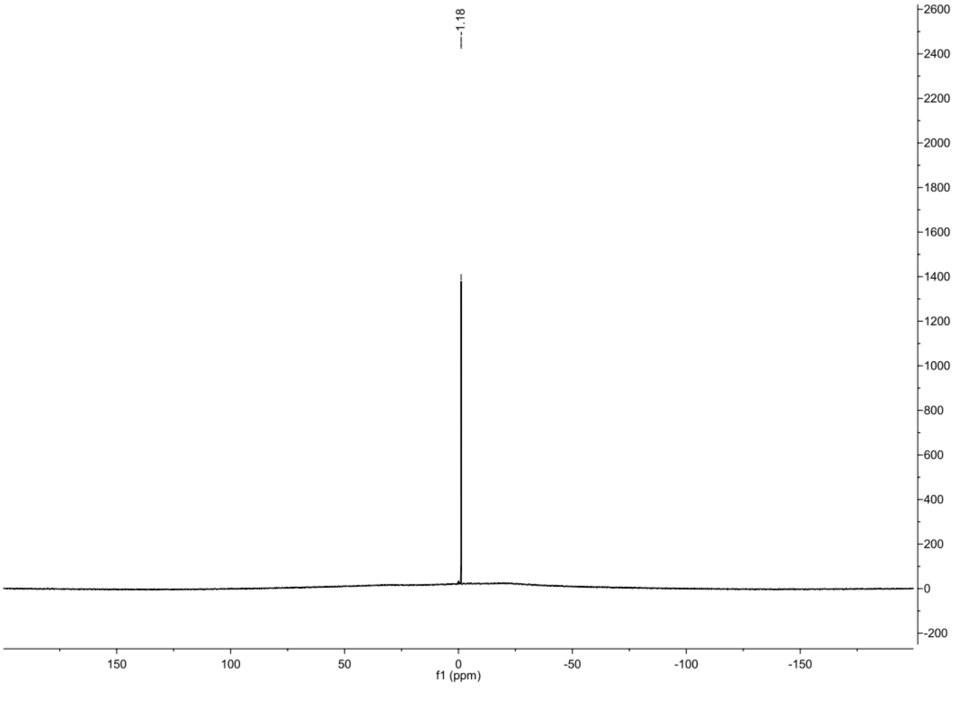
-1.18
f1 (ppm)
150 100 50 0 -50 -100 -150
2600 2400 2200 2000 1800 1600 1400 1200 1000 800 600 400 200 0 -200

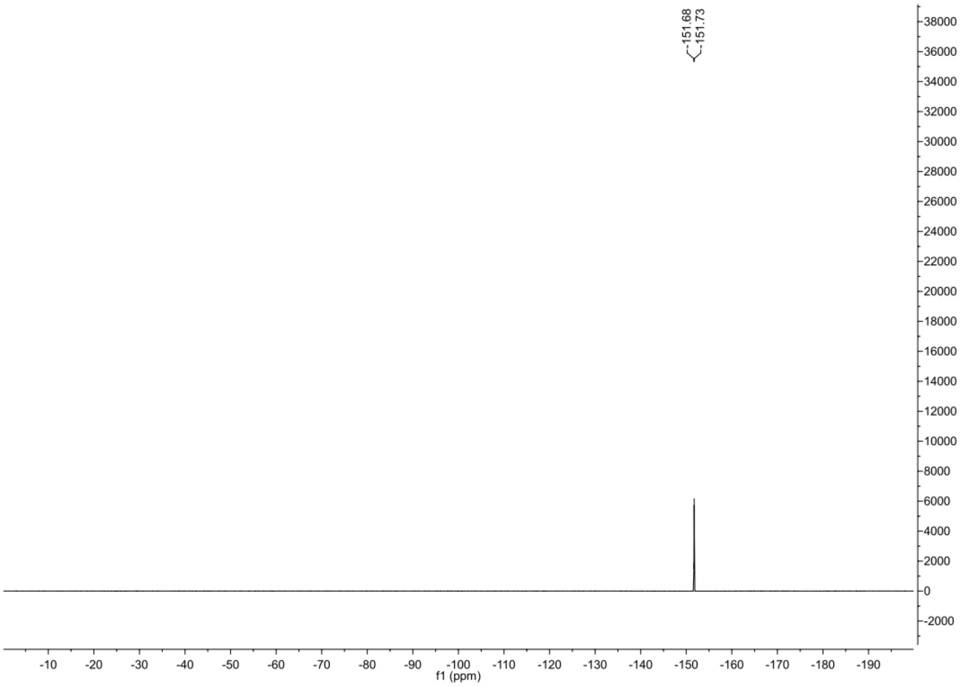

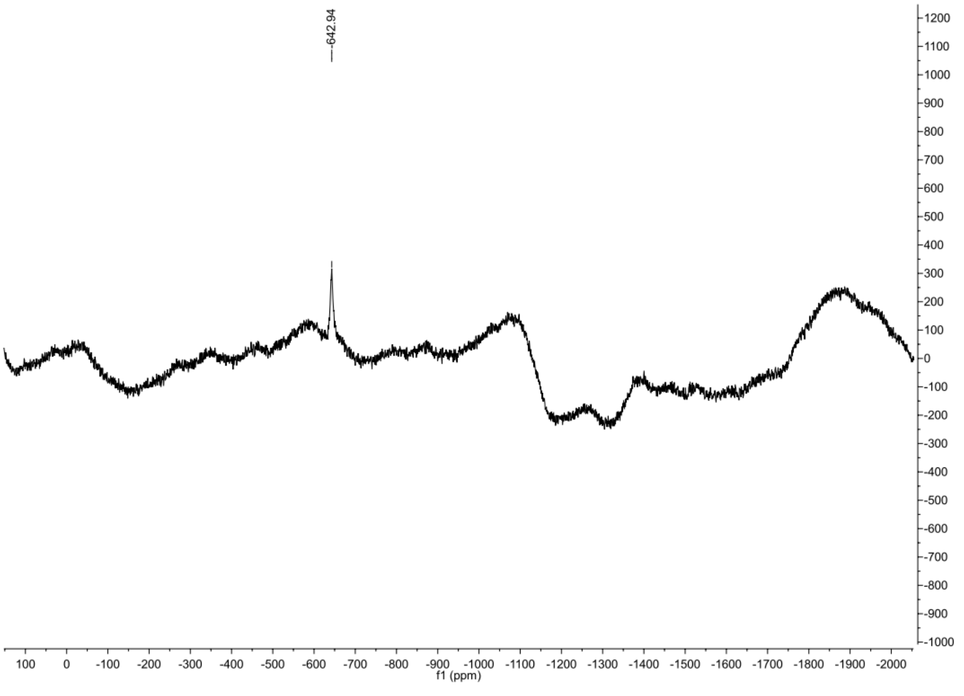

Table 3.5. Recycling for precatalyst 2 for epoxidation of cis-cyclooctene in RTIL [OMIM]NTf$_2$ with TBHP (n-decane)

Catalytic Run	**1**	**2**	**3**	**4**	**5**	**6**	**7**	**8**	**9**	**10**
Conversion%	98	99	100	100	100	100	100	100	100	100

3. The π*-acceptor ability of imidazo[1,5-*a*]pyridine-3-ylidene

Meyer et al. have summarized the structural changes that indicate the existence of metal to ligand π-backbonding [1] with imidazolium N-heterocyclic carbenes. On the basis of structural features, non-negligible π-interaction is indicated by elongated N-$C_{carbene}$ bonds and a smaller N-$C_{carbene}$-N bond angle. In Table 3.6, we have compared these structural features of ligand (obtained from Reference [2]) and that of complexes **2** and **3**.

Table 3.6. Comparison of structural data of ligand and complexes **2** and **3**. N2 refers to the nitrogen of fused pyridine moiety in imidazo[1,5-*a*]-3-pyridine ligand.

Parameter	[(ImPyMes)]Br	**2**	**3**
Bond Lengths (Å)			
$C_{carbene}$-N1	1.356	1.356	1.363
$C_{carbene}$-N2	1.357	1.374	1.380
Bond Angle (°)			
N1-$C_{carbene}$-N2	107.06	102.74	102.61

Thus, complexation of the carbene ligand to Mo in complexes **2** and **3** modifies the N-C-N bond angle significantly, and the slight elongation of carbene-N1 and carbene N2 bond lengths would indicate that the increase in *p* character of the carbene carbon is quite small. It is important to mention that the structural parameters of the carbene ligand are provided with Br^- as counter anion, while complex **3** has Cl^- as the anion. The π*-acceptor ability of imidazo[1,5-*a*]pyridine-3-ylidene ligands has been discussed before [3] and correlated with activity for Au complexes [4].

Supporting Information References

[1] X. Hu, Y. Tang, P. Gantzel, K. Meyer, Organometallics 22 (2003) 612–614.

[2] C. Burstein, C.W. Lehmann, F. Glorius, Tetrahedron 61 (2005) 6207–6217.

[3] R. Tonner, G. Heydenrych, G. Frenking, Chem. Asian J. 2 (2007) 1555–1567.

[4] M. Alcarazo, T. Stork, A. Anoop, W. Thiel, A. Fürstner, Angew. Chem. Int. Ed. Engl. 49 (2010) 2542–2546.

4 Cyclopentadienyl Molybdenum Alkylester Complexes as Catalyst Precursors for Olefin Epoxidation

Note: The work presented in this chapter will be submitted for publication.

Abstract

New molybdenum complexes of the type [$CpMo(CO)_3X$], containing ligands X = -$CHR^2CO(OR^1)$, where R^1 = ethyl (**1**), menthyl (**4**), bornyl (**5**) and R^2 = H; R^1 = ethyl and R^2 = methyl (**2**), phenyl (**3**), were synthesized and characterized by infrared (IR) and nuclear magnetic resonance (NMR) spectroscopy, elemental analysis, thermogravimetric analysis (TGA) and X-ray crystallography (complexes **1**, **2** and **5**). The compounds have been applied as catalysts precursors for achiral and chiral epoxidations of unfunctionalized olefins with *tert*-butyl hydroperoxide (TBHP) as oxidant at 22 °C (in dichloromethane, CH_2Cl_2) and 55 °C (in chloroform, $CHCl_3$). Substrates such as *cis*-cyclooctene, 1-octene, *cis*- and *trans*-stilbene, and *trans*-β-methylstyrene are selectively and quantitatively converted to their epoxides using a catalyst:substrate:oxidant ratio of 1:100:200 within 4 h at room temperature in CH_2Cl_2 and within 15 min at 55 °C in $CHCl_3$. Complexes **1**-**5** are precursors of highly active catalysts and turnover frequencies (TOFs) of ca. 1200 h^{-1} are obtained with *cis*-cyclooctene as substrate. No enantioselectivity is observed with *trans*-β-methylstyrene as substrate despite the application of enantiomerically pure precatalysts. The substituent effects of the side chain group on catalytic activity have been evaluated. A comparison of TOFs of epoxidation reaction of *cis*-cyclooctene at 55 °C and ^{95}Mo NMR shifts of complexes **1−5** suggests that there exists a trend between the stereoelectronic properties of different side chain substituents i.e. the Lewis acidity of the metal centre and catalytic activity.

4.1 Introduction

Since the development of the Halcon-ARCO process for industrial propylene oxide production using molecular Mo(VI) catalysts and organic hydroperoxides in homogeneous phase, improvements in stability, selectivity and applicability of specialized molybdenum complexes for homogeneous and heterogeneous epoxidation catalysis have been focal points of studies.[1] Mononuclear complexes such as [$MoO_2X_2L_n$] (X = halide, alkyl, siloxy, L = mono- or bidentate ligand),[2–6] [$(\eta^5-(C_5R_5)Mo(CO)_3X$] (R = H, Me, Bn; X = halide, Me, Et, *ansa*-bridged, CF_3)[7–10] and binuclear complexes of the type [$(\eta^5-(C_5R_5)_2M_2O_5$], (M = Mo, W)[11–12] have been used as epoxidation catalysts with *tert*-butyl hydroperoxide (TBHP) or H_2O_2 as oxidants.[12–14] Cyclopentadienyl (Cp) Mo complexes sometimes display activities even higher than the well-examined methyltrioxorhenium (MTO)-H_2O_2 system.[15–19] During the last decade, monomeric CpMo tricarbonyl complexes have been established as suitable precursors for catalytically active molybdenum dioxo or oxo-peroxo complexes, which are formed *in situ* with organic hydroperoxides after oxidative decarbonylation.[20–22] Homogeneous epoxidation activities of CpMo complexes as catalysts have been compared in a recent review[10] and other reviews have discussed heterogenization and epoxidation of the aforementioned category of molybdenum catalysts.[23–25]

Enantiopure epoxides are valuable intermediates and targets in organic synthesis and ubiquitous in pharmaceutical, agrochemical and other fine chemical industrial research initiatives.[26] Numerous molybdenum-based complexes have been utilized in enantioselective catalysis.[27,28] Specifically for epoxidation of unfunctionalized prochiral alkenes, chiral dioxo-molybdenum-based complexes have been extensively studied in both homogeneous and heterogeneous catalysis.[27,29] However, the limited enantioselectivity achieved with such complexes is, in general, a consequence of either weakly coordinating chiral ligands or transition states which are symmetrical during oxygen transfer in oxo-bisperoxo species.[30] Although stereoselective epoxidation in homogeneous phase is a lucrative target, particularly with readily available Mo catalysts, only very few examples are reported in literature and the enantiomeric excess (*ee*) do not exceed *ca.* 20% (for *trans*-β-methylstyrene as the substrate).[31] Efforts towards tailor-made chiral CpMo catalysts mostly involve the introduction of chiral substituents on the Cp ring.[31,32] However, as a consequence of the fast rotation of the Cp ring in solution, chiral information is lost and hence, the *ee* obtained are very poor. The rotation of the chiral Cp ligand can be suppressed by presence of an *ansa*-bridge from the Cp ligand to the Mo centre, either in a heteroatomic fashion[13] or σ-C bound.[33] In these cases, the chiral centres are located either at the *ansa*-bridge directly or at substituents at the bridge, which is usually too far away from the metal to be able to effectively transfer chiral information to the substrate. Royo et al. have investigated a chiral oxazoline substituted Cp molybdenum complex that forms a heteroatomic *ansa*-bridge, in order to introduce chiral centres in close proximity to the metal centre.[13] However, the oxazoline moiety decoordinates and loss of the Cp ligand during catalysis occurs. Hence, the efficiency of stereoselectivity in catalytic epoxidation with $[CpMo(CO)_3X]$ precatalysts also depends on the strength of the Mo–X bond.

Side chain functionalization of the fragment $[Cp'Mo(CO)_3]$ is a well-known route for synthesis of alkyl substituted complexes[34] and heterogenization of such catalysts in an ionic fashion on mesoporous silica and alumina MCM-41 and MCM-48.[35,36] In view of the strategic importance of enantiopure epoxides in many industrial endeavors, and the efficiency of CpMo complexes in achiral epoxidation,[37] we have synthesized side chain functionalized complexes **1−5** that are either substituted or unsubstituted at the Mo α-carbon (Scheme 4.1). It was then investigated whether epoxidation catalytic activity follows a trend on changing the side chain group, both sterically and electronically. Due to the presence of a chiral group in the side chain, it was possible to apply the enantiomerically pure precatalysts for stereoselective epoxidation of prochiral olefins. The side chain ligands utilized are alkyl moieties of the type $–CHR^2\text{-}COOR^1$, where the chiral information is located at the R^1 group. The ligand precursors to introduce the chiral menthyl and bornyl R^1 groups are easily derived from readily available natural products. The ester group serves to mediate the electronic situation at the Mo metal centre compared to the chloro and methyl group of complexes $[CpMo(CO)_3Cl]$ and $[CpMo(CO)_3Me]$. The presence of the ester moiety also eliminates the possibility of β-hydrogen elimination decomposition processes, which are possible for complexes where molybdenum is attached to a large alkyl group.[38]

An understanding of generic modes of induction, activation and reactivity of a given class of (pre)catalysts is required for developing ‘tailor-made’ catalysts. This can be done by evaluating available analytical data and identifying suitable parameters that help in defining principles of catalyst design. ^{95}Mo NMR chemical shifts are a suitable indicator of the electronic situation or Lewis acidity of the metal centre,[39] and conventionally turnover frequencies (TOFs) are chosen as an indicator of catalytic activity. Therefore we have attempted to find a correlation between ^{95}Mo chemical shifts and TOFs of epoxidation reaction with complexes **1−5**.

In this work the synthesis, characterization and applications of a hitherto unexplored class of cyclopentadienyl molybdenum complexes **1-5** for achiral and chiral epoxidation of unfunctionalized olefins such as *cis*-cyclooctene, 1-octene, *trans*- and *cis*-stilbene; and *trans*-β-methylstyrene respectively with TBHP as oxidant is reported. Complexes **1-5** demonstrate structural complexity, enabling a reasonable assessment of trends observed in epoxidation catalytic activity with regard to systematic manipulation of steric and electronic parameters when compared to literature known catalysts [CpMo(CO)$_3$Cl],[21] and [CpMo(CO)$_3$(CH$_3$)].[40]

4.2 Experimental

4.2.1 Methods and Materials

[Mo(CO)$_6$], NaH (60% dispersion in mineral oil), ethylchloroacetate, ethyllactate, ethylmandelate, (–)-borneol, (–)-menthol, *tert*-butylhydrogenperoxide (TBHP, ~5.5 M solution in *n*-decane), *trans*-β-methylstyrene were purchased from Sigma Aldrich. All manipulations involving air sensitive materials were performed under argon atmosphere using standard Schlenk techniques and dry solvents. Menthyl- and bornyl- chloroacetate side chain ligands were synthesized by reaction of L-(-) menthol and (-) borneol with chloroacetylchloride and *N*,*N*-dimethylamine at 0-30 °C. Side chain precursors for complexes **2** and **3**, namely ethyl lactate- and ethylmandelate- mesylate were also obtained by reaction with mesyl chloride in toluene.[51] The ligands were then either degassed and dried by freeze-pump-thaw method or distilled at low pressures prior to use for the synthesis of complexes **1-5**. High resolution NMR spectra were recorded using a Bruker Avance DPX-400 spectrometer. ^{1}H and ^{13}C spectra are referenced to solvent residual signals[41] and ^{95}Mo spectra to an internal standard of 2M Na$_2$MoO$_4$ in D$_2$O set to 0 ppm. Solid state MAS spectra were recorded on Bruker Avance 300 at room temperature in a 4mm ZrO$_2$ rotor, at 10 kHz or 12 kHz. As an external (secondary) standard for referencing adamantane was used, for TMS ^{1}H: 2.00 ppm, ^{13}C: 29.472 ppm were reference values. IR spectra were recorded on a Varian ATR-FTIR instrument. Thermogravimetric analyses were performed with a Netzsch TG 209 system at a heating rate of 10 °C min^{-1} under argon. Microanalyses were performed in the Mikroanalytisches Labor of the Technische Universität München, Garching. Mass spectra were recorded with Finnigan MAT 311 A and MAT 90 spectrometers. Catalysis was performed under ambient atmosphere and catalytic runs were monitored on a Varian CP-3800 instrument equipped with an FID and Optima 5 Amine column (*cis*-cyclooctene, 1-octene, *trans*- and *cis*-stilbene) and Optima Delta Amine column (*trans*-β-methylstyrene).

4.2.2 X-ray Crystallography

Data were collected on an X-ray single crystal diffractometer equipped with a CCD detector (APEX II, κ–CCD), a rotating anode (Bruker AXS, FR591) with MoK$_\alpha$ radiation (λ = 0.71073 Å) and a MONTEL-type focusing optic (compound **2**) or a fine-focussed sealed tube respectively (compounds **1** and **5**) and a graphite monochromator by using the SMART software package.[42] The measurements were performed on single crystals coated with perfluorinated ether. The crystals were fixed on the top of a glass fiber and transferred to the diffractometer. Crystals were frozen under a stream of cold nitrogen. A matrix scan was used to determine the initial lattice parameters. Reflections were merged and corrected for Lorenz and polarization effects, scan speed, and background using SAINT.[43] Absorption corrections, including odd and even ordered spherical harmonics were performed using SADABS.[43] Space group assignments were based upon systematic absences, *E* statistics, and successful refinement of the structures. Structures were solved by direct methods with the aid of successive difference Fourier maps, and were refined against all data using the APEX 2 software[42,44] in conjunction with SHELXL-97[45] and SHELXLE.[46] Unless stated otherwise, methyl hydrogen atoms were refined as part of rigid rotating groups, with a C–H distance of 0.98 Å and $U_{iso(H)} = 1.5 \cdot U_{eq(C)}$. Other H atoms were placed in calculated positions and refined using a riding model, with methylene and aromatic C–H distances of 0.99 and 0.95 Å, respectively, and $U_{iso(H)} = 1.2 \cdot U_{eq(C)}$. If not mentioned otherwise, non-hydrogen atoms were refined with anisotropic displacement parameters. Full-matrix least-squares refinements were carried out by minimizing $\Sigma w(F_o^2 - F_c^2)^2$ with SHELXL-97 [45] weighting scheme. Neutral atom scattering factors for all atoms and anomalous dispersion corrections for the non-hydrogen atoms were taken from *International Tables for Crystallography.*[47] Images of the crystal structures were generated by PLATON.[48]

Special remarks to the refinements:

1: Full refinement was possible without running into problems.

2: The ethyl moieties were refined using split layer positions.

5: Due to physical meaningless ADPs, the following restraints were applied: SIMU for C1 > C5 (Cp-Moiety) and ISOR for C10.

Crystallographic data (excluding structure factors) for the structures reported in this paper have been deposited with the Cambridge Crystallographic Data Centre as supplementary publication Nos. CCDC-934898 (**1**), CCDC-934899 (**2**) and CCDC-934900 (**5**). Copies of the data can be obtained free of charge on application to the CCDC, 12 Union Road, Cambridge CB2 1EZ, U.K. (Fax: (+44)1223-336-033; e-mail, deposit@ccdc.cam.ac.uk).

*4.2.3 General procedure for synthesis of **1-5***

$Na[CpMo(CO)_3]$ (1 equiv.) was prepared by refluxing $Mo(CO)_6$ and NaCp in freshly distilled, dry THF overnight. The yellow-orange oily residue obtained after removing THF in vacuo was purified by washing with cold, dry Et_2O (3x10 mL). 40 mL dry THF was then added followed by dropwise addition of degassed respective chloro- or mesylate ligands (1.05 equiv.) in 10 mL THF under a steady argon flow in the dark at -40 °C. The reaction flask was then stirred at r.t. in the dark for a suitable time, followed by evaporation of solvent to dryness. The obtained residues were extracted with dry pentane or hexane and concentrated in vacuo. The red-yellow products were then purified by column chromatography. Complexes **1-5** eluted as yellow bands after a deep red band of $Cp_2Mo_2(CO)_6$ using pentane:diethyether = 9:1. The fractions were concentrated under vacuum and **1-5** were obtained as yellow solids/oil in yields 54-85%.

$CpMo(CO)_3(CH_2COOC_2H_5)$ (1) Reaction time = 6 h, Yield = 73%. ^1H NMR (400 MHz, C_6D_6) δ 4.62 (s, 4H, Cp), 4.07 (q, *J* = 7.1 Hz, 2H), 1.88 (s, 2H, Mo-C*H*$_2$), 1.11 (t, *J* = 7.1 Hz, 3H). $\{^1H\}^{13}C$ NMR (101 MHz, C_6D_6) δ 240.63, 226.99 (Mo-*C*O); 181.07 (*C*=O), 93.44 (Cp), 59.37, 14.74, -3.77 (Mo-*C*H$_2$). ^{95}Mo (C_6D_6) = δ -1546. Elemental analysis calcd. (%): C 43.39, H 3.64; found: C 43.56, H 3.70. IR (cm^{-1}) 3110 *vw*, 2026 *s*, 1926 *vs*, 1682 *w*, 1423 *vw*, 1240 *w*, 1093, 1039, 823, 578, 550, 483, 443.

$CpMo(CO)_3(CH(CH_3)COOC_2H_5)$ (2) Reaction time = 24 h, Yield = 54%. ^1H NMR (400 MHz, C_6D_6) δ 4.63 (s, 5H, Cp), 4.05 (q, 2H), 2.90 (d, *J* = 7.1 Hz, 1H, Mo-C*H*), 1.61 (d, J = 7.1 Hz, 3H, Mo-CH-C*H*$_3$), 1.11 (t, J = 7.1 Hz, 3H). $\{^1H\}^{13}C$ NMR (101 MHz, C_6D_6) δ 241.00, 228.28, 227.63 (Mo-*C*O), 182.63 (C=O), 93.90 (Cp), 59.33, 23.61 (Mo-*C*H), 14.68, 11.32 (Mo-CH-*C*H$_3$). ^{95}Mo (C_6D_6, 2M Na_2MoO_4 in D_2O) = δ -1484. Elemental analysis calcd. (%): C 45.10, H 4.08, Mo 27.71; found: C 45.72, H 4.23, Mo 25.65. IR (cm^{-1}) 3324, 3089, 2962, 2925, 2010 s, 1914 *vs*, 1666 *vs*, 1445, 1423,1387, 1367, 1331, 1305, 1232, 1161 *vs*, 1098, 1050, 982, 899, 866, 828, 758, 704, 676, 579, 546, 484, 449.

$CpMo(CO)_3(CH(Ph)COOC_2H_5)$ (3) Reaction time = 48 h, Yield = 65%. ^1H NMR (400 MHz, C_6D_6) δ 7.63 (d, *J* = 7.3 Hz, 2H), 7.15 (m, 2H), 6.95 (t, *J* = 7.3 Hz, 1H), 4.48 (s, 5H, Cp), 4.15 (s, 1H, Mo-C*H*), 4.04 (m, 2H), 1.08 (t, 3 H). $\{^1H\}^{13}C$ NMR (101 MHz, C_6D_6) δ 241.35, 228.81, 228.72 (Mo-CO); 178.80 (C=O), 147.97, 128.15, 124.74, 94.82 (Cp), 59.53, 21.39 (Mo-*C*H), 14.53. ^{95}Mo (C_6D_6, 2M Na_2MoO_4 in D_2O) = δ -1515. Elemental analysis calcd. (%): C 52.96, H 3.95, Mo 23.50; found: C 54.10, H 4.06, Mo 22.43. IR (cm^{-1}) 3108 *vw*, 2979, 2926, 2257, 2023 *s*, 1930 *vs*, 1689, 1593, 1489, 1451, 1371, 1274, 1226, 1142, 1041, 822, 772, 701, 576, 547, 478, 446.

$CpMo(CO)_3(CH_2COOMenthyl)$ (4) Reaction time = 12 h, Yield = 70%. ^1H NMR (400 MHz, C_6D_6) δ 4.85-4.95 (m, 1H), 4.7 (s, 4H, Cp), 2.1-2.3 (m, 2H), 1.84-1.97 (m, 2H), 1.41-1.60 (m, 3H), 1.20-1.38 (m, 1H), 1.07-1.09 (m, 1H), 0.89-1.04 (m, 10H), 0.67-0.8 (m, 1H). $\{^1H\}^{13}C$ NMR (101 MHz, C_6D_6) δ 240.72, 226.91, 226.77 (Mo-*C*O), 180.71 (C=O), 93.44 (Cp), 73.00, 47.78, 41.89, 34.65, 31.75, 26.65, 23.82, 22.43, 21.16, 16.76, -3.36 (Mo-*C*H$_2$). ^{95}Mo (C_6D_6, 2M Na_2MoO_4 in D_2O) = δ -1553. Elemental analysis calcd. (%): C 54.30, H 5.92, Mo 21.69; found: C 55.36, H 6.28, Mo 21.85. IR (cm^{-1}) 3110, 2953, 2868, 2028, 1934, 1679, 1455, 1422, 1369, 1243, 1094, 1012, 821, 579, 550, 484, 445.

$CpMo(CO)_3(CH_2COOBornyl)$ (5) Reaction time = 12 h, Yield = 85%. ^1H NMR (400 MHz, C_6D_6) δ 5.13-5.17 (m, 1H), 4.66 (s, 4H, Cp), 2.42-2.55 (m, 1H), 2.28-2.38 (m, 1H), 1.88-2.01 (m, 2H), 1.66-1.80 (m, 1H), 1.53-1.60 (m, 1H), 1.30-1.47 (m, 2H), 1.14-1.24 (m, 1H), 0.70-1.01 (m, 9H), 0.43-0.55 (m, 1H). $\{^1H\}^{13}C$ NMR (101 MHz, C_6D_6) δ 240.58, 227.00, 226.85 (Mo-*C*O), 181.48 (C=O), 93.53 (Cp), 79.27, 48.91, 48.04, 45.40, 37.54, 28.56, 27.74, 19.92, 18.99, 13.98, -3.35 (Mo-*C*H$_2$). ^{95}Mo (C_6D_6, 2M Na_2MoO_4 in D_2O) δ -1555. Elemental analysis calcd. (%): C 54.55, H 5.49, Mo 21.79; found: C 54.81, H 5.62, Mo 21.91. IR (cm^{-1}) 3105, 2948, 2868, 2490, 2158, 2023 *s*, 1931 *vs*, 1669 *s*, 1420, 1366, 1300, 1247 *vs*, 1135, 1095, 1022, 982, 955, 860, 827, 740, 577, 547, 520, 483, 445.

4.2.4 Epoxidation catalysis

All catalytic investigations were carried out under ambient atmosphere, at 22 °C either with solvent CH_2Cl_2 or solventless conditions and at 55 °C in $CHCl_3$. Under standardized conditions, 1 mol% or 0.1 mol% catalyst and the substrate were dissolved in 5 mL solvent. Catalysis was started with the addition of TBHP to the catalyst and substrate reaction mixture. Aliquots were obtained from the reaction flask at suitable time intervals and treated with activated MnO_2 to destroy the oxidant, followed by filtration through a $MgSO_4$ plug to remove traces of water. Appropriate amount of external standard solution (indane and *p*-xylene for *cis*-cyclooctene, toluene and mesitylene for 1-octene, hexadecane and octadecane for *cis*- and *trans*-stilbene, 1,2,4-trimethylbenzene and tetraline for *trans*-β-methylstyrene in isopropanol) was then added to the aliquot and the sample was injected into GC instrument having a column pre-calibrated with $r^2 = 0.999$ to the chosen substrate. Enantiomeric excess (*ee*) was calculated from integration of the two peaks relative to calibration method optimized with pure sample injections of (2*S*,3*S*)-2-methyl-3-phenyloxirane and (2*R*,3*R*)-2-methyl-3-phenyloxirane.

4.3 Results and Discussion

*4.3.1 Synthesis and characterization of complexes **1-5***

Complexes **1-5** were synthesized by procedures analogous to previous reports of synthesis of complex **1**.[49,50] $Na[CpMo(CO)_3]$ was prepared according to literature[34] and used as the metal precursor for complexes **1**-**5** (Scheme 4.1).

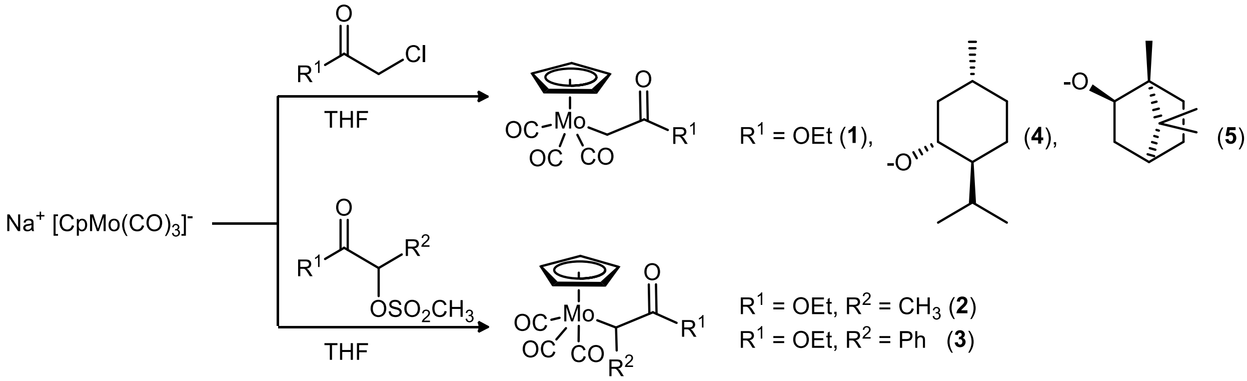

Scheme 4.1. Synthesis of cyclopentadienyl molybdenum tricarbonyl alkylester complexes **1-5**.

As side chain precursors, α-chloroesters were suitable for alkylation of the $Na[CpMo(CO)_3]$ fragment (for complexes **1, 4** and **5**) while α-methanesulfonoxyesters were more suited for synthesis of secondary η^1-oxoalkyl side chains (complexes **2** and **3**). However, the reaction time was longer for the synthesis of complexes **2** and **3**, requiring stirring at room temperature for several days. Reaction of the chloro- and mesylate precursors with $Na[CpMo(CO)_3]$ at room temperature for 6-48 h thus gave complexes **1-5** in yields of 54-85%.

Complexes **1**-**3** and **5** are yellow solids and complex **4** is obtained as bright yellow oil after column purification. They are soluble in common organic solvents, such as benzene, toluene, tetrahydrofuran and dichloromethane. In the solid state, the synthesized complexes are stable to air and moisture for several hours. In solution, all complexes are significantly more sensitive showing visible decomposition to blue-green residues overnight. Compounds **1-5** can be handled briefly under ambient conditions without any apparent decomposition, but complexes of this type are known to be susceptible to slow photochemical transformation in solution to either the μ-CO bridged species as known[52] or rearrangement to the η^3-coordinated side chain on loss of a carbonyl ligand.[53] Complexes similar to **2** are known to be susceptible to β-hydrogen elimination[54] but in this case, decomposition of **2** to an α-alkenyl type of complex was not observed. All synthesized complexes are stable for over a year when stored in the dark under argon at -30 °C. While complexes **2** and **3** decompose at 150 and 110 °C, respectively, Mo complexes **4** and **5** bearing menthyl and bornyl moieties decompose at 210 and 205 °C respectively, as shown by TGA-MS measurements (see the Supporting Information, SI).

4.3.2 NMR spectroscopy

^{1}H NMR spectra of compounds **1-5** (in C_6D_6) show the C_5H_5 ligand in the range 4.5-4.7 ppm and 93.4-94.8 ppm in ^{13}C NMR (Table 4.1). These chemical shift values for the Cp ligand are in the range observed for other structurally similar complexes [CpMo(CO)$_3$X] (where X = Cl, CH_3). The Mo-CH_2 protons of the alkyl ligands appear upfield (1.8-2.1 ppm) for **1**, **4** and **5** as the deshielding effect of the ester group is partly offset by the metal centre, which is coordinated to three backbonding CO ligands. On the other hand, the methylene signals in **2** and **3** are highly deshielded, appearing downfield at 2.9 and 4.1 ppm, respectively. This de-shielding effect of the methyl and phenyl substituents is also reflected in the respective ^{13}C NMR shifts of the α-carbon, observed at 21-23 ppm for complexes **2** and **3** in contrast to the highly upfield signals at -3 ppm for **1**, **4** and **5**.

In ^{13}C NMR the carbonyl resonances of complexes **2-5** (in C_6D_6) appear as three well resolved peaks, one *each* for the two *syn* carbonyls and one for the third *trans* carbonyl known to appear downfield to the two *cis* CO.[55] Similar to complexes [CpMo(CO)$_3$X] (X = Me, Cl), compound **1** shows no such in-equivalence in chemical shift for the terminal carbonyl groups and only two signals are observed.

Table 4.1. Selected NMR Spectroscopic data for complexes **1-5** and comparison with [CpMo(CO)$_3$Cl] and [CpMo(CO)$_3$CH$_3$].

Complex	^{1}H NMR^{a}		^{13}C{^{1}H} NMR^{a}			
	Cp	Mo-$^{\alpha}$C$\underline{H}$	Cp	Mo-$^{\alpha}\underline{C}$H	$\underline{C}$(=O)O	Mo–$\underline{C}$≡O
1^{b}	4.68	1.84 (s,2H)	–	-3.94	–	227.04, 240.63
1	4.62	1.88 (s,2H)	93.44	-3.78	181.05	226.99, 240.63
2	4.63	2.87-2.93 (q,1H)	93.90	23.61	182.63	227.63, 228.28, 241.00
3	4.48	4.15 (s,1H)	94.82	21.39	178.80	228.72, 228.81, 241.35
4	4.70	2.16 (m,2H)	93.44	-3.36	180.71	226.77, 226.91, 240.72
5	4.66	1.93 (m,2H)	93.53	-3.35	181.48	226.85, 227.00, 240.58
[CpMo(CO)$_3$Cl]	4.62	–	95.58	–	–	225.21, 242.99
[CpMo(CO)$_3$CH$_3$]	4.42	0.39	92.41	1.44	–	227.37, 240.49

^{a} All signals are referenced to deuterated solvent C_6D_6 δ7.16 (for ^{1}H) and δ128.06 (for ^{13}C{^{1}H}).

^{b} Reference 49.

Variable temperature ^{13}C NMR studies for **5** in C_6D_6 show that the stereoelectronic asymmetry observed in the form of two suitably resolved peaks for the electronically in-equivalent '*cis*-CO' is present even until 70 °C. Coalescence of the two carbonyl signals does not occur even at this high temperature (Figure 4.5, Supporting Information). Solid state ^{1}H MAS and ^{13}C CPMAS spectra of **5** has been compared to that of [CpMo(CO)$_3$Me] (Figure 4.6, SI). For complex **5**, all three Mo bound carbonyl groups show chemical shift anisotropy in the solid state and appear at δ 226.59, 230.16 and 242.25, in contrast to [CpMo(CO)$_3$Me] where the two *cis*-CO are equivalent at 230.3 ppm and the third appears at 242.3 ppm. This shows that the possible fluxional processes, namely, rotation of Cp about the Mo-(η^5-Cp) C$_5$ axis, rapid interchangability equivalence of the square pyramidal basal *cis*-CO ligands, and rotation about the Mo- αC σ bond[56−59] − are slower or restricted, in likelihood of the presence of bulky substituents for **5** and for complexes **2−4** as well. For [CpMo(CO)$_3$Me] however, no such in-equivalence is apparent and only two carbonyl peaks can be observed in solution and solid state ^{13}C NMR. Complexes **2−5** are thus examples of monomeric cyclopentadienyl tricarbonyl molybdenum piano stool complexes where the barriers to rotation of Cp and basal ligands although quite small in magnitude, are significant even at high temperatures.

It is important to note that the solution NMR of complexes **4** and **5**, and X-ray structure for **5** (Flack parameter 0.02(7), see SI) confirm the enantiopurity of the prepared complexes. ^{95}Mo NMR data for complexes **1**-**5** are summarized in Table 4.4. For a discussion of ^{95}Mo NMR shifts and catalytic activity, see Section 4.3.7.

4.3.3 Vibrational spectroscopy

The carbonyl ester group in **1-5** absorbs in the range of 1666-1690 cm^{-1}, which is typical for complexes of this type.[50] The absorption frequencies for the terminal carbonyl groups differ only about 10 cm^{-1} in **1, 3−5**. The chemical shift anisotropy which is observed in solution and solid state NMR for metal bound carbonyl groups is not clearly evident in the absorption pattern and only two bands are seen in the range of 2023-2028 cm^{-1} and 1926-1931 cm^{-1}.[60] This is not altogether unusual as deviation from the original D$_{4h}$ geometry to slightly perturbed C$_{3v}$ geometry in piano-stool complexes results in experimental observation of only two bands A′ and A″ out of the three possible ν_{CO}. There is however, a difference in absorption frequencies for the metal bound carbonyl groups in complex **2** when compared to complexes **1, 3, 4** and **5**. Bands at 2010 cm^{-1} and 1914 cm^{-1} for **2** are slightly lower wavenumbers compared to ν_{CO} for the other precatalysts which absorb averagely at 2026 cm^{-1} and 1930 cm^{-1}. The lower absorption frequencies for terminal CO groups in **2** reflect that the metal is more electron rich and there is stronger back-bonding. This observation is curious when considered in conjunction with the NMR data for complexes **2** and **3** (Section 4.3.2). If an unhindered transmission of the negative inductive effect of the α-carbon substituent is considered from the observed de-shielded ^{1}H and ^{13}C NMR shifts of the α-carbon and also affecting the metal centre, then the molybdenum central atom can be considered electron poor. However, because of its inherent Lewis acidic nature, the consequences of substituent inductive effect are partly offset by elongation of the Mo-α-carbon bond length (see Section 4.3.5).

4.3.4 Thermogravimetry and Mass Spectrometry

Thermogravimetric analysis combined with mass spectrometry data for complexes **2-5** indicate that loss of a Mo bound carbonyl group (as CO$^+$) initiates their decomposition. This is followed by a nearly simultaneous loss of Cp or other two carbonyls or the alkylester side chain. These transformations are responsible for complete decomposition of the precatalysts. The propensity of both processes is accentuated when one CO is lost. Mass spectrometry and decomposition points determined from TGA-MS are given in Table 4.2.

Table 4.2. Mass spectrometry data and decomposition points for complexes **1-5**.

Complex	MI[a,b]	Base Peak	Method[d]	Decomposition point (°C)[e]
1[c]	333	89	CI	32.5 - 33.5[c]
2	348.6 (14.8)	182.8	CI (+)	150
3	410.5 (13.7)	164.9	CI (+)	110[f]
4	444.6 (4.6)	146.9	FAB (+)	210 – 220[f]
5	442.5 (19.9)	246.6	FAB (+)	205

[a] % Relative abundance in parenthesis. [b] CI-MS (+) *m/z* are M+1 peaks. [c] Reference [50] [d] CI refers to chemical ionization, FAB refers to fast atom bombardment method. [e] Determined by TGA-MS under inert Argon with Al_2O_3 correction; temperature gradient 10 K min^{-1}. [f] Gradual decomposition, triggered by loss of one CO^+.

4.3.5 Single crystal X-ray diffraction

Crystals for complexes **1**, **2** and **5** were obtained from a pentane-diethyl ether solvent mixture by slow vapor diffusion and were suitable for single crystal X-ray diffraction experiments. The crystal structures for these complexes prove the η^1-coordination of the ester side chain (Figures 4.1−4.3). More detailed data are presented in Supplementary Information. The bond length Mo1-C9 (Mo-$^{\alpha}$C) in the crystal structures of complexes **1**, **2** and **5** differs significantly. This bond distance is the shortest for complex **1** (2.325(2) Å) due to least steric demand in the absence of any α-C substituent while in complex **2** (2.377(2) Å), presence of the methyl substituent exerts a higher steric demand and the bond length increases. For complex **5**, the bond length Mo1-C9 is 2.349(5) Å, which is in between those for **1** and **2**. Here, the steric influence is a result of the bulky bornyl ester group even though there is no additional α-C substituent. The Mo-$^{\alpha}$C bond length in complex [$CpMo(CO)_3CH_3$] is 2.326(3) Å[61] which is almost identical to the bond length in complex **1**. Since the metal centre is inherently Lewis acidic, there is a reluctance to donate electron density to the α-carbon in order to alleviate the de-shielding effect of methyl (complex **2**) or phenyl (**3**) substituent. Consequently, for these electronic reasons as well, bond length Mo1-C9 is elongated in **2** compared to **1**.

All terminal Mo–CO bonds and the C–O bond lengths for **1**, **2** and **5** are equal (within statistical error) and lie in the expected range. Furthermore, the bond angle Cp–Mo1–C9 is the smaller 109.01(6)° for complex **1** when compared to complexes **2** and **5** (110.71(6)° and 111.0(2)° respectively). This is possibly due to packing effects which enable the ester moiety to rotate freely in **2** and **5**, however in complex **1** only a staggered conformation of Cp–Mo1–C9–C10 is possible. This is also made evident on comparing the torsion angle Cp–Mo1–C9–C10 = -177.8(2)° in **1**, -59.8(2)° in **2** and -51.2(4)° in **5**. Additionally, C7–Mo1–C9 torsion angle differs in the three complexes significantly. It has the highest value for **1** (136.2(1)° which is possibly a consequence of conformation or packing effects; while in complex **2** (134.4(1)°) and **5** (132.7(3)°), the higher steric demand and *gauche* conformation to Mo1–Cp makes a close proximity between C9 and CO ligands possible, making the torsion angle smaller than for **1**.

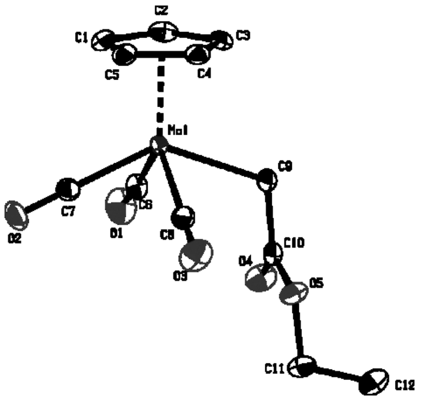

Figure 4.1. ORTEP view of the single crystal X-ray structure of compound **1**.

Thermal ellipsoids are drawn at the 50% probability level. Hydrogen atoms are omitted for clarity. Selected bond distances [Å], angles [°] and torsion angles [°]: Mo1–C9 2.325(2), Mo1···Cp 1.9956(2), Mo1–C6 2.002(3), Mo1–C7 1.990(3), Mo1–C8 2.000(3), C6–O1 1.148(4), C7–O2 1.143(3), C8–O3 1.138(4), Cp–Mo1–C9 109.01(6), Mo1–C9–C10 116.0(2); C6–Mo1–C9 77.7(2), C7–Mo1–C9 136.2(1), C8-Mo1–C9 78.4 (2), Mo1–C9–C10–O4 88.1(3), Cp–Mo1–C9–C10 -177.8(2).

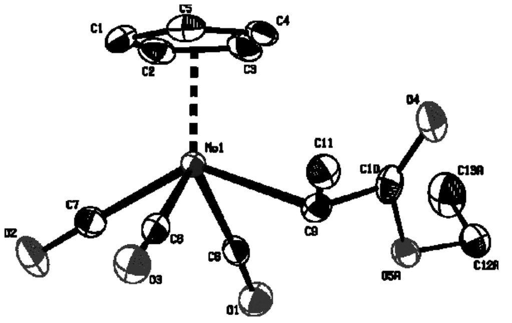

Figure 4.2. ORTEP view of the single crystal X-ray structure of compound **2**.

Thermal ellipsoids are drawn at the 50% probability level. Hydrogen atoms and the disorder in the ester moiety are omitted for clarity. Selected bond distances [Å], angles [°] and torsion angles [°]: Mo1–C9 2.377(2), Mo1···Cp 2.0118(3), Mo1–C6 1.997(2), Mo1–C7 1.997(3), Mo1–C8 2.004(2), C6–O1 1.145(3), C7–O2 1.145(3), C8–O3 1.141(3), Cp–Mo1–C9 110.71(6), Mo1–C9–C10 108.3(2); C6–Mo1–C9 78.9(1), C7–Mo1–C9 134.4(1), C8-Mo1–C9 73.6(1), Mo1–C9–C10–O4 96.3(3), Cp–Mo1–C9–C10 -59.8(2).

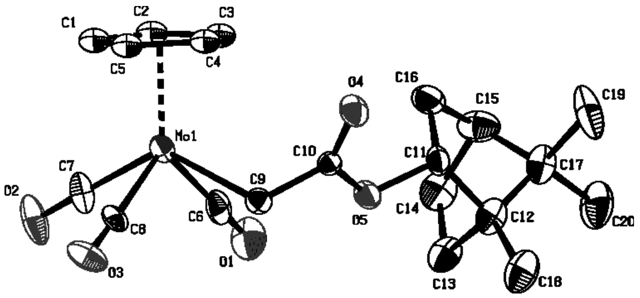

Figure 4.3. ORTEP view of the single crystal X-ray structure of compound **5**.

Thermal ellipsoids are drawn at the 50% probability level. Hydrogen atoms are omitted for clarity. Selected bond distances [Å], angles [°] and torsion angles [°]: Mo1–C9 2.349(5), Mo1···Cp 1.9917(5), Mo1–C6 2.008(5), Mo1–C7 1.983(7), Mo1–C8 1.978(7), C6–O1 1.141(6), C7–O2 1.170(8), C8–O3 1.161(7), Cp–Mo1–C9 111.0(2), Mo1–C9–C10 111.0(4); C6–Mo1–C9 77.6(2), C7–Mo1–C9 132.7(3), C8-Mo1–C9 73.5 (2), Mo1–C9–C10–O4 91.4(6), Cp–Mo1–C9–C10 -51.2(4).

4.3.6 Epoxidation Catalysis

All complexes were applied as catalyst precursors for the epoxidation of *cis*-cyclooctene, 1-octene, as well as the prochiral olefins *trans*- and *cis*-stilbene and *trans*-β-methylstyrene. TBHP (5.5 M in n-decane) was used as an oxidant. Different molar ratios of the catalysts, 1 mol% and 0.1 mol% were investigated and ratio of substrate:TBHP = 1:2 was utilized in all reactions which were carried out at 22 and 55 °C. Catalytic reactions were investigated under air in 5 mL of solvent dichloromethane, chloroform or in the absence of a solvent. For all catalytic reactions, <1% conversion of all substrates to their epoxides was observed in the absence of the molybdenum precatalyst and similarly, the oxidants alone without the catalyst were ineffective in any appreciable epoxidation of the chosen substrates.

During catalysis with complexes **1−5** at room temperature, an induction period is observed lasting from 30 min - 2 h depending on the catalyst with *cis*-cyclooctene (and 200 equiv. TBHP) which is attributed to the period of oxidative decarbonylation of the precatalyst to give the catalytically active species (see Figure 4.4).[20,21,62] ^{1}H and ^{13}C kinetic NMR experiments have shown that the complexes are stable under oxidative conditions and the ester side chain does not dissociate, neither during oxidative decarbonylation of the precatalyst nor during the catalytic epoxidation reaction (see Chapters 5 and 6).

Since complete decarbonylation for complexes **1-5** (indicated by the induction period in conversion *vs.* time plots) is slower than for complexes [CpMo(CO)$_3$X] (X = Me, Cl), the concentration of active species present initially in the mixture is very small until about 30 min after addition of TBHP. Once a critical amount of oxidized species is present in the reaction mixture, epoxidation of the substrate is quite fast. **1-5** are active catalysts for the epoxidation of *cis*-cyclooctene forming cyclooctene oxide selectively and quantitatively within 2-4 h (1 mol% catalyst) at room temperature in dichloromethane (Figure 4.4(a)). Activities in the range of 120-190 cycles per hour are observed for cyclooctene oxide formation (see Table 4.3 and Table 4.5 in SI), which increase marginally to 230 – 360 h^{-1} when 0.1 mol% of the precatalysts are used (Figure 4.4(b)). In the absence of a co-solvent, catalytic epoxidation of *cis*-cyclooctene was accompanied with evolution of heat, indicating that oxidative decarbonylation is exothermic. This is, at least in part, responsible for faster conversions to cyclooctene oxide along with the smaller dilution factor and thus increased TOFs of 210-500 h^{-1} (Figure 4.4(c)).

Table 4.3. Yield%[a] and TOF[b] range observed for epoxidation of olefin substrates with complexes **1-5**; 1 mol% catalyst, CH_2Cl_2 solvent at 22 °C unless stated otherwise.

S. No.	Substrate	Yield % (at 4 h)	Yield % (at 24 h)	TOF (h^{-1})
(a)	*cis*-cyclooctene	99	99	120 – 190
(b)	*cis*-cyclooctene + 0.1 mol% catalyst	22 – 44	99	230 – 360
(c)	*cis*-cyclooctene (no co-solvent)	99	99	210 – 500
(d)	*cis*-cyclooctene, 55 °C, $CHCl_3$	99	99	775 – 1190
(e)	*cis*-stilbene	28 – 52[c]	43 – 60	20 – 40
(f)	*trans*-stilbene	34 – 48[c]	48 – 63	30 – 90
(g)	1-octene	16 – 27	21 – 38	10 – 40
(h)	*trans*-β-methylstyrene	51 – 64	62 – 77	50 – 100

[a] GC-MS yield of corresponding epoxides. [b] Determined at the steepest part of conversion *vs* time slope. [c] Only their respective epoxides were formed.

At a higher reaction temperature of 55 °C, conversion of cis-cyclooctene to its epoxide is very fast and quantitative yields are obtained within 10 min of addition of the oxidant (Figure 4.4(d)). There is no clearly discernible induction period for these catalyses and TOFs in the range of 775-1190 h^{-1} are obtained. For catalysis with complexes **2** and **3**, within 5 min of addition of TBHP, rapid evolution of gases is observed with a simultaneous increase in temperature over 55 °C. This temperature increase is a result of oxidative decarbonylation of the tricarbonyl complexes and responsible for the high activity (as indicated by TOFs) of the complexes. During catalysis with complexes **1**, **4** and **5** such violent exothermic reactions are not observed, however, due to the high reaction temperature, the conversion of *cis*-cyclooctene is very fast and for all complexes, quantitative yield of the epoxide is obtained within 15 min.

The stilbene substrates are selectively transformed to their respective epoxides in yields of up to 50% within 4 h and these yields only marginally increase up to 60% after 24 h at room temperature (Figure 4.4(e) and (f)). More challenging substrate 1-octene is converted to the epoxide slowly, and yields of about 40% are obtained after 24 h at room temperature with 1 mol% of the catalysts. There is little influence of the increasing steric bulk of the ester alkyl group from ethyl (**1, 2** and **3**) to menthyl (**4**) or bornyl (**5**) on catalytic activity, which is not surprising as the electronic situation at the metal centre is similar for the three α-carbon unsubstituted precatalysts. Additionally, the reaction site is farther from the ethyl group or sterically encumbered menthyl or bornyl groups located at the end of the oxoalkyl side chain.

Although epoxidation of *trans*-β-methylstyrene is selective towards the epoxide product, there is negligible (with experimental error) stereo-differentiation during catalysis and only equimolar amounts of (2*S*,3*S*)-2-methyl-3-phenyloxirane and (2*R*,3*R*)-2-methyl-3-phenyloxirane are obtained. Poor ee obtained with these complexes can be reasoned to be due to location of chiral information being still too far away from the reactive metal centre. Complexes **2** and **3** with methyl and phenyl substituent on Mo-$^{\alpha}$C respectively are in general, more active than complexes **1**, **4, 5** which are unsubstituted at this position. Furthermore, **3** displays higher activity than **2** for nearly all substrates tested. This trend may be accounted for by the fact that the molybdenum centre is rendered slightly more electron deficient due to presence of methyl and phenyl groups compared to precatalysts **1**, **4** and **5**.

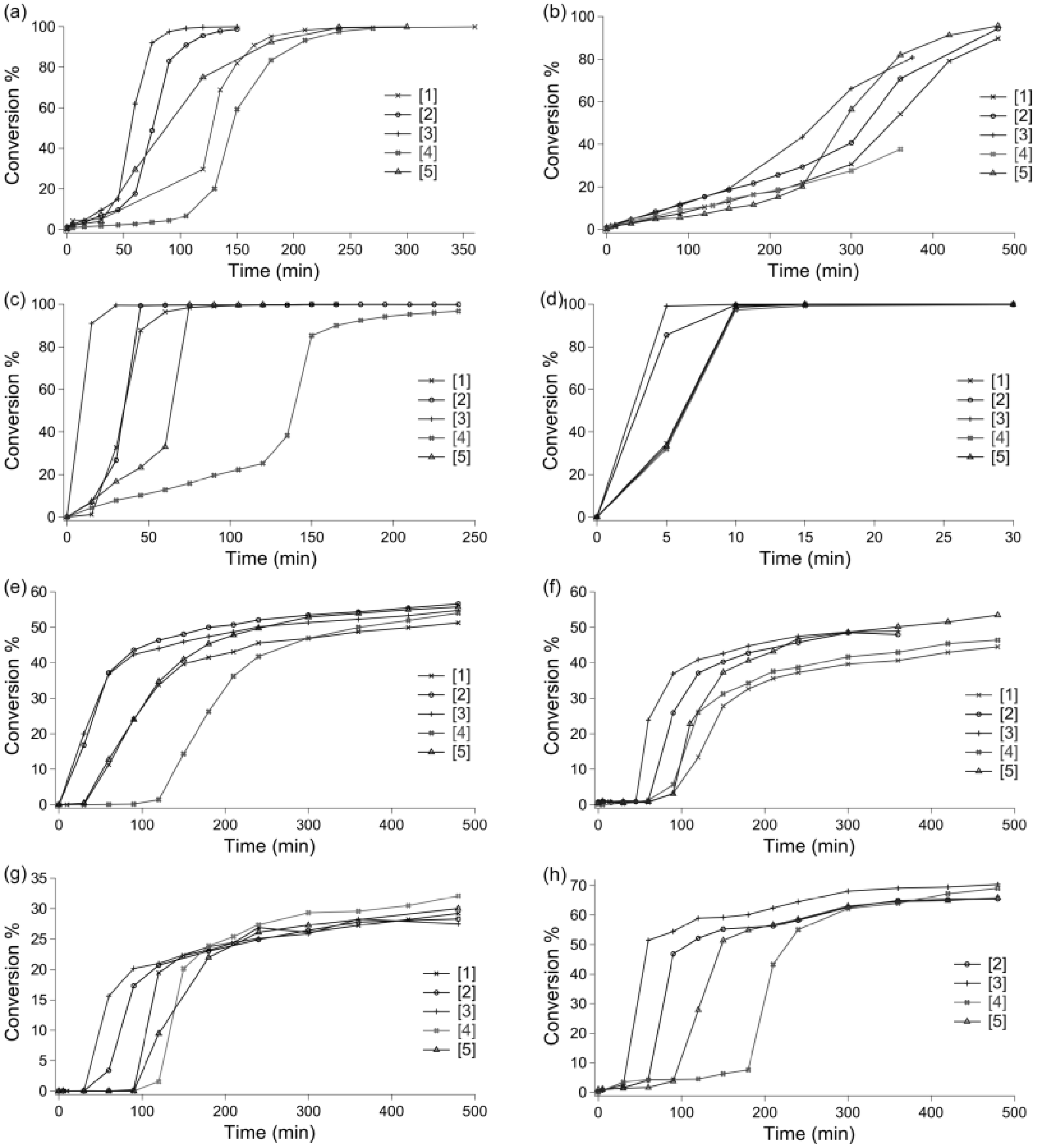

Figure 4.4. Conversion *vs.* time plot for different substrates with 1 mol% complexes 1-5 and TBHP oxidant at room temperature in dichloromethane unless stated otherwise. (a) *cis*-cyclooctene, (b) *cis*-cyclooctene + 0.1 mol% catalyst, (c) *cis*-cyclooctene, no co-solvent, (d) *cis*-cyclooctene, 55 °C, $CHCl_3$ solvent, (e) *cis*-stilbene, (f) *trans*-stilbene, (g) 1-octene, (h) *trans*-β-methylstyrene; ratio catalyst:substrate:oxidant = 1:100:200.

For catalysis reactions performed at room temperature with all complexes in CH_2Cl_2, the reaction vessel was immersed in an oil bath to control ambient temperature. However, as mentioned before, an increase in temperature was observed on addition of TBHP to the cis-cyclooctene substrate mixture with complexes **2** and **3**, but not for 1-octene, stilbene substrates or trans-β-methylstyrene.

The mechanism of oxidative decarbonylation and the nature of oxidized species formed during the transformation of Mo(II) precatalysts to Mo(VI) complexes has not been addressed in literature until now. Hence a satisfactory explanation for why oxidative decarbonylation should be quite exothermic for some complexes and not others, and observed during catalytic epoxidation of some substrates and not others is not available. One argument might be made from the slower reactivity of less nucleophilic 1-octene or sterically bulky stilbene or methylstyrene substrates and thus slower, less 'violent' reactions. However, we consider such an explanation to be insufficient and are undertaking efforts to resolve this issue.

4.3.7 Catalytic Activity (TOFs) and ^{95}Mo NMR Chemical Shift

Turnover frequencies (TOFs) calculated for epoxidation of *cis*-cyclooctene at room temperature in CH_2Cl_2 solvent catalyzed by complexes **1**, **2** and **4** are similar at *ca.* 120 h^{-1} (see Table 4.5) but for complexes **3** and **5** they are slightly higher at 180 h^{-1} under these conditions. This implies that both electronic and steric parameters of the side chain X in [$CpMo(CO)_3X$] complexes determine the catalytic activity at room temperature. From experimental observations it is known that in the induction stage of epoxidation, oxidative decarbonylation results in the formation of the catalytically active dioxo and oxo-peroxo complexes. Additionally, this reaction is exothermic to an appreciable degree in some cases (α-C substituted **2** and **3**) and not for others (unsubstituted complexes **1**, **4** and **5**) when 1 mol% of the catalyst is used for epoxidation of *cis*-cyclooctene. The increase in temperature thus increases the rate of the epoxidation reaction more in the initial phase which gradually slows with time. Furthermore, when reaction progress is illustrated in conversion% *vs.* time plots for the different complexes, it is obvious that the two reactions − oxidative decarbonylation and catalytic epoxidation are not mutually exclusive and therefore a true sigmoidal curve is not obtained. Therefore, when TOFs are calculated for the steepest part of the conversion curves, and considered as a parameter to evaluate activity of a class of structurally similar precatalysts, changes that occur during the induction period must be taken into account.

^{95}Mo chemical shifts for complexes **1, 4** and **5** are similar, seen at ca. -1550 ppm. For complexes **2** and **3**, the chemical shifts are observed at -1484 ppm and -1349 ppm respectively (Table 4.4). These lie in between the ^{95}Mo shift for known tricarbonyl complexes [$CpMo(CO)_3Cl$] (at -887 ppm) and [$CpMo(CO)_3CH_3$] (at -1736 ppm).

The trend in chemical shifts (−Cl compared to $-CH_3$ complex) can be interpreted to indicate that an electron withdrawing substituent at the Mo centre shows a downfield shift in comparison to an electron donating group.[39] This implies that the phenyl group in **3** makes the Mo centre more electron deficient than the methyl substituent in **2** which is in accordance with expected substituent effects ($-CH_3$ *vs.* $-C_6H_5$ at α-C in conjunction with ester functional group). Additionally, in both complexes **2** and **3** there is a net –I effect on the metal (which is only partly offset by the elongation of Mo−αC9 bond length) in comparison to complexes **1**, **4** and **5**.

Table 4.4. ^{95}Mo NMR shifts[a] and TOFs of epoxidation of *cis*-cyclooctene at 55 °C with TBHP (catalyst:substrate:TBHP = 1:100:200) for complexes **1−5**, [CpMo(CO)$_3$Cl] and [CpMo(CO)$_3$CH$_3$] in CHCl$_3$.

Complex	^{95}Mo chemical shift (ppm)	TOF (h^{-1})	Reference
1	-1546	775	This work
2	-1484	1024	This work
3	-1349	1187	This work
4	-1553	784	This work
5	-1555	781	This work
[CpMo(CO)$_3$Cl]	-887	1300	20
[CpMo(CO)$_3$(CH$_3$)]	-1736	820	40

[a] All signals are referenced to 2M Na$_2$MoO$_4$ in D$_2$O set to 0 ppm.

Thus in our understanding, TOFs determined at room temperature for the purpose of judging catalytic performance are insufficient since oxidative decarbonylation is exothermic in some cases (see above) and not others. Since this exothermicity of decarbonylation process can also increase the reaction rate and result in faster conversion of the substrate to the epoxide, TOFs determined from these reactions would be influenced by the “induction phase”.

We then chose to study the reactions at a higher temperature, specifically 55°C, since catalytic reactions reported in almost every related scientific literature of CpMo epoxidation catalysts[10] utilize these high temperature conditions. For sake of consistency and comparison we employed this high temperature as well.

In the limited number of literature reports that do report conversion *vs.* time plots, at 55°C the induction phase is usually not observed. Once we could eliminate the influence of the conversion of Mo(II) to Mo(VI) complexes on epoxidation activity in this manner, the differences in catalytic activity (illustrated in Figure 4.4(d) and Table 4.5) and ^{95}Mo chemical shifts for **1−5** became easier to evaluate than at room temperature.

At 55 °C, while TOFs for the unsubstituted complexes **1**, **4** and **5** are similar at 780 h^{-1} and ^{95}Mo shifts average at -1550 ppm; TOFs of 1024 h^{-1} and 1187 h^{-1} for complexes **2** and **3** respectively are in agreement with the trend of chemical shift – relatively more electron ‘rich’ metal centre in **2** (-1484 ppm) performs slightly poorly than complex **3** (-1349 ppm) in the epoxidation of *cis*-cyclooctene substrate. Even as the ^{95}Mo shifts of complexes **1−5** are in between those for [CpMo(CO)$_3$Cl] and [CpMo(CO)$_3$CH$_3$], the differences in catalytic activity when compared to complexes **1-5** are not very large (Table 4.3).[10] The order of TOFs is therefore –Cl > **3** > **2** > −CH$_3$ ≈ **4** ≈ **5** ≈ **1**; which is in good agreement with the ^{95}Mo chemical shift values.

It can be concluded that a trend in catalytic activity on the basis of stereoelectronic effects of side chain substituents is possible by considering ^{95}Mo NMR shifts. However, to explain the differences observed in catalytic activity, the fundamental differences in structure, stability and reactivity of the oxidized complexes (dioxo and oxo-peroxo)[22] cannot be entirely disregarded in favor of one parameter, i.e. ^{95}Mo chemical shifts. In addition, such a trend is observed only when initial phase of the epoxidation reaction is ignored, for example, by following reaction progress at a high temperature (55 °C).

Note that the above discussion does not intend to convey that such a correlation has a very broad scope. We do not believe ^{95}Mo chemical shifts can be used to predict catalytic activity of all [CpMo(CO)$_3$R] catalysts with R = any group. Complexes **1-5** are electronically (from IR data) and structurally (space group P212121 for **1** and **5**, Pbca for **2**) quite similar. Furthermore, their ^{95}Mo chemical shifts are similar as well (**1**, **4** and **5**; and **2** and **3**). Thus analysing the analytical data and outlining a trend in catalytic activity for these complexes is reasonable.

As such, electrophilicity (w.r.t. reactivity of the metal with olefin) and the Lewis acidic nature of the metal centre (indicated by the ^{95}Mo shifts, which are themselves quite sensitive to changes in structure and electronic effects of ligands) may be quite different. In this context, a universality of the proposed trend is both false and inaccurate. Lewis acidity of the metal centre and catalytic activity need not necessarily support each other. Therefore we restrict the discussion to only this small library of precatalysts.

4.4 Conclusion

Cyclopentadienyl molybdenum complexes with different oxoalkyl side chains have been synthesized and investigated for achiral and chiral epoxidation catalysis. The chiral ligands for the synthesized complexes are derived from cheap and readily available chiral pool compounds. A comparison between complexes substituted and unsubstituted at α-carbon to molybdenum has been presented. The former are more active for epoxidation of olefins on account of a more electron deficient metal centre and **3** proved to be the best catalyst for nearly all substrates. **1-5** display good activities in epoxidation catalysis at room temperature than most other half sandwich tricarbonyl Mo(II) complexes previously reported (TOFs mostly reported for epoxidation carried out at 55 °C, see Chapter 1), and unfortunately no stereoselectivity is achieved with prochiral substrates. Additionally, the stereoelectronic influences of side chain substituents in CpMo(CO)$_3$ complexes on observed catalytic activity in epoxidation reactions (TOFs) have been discussed using ^{95}Mo NMR data. It has been established that an electron deficient Mo centre in the tricarbonyl precatalysts, in general, gives oxidized dioxo and oxo-peroxo complexes that perform better in olefin epoxidation than a [CpMo(CO)$_3$R] complex where the metal centre is more electron rich.

4.5 References

[1] S. T. Oyama (ed.), Mechanisms in Homogeneous and Heterogeneous Epoxidation Catalysis, Elsevier, 2011.

[2] S. M. Bruno, B. Monteiro, M. S. Balula, C. Lourenço, A. A. Valente, M. Pillinger, P. Ribeiro-Claro, I. S. Gonçalves, Molecules 11 (2006) 298–308.

[3] A. Günyar, F. E. Kühn, J. Mol. Catal. A: Chem. 319 (2010) 108–113.

[4] A. M. Al-Ajlouni, A. Günyar, M.-D. Zhou, P. N. W. Baxter, F. E. Kühn, Eur. J. Inorg. Chem. 2009 (2009) 1019–1026.

[5] F. E. Kühn, A. M. Santos, M. Abrantes, Chem. Rev. 106 (2006) 2455–75.

[6] A. Günyar, M.-D. Zhou, M. Drees, P. N. W. Baxter, G. Bassioni, E. Herdtweck, F. E. Kühn, Dalton Trans. (2009) 8746–8754.

[7] A. Capapé, A. Raith, F. E. Kühn, Adv. Synth. Catal. 351 (2009) 66–70.

[8] C. Freund, W. A. Herrmann, F. E. Kühn, Top. Organomet. Chem. 22 (2007) 39–77.

[9] S. A. Hauser, M. Cokoja, M. Drees, F. E. Kühn, J. Mol. Catal. A: Chem. 363-364 (2012) 237–244.

[10] N. Grover, F. E. Kühn, Curr. Org. Chem. 16 (2012) 16–32.

[11] A. M. Martins, C. C. Romão, M. Abrantes, M. C. Azevedo, J. Cui, A. R. Dias, M. T. Duarte, M. A. Lemos, T. Lourenço, R. Poli, Organometallics 24 (2005) 2582–2589.

[12] C. Dinoi, M. Ciclosi, E. Manoury, L. Maron, L. Perrin, R. Poli, Chem. Eur. J. 16 (2010) 9572–84.

[13] P. M. Reis, C. A. Gamelas, J. A. Brito, N. Saffon, M. Gómez, B. Royo, Eur. J. Inorg. Chem. 2011 (2011) 666–673.

[14] V. V. K. M. Kandepi, J. M. S. Cardoso, B. Royo, Catal. Lett. 136 (2010) 222–227.

[15] T. Michel, M. Cokoja, V. Sieber, F. E. Kühn, J. Mol. Catal. A: Chem. 358 (2012) 159–165.

[16] P. Altmann, M. Cokoja, F. E. Kühn, Eur. J. Inorg. Chem. 2012 (2012) 3235–3239.

[17] T. Michel, D. Betz, M. Cokoja, V. Sieber, F. E. Kühn, J. Mol. Catal. A: Chem. 340 (2011) 9–14.

[18] F. E. Kühn, A. Scherbaum, W. A. Herrmann, J. Organomet. Chem. 689 (2004) 4149–4164.

[19] F. E. Kühn, A. M. Santos, W. A. Herrmann, Dalton Trans. (2005) 2483–2491.

[20] M. Abrantes, A. M. Santos, J. Mink, F. E. Kühn, C. C. Romão, Organometallics 22 (2003) 2112–2118.

[21] A. A. Valente, J. D. Seixas, I. S. Gonçalves, M. Abrantes, M. Pillinger, C. C. Romão, Catal. Lett. 101 (2005) 127–130.

[22] A. M. Al-Ajlouni, D. Veljanovski, A. Capapé, J. Zhao, E. Herdtweck, M. J. Calhorda, F. E. Kühn, Organometallics 28 (2009) 639–645.

[23] D. Betz, A. Raith, M. Cokoja, F. E. Kühn, ChemSusChem 3 (2010) 559–562.

[24] D. Betz, W. A. Herrmann, F. E. Kühn, J. Organomet. Chem. 694 (2009) 3320–3324.

[25] K. R. Jain, F. E. Kühn, Dalton Trans. (2008) 2221–2227.

[26] A. K. Yudin (ed.), Aziridines and Epoxides in Organic Synthesis, Wiley-VCH Weinheim, 2006.

[27] K. R. Jain, W. A. Herrmann, F. E. Kühn, Coord. Chem. Rev. 252 (2008) 556–568.

[28] J. A. Brito, B. Royo, M. Gómez, Catal. Sci. Technol. 1 (2011) 1109–1118.

[29] F. E. Kühn, J. Zhao, W. A. Herrmann, Tetrahedron: Asymmetry 16 (2005) 3469–3479.

[30] A. J. Burke, Coord. Chem. Rev. 252 (2008) 170–175.

[31] M. Abrantes, A. Sakthivel, C. C. Romão, F. E. Kühn, J. Organomet. Chem. 691 (2006) 3137–3145.

[32] M. Abrantes, F. A. A. Paz, A. A. Valente, C. C. L. Pereira, S. Gago, A. E. Rodrigues, J. Klinowski, M. Pillinger, I. S. Gonçalves, J. Organomet. Chem. 694 (2009) 1826–1833.

[33] J. Zhao, E. Herdtweck, F. E. Kühn, J. Organomet. Chem. 691 (2006) 2199–2206.

[34] T. S. Piper, G. Wilkinson, J. Inorg. Nucl. Chem. 3 (1956) 104–124.

[35] J. Zhao, A. Sakthivel, A. M. Santos, F. E. Kühn, Inorg. Chim. Acta 358 (2005) 4201–4207.

[36] A. Sakthivel, J. Zhao, F. E. Kühn, Stud. Surf. Sci. Catal. 156 (2005) 237–242.

[37] A. Capapé, A. Raith, E. Herdtweck, M. Cokoja, F. E. Kühn, Adv. Synth. Catal. 352 (2010) 547–556.

[38] J. K. P. Ariyaratne, A. M. Bierrum, M. L. H. Green, M. Ishaq, C. K. Prout, M. G. Swanwick, J. Chem. Soc. A. Inorg. Phys. Theor. (1969) 1309–1321.

[39] C. G. Young, M. Minelli, J. H. Enemark, G. Miessler, N. Janietz, H. Kauermann, J. Wachter, Polyhedron 5 (1986) 407–413.

[40] J. Zhao, A. M. Santos, E. Herdtweck, F. E. Kühn, J. Mol. Catal. A: Chem. 222 (2004) 265–271.

[41] G.R. Fulmer, A.J.M. Miller, N.H. Sherden, H.E. Gottlieb, A. Nudelman, B.M. Stoltz, J.E. Bercaw, K.I. Goldberg, Organometallics 29 (2010) 2176-2179

[42] APEX suite of crystallographic software. APEX 2 Version 2008.4. Bruker AXS Inc., Madison, Wisconsin, USA (2008).

[43] SAINT, Version 7.56a and SADABS Version 2008/1. Bruker AXS Inc., Madison, Wisconsin, USA (2008).

[44] Sheldrick, G. M. "SHELXS-97", Program for Crystal Structure Solution, Göttingen, (1997).

[45] Sheldrick, G. M. "SHELXL-97", University of Göttingen, Göttingen, Germany, (1998).

[46] Huebschle, C. B., Sheldrick, G. M. & Dittrich, B. “SHELXLE”, J. Appl. Cryst. 44 (2011) 1281-1284.

[47] International Tables for Crystallography, Vol. C, Tables 6.1.1.4 (pp. 500-502), 4.2.6.8 (pp. 219-222), and 4.2.4.2 (pp. 193-199), Wilson, A. J. C., Ed., Kluwer Academic Publishers, Dordrecht, The Netherlands, 1992.

[48] Spek, A. L. "PLATON", A Multipurpose Crystallographic Tool, Utrecht University, Utrecht, The Netherlands, (2010).

[49] E. R. Burkhardt, J. J. Doney, R. G. Bergman, C. H. Heathcock, J. Am. Chem. Soc.1987, 109, 2022–2039.

[50] R. B. King, M. B. Bisnette, A. Fronzaglia, J. Organomet. Chem. 5 (1966) 341–356.

[51] L. R. Hillis, R. C. Ronald, J. Org. Chem. 46 (1981) 3348–3349.

[52] R. B. King, J. Organomet. Chem. 100 (1975) 111–125.

[53] R. B. King, A. Fronzaglia, J. Am. Chem. Soc. 88 (1966) 709–712.

[54] J. K. P. Ariyaratne, M. L. H. Green, J. Chem. Soc. Res. (1964) 1–5.

[55] L. J. Todd, J. R. Wilkinson, J. P. Hickey, D. L. Beach, K. W. Barnett, J. Organomet. Chem. 154 (1978) 151–157.

[56] R. Mynott, H. Lehmkuhl, E.-M. Kreuzer, E. Joussen, Angew. Chem. Int. Ed. Engl. 29 (1990) 289–290.

[57] R. F. Jordan, E. Tsang, J. R. Norton, J. Organomet. Chem. 149 (1978) 53–56.

[58] J. W. Faller, A. S. Anderson, C.-C. Chen, J. Chem. Soc. D Chem. Comm. 13 (1969) 719–720.

[59] R. Poli, Organometallics 9 (1990) 1892–1900.

[60] R. B. King, L. W. Houk, Can. J. Chem. 47 (1969) 2959–2964.

[61] M. Abrantes, P. Neves, M. M. Antunes, S. Gago, F. A. Almeida Paz, A. E. Rodrigues, M. Pillinger, I. S. Gonçalves, C. M. Silva, A. A. Valente, J. Mol. Catal. A: Chem. 320 (2010) 19–26.

[62] M. K. Trost, R. G. Bergman, Organometallics 10 (1991) 1172–1178.

4.6 Supporting Information

1. (a) ^{1}H, (b) ^{13}C, (c) ^{95}Mo (d) IR spectra for complex **1**

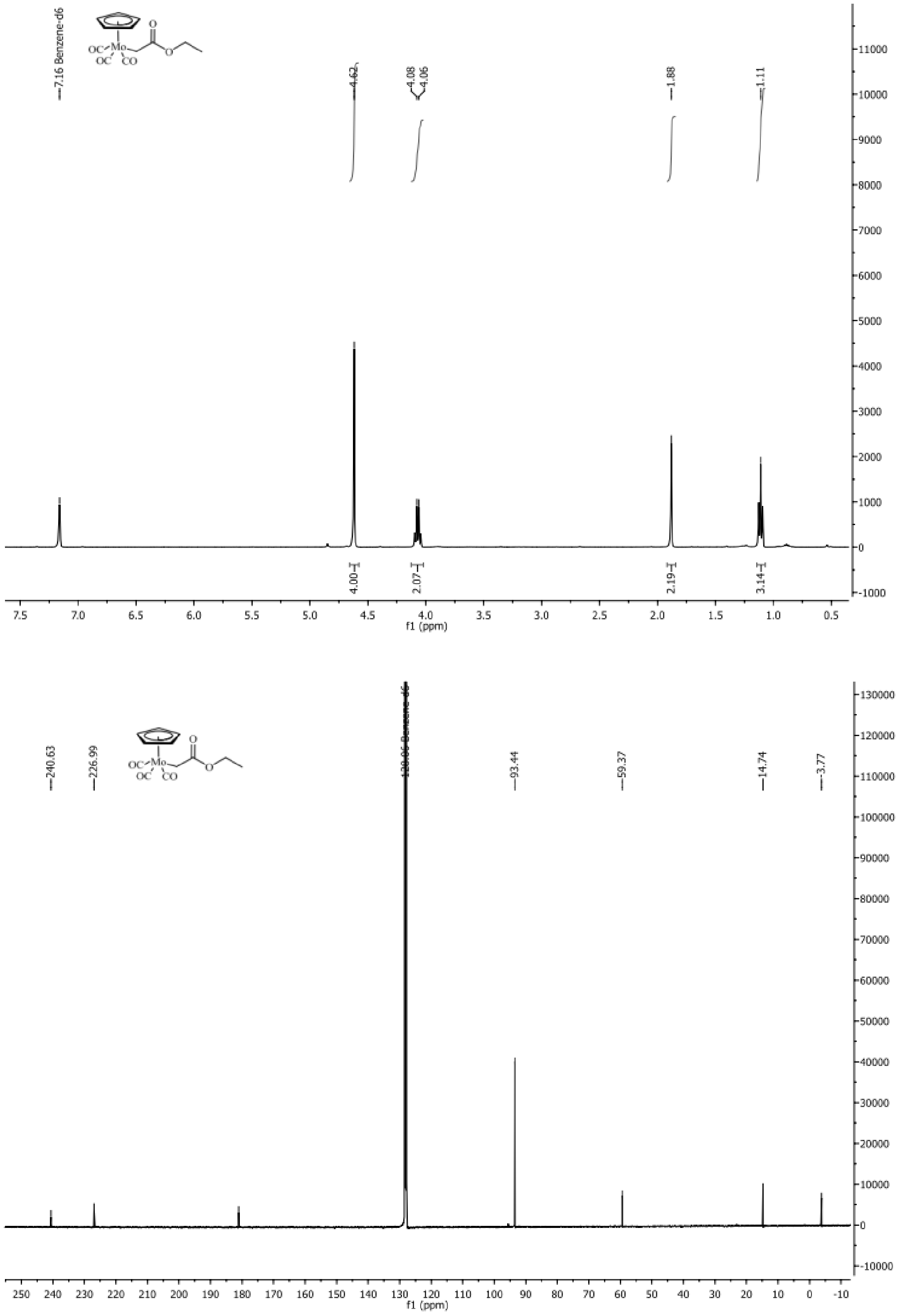

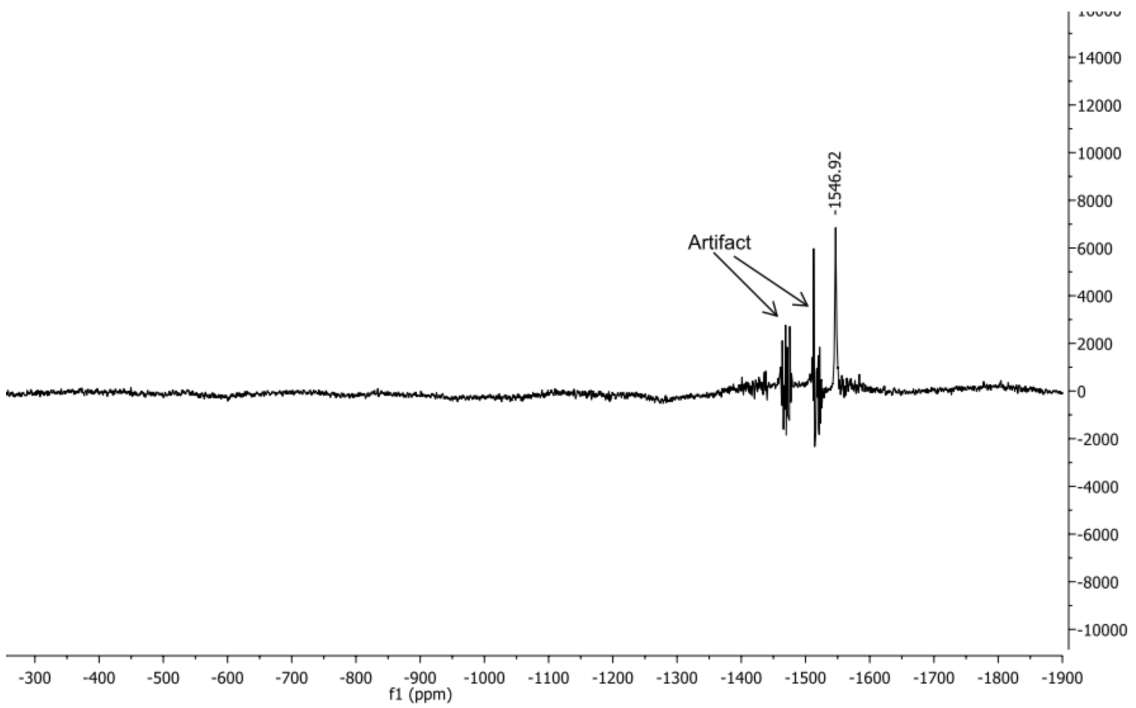
-1546.92
Artifact
14000
12000
10000
8000
6000
4000
2000
0
-2000
-4000
-6000
-8000
-10000
-300
-400
-500
-600
-700
-800
-900
-1000
-1100
-1200
-1300
-1400
-1500
-1600
-1700
-1800
-1900
f1 (ppm)

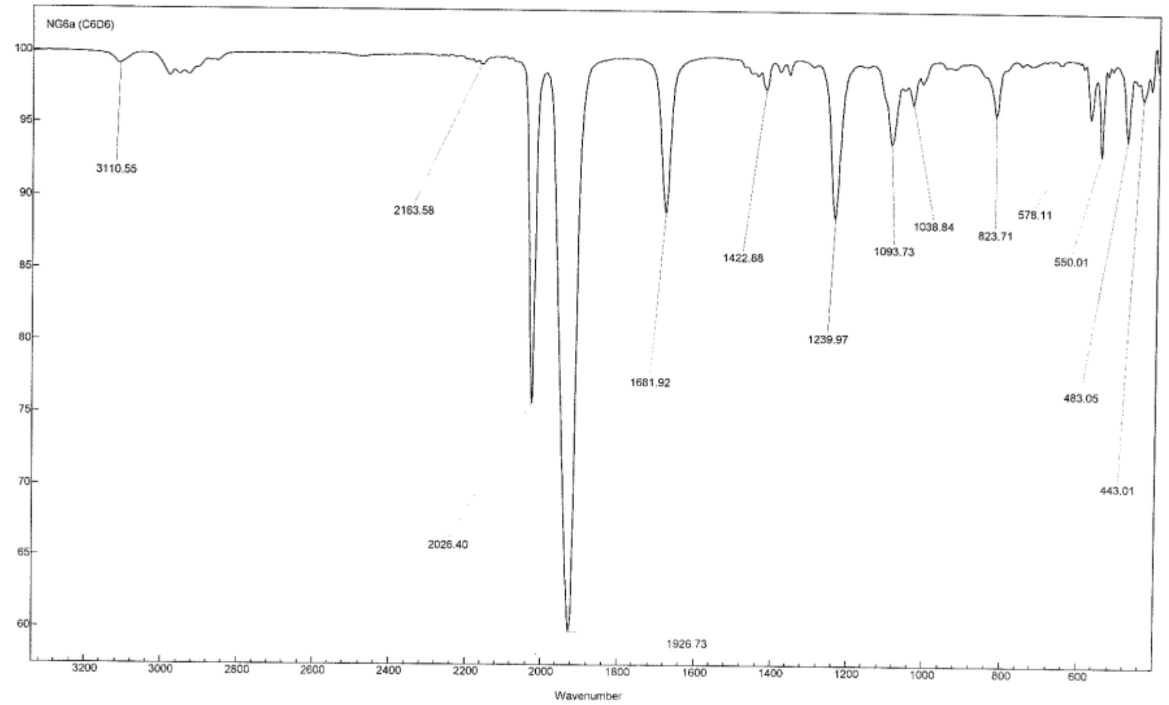
NG6a (C6D6)
100
95
90
85
80
75
70
65
60
3110.55
2163.58
2026.40
1926.73
1681.92
1422.88
1239.97
1093.73
1038.84
823.71
578.11
550.01
483.05
443.01
3200
3000
2800
2600
2400
2200
2000
1800
1600
1400
1200
1000
800
600
Wavenumber

2. (a) ^{1}H, (b) ^{13}C, (c) ^{95}Mo, (d) IR, (e) TGA-MS spectra for complex **2**

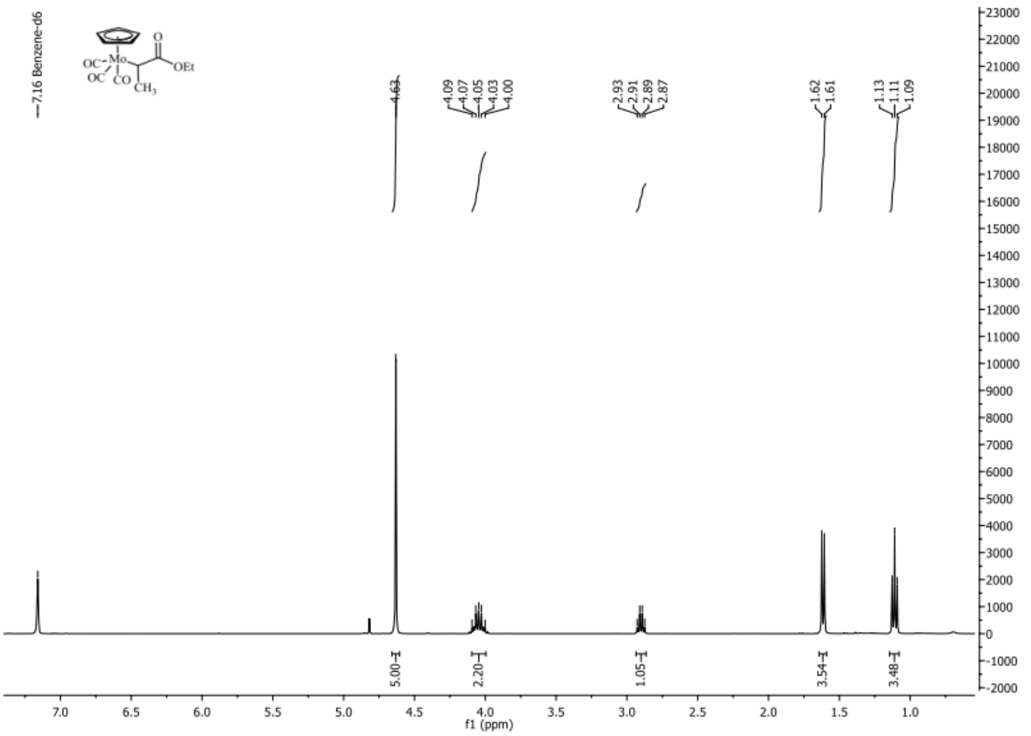

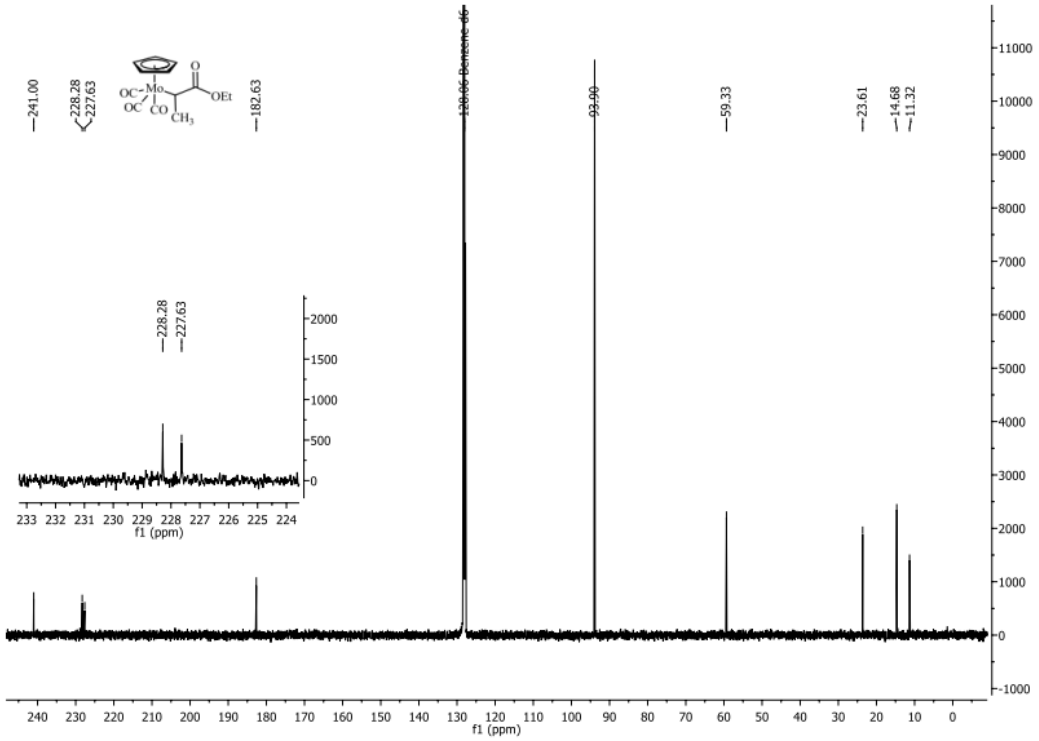

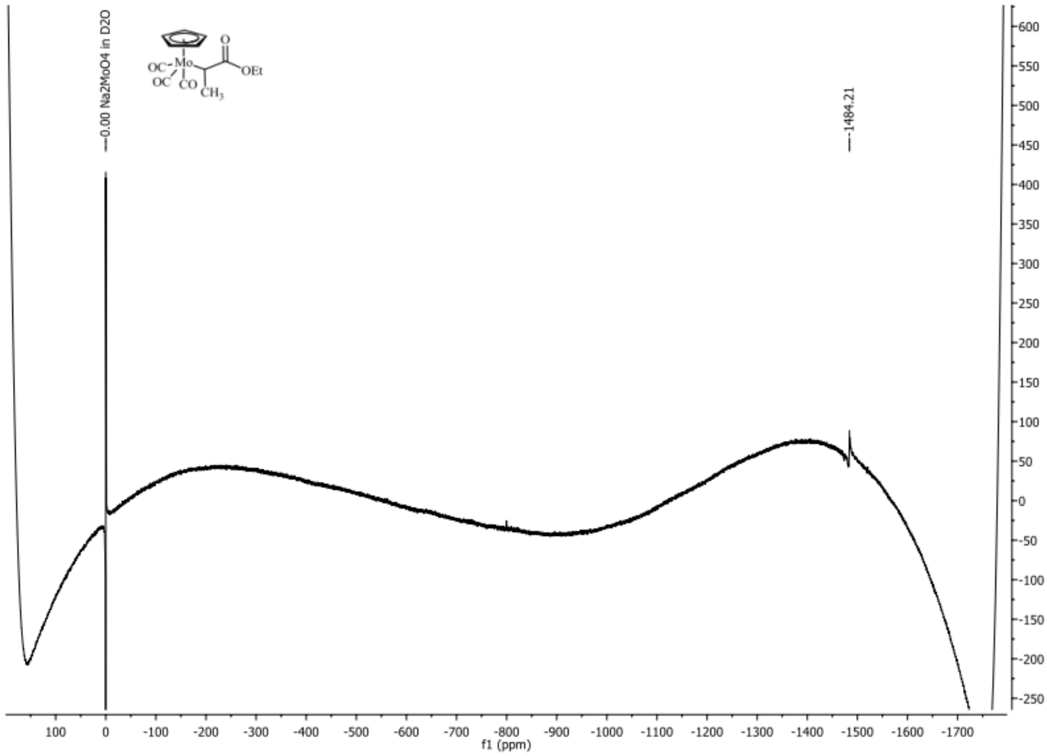
0.00 Na2MoO4 in D2O
-1484.21
OC
Mo
OC
CO
O
OEt
CH3
600
550
500
450
400
350
300
250
200
150
100
50
0
-50
-100
-150
-200
-250
100
0
-100
-200
-300
-400
-500
-600
-700
-800
-900
-1000
-1100
-1200
-1300
-1400
-1500
-1600
-1700
f1 (ppm)

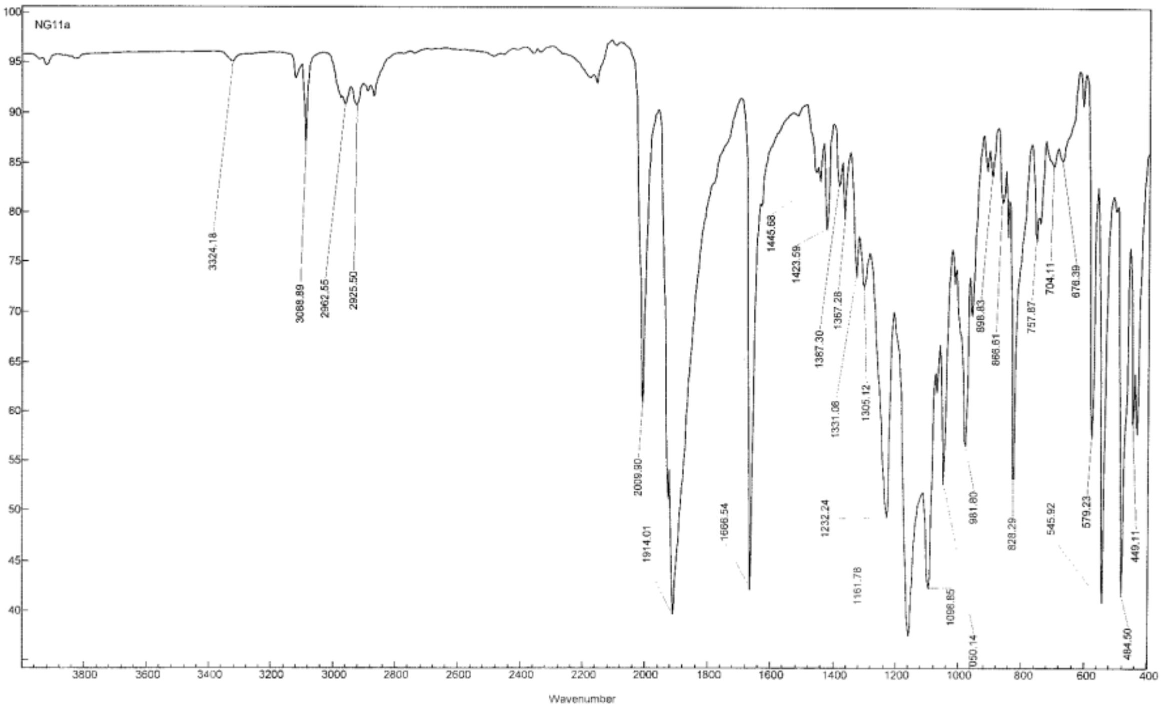
NG11a
100
95
90
85
80
75
70
65
60
55
50
45
40
3324.18
3068.89
2962.55
2925.50
2009.90
1914.01
1666.54
1445.68
1423.59
1387.30
1367.28
1331.08
1305.12
1232.24
1161.78
1098.85
050.14
981.80
898.83
868.61
828.29
757.87
704.11
678.39
545.92
579.23
484.50
449.11
3800
3600
3400
3200
3000
2800
2600
2400
2200
2000
1800
1600
1400
1200
1000
800
600
400
Wavenumber

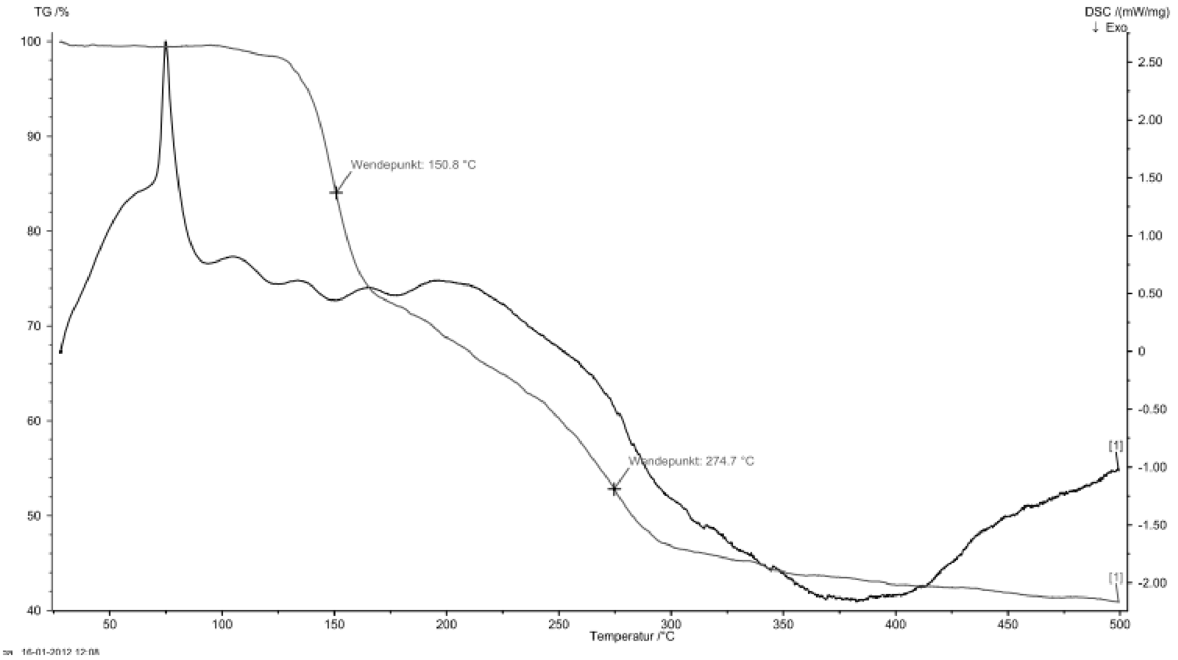

3. (a) ^{1}H, (b) ^{13}C, (c) ^{95}Mo, (d) IR, (e) TGA-MS spectra for complex **3**

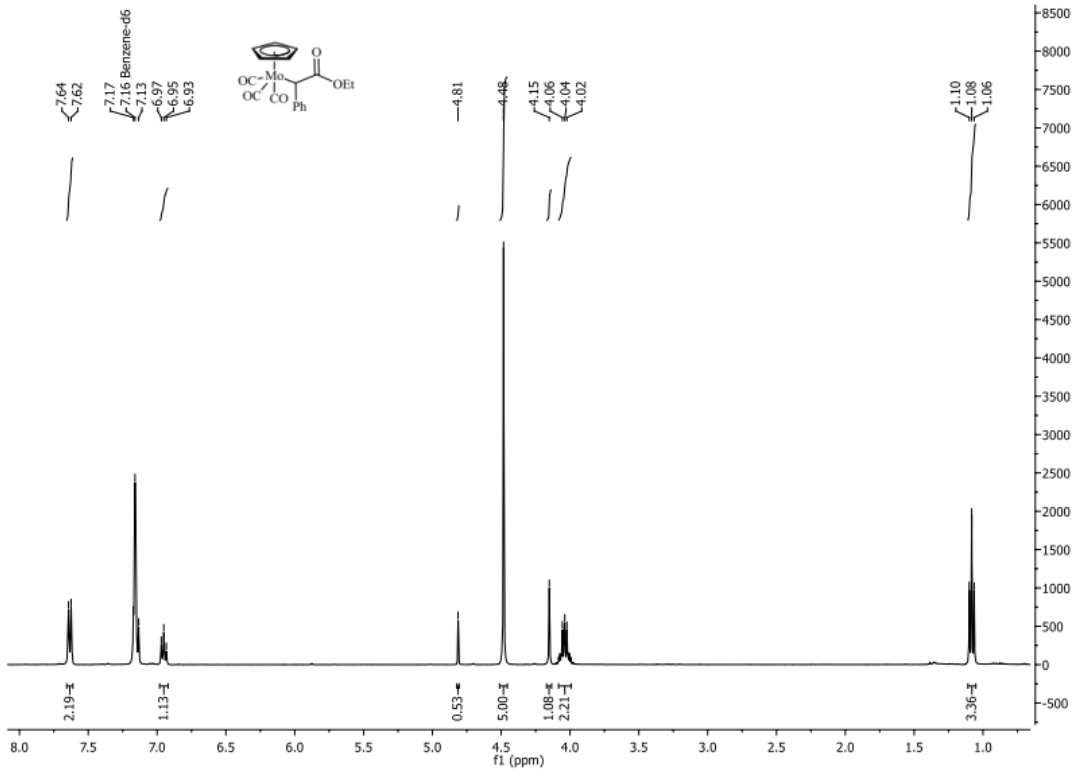

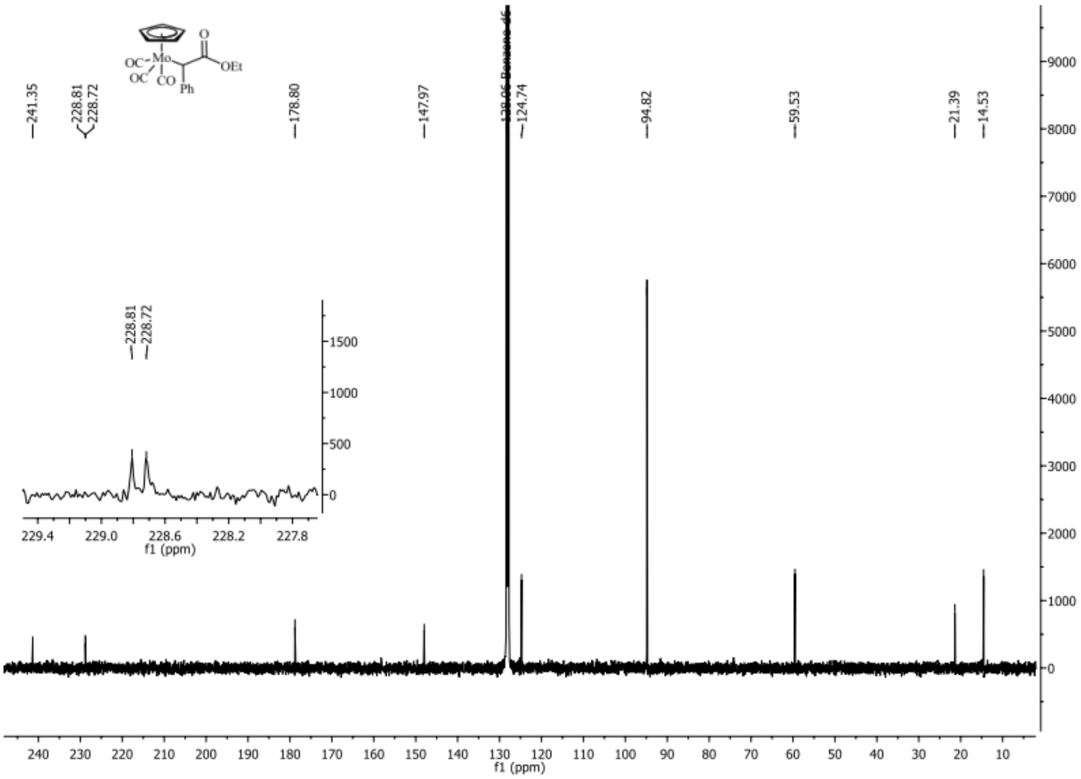
241.35
228.81
228.72
OC
Mo
OC
CO
O
OEt
Ph
178.80
147.97
128.06 Benzene-d6
124.74
94.82
59.53
21.39
14.53
228.81
228.72
1500
1000
500
0
229.4
229.0
228.6
228.2
227.8
f1 (ppm)
9000
8000
7000
6000
5000
4000
3000
2000
1000
0
240
230
220
210
200
190
180
170
160
150
140
130
120
110
100
90
80
70
60
50
40
30
20
10
f1 (ppm)

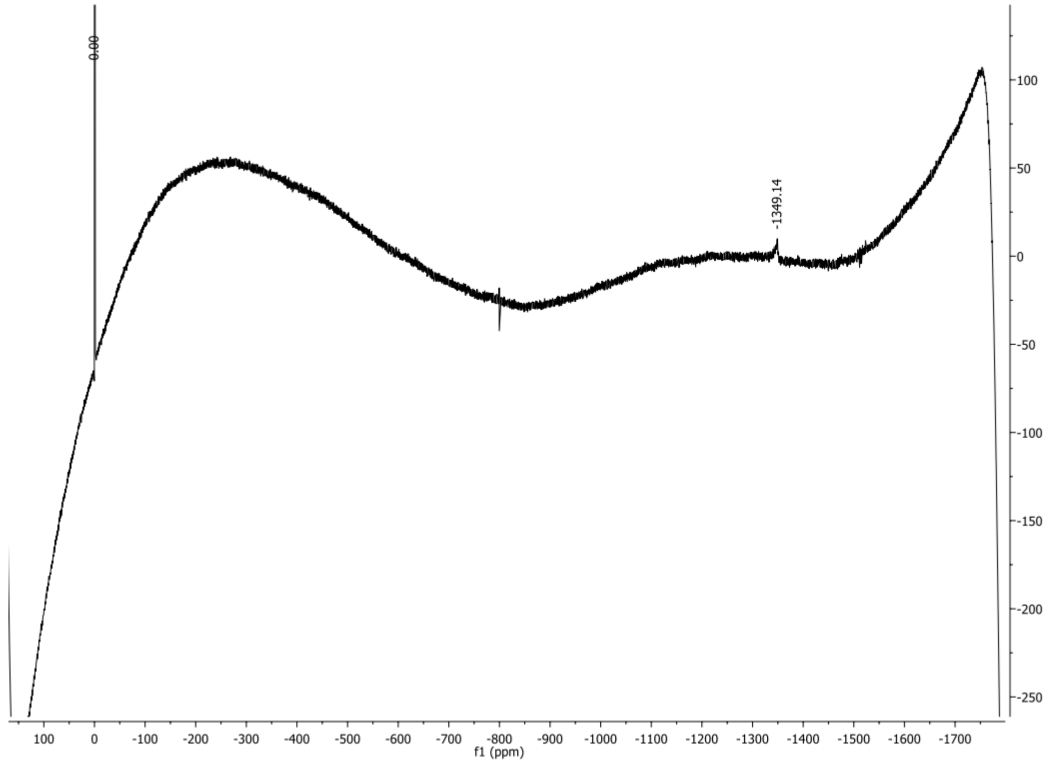
0.00
-1349.14
100
50
0
-50
-100
-150
-200
-250
100
0
-100
-200
-300
-400
-500
-600
-700
-800
-900
-1000
-1100
-1200
-1300
-1400
-1500
-1600
-1700
f1 (ppm)

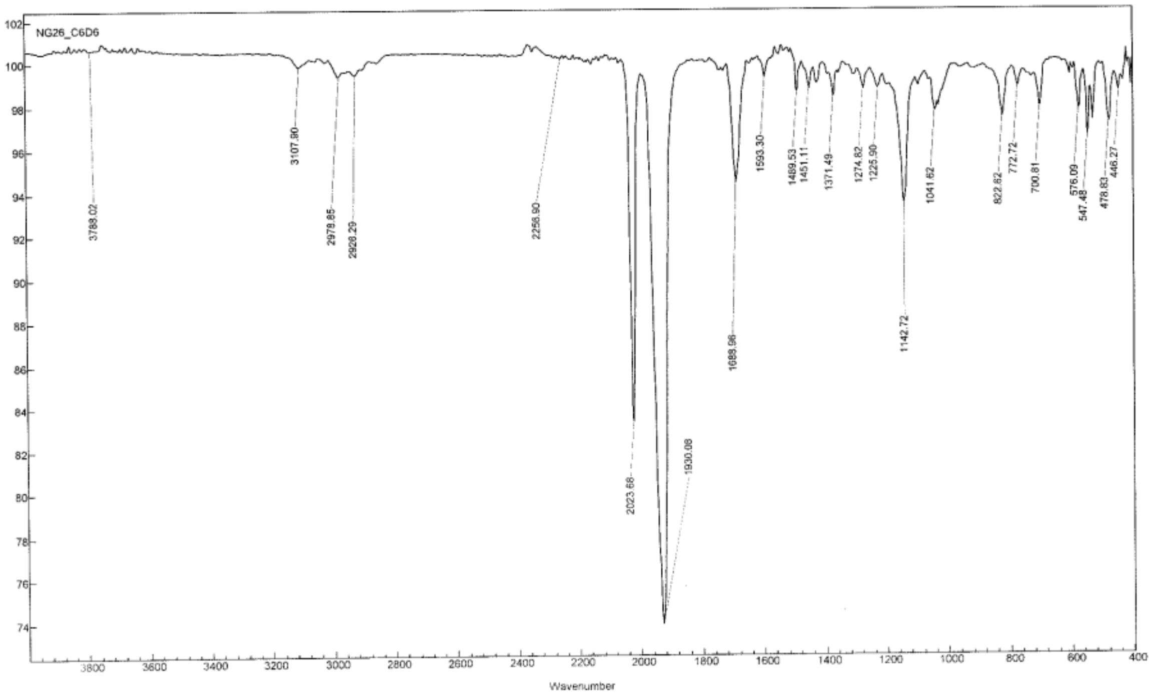
NG26_C6D6
102
100
98
96
94
92
90
88
86
84
82
80
78
76
74
3788.02
3107.80
2978.85
2928.29
2258.90
2023.68
1930.08
1688.96
1593.30
1489.53
1451.11
1371.49
1274.82
1225.90
1142.72
1041.62
822.82
772.72
700.81
576.09
547.48
478.83
446.27
3800
3600
3400
3200
3000
2800
2600
2400
2200
2000
1800
1600
1400
1200
1000
800
600
400
Wavenumber

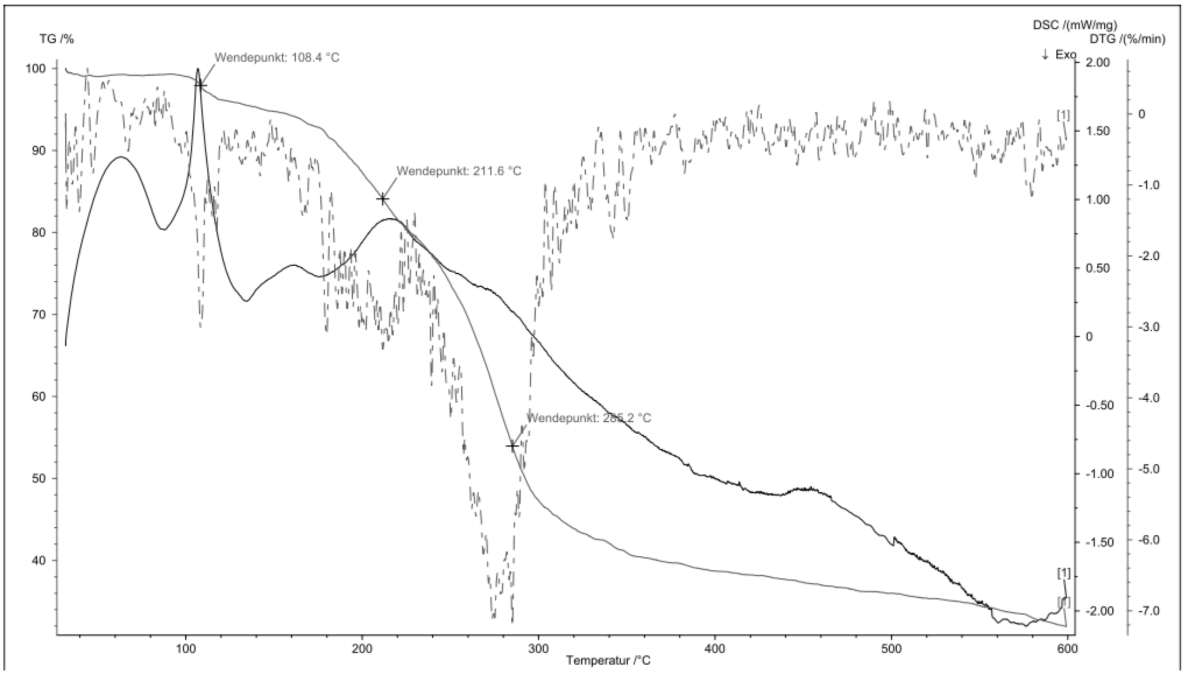
TG /%
DSC /(mW/mg)
DTG /(%/min)
↓ Exo
Wendepunkt: 108.4 °C
Wendepunkt: 211.6 °C
Wendepunkt: 285.2 °C
100
90
80
70
60
50
40
2.00
1.50
1.00
0.50
0
-0.50
-1.00
-1.50
-2.00
0
-1.0
-2.0
-3.0
-4.0
-5.0
-6.0
-7.0
[1]
[1]
[1]
100
200
300
400
500
600
Temperatur /°C

4. (a) ^{1}H, (b) ^{13}C, (c) ^{95}Mo, (d) IR, (e) TGA-MS spectra for complex **4**.

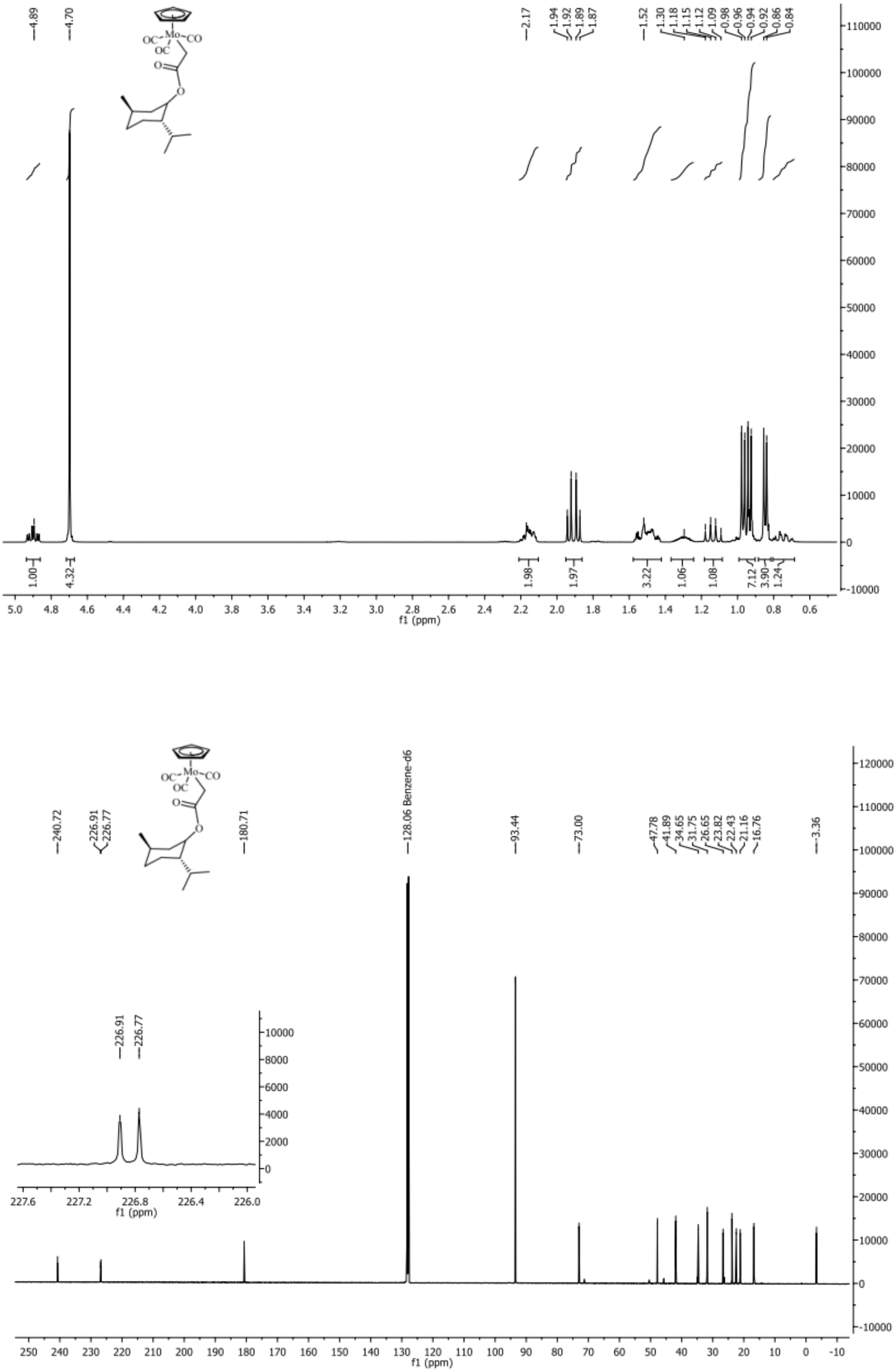

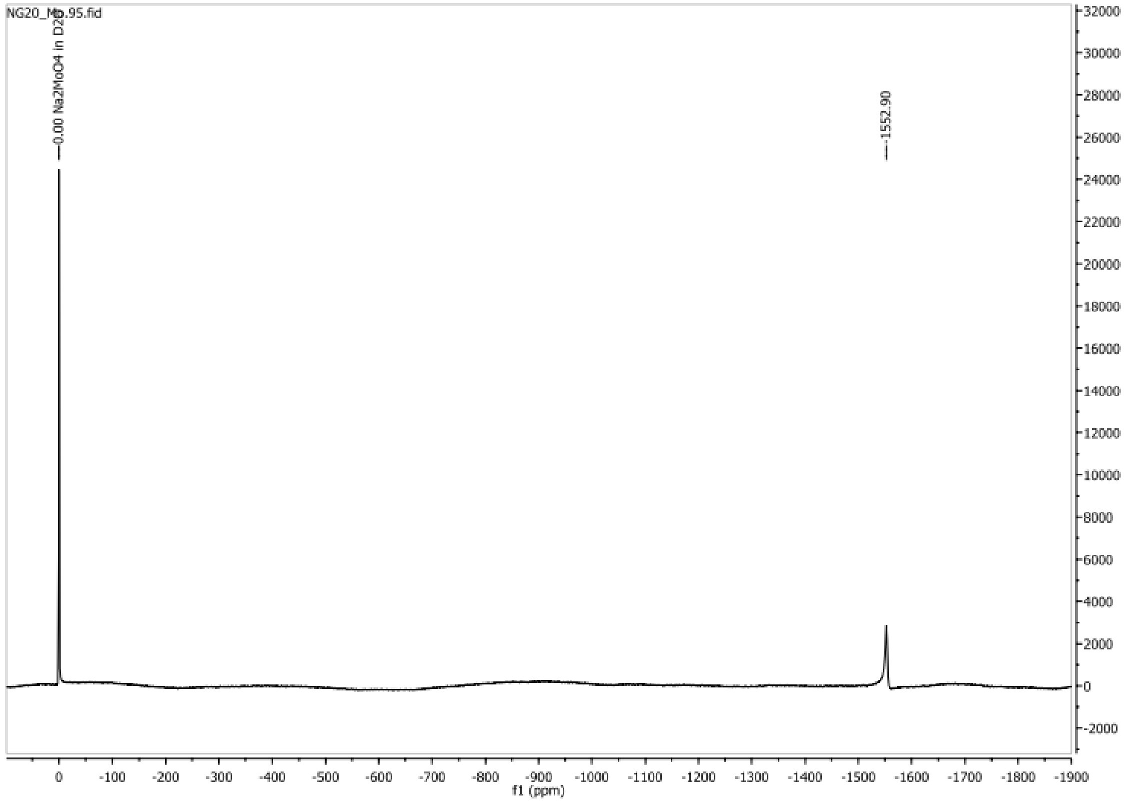
NG20_Mo.95.fid
0.00 Na2MoO4 in D2O
-1552.90
32000
30000
28000
26000
24000
22000
20000
18000
16000
14000
12000
10000
8000
6000
4000
2000
0
-2000
0
-100
-200
-300
-400
-500
-600
-700
-800
-900
-1000
-1100
-1200
-1300
-1400
-1500
-1600
-1700
-1800
-1900
f1 (ppm)

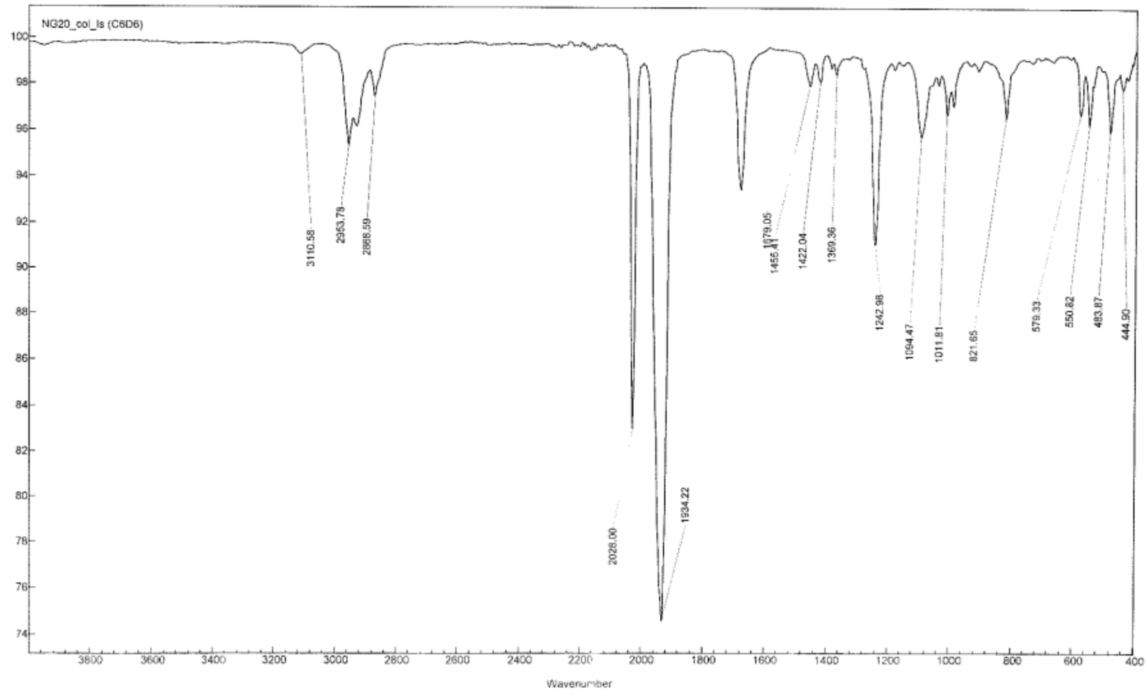
NG20_col_ls (C6D6)
100
98
96
94
92
90
88
86
84
82
80
78
76
74
3110.58
2953.78
2868.59
2028.00
1934.22
1679.05
1455.41
1422.04
1369.36
1242.98
1094.47
1011.81
821.65
579.33
550.82
483.87
444.90
3800
3600
3400
3200
3000
2800
2600
2400
2200
2000
1800
1600
1400
1200
1000
800
600
400
Wavenumber

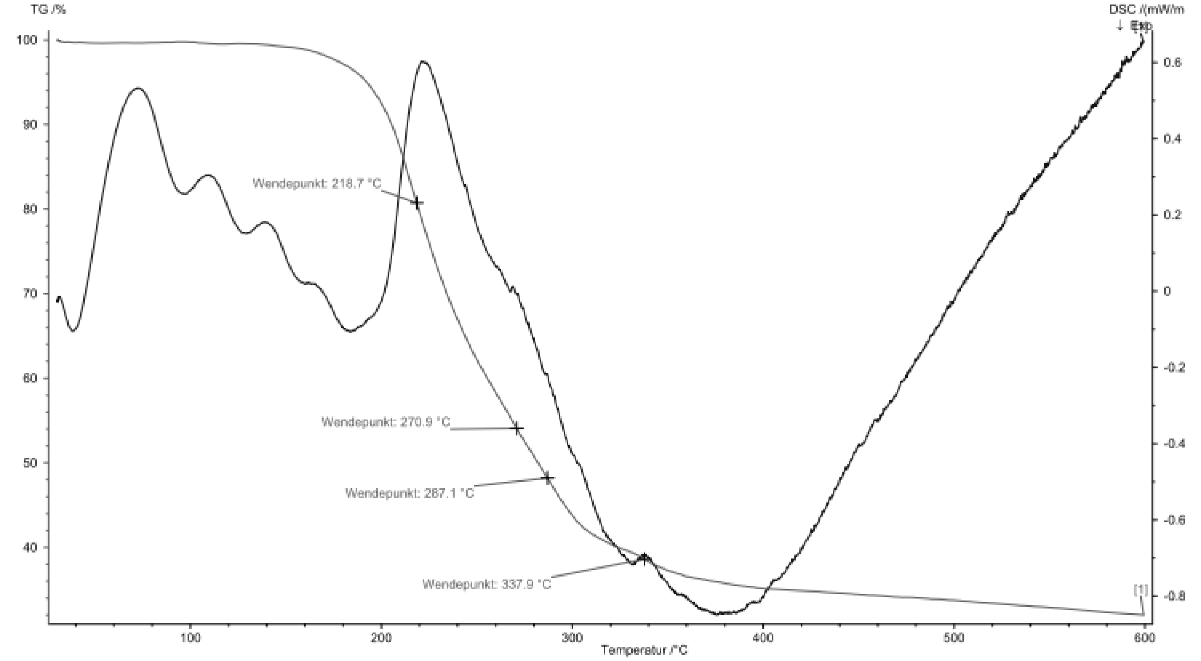

5. (a) ^{1}H, (b) ^{13}C, (c) ^{95}Mo, (d) IR, (e) TGA-MS spectra for complex **5**

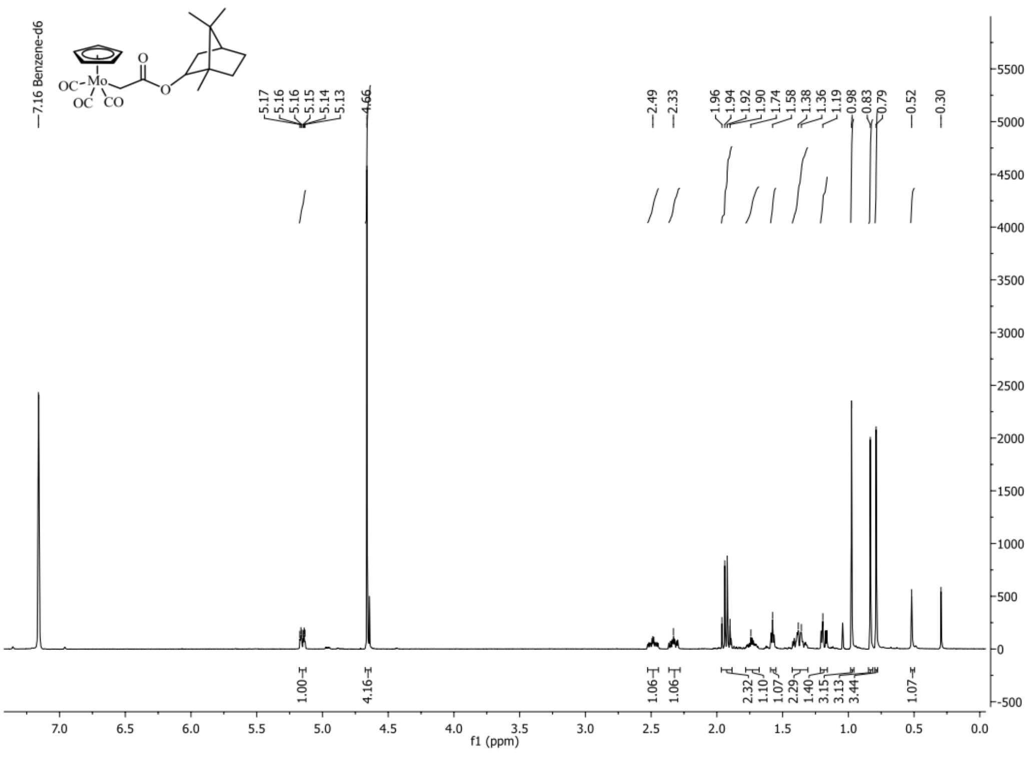

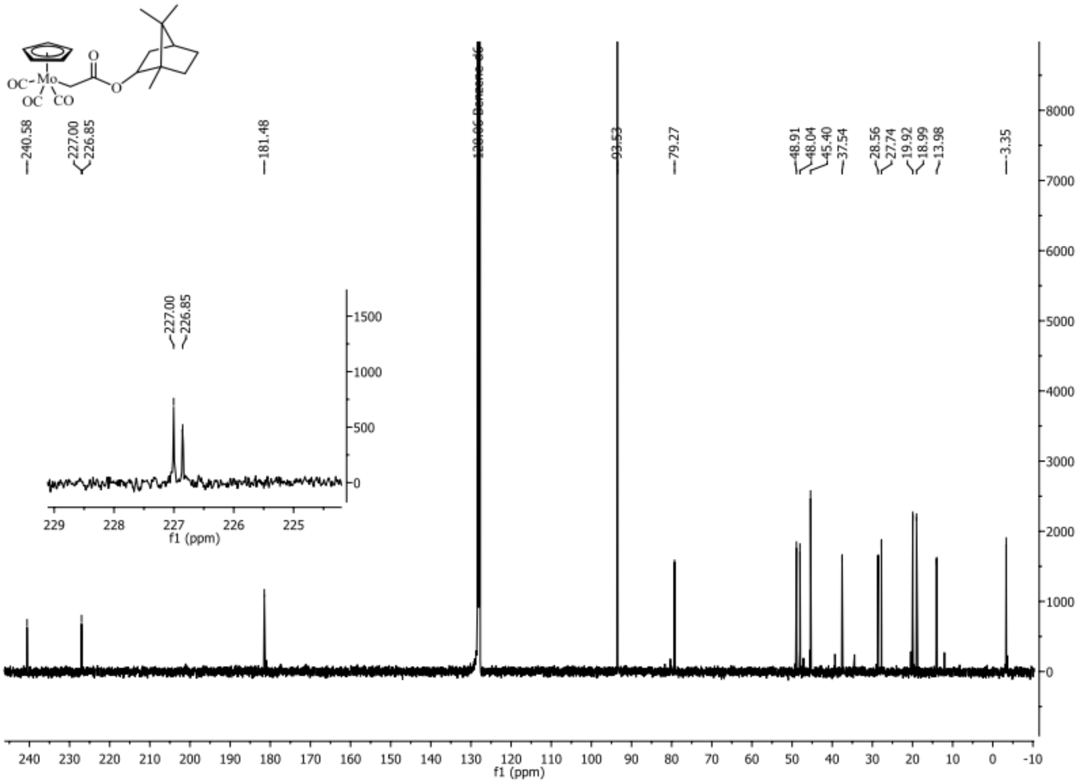
OC
Mo
OC
CO
O
O
240.58
227.00
226.85
181.48
128.06 Benzene-d6
93.53
79.27
48.91
48.04
45.40
37.54
28.56
27.74
19.92
18.99
13.98
-3.35
8000
7000
6000
5000
4000
3000
2000
1000
0
227.00
226.85
1500
1000
500
0
229
228
227
226
225
f1 (ppm)
240
230
220
210
200
190
180
170
160
150
140
130
120
110
100
90
80
70
60
50
40
30
20
10
0
-10
f1 (ppm)

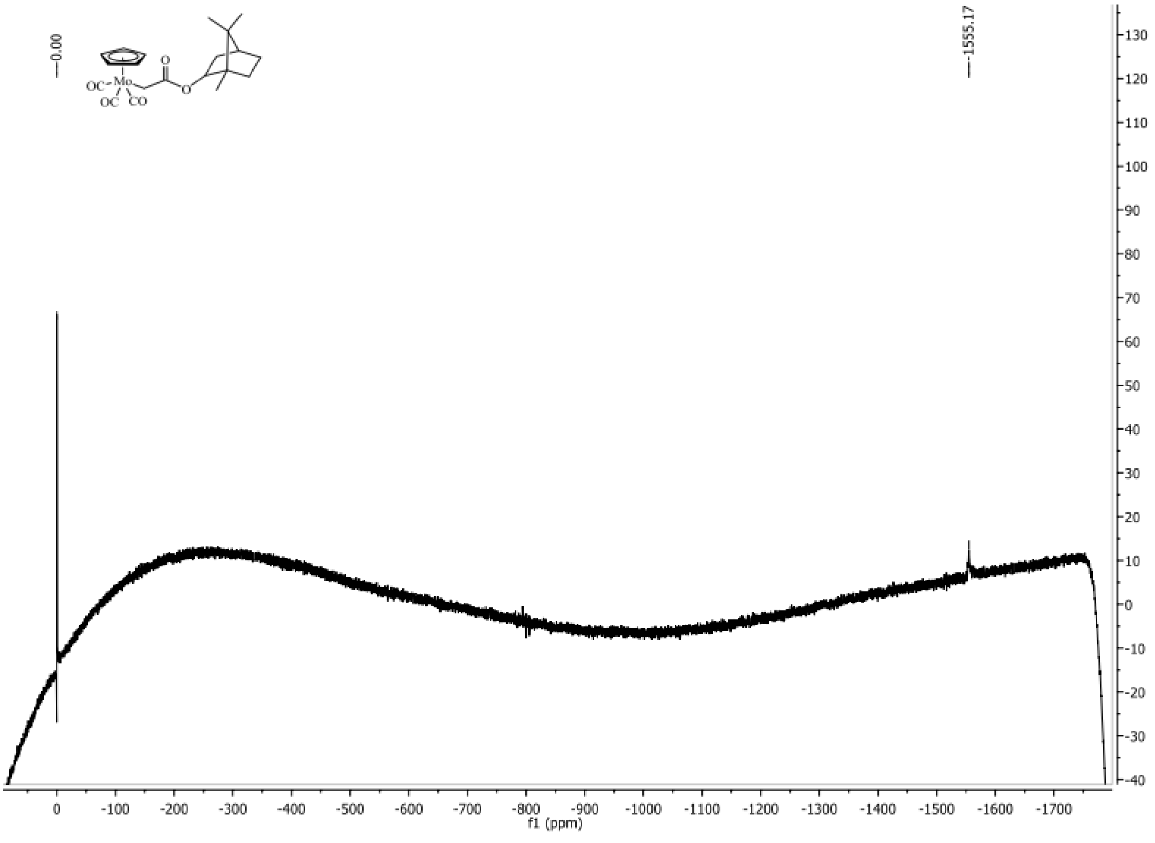
0.00
OC
Mo
OC
CO
O
O
-1555.17
130
120
110
100
90
80
70
60
50
40
30
20
10
0
-10
-20
-30
-40
0
-100
-200
-300
-400
-500
-600
-700
-800
-900
-1000
-1100
-1200
-1300
-1400
-1500
-1600
-1700
f1 (ppm)

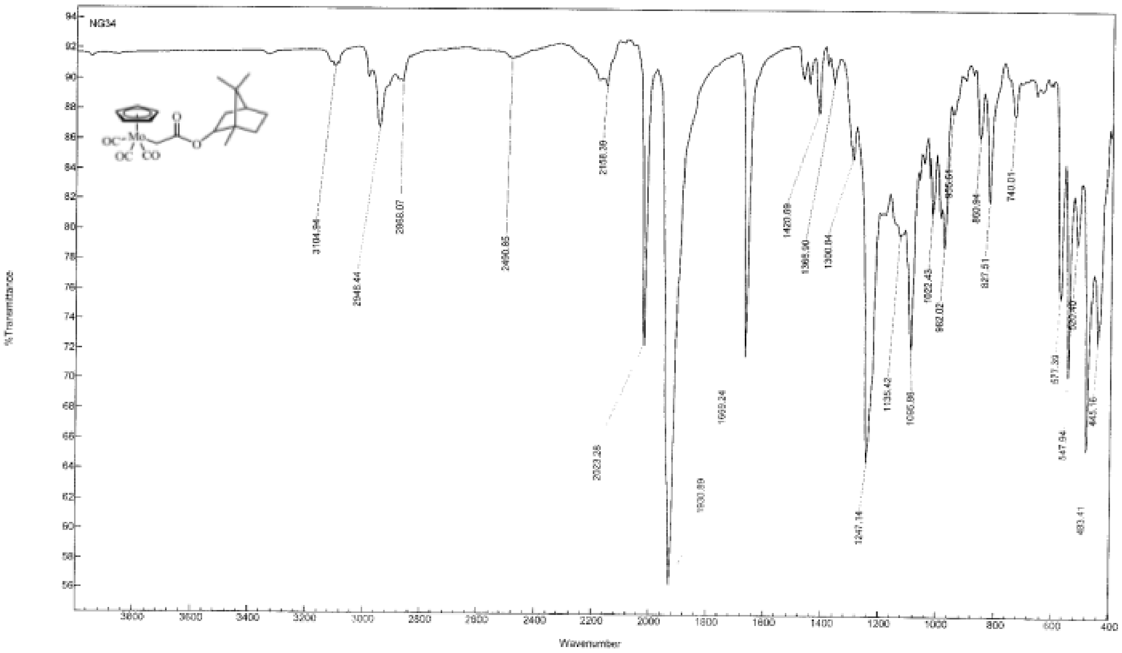
NG34
%Transmittance
94
92
90
88
86
84
82
80
78
76
74
72
70
68
66
64
62
60
58
56
OC
Mo
OC
CO
O
O
3104.94
2948.44
2868.07
2490.85
2158.39
2023.28
1930.89
1669.24
1420.69
1368.90
1300.84
1247.14
1135.42
1086.88
1022.43
962.02
935.61
860.94
827.51
740.01
571.33
520.40
547.94
493.41
445.16
3800
3600
3400
3200
3000
2800
2600
2400
2200
2000
1800
1600
1400
1200
1000
800
600
400
Wavenumber

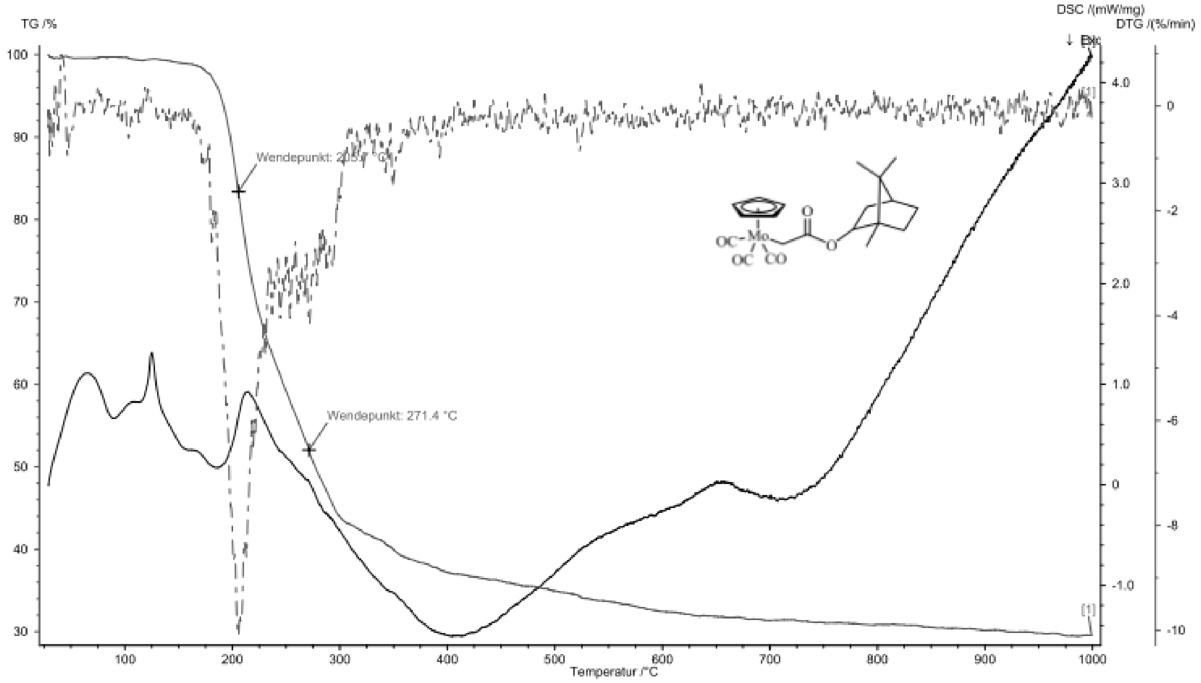
TG /%
DSC /(mW/mg)
DTG /(%/min)
↓ Exo
Wendepunkt: 205.7 °C
Wendepunkt: 271.4 °C
OC
Mo
OC
CO
O
O
[1]
[1]
100
90
80
70
60
50
40
30
4.0
3.0
2.0
1.0
0
-1.0
0
-2
-4
-6
-8
-10
100
200
300
400
500
600
700
800
900
1000
Temperatur /°C

6. Inequivalence of terminal CO groups in complex **5**, a variable temperature study.

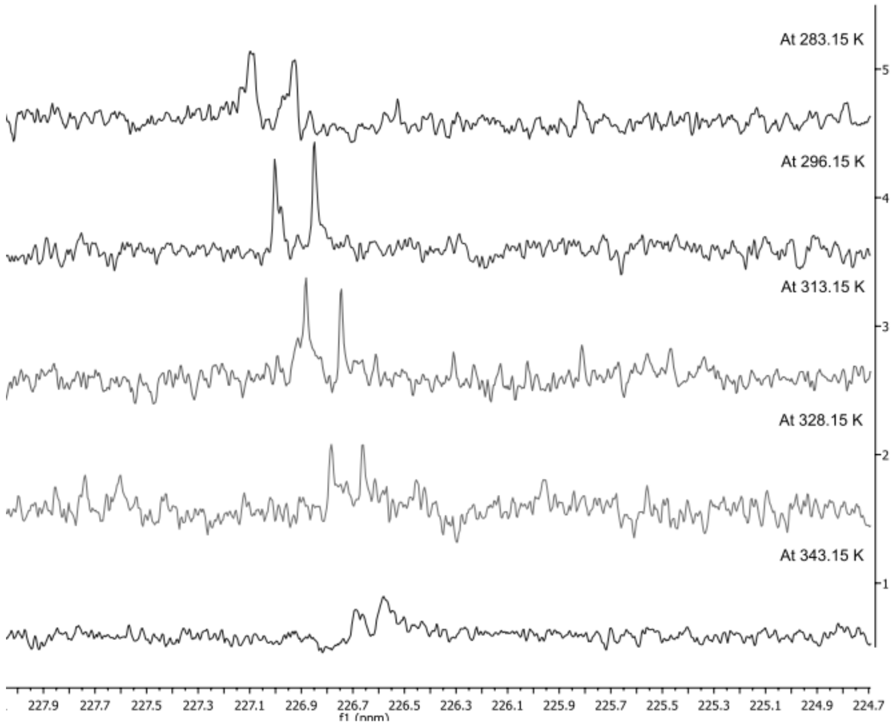

Figure 4.5. Variable temperature ^{13}C NMR (C_6D_6) of 5 in the *cis*-CO region, showing electronic inequivalence or asymmetry of the carbonyl ligands even at 70°C.

7. Solid state NMR comparison study of CpMo(CO)$_3$CH$_3$ and **5**.

There are two signals in the ^{1}H-MAS spectrum for CpMo(CO)$_3$CH$_3$ at 5.52 ppm (for $C_5\mathit{H}_5$) and 0.53 ppm (for -$C\mathit{H}_3$) and for **5**, Cp ligand appears at 5.57 ppm as a broad signal. In ^{13}C-CPMAS spectrum of the methyl complex, side bands of the Cp signal at 94.68 ppm appear at 253.67 ppm and -64.37 ppm(12 kHz). The -CH$_3$ group appears at -22.6 ppm and the molybdenum bound carbonyl ligands at 242.35 and 230.34 ppm. However, ^{13}C-CPMAS for complex **5** shows three distinct peaks for the three Mo-CO groups at 242.25, 230.16 and 226.59 ppm. The first rotational side bands of the Cp ligand of **5** appear at 254.96 and -63.01 ppm.

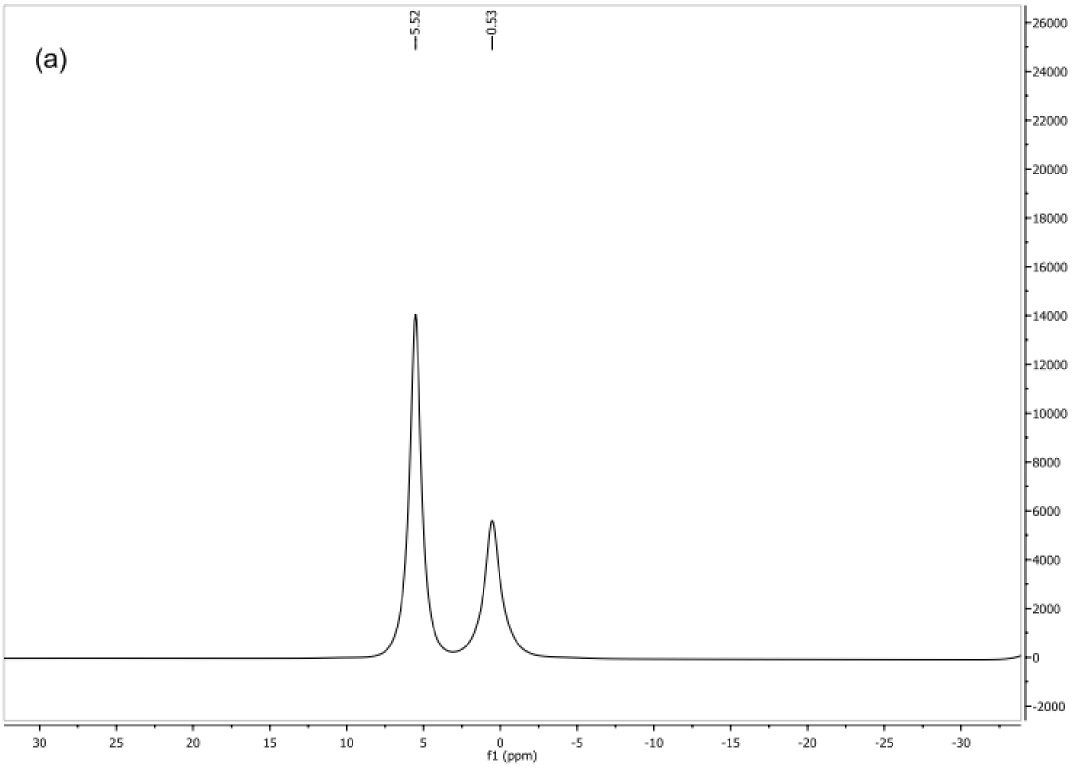
(a)
5.52
0.53
26000
24000
22000
20000
18000
16000
14000
12000
10000
8000
6000
4000
2000
0
-2000
30 25 20 15 10 5 0 -5 -10 -15 -20 -25 -30
f1 (ppm)

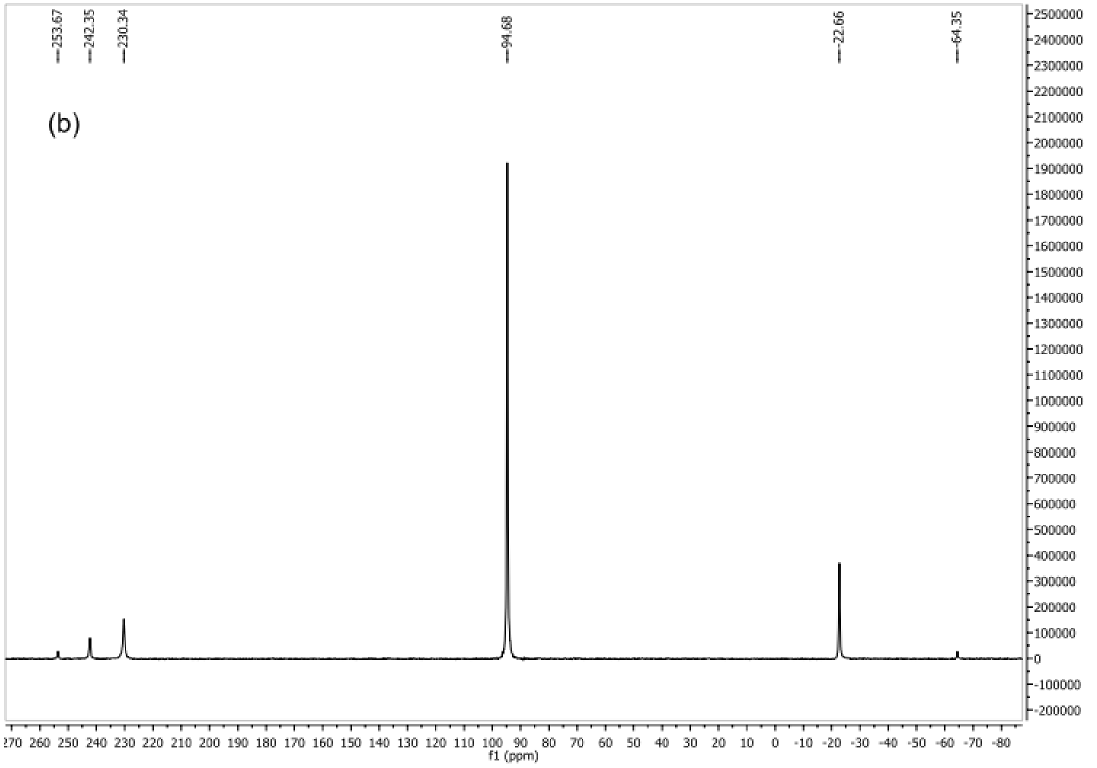
(b)
253.67
242.35
230.34
94.68
-22.66
-64.35
2500000
2400000
2300000
2200000
2100000
2000000
1900000
1800000
1700000
1600000
1500000
1400000
1300000
1200000
1100000
1000000
900000
800000
700000
600000
500000
400000
300000
200000
100000
0
-100000
-200000
270 260 250 240 230 220 210 200 190 180 170 160 150 140 130 120 110 100 90 80 70 60 50 40 30 20 10 0 -10 -20 -30 -40 -50 -60 -70 -80
f1 (ppm)

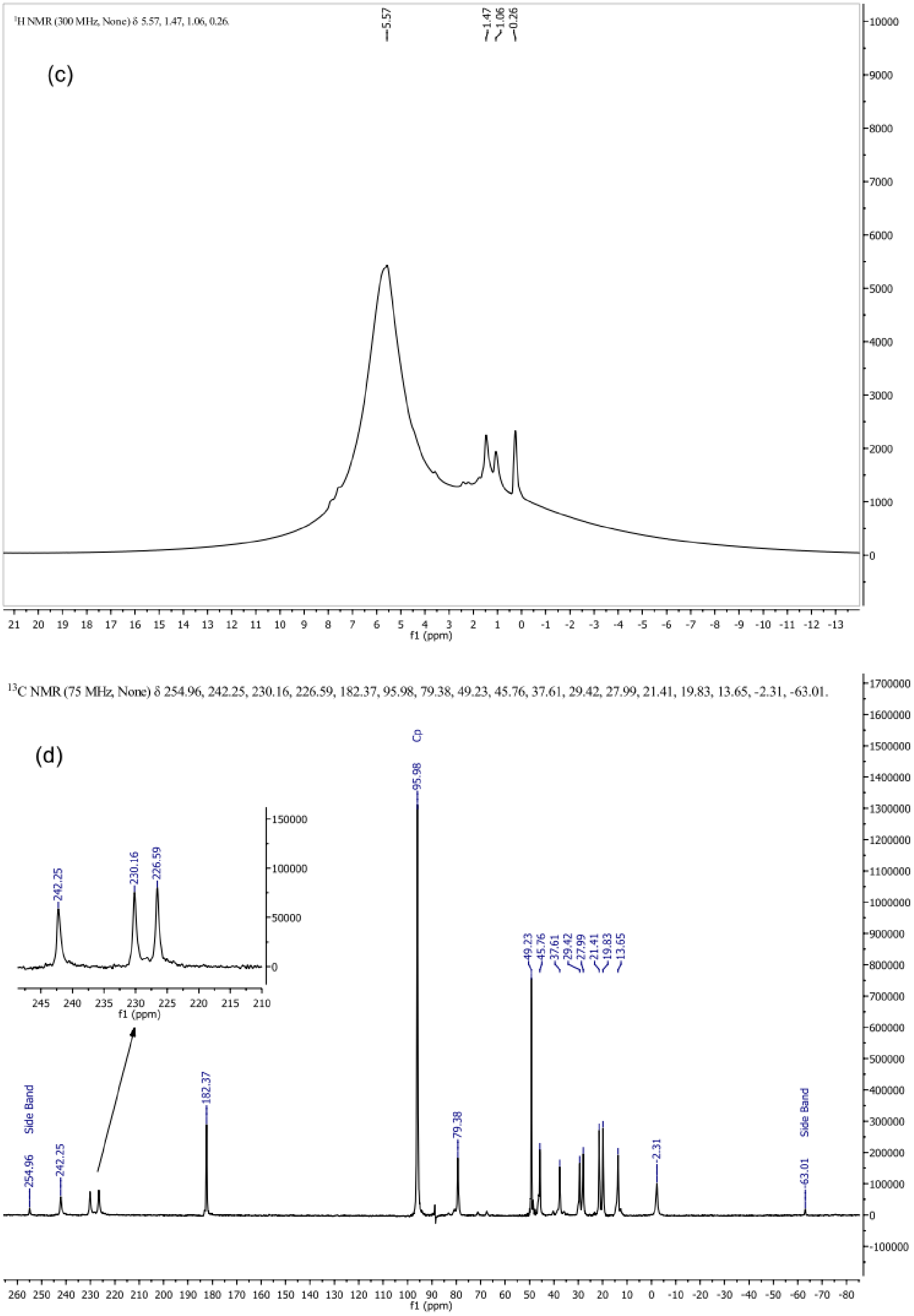

Figure 4.6. (a) ^{1}H-MAS and (b) ^{13}C-CPMAS spectra for complex $CpMo(CO)_3(CH_3)$; (c) ^{1}H-MAS and (d) ^{13}C-CPMAS for complex 5.

8. X-ray Crystallographic Data for **1, 2** and **5**

Compound **1** (CCDC 934898)

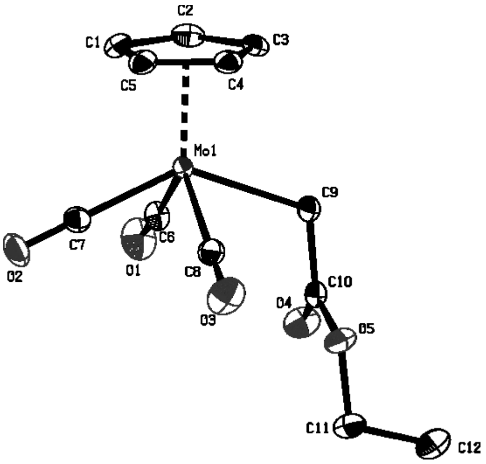

Figure 4.7. ORTEP drawing with 50% ellipsoids for complex **1**.

A clear light yellow fragment-like specimen of $C_{12}H_{12}MoO_5$, approximate dimensions 0.258 mm x 0.358 mm x 0.480 mm, was used for the X-ray crystallographic analysis. The X-ray intensity data were measured on a Bruker Kappa APEX II CCD system equipped with a graphite monochromator and a Mo fine-focus tube (λ = 0.71073 Å).

```
                         Crystal Data

Formula                                              C12 H12 Mo O5
Formula Weight                                              332.16
Crystal System                                        Orthorhombic
Space group                                  P212121      (No. 19)
a, b, c [Angstrom]             8.5556(1)   10.4982(2)   14.8086(2)
V [Ang**3]                                              1330.09(3)
Z                                                                4
D(calc) [g/cm**3]                                            1.659
Mu(MoKa) [ /mm ]                                             0.995
F(000)                                                         664
Crystal Size [mm]                             0.26 x  0.36 x  0.48

                       Data Collection

Temperature (K)                                                123
Radiation [Angstrom]                             MoKa      0.71073
Theta Min-Max [Deg]                                     2.4,  25.5
Dataset                                -10: 10 ; -12: 12 ; -17: 17
Tot., Uniq. Data, R(int)                     37426,   2464,  0.027
Observed data [I > 2.0 sigma(I)]                              2449

                          Refinement

Nref, Npar                                              2464,  164
R, wR2, S                                     0.0208, 0.0544, 1.11
w = 1/[\s^2^(Fo^2^)+(0.0366P)^2^+0.7711P] where P=(Fo^2^+2Fc^2^)/3
Max. and Av. Shift/Error                                0.00, 0.00
Flack x                                                    0.50(4)
Min. and Max. Resd. Dens. [e/Ang^3]                    -0.29, 1.82
```

Compound **2** (CCDC 934899)

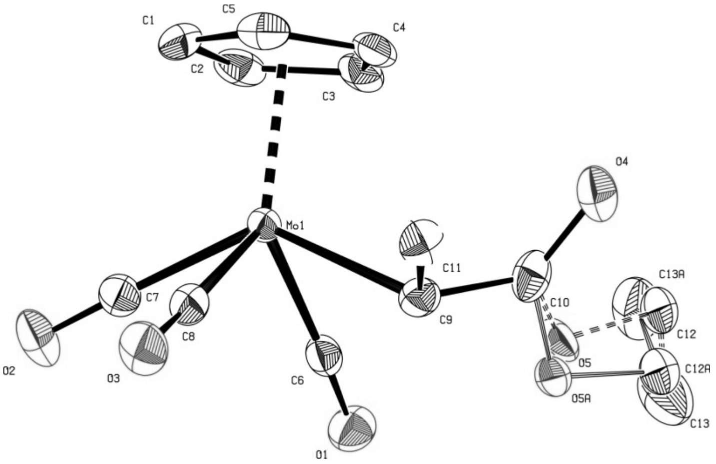

Figure 4.8. ORTEP drawing with 50% ellipsoids for complex **2**.

A clear intense yellow fragment-like specimen of $C_{13}H_{14}MoO_5$, approximate dimensions 0.150 mm x 0.359 mm x 0.554 mm, was used for the X-ray crystallographic analysis. The X-ray intensity data were measured on a Bruker Kappa APEX II CCD system equipped with a Montel mirror monochromator and a Mo FR591 rotating anode (λ = 0.71073 Å).

```
                         Crystal Data

Formula                                              C13 H14 Mo O5
Formula Weight                                              346.18
Crystal System                                        Orthorhombic
Space group                                    Pbca       (No. 61)
a, b, c [Angstrom]          10.3022(8)   11.1065(9)  23.6758(19)
V [Ang**3]                                               2709.0(4)
Z                                                                8
D(calc) [g/cm**3]                                            1.698
Mu(MoKa) [ /mm ]                                             0.981
F(000)                                                        1392
Crystal Size [mm]                                0.15 x  0.36 x  0.55
                         Data Collection

Temperature (K)                                                123
Radiation [Angstrom]                               MoKa      0.71073
Theta Min-Max [Deg]                                      1.7,  25.4
Dataset                                -12: 12 ; -13: 13 ; -28: 28
Tot., Uniq. Data, R(int)                      55418,   2486,  0.032
Observed data [I > 2.0 sigma(I)]                              2067
                           Refinement

Nref, Npar                                               2486,  203
R, wR2, S                                    0.0231, 0.0524, 1.13
w = 1/[\s^2^(Fo^2^)+(0.0135P)^2^+4.3243P] where P=(Fo^2^+2Fc^2^)/3
Max. and Av. Shift/Error                                0.00, 0.00
Min. and Max. Resd. Dens. [e/Ang^3]                    -0.37, 0.67
```

Compound **5** (CCDC 934900)

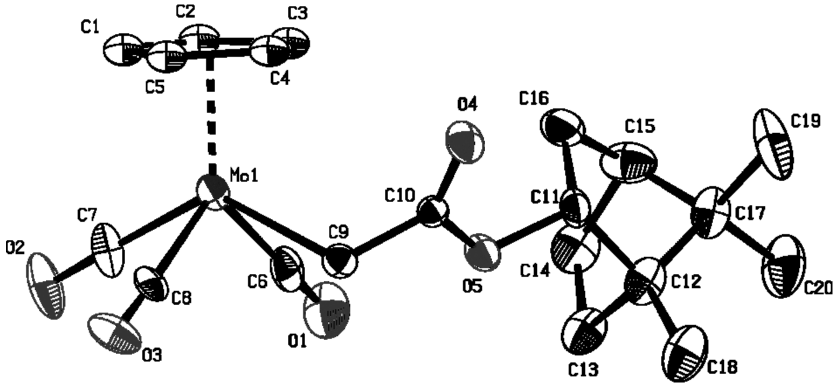

Figure 4.9. ORTEP drawing with 50% ellipsoids for complex **5.**

A clear light yellow plate-like specimen of $C_{20}H_{24}MoO_5$, approximate dimensions 0.030 mm x 0.230 mm x 0.330 mm, was used for the X-ray crystallographic analysis. The X-ray intensity data were measured on a Bruker Kappa APEX II CCD system equipped with a graphite monochromator and a Mo fine-focus tube (λ = 0.71073 Å).

```
                              Crystal Data

        Formula                                             C20 H24 Mo O5
        Formula Weight                                             440.33
        Crystal System                                       Orthorhombic
        Space group                                  P212121      (No. 19)
        a, b, c [Angstrom]           7.4170(2)     7.6621(2)   34.3794(9)
        V [Ang**3]                                             1953.77(9)
        Z                                                               4
        D(calc) [g/cm**3]                                           1.497
        Mu(MoKa) [ /mm ]                                            0.698
        F(000)                                                        904
        Crystal Size [mm]                             0.03 x  0.23 x  0.33

                            Data Collection

        Temperature (K)                                               123
        Radiation [Angstrom]                            MoKa      0.71073
        Theta Min-Max [Deg]                                     2.4,  25.4
        Dataset                                -8:  8 ;  -9:  9 ; -41: 41
        Tot., Uniq. Data, R(int)                     37467,   3579,  0.089
        Observed data [I > 2.0 sigma(I)]                             3025

                               Refinement

        Nref, Npar                                             3579,  238
        R, wR2, S                                  0.0550, 0.0943, 1.15
        w = 1/[\s^2^(Fo^2^)+(0.0133P)^2^+6.0706P] where P=(Fo^2^+2Fc^2^)/3
        Max. and Av. Shift/Error                               0.00, 0.00
        Flack x                                                   0.02(7)
        Min. and Max. Resd. Dens. [e/Ang^3]                   -1.29, 0.65
```

9. Turnover frequencies (TOFs) for catalysis reactions with **1-5** and different substrates.

Table 4.5. TOFs[a] for complexes 1-5 (in mol mol_{Mo}^{-1} h^{-1}) utilized for olefin epoxidation in DCM at 22 °C using TBHP with catalyst:substrate:oxidant = 1:100:200 unless stated otherwise.

Experiment	Substrate	**1**	**2**	**3**	**4**	**5**
(a)	*cis*-cyclooctene, 1 mol% catalyst	120	124	188	118	189
(b)	*cis*-cyclooctene, 0.1 mol% catalyst	236	302	262	263	362
(c)	*cis*-cyclooctene, no co-solvent	220	290	500	188	210
(d)	cis-cyclooctene, 55 °C, $CHCl_3$	775	1024	1187	784	781
(e)	*cis*-stilbene	25	40	33	26	24
(f)	*trans*-stilbene	26	50	91	40	60
(g)	1-octene	38	27	31	37	12
(h)	*trans*-β-methylstyrene	-	85	97	70	48

[a] All values were determined from the steepest part of the conversion vs. time slope.

III. Kinetics and Mechanisms

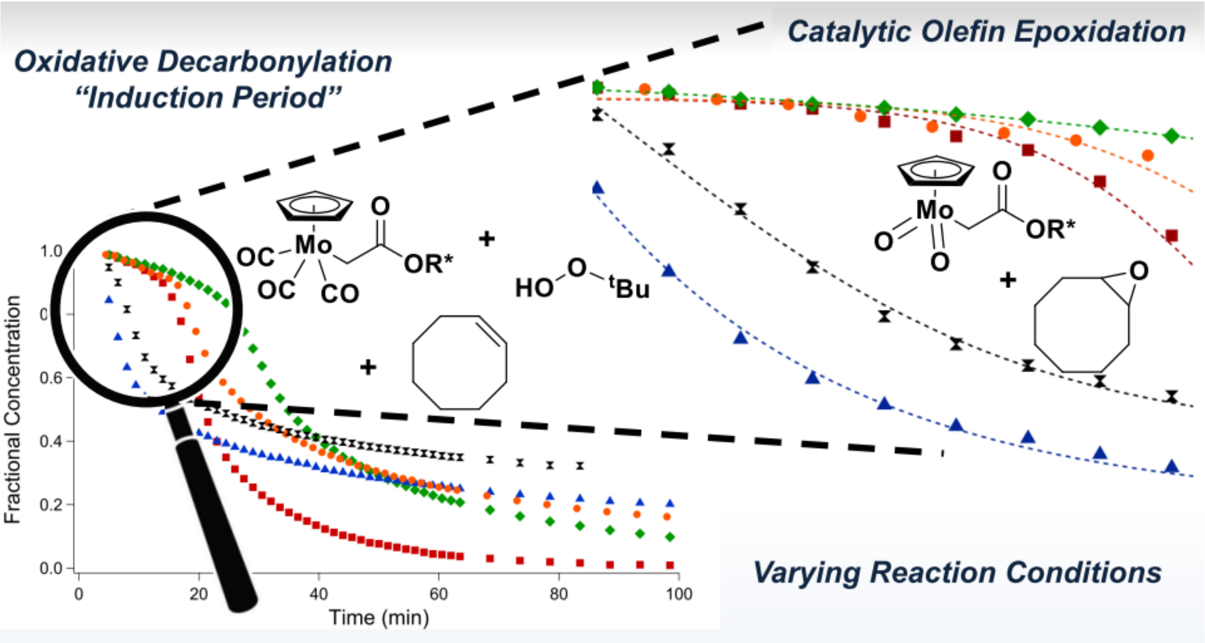

- *In situ* oxidative decarbonylation of [CpMo(CO)$_3$R*] precatalysts and catalytic alkene epoxidation have been studied by kinetic NMR.
- Effect of varying reaction conditions on the catalytic epoxidation has been studied.
- Implications of the induction phase behaviour have been utilized to propose a probable kinetic model.

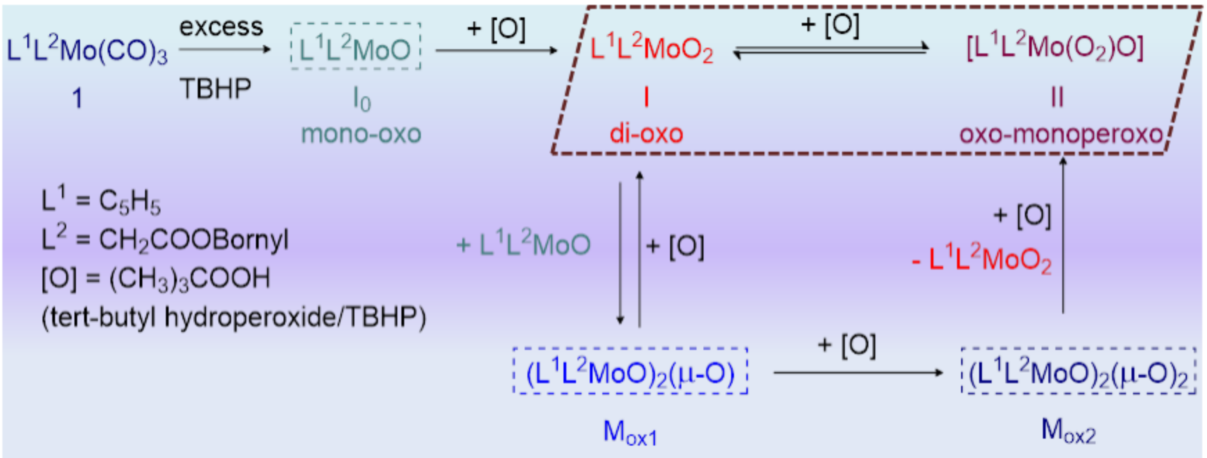
L¹L²Mo(CO)₃
1
excess
TBHP
L¹L²MoO
I₀
mono-oxo
+ [O]
L¹L²MoO₂
I
di-oxo
+ [O]
[L¹L²Mo(O₂)O]
II
oxo-monoperoxo
L¹ = C₅H₅
L² = CH₂COOBornyl
[O] = (CH₃)₃COOH
(tert-butyl hydroperoxide/TBHP)
+ L¹L²MoO
+ [O]
+ [O]
- L¹L²MoO₂
(L¹L²MoO)₂(μ-O)
Mox1
+ [O]
(L¹L²MoO)₂(μ-O)₂
Mox2

- Oxidative decarbonylation of [CpMo(CO)$_3$R] precatalysts with TBHP oxidant has been studied.
- Existence of Mo(IV) and Mo(V) intermediates during conversion of Mo(II) to Mo(VI) is proposed.
- Catalyst robustness with respect to side reactions is evaluated.

5 A Kinetic Study of Catalytic Olefin Epoxidation with [CpMo(CO)$_3$(η^1-CH$_2$COOR)] Precatalysts using NMR

Abstract

In this work, the epoxidation of *cis*-cyclooctene with mononuclear precatalysts of the type [CpMo(CO)$_3$R*], (Cp = C_5H_5, R* = CH$_2$COOBornyl, **5**) with *tert*-butylhydroperoxide (TBHP) as oxidant has been studied using kinetic ^{1}H and ^{13}C NMR spectroscopy. When **5** is treated with TBHP in the presence of *cis*-cyclooctene, the Mo(VI) dioxo complex [CpMoO$_2$R*] **I** is primarily involved in activating TBHP and subsequent oxygen transfer to the olefin. Catalytic epoxidation reaction takes precedence over complete oxidation of the precatalyst and after quantitative yield of the epoxide is obtained, **I** is further oxidized to oxo-peroxo complex [CpMo(O)(O$_2$)R*] **II**. Both **I** and **II** are catalytically active for the epoxidation of *cis*-cyclooctene with TBHP. The effect of varying oxidant, substrate and catalyst concentrations on the induction period of epoxidation reaction has been studied. These experiments illustrate that *in situ* oxidative decarbonylation is not an economical process. It is found that catalysis at high reaction temperatures (usually 55 °C) is detrimental to kinetic and thermodynamic control, and thus partly responsible for lack of effective asymmetric induction. Furthermore, in its role as a reductant, the substrate affects the induction period and evolution of reaction kinetics thereafter. At high substrate concentrations, olefin pre-coordination at Mo is proposed (saturation kinetics). Previously published kinetic models of epoxidation of olefins with Mo(VI) oxo catalysts have been critically re-addressed.

5.1 Introduction

A large number of structurally diverse complexes of the type [Cp′M(CO)$_3$R] (where Cp′ = unsubstituted or substituted cyclopentadienyl ligand, R = halide, alkyl, etc.) have been employed for catalytic epoxidation of unfunctionalized olefins in the last decade.[1] Several research groups have investigated kinetic and theoretical models outlining oxygen transfer to olefin substrates with CpMo complexes using oxidants such as *tert*-butylhydroperoxide (TBHP) and H_2O_2.[2–6] It is now generally accepted that *in situ* oxidative decarbonylation of these precatalysts with excess TBHP results in the formation of the complex [Cp′MoO$_2$R] (dioxo), which is then further oxidized to oxo-peroxo complex [Cp′MoO(O$_2$)R].[3,7] In fact, several of such oxidized species have been isolated and identified by X-ray crystallography.[3,8–11] Depending on the substitution pattern of Cp and the nature of group R, these oxidized complexes are either catalytically active or inactive in olefin epoxidation. For example, both [CpMoO$_2$Cl] and [CpMoO(O$_2$)Cl] obtained from [CpMo(CO)$_3$Cl] are catalytically active,[2] however the C$_5$Me$_5$ (Cp*) oxo-peroxo analogue [Cp*MoO(O$_2$)Cl] is a catalytically dead-end species[11,12] and only the dioxo complex [Cp*MoO$_2$Cl] is active.[5] Furthermore, both the dioxo species [CpMoO$_2$R] and the oxo-peroxo complex [CpMoO(O$_2$)R] have been shown to be catalytically active for R = CH$_3$.[3,13] The formation and fate of these oxidized complexes and epoxidation of olefins with them has been followed by different spectroscopic techniques (UV-Vis, ^{19}F NMR, FTIR, Raman) to develop kinetic models of the oxidation reactions.[3,13] It is noteworthy that the Cp ligand is retained during these oxidative processes, although, depending on the extent of substitution (or steric bulk) of the ligand, loss of the (alkylcyclopentadienyl) ligand during catalysis has also been reported.[14] Additionally, the high activity of the oxidized complexes has been attributed to catalysis-facilitating haptotropic shifts.[14] The side chain groups R are also retained during the oxidation reactions.[15]

Although the synthesis of structurally diverse half-sandwich Mo catalysts is quite straightforward,[1,16] efficient stereoselective epoxidation of prochiral olefins has not been achieved so far and an adequate explanation for the poor enantiomeric excess (*ee*) obtained is lacking.[17–21] Catalytic epoxidation with these complexes is stereospecific, i.e. epoxidation of *cis*- and *trans*-stilbene results in formation of their respective epoxides with a high selectivity (>99% within experimental error). However, differences in the reactivity of these catalysts with the different olefin substrates (e.g. conversion of internal alkenes to their epoxides is faster than that of terminal alkenes) cannot be satisfactorily explained.

Despite widespread interest in these CpMo epoxidation precatalysts, only very few published reports undertake efforts to describe the nature and stability of the oxidized complexes.[20,22,23] For industrial applications and intended reusability/recyclability of the catalysts, more information about process robustness is required.[24,25] Therefore, a careful kinetic study can help to provide an insight into the role of secondary processes such as side reactions and catalyst deactivation.[26]

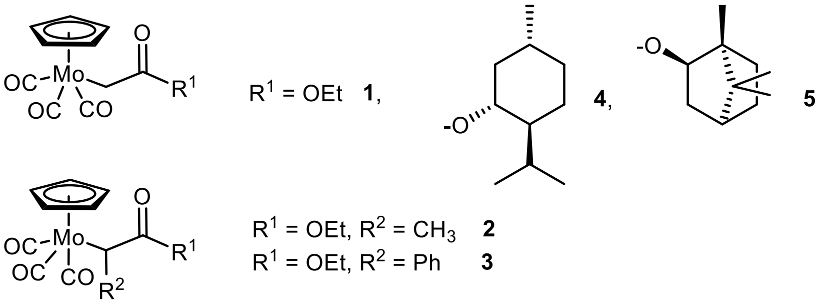

Figure 5.1. Cyclopentadienyl molybdenum tricarbonyl alkylester precatalysts 1-5.[27]

The synthesis, characterization and catalytic potential of complexes of the type [CpMo(CO)$_3$(CHR^{2}COOR^1)] containing η^1-coordinated chiral alkylester side chain (**1−5**, R^1 = Et, menthyl, bornyl; R^2 = Me, Ph; Figure 5.1) has been described.[27] This study concludes that a general prediction of catalytic activity (TOFs) by comparing stereoelectronic effects of different side chain R groups in [CpMo(CO)$_3$R] complexes and ^{95}Mo NMR data is possible, similar to the structure-activity relationship based on the substitution pattern of the Cp ligand.[7,28,29] This has been illustrated by comparing the catalytic activity of complexes [CpMo(CO)$_3$Cl] and [CpMo(CO)$_3$CH$_3$], with complexes **1−5** at 55 °C in CHCl$_3$ solvent.[27,30] Additionally, it is found that even though the complexes are enantiomerically pure and highly selective towards epoxide formation, epoxidation of the model prochiral olefin substrate *trans*-β-methylstyrene gives negligible enantioselectivity and equimolar amounts of (2*S*,3*S*)-2-methyl-3-phenyloxirane and (2*R*,3*R*)-2-methyl-3-phenyloxirane are obtained. These observations have motivated us to investigate whether there are some fundamental features of the catalytic activity of these complexes. The objective of this study is to gain more information about the induction period, wherein Mo(II) precatalysts are oxidized to Mo(VI) complexes. This information might help provide clues to explain the lack of kinetic and thermodynamic control in the epoxidation reaction.

Oxidative decarbonylation of precatalysts **1**, **4** and **5** with TBHP (in n-decane) is slower in comparison to precatalysts **2**, **3**, [CpMo(CO)$_3$Cl] and [CpMo(CO)$_3$CH$_3$]; indicated by an induction period that lasts about 30 min–1 h during catalytic epoxidation at room temperature. We have chosen complex **5** (R* = CH$_2$COOBornyl) for our study, since its X-ray structure[27] and ^{1}H and ^{13}C NMR confirm the enantiopurity of the complex. Additionally, the incumbent stereoelectronic effects in **5** make the oxidative transformations slow enough to be followed on a suitable time scale in NMR. We have also anticipated that pseudo-first order "initial rate" conditions that are usually employed for deriving kinetic rate law, can affect the overall kinetic progress of catalytic epoxidation and therefore information about the processes taking place in the induction period will be less evident.[26] For this reason, we have deliberately chosen to study the progress of the epoxidation reaction by NMR under varying reaction conditions that mimic laboratory scale catalysis conditions. Monitoring the kinetic reaction progress in entirety (and not simply initial rate conditions) can also provide information about catalyst activation and deactivation, and substrate and product inhibition.[26]

5.2 Experimental

All chemicals, *tert*-butylhydroperoxide (5.5 M solution in *n*-decane over molecular sieves, containing <4% water, Sigma Aldrich), *cis*-cyclooctene (95%, Acros Organics) were used as received. Complexes **1-5** were prepared according to Ref. 27. All manipulations involving air sensitive materials were performed under argon atmosphere using standard Schlenk techniques and dry solvents. High resolution NMR spectra were recorded using a Bruker© Avance DPX-400 spectrometer. ^{1}H and ^{13}C spectra are referenced to solvent residual signals.

Typical reaction conditions and data acquisition in kinetic ^{1}H and ^{13}C NMR study

For catalytic epoxidation of *cis*-cyclooctene – A mixture of *ca.* 0.1 mmol of **5** and mesitylene or naphthalene was dissolved in 0.4 mL CDCl$_3$ in an NMR tube and its ^{1}H and ^{13}C spectra were recorded. 10 equiv. of *cis*-cyclooctene was then added to the NMR tube and after mixing properly; ^{1}H and ^{13}C NMR were measured. Subsequently, 20 equiv. of TBHP (5.5 M *n*-decane solution) was added at 22 °C, mixed with the precatalyst and substrate solution, and analysed by *multizg* acquisition program of Bruker© TopSpin spectrometer. After shimming, ^{1}H spectra (16 scans) were first recorded at 5 min and subsequently at intervals of 10 min, and ^{13}C (164 scans) spectra first after 15 min and thereafter at 10 minute intervals, for a total time of 4 h.

Effect of temperature on epoxidation – The mixture of **5**, mesitylene, CDCl$_3$, and *cis*-cyclooctene was maintained at the desired temperature (10 °C or 30 °C) using *edte* GUI in the 400 MHz Bruker© spectrometer. 10 equiv. TBHP (5.5 M n-decane solution) was then added and the solution was mixed properly before the start of reaction monitoring by *multizg* acquisition program. After shimming, ^{1}H spectra were first recorded at 5 min and subsequently at intervals of 10 min, and ^{13}C spectra first after 15 min and thereafter at 10 minute intervals, for the duration of 4 or 6 h.

Data Analysis for all quantitative kinetic ^{1}H NMR Using NMR software MestReNova©, the characteristic signals at 6.65 ppm (mesitylene) and 7.8–8.0 ppm (naphthalene) for the internal standards were integrated to 3 H and 4 H respectively in all ^{1}H NMR. The concentration of different oxidized species was determined by integrating the area of Cp signals for these species as equivalent to 5 H (in case of **I** and **II**).

5.3 Results and Discussion

In analogy with previous reports,[3,13] we have proposed that the reaction of **5** with TBHP proceeds as illustrated in Scheme 5.1. The progress of catalytic epoxidation of *cis*-cyclooctene has been studied by kinetic ^{1}H and ^{13}C NMR in Section 5.3.1. The influence of varying oxidant, precatalyst and substrate concentrations on this transformation has been studied in Section 5.3.2. Finally in Section 5.3.3, an evaluation of kinetic models proposed before[3,14] for oxidation reactions of [CpMo(CO)$_3$R] tricarbonyl complexes is presented.

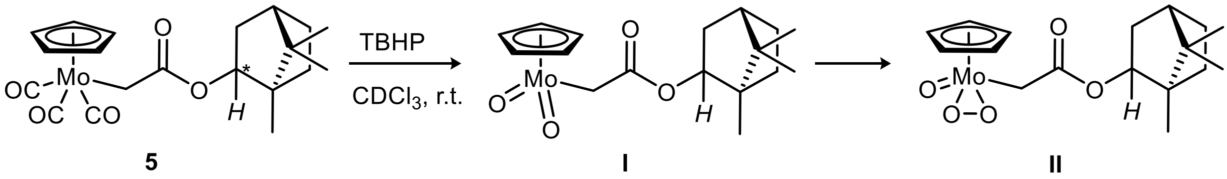

Scheme 5.1. Oxidation of tricarbonyl precatalyst 5 with 10 equiv. TBHP (in n-decane) results in the formation of both dioxo (I) and oxo-peroxo (II) species at room temperature in CDCl$_3$.

5.3.1 Catalytic Epoxidation of cis-Cyclooctene

A mixture of *ca.* 0.1 mmol of **5** in CDCl$_3$ and 10 equiv. of *cis*-cyclooctene was treated with 20 equiv. TBHP at 22 °C and the reaction progress was monitored by ^{1}H (Figure 5.2) and ^{13}C NMR (Figure 5.3). Quantitative epoxidation of *cis*-cyclooctene to its epoxide takes place within 3.5 h, as indicated by the disappearance of *cis*-cyclooctene multiplet at 5.68−5.85 ppm. However, complex **5** does not undergo complete oxidative decarbonylation and all three terminal CO signals can be observed even after 4 h in ^{13}C NMR (Figure 5.3(a)). This indicates that although only part of the precatalyst is converted to the active species, the rate of epoxidation is quite high. The signal for Cp of precatalyst **5** at 5.22 ppm and a new signal for the oxidized complex at 6.28 ppm can both be observed after 4 h of monitoring of the catalysis reaction, providing confirmation that Cp ligand is retained after the oxidative transformation.

In ^{13}C NMR, a prominent signal from the Cp ligand of the oxidized complex (Cp(ox)) is observed at 111.3 ppm evolving from the Cp signal at 93.4 ppm of the tricarbonyl precatalyst **5** and is assigned to the dioxo complex **I** (Scheme 5.1). A small signal at 111.7 ppm of the Cp ligand of oxo-peroxo complex can be seen once cyclooctene is quantitatively oxidized (Figure 5.3(d)). Since cyclooctene is converted to its epoxide before the amount of oxo-peroxo complex is significant, it is evident that rate of oxidation of olefin with the dioxo complex is quite high. In conclusion, this observation indicates that the presence of the olefin (in its role as a reductant) affects the oxidation of the precatalyst, i.e. by suppressing the conversion of **I** to **II**.

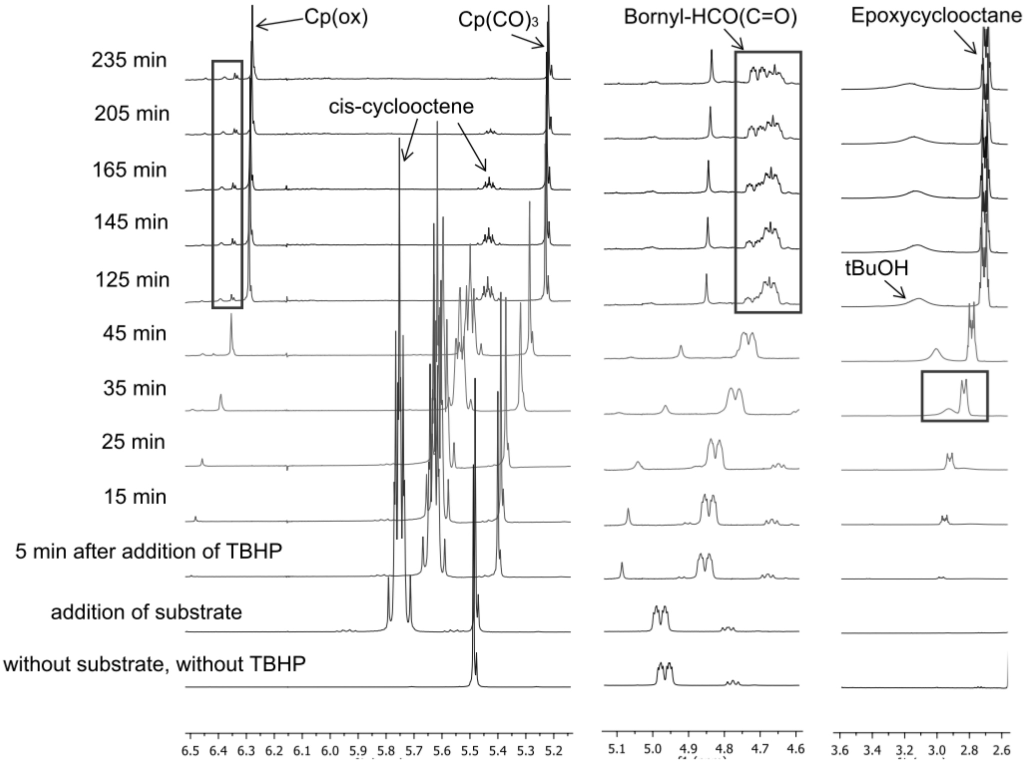

Figure 5.2. ^{1}H kinetic NMR profile for reaction of 5 with 10 equiv. of *cis*-cyclooctene and 20 equiv. of TBHP (in decane) in $CDCl_3$ at 22 °C (with mesitylene as internal standard).

Note that in Figure 5.3(b), the signals for the ester carbonyl carbon are not clearly observed in the period following oxidative decarbonylation (between 15–45 min) but reappear at about 55 min. It is unclear why this might occur since the signals for other quaternary carbon (CO group) can still be observed. The chiral side chain does not dissociate during the catalysis reaction, as evident from a persistent multiplet in ^{1}H NMR from 4.6-4.76 ppm after 4 h (corresponding to the hydrogen at bornyl chiral centre from dioxo complex **I**) and a signal at 170.8 ppm (for the ester carbonyl) in ^{13}C NMR. Additionally, *tert*-butanol is evolved as a side product, appearing as a broad signal in ^{1}H spectra from 2.9−3.3 ppm. The complete assignment of observed ^{1}H and ^{13}C NMR chemical shifts is given in Table 5.1.

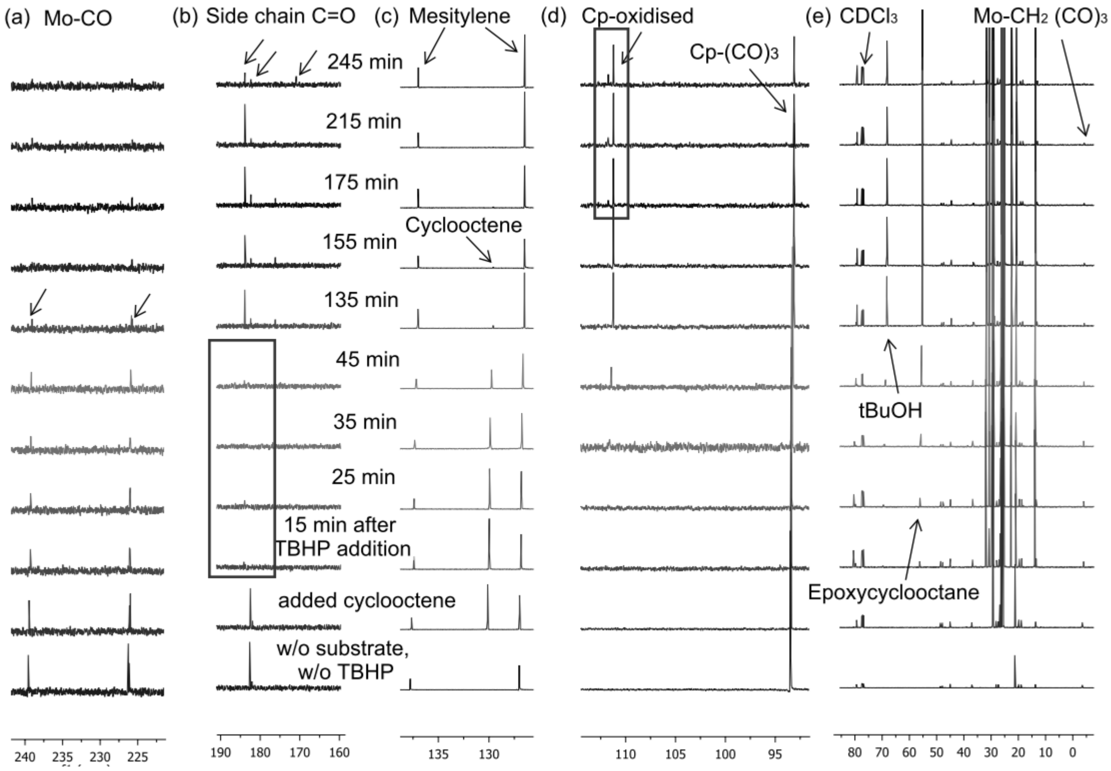

Figure 5.3. ^{13}C kinetic NMR profile for reaction of 5 with 10 equiv. of *cis*-cyclooctene and 20 equiv. of TBHP (in *n*-decane) in $CDCl_3$ at 22 °C (using mesitylene as internal standard).

Table 5.1. Assignment of ^{1}H and ^{13}C NMR chemical shifts (in ppm) observed during catalytic epoxidation of *cis*-cyclooctene with 5 and TBHP oxidant in $CDCl_3$ at 22 °C (5:CyOc:TBHP = 1:10:20). R* = $CH_2COOBornyl$, CyOc = *cis*-cyclooctene, EpCy = Epoxycyclooctane.

Complex	^{1}H NMR, δ (ppm)		^{13}C NMR, δ (ppm)		Time
5	Cp	5.22	Cp	93.4	0–4 h
	C(O)OC$\underline{H}$	4.93–4.99	Mo-$\underline{C}$O	226.14, 226.36, 239.67	
			(O=$\underline{C}$)OR*	182.3 → 184.0[b]	
I	Cp	6.28	Cp	111.3	35 min–4 h
	C(O)OC$\underline{H}$	4.6–4.76[a]	(O=$\underline{C}$)OR*	176.16	
II	Cp	6.27	Cp	111.7[c]	175 min–4 h
	C(O)OC$\underline{H}$	[a]	(O=$\underline{C}$)OR*	171.4[c]	
CyOc	–$\underline{H}$C=C$\underline{H}$–	5.68–5.85	–H$\underline{C}$=$\underline{C}$H–	130.0	0–165 min
EpCy	–$\underline{H}$C-(O)-C$\underline{H}$–	2.64–2.75	–H$\underline{C}$-(O)-$\underline{C}$H–	55.5	15 min–4 h

[a] See Figure 5.2, 'Bornyl-$\underline{H}$C-O-C(=O)' for changes in observed multiplet of this proton. [b] Chemical shift changes due to change in polarity. [c] Observed after 3.5 h when epoxidation of cyclooctene is complete.

The concentration *vs.* time plots illustrated in Figure 5.4 follow the progress of catalytic epoxidation and the changes in the concentrations of the substrate, precatalyst **5** and dioxo complex **I**. From a starting concentration of [**5**] = 0.249 M, the amount of **5** present in solution after 3.5 h left unreacted is 0.079 M (31.7%) and the concentration of the catalytically active dioxo species is 0.083 M (~33.3%). This suggests that *in situ* generation of catalytically active complexes is not very efficient. Alternatively, since *ca.* one-third of the precatalyst is left unreacted during catalytic epoxidation, it can be inferred that the conversion of cyclooctene substrate to epoxide takes precedence over complete oxidative decarbonylation.

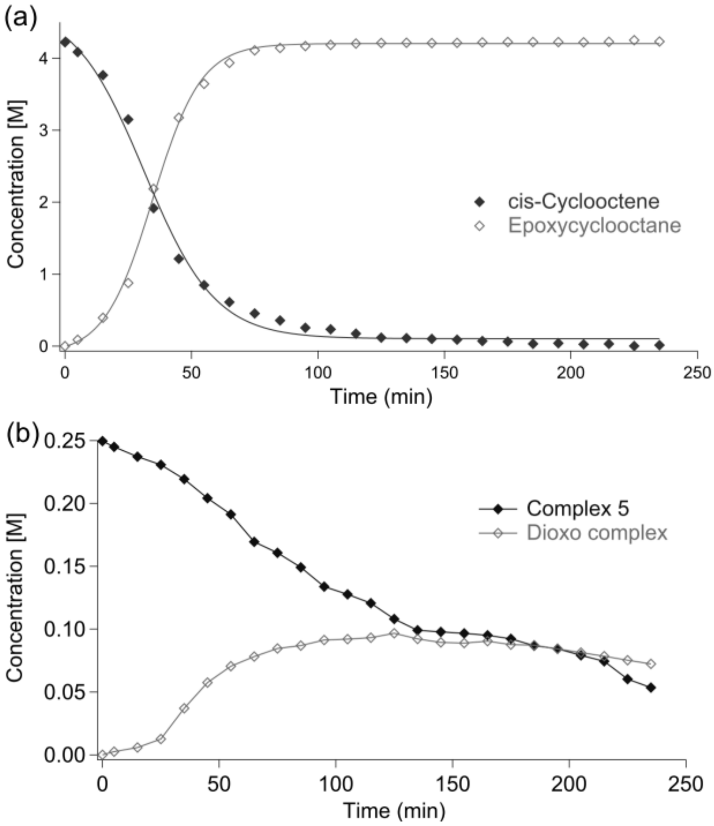

Figure 5.4. Concentration *vs.* time plots for (a) catalytic epoxidation of *cis*-cyclooctene with TBHP and, (b) concentration of precatalyst 5 and the catalytically active oxidized complex I during epoxidation.

In an attempt to evaluate how such homogeneous catalysts perform in subsequent catalytic runs without isolating the active oxo complex, cyclooctene was added after the catalyst was treated with TBHP. On treating **5** with 50 equiv. of TBHP, ^{95}Mo NMR of the reaction mixture shows a broad signal at -628 ppm (Figure 5.9 in the Supporting Information). This chemical shift is similar to ^{95}Mo signals for other [CpMo(O)(O$_2$)R] complexes (R = CH$_3$, -609 ppm; R = CF$_3$, -709 ppm).[3,13] For this reason, the persistent Cp signal at 6.27 ppm in ^{1}H NMR and 111.7 ppm in ^{13}C NMR is assigned to the oxidized species **II**. This complex is quite stable and in contrast to our observations when **5** is oxidized with 10 or 20 equiv. of TBHP, no precipitate is observed in the NMR tube. After 48 h, *cis*-cyclooctene (10 equiv.) was added into the NMR tube containing the pre-oxidized complex **II**. The concentration of the oxidized complex available for epoxidation of the substrate was determined to be *ca.* 0.054 M. This amount is ~ 50% than was present after 4 h of oxidation of the precatalyst (*ca.* 0.11 M), indicating either that **II** is slowly transformed into another species or that it undergoes decomposition. Complex **II** also catalyses the transformation of *cis*-cyclooctene to its epoxide, though conversion occurs at a slower rate (see Figure 5.10 in the SI). This may be attributed to both − lower activity of the oxo-peroxo species and the auto-retardation effect of *tert*-butanol which is present in the reaction mixture after *in situ* oxidation of the precatalyst.[31]

We thus conclude from results observed so far that oxidation of **5** with TBHP forms complexes **I** (dioxo) and **II** (oxo-peroxo) complexes and both are catalytically active for olefin epoxidation (Scheme 5.2). As mentioned before, the dioxo complex **I** is the primary active species and thus important to consider for the kinetic model of the epoxidation reaction.

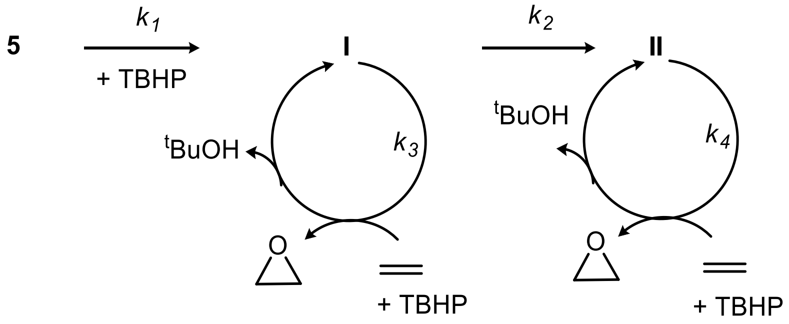

Scheme 5.2. Oxidation of **5** with TBHP to give complexes **I** and **II**. In the absence of olefin *cis*-cyclooctene, k_2 is large. In the presence of olefin, k_1, $k_3 >> k_2$ and k_4 is small but positive. k_1, k_2, k_3 and k_4 refer to rate constants for the oxidative transformations.

5.3.2 Effect of Varying Reaction Conditions

5.3.2.1 Effect of Temperature

Several research groups report that oxidative decarbonylation of [CpMo(CO)$_3$R] complexes with TBHP (n-decane) is very exothermic,[2] and in our experience, as an example, very rapid and violently exothermic at high concentration (~1-2 mol%) of the precatalysts R = Cl, CH(CH$_3$)COOC$_2$H$_5$ and CH(C$_6$H$_5$)COOC$_2$H$_5$, or when catalysis is carried out in the absence of a co-solvent. This exothermic conversion is, in part, responsible for high initial conversions of olefin substrates to their epoxides. Nevertheless, in majority of the published research epoxidation reactions have been carried out at a temperature of 55 °C and influence of exothermicity of oxidative decarbonylation is not taken into account.[1]

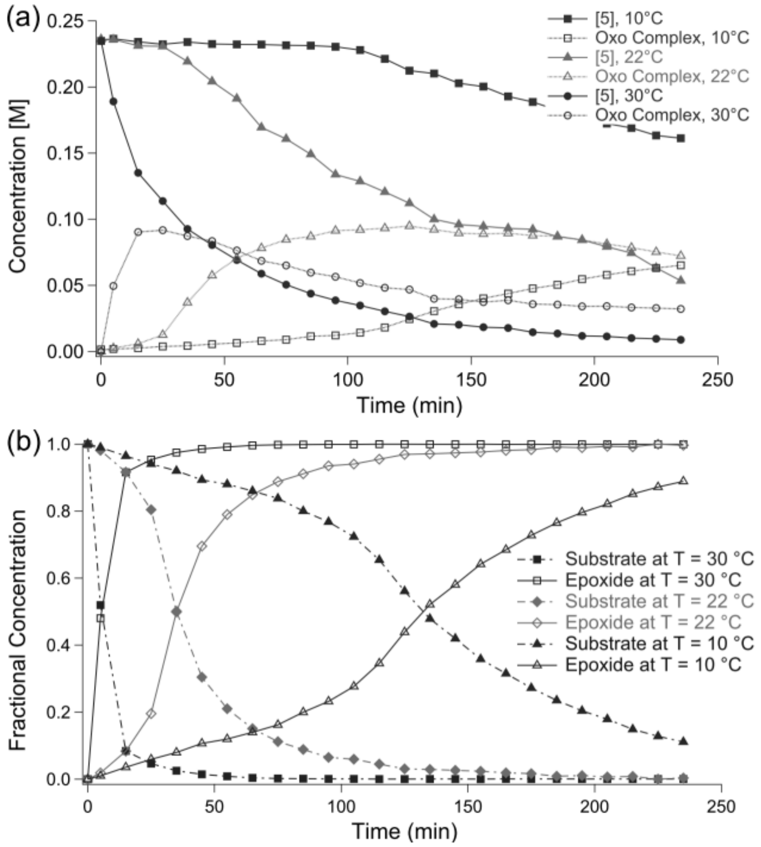

Figure 5.5. Concentration *vs.* time profiles for catalytic epoxidation of *cis*-cyclooctene with catalyst:substrate:TBHP = 1:10:20; at 10 °C (blue), 22 °C (green) and 30 °C (red) in $CDCl_3$. (a) Concentration of 5 and sum concentration of oxidized species **I** and **II** *vs.* time, (b) fractional concentration of *cis*-cyclooctene and epoxycyclooctane *vs.* time.

Therefore, the progress of epoxidation of *cis*-cyclooctene at different temperatures using 0.1 mmol of **5** was studied (catalyst:substrate:oxidant = 1:10:20). Figure 5.5(a) illustrates the changes in concentration of **5** and **(I + II)** during the epoxidation reaction at 10, 22 and 30 °C. At low temperature, complete oxidative decarbonylation takes longer. Hence, the catalytically active species **I** is formed slowly, resulting in a gradual conversion of cyclooctene to its epoxide. Figure 5.5(b) also shows the selective conversion of the cyclooctene to epoxycyclooctane at different reaction temperatures. It is found that ~ 90% of the substrate is converted into its epoxide within 15 min at 30 °C using 1 mol% of **5**. TOF determined from the steepest part of the slope and from amount of oxidized complexes in solution at 30 °C is 535 h^{-1}. There is no perceptible induction period as observed for epoxidation carried out at 10 °C and 22 °C. Complete conversion of cyclooctene at 22 °C is achieved after 75 min of addition of TBHP (TOF = 211 h^{-1}) while at 10 °C, epoxidation is very slow and cyclooctene is quantitatively consumed after about 4.5 h (at 10 °C, TOF = 90 h^{-1}). During olefin epoxidation no precipitate formed even at high temperatures.

Interestingly, after cyclooctene epoxide is quantitatively formed in epoxidation carried out at 30 °C, the concentration of the oxidized catalyst begins to decrease with time. This is also observed for the reaction carried out at 22 °C and confirms that further oxidative conversions take place; such as conversion of **I** to **II**, *vide supra* Figure 5.2 and Figure 5.3. Furthermore, the *highest* amount of catalytically active species present at 30 °C during epoxidation is *ca.* 39.5% (0.096 M) of original precatalyst concentration (0.245 M). Subsequent to complete epoxidation, precatalyst concentration decreases, but apparently concentration of **I** or **II** does not increase.

5.3.2.2 Effect of Oxidant Concentration

A survey of published literature shows that use of a very large excess of the oxidant (150 or 200 equiv. of TBHP) for catalysis reactions is standard practice.[1] To determine how the concentration of the oxidant affects the induction period during catalysis, we treated 10 equiv. of *cis*-cyclooctene and 0.05 mmol of precatalyst **5** in $CDCl_3$ at 22 °C with various equivalents of TBHP. No precipitate is formed in these reactions and after quantitative conversion to the epoxide, further oxidation of the dioxo complex to oxo-peroxo species **II** is observed in ^1H and ^{13}C NMR (see Section 5.3.1).

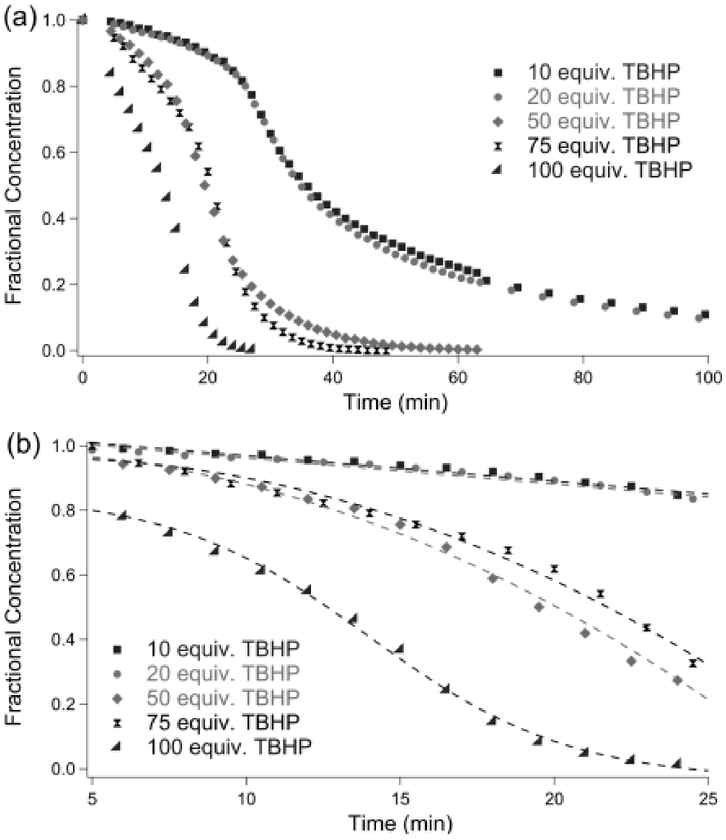

Figure 5.6. (a) Fractional concentration of *cis*-cyclooctene (in all cases, [S] = 10 equivalents with respect to 5) *vs.* time (min) during the epoxidation reaction using *ca.* 0.05 mmol of 5 with different concentrations of TBHP oxidant. Note: The fractional concentration of cyclooctene epoxide has been omitted for clarity. In all cases, mole fraction $n_{epoxide}$ = $[1-(n_{CyOc})]$ within experimental error. (b) Induction phase behaviour differs on varying oxidant concentration.

The rate of *cis*-cyclooctene conversion under these conditions is primarily influenced by the oxidant concentration since other factors such as concentration of **5** and cyclooctene, and the reaction temperature (22 °C) are kept identical. With 10 and 20 equiv. of TBHP (catalyst:substrate ratio = 1:10) utilized for the epoxidation reaction, a clearly discernible “slow phase” of 25 min is seen (Figure 5.6(a)). Increasing the amount of TBHP from 10 to 20 equiv. does not affect the reaction progress appreciably. The fractional conversion of the substrate to its epoxide is gradual and yield of cyclooctene epoxide is *ca.* 92% after 4 h of reaction monitoring. Quantitative conversion of the substrate is not achieved since 10 equiv. of TBHP are insufficient for oxidation of the precatalyst as well as epoxidation. However, as mentioned in Section 5.3.1, only two-thirds of the precatalyst is transformed on reaction with TBHP, and the concentration of active species is 33%. Hence, the observation that epoxidation reaches near completion with a small amount of active species is testament to the fact that these catalysts are quite active.

As mentioned before, epoxidation takes precedence over oxidative decarbonylation, but it is required that sufficient amount of the active species is present. This is illustrated in the time period of the induction phase (Figure 5.6(b)). At lower concentrations of the oxidant (10 and 20 equiv.), a linear fit to the change in substrate concentration with time is seen. At higher concentrations (50 and 75 equiv.) linear dependence is a poor approximation and induction phase curve fits a polynomial of third order. When a larger excess of 100 equiv. of TBHP is present, the initial period shows sigmoidal behaviour. This follows from an understanding that a sufficient amount of precatalyst is oxidized since oxidant concentration is not limiting. Overall, the initial period in these cases lasts for 5−10 min, followed by a rather steeper decline until quantitative conversion of the substrate is achieved.

5.3.2.3 *Effect of Precatalyst Concentration*

A study of epoxidation of *cis*-cyclooctene with different concentrations of **5** using substrate:TBHP = 1:2 in all cases is illustrated in Figure 5.7.

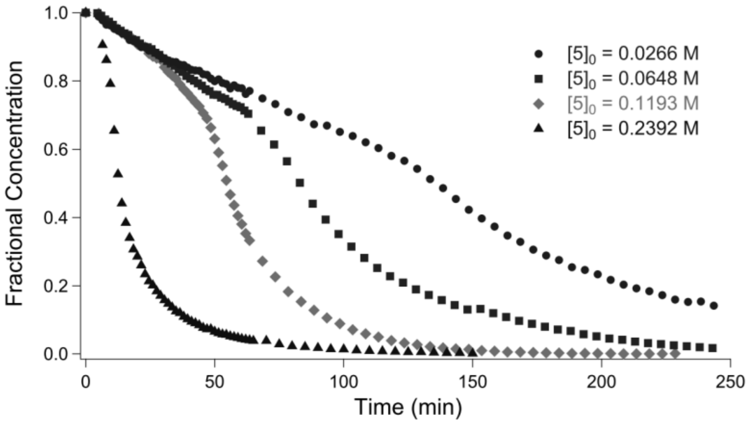

Figure 5.7. Plot of fractional concentration of *cis*-cyclooctene *vs.* time during its epoxidation with TBHP (substrate:TBHP = 1:2) as dependent on varying concentrations of precatalyst 5. Reactions performed in 0.4 mL $CDCl_3$ at 22 °C.

A plot of fractional concentration of *cis*-cyclooctene with time illustrates that at a low precatalyst concentrations, the induction period lasts up to an hour. Even though a relatively larger amount of the oxidant is available for oxidation of 0.0266 M and 0.0648 M of **5**, due to the dilution effect, formation of the epoxide is slow as well. In the first hour, *ca.* 30% of *cis*-cyclooctene is consumed and once a critical amount of the active species is formed, the larger excess of TBHP accelerates the reactions. The same behaviour is observed when precatalyst concentration is 0.1193 M. On increasing the concentration of **5** to 0.2392 M (*ca.* 0.1 mmol of **5** in 0.4 mL of $CDCl_3$), a larger amount of catalyst is present so that the formation of active dioxo species is not limiting on the epoxidation reaction. This explains the absence of an induction phase for the epoxidation of *cis*-cyclooctene using a higher catalyst amount.

5.3.2.4 Effect of Substrate Concentration

The progress of epoxidation reaction was studied by varying the amount of *cis*-cyclooctene. 0.05 mmol of **5** and 20 equiv. of TBHP were employed for this study, at 22 °C in $CDCl_3$ solvent (Figure 5.8). A lesser amount of the substrate (5 equiv.) is nearly quantitatively converted to the epoxide within an hour after addition of TBHP. An induction period that lasts about 15 min is observed. During epoxidation of 10 equiv. of substrate, the relative amount of active catalyst species available is lesser compared to oxidation of 5 equiv. of substrate. Nevertheless, after an induction phase of 25 min, ca. 80% of *cis*-cyclooctene is converted to the epoxide after 1 h, albeit in a more gradual fashion. As expected, conversion to the epoxide in the experiment with catalyst:substrate:TBHP ratio = 1:20:20 and 1:25:20 is incomplete, because (a) there is a lesser equivalent of the active catalyst available per equivalent substrate and, (b) there is insufficient oxidant TBHP for both oxidation reactions, i.e. precatalyst oxidation and epoxidation.

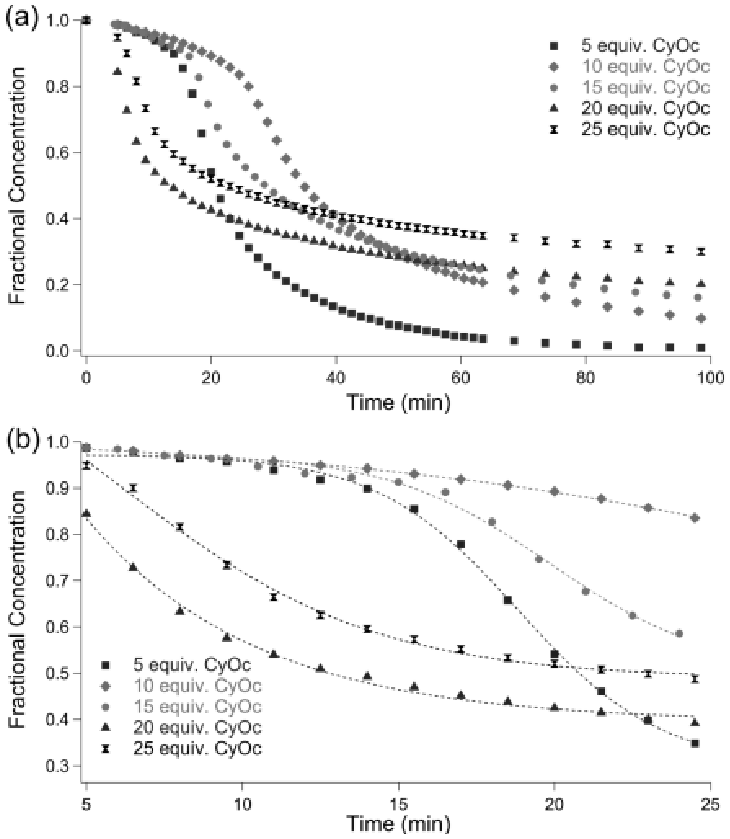

Figure 5.8. (a) Plot of fractional concentration of *cis*-cyclooctene *vs*. time during epoxidation with 20 equiv. of TBHP (in n-decane) using 0.05 mmol of 5 (1 equiv.) in 0.4 mL of $CDCl_3$ at 22 °C. (b) Induction period behaviour on varying substrate concentrations for catalytic epoxidation.

Curiously, the induction or ‘slow’ phase of the catalysis reaction during epoxidation of 20 and 25 equiv. of the substrate lasts for only about 5 min. Here, it is evident that as soon as the active oxidized species is formed from the oxidation of the precatalyst, it reacts faster with the overwhelming excess of substrate to form the epoxide. Consequently, the induction period is of a shorter duration compared to lower concentrations of the substrate. This behaviour is indicative of saturation kinetics.

5.3.3 Epoxidation with [CpMo(CO)$_3$R] complexes

A kinetic model for the complex [CpMo(CO)$_3$CH$_3$] has been published before.[3] The assumptions made for the derivation of the rate law for R = CH$_3$ complex can be considered as sound arguments to derive a rate equation that is reasonably well-supported by experimental data generated using the initial rate method. According to results discussed here, the 'Ajlouni kinetic model' can only be credible as an approximation since the induction period is greatly influenced by the initial reaction conditions.

In this study, it has been demonstrated that the transformations occurring in the 'slow' phase have an impact on the progress of the 'fast phase'. For example, at the beginning of the epoxidation reaction there is a 'higher' substrate concentration and a low concentration of active catalyst. At this stage, oxidative decarbonylation takes precedence over catalytic epoxidation until a sufficient amount of active catalyst is present. However, this does not imply that rate of epoxidation or conversion of substrate must necessarily be zero. In fact, the two oxidative transformations – oxidative decarbonylation and catalytic epoxidation occur in a competitive fashion in the early stages of the overall catalysis reaction.

The concentration of the substrate decreases with time as catalytic epoxidation progresses and side product *tert*-butanol is formed. This naturally affects the rate of the transformations shown in Scheme 5.2, and catalyst decomposition processes and competitive equilibria (coordination of ^{t}BuOH at the metal centre instead of TBHP[31]) are likely to become important at this later stage. Furthermore, in the presence of higher oxidant concentration and a low substrate concentration, a part of the active catalyst **I** is likely to undergo further oxidation to **II** and thus simultaneously, both **I** and **II** can contribute to the catalytic reaction.

Since reaction progress is quite sensitive to initial reaction conditions, a well-defined asymmetric transition state for chirality transfer in each catalytic cycle is unlikely to persist. Thus poor kinetic control during epoxidation of prochiral substrates can be explained.

Previously published kinetic and theoretical models[3,5,32] consider the formation of an intermediate of the type [CpMo(OH)(OO^{t}Bu)(O)(R)] from [CpMo(O)$_2$R] (R = CH$_3$) and TBHP.[3] This intermediate is present in equilibrium with the dioxo complex and in presence of the substrate alkene, it participates in the catalysis reaction. There may either occur an exogenous attack of the olefin *via* the Sharpless-like transition state or insertion of the olefin into Mo-O(O^{t}Bu) bond to give the epoxide. This is the main tenet of the Ajlouni kinetic model.[3] Hauser et al. have considered the formation of intermediate [CpMo(OOH)(OO^{t}Bu)(O)(CF$_3$)] in a similar manner for the reaction of oxo-peroxo complex [CpMo(O$_2$)(O)(CF$_3$)] with TBHP.[13] Kinetic studies by Colbran et al. with the complex [Cp'Mo(O)$_2$Br] (Cp' is a pentaaryl substituted cyclopentadienyl ligand) on the other hand propose that at least partially, the loss of Cp' ligand is imminent as catalysis proceeds.[14] Furthermore, it might be possible that such a non-Cp containing species is a better catalyst than the dioxo complex. Interestingly, *three* complex species, related to each other by a set of consecutive transformations (referred as **A** → **B** →

C) are required to fit the kinetic data of Colbran et al. The authors observe that both species **A** and **C** are catalytically active for epoxidation; **C** relatively more active than **A**. Furthermore, although **C** is obtained from **B**, the latter is catalytically inactive. The identity of either of these species has not been unequivocally established in this study.[14]

In the context of pre-equilibrium saturation kinetics observed with high substrate concentration with alkylester complex **5** discussed in this work, and epoxidation with Mo dioxo σ-peroxo complexes of Mitchell and Finney,[33] the following conclusion can be drawn. Observed saturation behaviour (Section 5.3.2.4) with the oxidized complex formed from **5** suggests that olefin coordination to the metal centre is likely (Michaelis-Menten model), even though it is not necessary for this η^2-olefin Mo adduct to be catalytically active. Note that the synthesis of Mo-olefin complexes[34] and their participation in catalysis has also been invoked before in published literature to explain kinetic data.[35,36]

As seen in Figure 5.4(b) and Figure 5.5(a), the concentration of the active species obtained from **5** decreases over time during the catalytic reaction. The various possibilities that may explain this observation are that (A) the active dioxo complex begins to transform into another species (which is not oxo-peroxo) that cannot be detected by NMR, (B) the pre-catalyst also decomposes into a complex Mo species (at least partially) that too cannot be quantified by NMR spectroscopic method, or (C) another species is formed (either with the substrate or with TBHP) that is the resting stage of the catalyst.

Thus, it is evident that further research with tricarbonyl complexes must attempt to unambiguously establish the nature of the primary catalytically active species i.e. dioxo *versus* oxo-peroxo. A description of the stability and reactivity of the active species can help in understanding the fundamental differences in reactivity of different CpMo complexes, and perhaps even in the synthesis of ‘tailor-made’ Mo-based epoxidation catalysts.

Despite the advantage of tricarbonyl pre-catalysts as stable, easily storable precursors that are less susceptible to decomposition in air and moisture than corresponding oxo complexes; it is shown that oxidative decarbonylation (illustrated by the “induction phase”) is not a straightforward route for the synthesis of CpMo oxo species. This knowledge is a useful addition for rational molecular catalyst design. DFT calculations to help elaborate on the mechanism of oxidative decarbonylation are discussed in Chapters 6 and 7.

5.4 Conclusion

The oxidized complexes formed by *in situ* oxidation of [CpMo(CO)$_3$(CH$_2$COOR)] precursors are stable, i.e. the Cp ligand and the chiral side chain are retained during the various transformations. Both complexes [CpMo(O)$_2$(CH$_2$COOR)] **I** and [CpMoO(O$_2$)(CH$_2$COOR)] **II**, are catalytically active and selective towards epoxide formation. Other factors, such as distance of the chiral centre from the metal reaction site and formation of more than one catalytically active species notwithstanding, poor asymmetric induction is a consequence of insufficient kinetic and thermodynamic control during the initial phase of the oxidation reaction. During catalytic epoxidation, dioxo complex **I** is the main catalytic species for epoxidation of *cis*-cyclooctene. Epoxidation reaction takes precedence over further oxidation of **I** to the oxo peroxo complex **II**. Initial reaction conditions such as oxidant, substrate, pre-catalyst concentrations and temperature exert a significant influence on the overall progress of the epoxidation reactions. For catalytic epoxidation carried out at an ambient temperature (>10 °C), *in situ* oxidation of the pre-catalyst is not a particularly robust and efficient process. A high oxidant concentration enforces poor kinetic control and multiple catalytically active species are likely to be formed. At a high substrate concentration, saturation kinetics is observed. A lower concentration of such pre-catalysts is preferable during epoxidation since deactivation and side processes are minimised.

5.5 References

[1] N. Grover, F.E. Kühn, Curr. Org. Chem. 16 (2012) 16–32.

[2] A.A. Valente, J.D. Seixas, I.S. Gonçalves, M. Abrantes, M. Pillinger, C.C. Romão, Catal. Lett. 101 (2005) 127–130.

[3] A.M. Al-Ajlouni, D. Veljanovski, A. Capapé, J. Zhao, E. Herdtweck, M.J. Calhorda, F.E. Kühn Organometallics 28 (2009) 639–645.

[4] M. Groarke, I.S. Gonçalves, W.A. Herrmann, F.E. Kühn, J. Organomet. Chem. (2002) 108–112.

[5] A. Comas-Vives, A. Lledós, R. Poli, Chem. Eur. J. 16 (2010) 2147–2158.

[6] P. Chandra, S.L. Pandhare, S.B. Umbarkar, M.K. Dongare, K. Vanka, Chem. Eur. J. 19 (2013) 2030–2040.

[7] M. Abrantes, A.M. Santos, J. Mink, F.E. Kühn, C.C. Romão, Organometallics 22 (2003) 2112–2118.

[8] A.M. Martins, C.C. Romão, M. Abrantes, M.C. Azevedo, J. Cui, A.R. Dias, M. T. Duarte, M. A. Lemos, T. Lourenço, R. Poli Organometallics 24 (2005) 2582–2589.

[9] D. Saurenz, F. Demirhan, P. Richard, R. Poli, H. Sitzmann, Eur. J. Inorg. Chem. (2002) 1415–1424.

[10] M. V Galakhov, P. Gómez-Sal, T. Pedraz, M.A. Pellinghelli, P. Royo, A. Tiripicchio, A. V. de Miguel J. Organomet. Chem. 579 (1999) 190–197.

[11] D. Chakraborty, M. Bhattacharjee, R. Krätzner, R. Siefken, H.W. Roesky, I. Uson, H.-G. Schmidt Organometallics 18 (1999) 106–108.

[12] M.K. Trost, R.G. Bergman, Organometallics 10 (1991) 1172–1178.

[13] S.A. Hauser, M. Cokoja, M. Drees, F.E. Kühn, J. Mol. Catal. A Chem. 363-364 (2012) 237–244.

[14] M. Pratt, J.B. Harper, S.B. Colbran, Dalton Trans. (2007) 2746–2748.

[15] P. Legzdins, E.C. Phillips, S.J. Rettig, L. Sanchez, J. Trotter, V.C. Yee, Organometallics 7 (1988) 1877–1878.

[16] F.E. Kühn, A.M. Santos, M. Abrantes, Chem. Rev. 106 (2006) 2455–75.

[17] J.A. Brito, B. Royo, M. Gómez, Catal. Sci. Technol. 1 (2011) 1109.

[18] M. Abrantes, A. Sakthivel, C.C. Romão, F.E. Kühn, J. Organomet. Chem. 691 (2006) 3137–3145.

[19] J. Zhao, E. Herdtweck, F.E. Kühn, J. Organomet. Chem. 691 (2006) 2199–2206.

[20] M. Abrantes, F.A.A. Paz, A.A. Valente, C.C.L. Pereira, S. Gago, A.E. Rodrigues, J. Klinowski, M. Pillinger, I. S. Gonçalves J. Organomet. Chem. 694 (2009) 1826–1833.

[21] P.M. Reis, C.A. Gamelas, J.A. Brito, N. Saffon, M. Gómez, B. Royo, Eur. J. Inorg. Chem. 2011 (2011) 666–673.
[22] S. Li, Z. Wang, T.S.A. Hor, J. Zhao, Dalton Trans. 41 (2012) 1454–1456.
[23] S. Li, C.W. Kee, K. Huang, T.S.A. Hor, J. Zhao, Organometallics 29 (2010) 1924–1933.
[24] S.A. Hauser, M. Cokoja, F.E. Kühn, Catal. Sci. Technol. 3 (2013) 552.
[25] D. Betz, W.A. Herrmann, F.E. Kühn, J. Organomet. Chem. 694 (2009) 3320–3324.
[26] D.G. Blackmond, Angew. Chem. Int. Ed. 44 (2005) 4302–4320.
[27] Chapter 4.
[28] J. Zhao, A.M. Santos, E. Herdtweck, F.E. Kühn, J. Mol. Catal. A Chem. 222 (2004) 265–271.
[29] P. Neves, C. C. L. Pereira, F. A. A. Paz, S. Gago, M. Pillinger, C. M. Silva, A. A. Valente, C. C. Romão, I. S. Gonçalves J. Organomet. Chem. 695 (2010) 2311–2319.
[30] J.A. Brito, H. Teruel, S. Massou, M. Gómez, Magn. Reson. Chem. 47 (2009) 573–577.
[31] A.M. Al-Ajlouni, A.A. Valente, C.D. Nunes, M. Pillinger, A.M. Santos, J. Zhao, C. C. Romão, I. S. Gonçalves, F. E. Kühn Eur. J. Inorg. Chem. (2005) 1716–1723.
[32] P.J. Costa, M. José Calhorda, F.E. Kühn, Organometallics. 29 (2010) 303–311.
[33] J.M. Mitchell, N.S. Finney, J. Am. Chem. Soc. 123 (2001) 862–869.
[34] W.R. Thiel, T. Priermeier, Angew. Chem. Int. Ed. English. 34 (1995) 1737–1738.
[35] H. Mimoun, I.S. de Roch, L. Sajus, Tetrahedron 26 (1970) 37–50.
[36] C. Su, J.W. Reed, E.S. Gould, Inorg. Chem. 12 (1973) 337–342.

5.6 Supporting Information

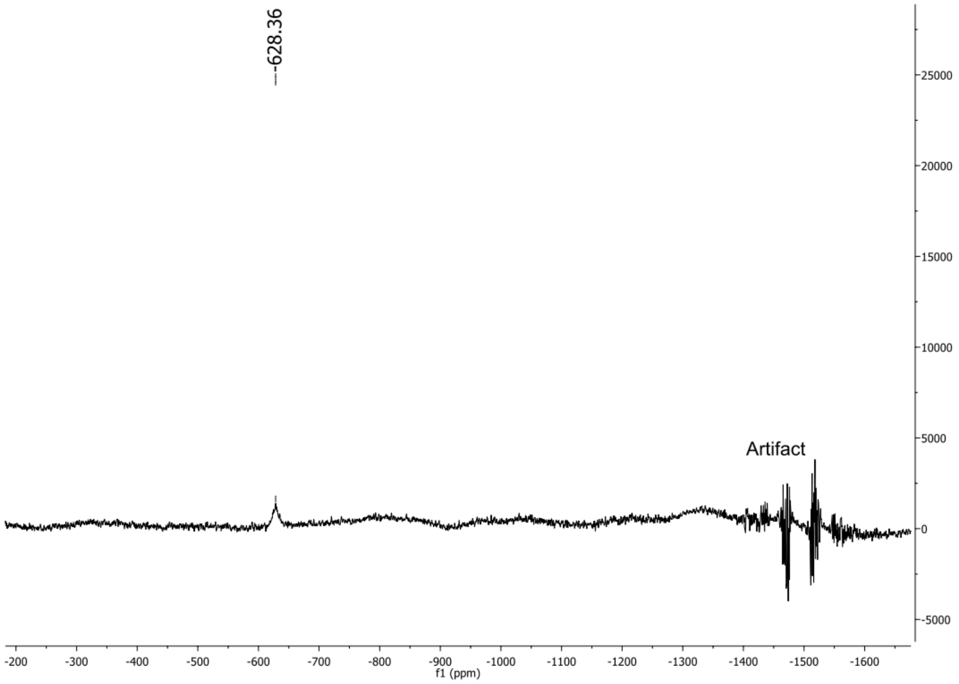

Figure 5.9. ^{95}Mo NMR measured after 24 h of oxidation of precatalyst 5 with 10 equiv. of TBHP (n-decane) in CDCl3.

Pre-catalyst **5** (0.2335 M in $CDCl_3$) was first oxidized with 50 equiv. TBHP (0.85 mL of 5.5 M in n-decane) at room temperature. After 48 h, 10 equiv. of *cis*-cyclooctene (0.12 mL) was added to the NMR tube and the reaction was monitored for 4 h. The rate of epoxidation of *cis*-cyclooctene is slower and there is an incomplete conversion of cyclooctene even after 4 h and presence of initial excess of TBHP (50 equiv.). (Figure 5.10)

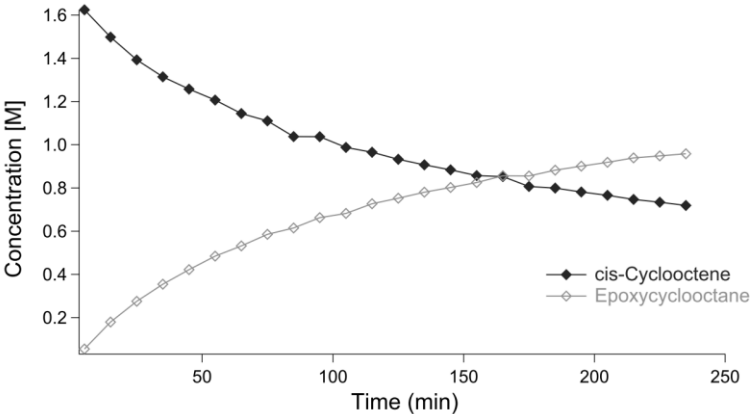

Figure 5.10. Kinetic plot of epoxidation of *cis*-cyclooctene with TBHP and oxo-peroxo complex obtained after oxidation of **5**.

6 Oxidation of [CpMo(CO)$_3$R*] Pre-catalysts with *tert*-Butyl Hydroperoxide

Abstract

Oxidative transformation of [CpMo(CO)$_3$R] (R = various alkyl groups) Mo(II) pre-catalysts with *tert*-butylhydroperoxide (TBHP) has been studied by kinetic NMR and *in situ* IR. ^{1}H and ^{13}C NMR profiles show that two Mo(VI) complexes − dioxo [CpMoO$_2$R], **I** and oxo-peroxo [CpMo(O)(O$_2$)R], **II** are formed. Additionally, NMR signals for two intermediate species arbitrarily assigned as **A** and **B**, are also observed during this transformation. Under certain conditions, oxidation of these pre-catalysts is accompanied by the formation of a precipitate which is not easily characterized. It is proposed that the precipitate is formed *via* an intermediate with σ-bonded Cp which corresponds to the NMR signal assigned **A**. In addition to the two Mo(VI) complexes, calculated thermodynamic data indicates that existence of Mo(IV) mono-oxo complex [CpMo(O)R] and Mo(V) μ-oxo dimers during oxidative decarbonylation is feasible for R = CH$_2$COOCH$_3$. Thus in ^{1}H NMR, it is proposed that signal **B** corresponds to Cp signal either in intermediate of the type [CpMo(OH)(OO^{t}Bu)(O)R] or in Mo(V) *mono*- or *bis*-μ-oxo dimers [(CpMo(O)R)$_2$(μ-O)$_{1,2}$] . The NMR signals assigned to the species **A** and **B**, and precipitate formation are not observed during catalytic olefin epoxidation reaction. A study of oxidative decarbonylation under different reaction conditions illustrates that this process is not very efficient, primarily on account of formation of a precipitate. A general overall scheme of transformations of [CpMo(CO)$_3$R] complexes when they are treated with TBHP has been proposed.

6.1 Introduction

The catalytic activity and mechanism of homogeneous olefin epoxidation with MoO$_2$,[1−5] Mo(O)(O$_2$)$_2$,[6] MoO$_3$,[7−9] and (MoO)$_2$(μ-O)[10,11] based complexes has been extensively addressed in literature.[12−14] In 2003, Kühn and co-workers demonstrated that cyclopentadienyl tricarbonyl complexes of molybdenum, [Cp'Mo(CO)$_3$Cl] (where Cp' = C$_5$H$_5$, C$_5$Me$_5$, C$_5$(CH$_2$Ph)$_5$) are oxidized with alkylhydroperoxides such as *tert*-butylhydroperoxide (TBHP) to dioxo complexes [Cp'Mo(O)$_2$Cl].[15] These dioxo complexes are highly active catalysts for the epoxidation of unfunctionalized olefins, but more sensitive to air and moisture compared to their tricarbonyl precursors. A decade later, numerous tricarbonyl complexes of this type ([CpMo(CO)$_3$R], where R = halide, alkyl, N-heterocyclic carbene, alkylester, *ansa* bridged alkyl or cycloalkyl group etc.) have been synthesized and applied *in situ* as highly selective pre-catalysts for epoxidation with TBHP.[16] Subsequent kinetic and mechanistic work with these complexes has shown that the dioxo complexes are further oxidized to oxo-peroxo complexes in excess TBHP and the latter complexes may or may not be active catalysts.[17−21] There is extensive data available regarding catalytic activity under diverse reaction conditions for the different structural types of these complexes.[16] Despite this, progress with deriving structure-activity relationships is slow and identifying key catalyst design principles for a specific, desired functionality of these complexes is quite challenging. For example, catalytic activity trends for complexes that differ in the substitution pattern on the Cp ring,[15,22] or on the size of cycloalkyl ansa bridge[23] have been studied. In Chapter 3, an explanation for the high catalytic activity of the [CpMo(CO)$_2$(NHC)X] complexes has been sought by discussing the unique stereoelectronic features of the imidazo[1,5-a]pyridyl-3-ylidine NHC ligand. A correlation between ^{95}Mo NMR shifts and turnover frequencies (or TOFs) has been proposed for complexes with alkylester side chain substituents.[24] However, even now, attempts to predict catalytic activity on the basis of stereoelectronic effects of the ligands fail in some cases.[20] Subsequently, only elaborate theoretical calculations are able to propose explanations for differences in reactivity.[21]

In Chapter 5, catalytic epoxidation of *cis*-cyclooctene with η^1-oxoalkyl ester complex [CpMo(CO)$_3$(CH$_2$COOR*)] (R* = bornyl, **5**) with TBHP under varying reaction conditions has been studied. The conclusions of this kinetic NMR study are that the dioxo complex which is formed after oxidative decarbonylation is the primary catalyst species for epoxidation. Even though a sufficient excess of the oxidant is available, epoxidation reaction takes precedence over complete oxidative decarbonylation of the pre-catalyst. In the later stages of the reaction when nearly complete conversion of the substrate *cis*-cyclooctene has taken place, the dioxo complex is further oxidized to oxo-peroxo species. The oxo-peroxo complex [CpMo(O)(O$_2$)R] is also active for catalytic epoxidation of cyclooctene. Furthermore, the initial reaction conditions have a strong influence over how the reaction evolves. It has been shown that the rate of the epoxidation reaction shows a non-first order dependence on substrate concentration. When substrate:oxidant concentration ≥ 1, saturation kinetics is observed, implying that a Michaelis-Menten type equilibrium must exist. This hints that during the catalysed reaction olefin coordination is possible at high concentration of the substrate. In other words, TBHP and the olefin compete for coordination at the metal centre. Since the coordination of the alkene as a η^2-ligand with the dioxo complex [CpMoO$_2$R] is energetically unfavourable and the coordination sphere of the activated complex [CpMo(O)(OH)(OO^{t}Bu)] too crowded for π-coordinated alkene ligand, it is proposed that a coordinatively unsaturated Mo species exists during the transformation of [CpMo(CO)$_3$R] pre-catalyst to the Mo(VI) dioxo complex.

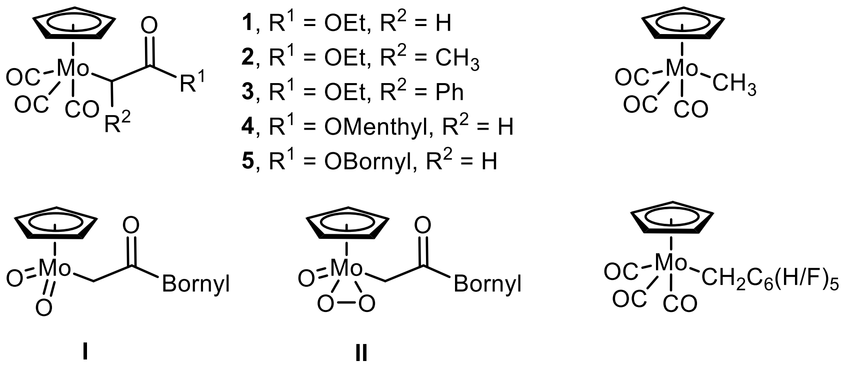

Figure 6.1. Complexes discussed in this chapter.

The technique of *in situ* pre-catalyst oxidation with TBHP for epoxidation of unfunctionalized olefins has been employed for obtaining oxo complexes in several structurally different Mo compounds. For example, not only CpMo tricarbonyl complexes, but several Mo and W dicarbonyl and tetracarbonyl complexes have been applied as pre-catalysts for olefin epoxidation *via* the *in situ* oxidation method with TBHP and H_2O_2 as oxidants.[25–28] Therefore we find it pertinent to re-evaluate the efficiency and selectivity of this process. The objective of this study is to find explanations for the exothermic nature of the oxidative decarbonylation reaction and lack of enantioselectivity during epoxidation of prochiral substrates. An attempt to assess of the stability of oxo complexes obtained from different pre-catalysts has also been made. The intention of the work discussed in this chapter is to identify the generic modes of activation and reactivity of $[CpMo(CO)_3R]$ complexes when they are treated with TBHP, and determine whether principles for molecular catalyst design are possible to derive.

6.2 Experimental

Theoretical Calculations – All computations have been performed by using Gaussian09 C.02. For all atoms excluding Mo, the optimizations, transition state searches (Berny algorithm)[29] and frequency/thermochemistry determinations have been conducted using the density functional method B3LYP[30–32] together with the basis set 6-31G**.[33,34] For Mo, effective-core potential (ECP) basis set was used (Stuttgart 1997).[35,36] All obtained geometries have been identified *via* the number of negative frequencies as minima (NImag=0) or transition states (NImag=1). All reported energies are un-scaled and reported in kcal mol^{-1} relative to a defined zero point. Free energy differences have been calculated for the gas phase in 298.15 K and 1.0 atm.

Materials and Methods – Complexes **1−5**, $[CpMo(CO)_3R]$ (R = CH_3, $CH_2C_6H_5$, $CH_2C_6F_5$) can be prepared by reaction of $Na[CpMo(CO)_3]$ and appropriate chloro- or mesylate precursors. The synthetic method is documented in published literature.[37–39] All NMR experiments were performed under ambient conditions. TBHP (5.5 M n-decane over molecular sieves, <4% H_2O) solution was purchased from Sigma Aldrich and used as such. Process analytics monitoring by *in situ* IR spectroscopy was carried out using Mettler-Toledo ReactIR™ 15 instrument at 25 °C under air.

Typical reaction conditions and data acquisition in kinetic ^1H and ^{13}C NMR study for pre-catalyst oxidation –

0.1 mmol of **5** was dissolved in 0.4 mL $CDCl_3$ in an NMR tube with mesitylene as an internal standard and its ^1H and ^{13}C spectra was recorded at room temperature. 10 equiv. of TBHP (5.5 M n-decane solution) was added and the solution was mixed properly before the start of reaction progress monitoring by *multizg* acquisition program of Bruker Topspin spectrometer. After shimming, ^1H spectra (16 scans) were first recorded at 5 min and subsequently at intervals of 10 min, and ^{13}C (164 scans) spectra first after 15 min and thereafter at 10 minute intervals, for the duration of 4 h. To obtain data at shorter intervals, the scans for ^{13}C NMR were reduced. In experiments for varying substrate, oxidant and catalyst concentrations, only ^1H NMR spectra were measured.

Effect of temperature on pre-catalyst oxidation The mixture of pre-catalyst **5**, mesitylene, $CDCl_3$ was maintained at the desired temperature (10 °C or 30 °C) using *edte* GUI in the 400 MHz Bruker spectrometer. 10 equiv. TBHP (5.5 M n-decane solution) was then added and the solution was mixed properly before the start of reaction monitoring by *multizg* acquisition program. After shimming, ^1H spectra were first recorded at 5 min and subsequently at intervals of 10 min, and ^{13}C spectra first after 15 min and thereafter at 10 minute intervals, for the duration of 4 or 6 h.

Data Analysis for all quantitative kinetic ^{1}H NMR Using NMR software MestReNova©, the characteristic signals at 6.65 ppm (mesitylene) and 7.8–8.0 ppm (naphthalene) for the internal standards were integrated to 3 H and 4 H respectively in all ^{1}H NMR. The concentration of different oxidized species was determined by integrating the area of Cp signals for these species as equivalent to 5 H (in case of **I** and **II**).

Oxidation of **5** with 10 equiv. TBHP at reflux conditions 0.678 mg (1.53 mmol) of pre-catalyst **5** was dissolved in 30 mL dry dichloromethane. 10 equiv. TBHP (15.3 mmol, 2.78 mL of 5.5 M *n*-decane solution) was then added to the solution which was brought to reflux (45 °C). Within an hour, formation of a white precipitate **5a** and change in colour of the bright yellow solution to pale yellow was observed. After 3h at reflux, the precipitate **5a** was separated from the light yellow supernatant, washed with dry DCM (3x10 mL) and dried under vacuum. The collected supernatant and washings were treated with a small amount of activated MnO_2. When effervescence ceased, the solution was dried with $MgSO_4$ and filtered again under argon. The filtrate was then concentrated under vacuum to obtain the air and moisture sensitive, light yellow oil **5b**.

5a IR (cm^{-1}) 1364 *w*, 1301 *vw*, 1241 *br*, 1150, 1125, 1044, 949 *vs*, 885 *vs*, 814 *vs*, 655 *vs*, 618 *s*, 586, 561, 531, 437. Analysis: C 24.59%, H 3.12%, Mo 34.33%; CI-MS 288.9 (MI), 136.9 (Base, 10.67%).

5b ^{95}Mo ($CDCl_3$, 2M Na_2MoO_4 in D_2O) δ -628. IR (cm^{-1}) 3394 *br*, 2923 *vs*, 2854 *w*, 2158 *vw*, 1735 *w*, 1691 *w*, 1455 *w*, 1363 *w*, 1247 *vs*, 1195, 1153, 1080, 1026 *s*, 951 *s*, 884 *s*, 818 *w*, 668 *w*, 571 *s*, 481 *vw*.

Pre-catalyst oxidation studied by *in situ* IR 98.9 mg of pre-catalyst **5** was dissolved in 10 mL $CHCl_3$ at 25 °C. This spectrum was measured as the baseline. 10 equiv. of TBHP was then added and the mixture was stirred for 4 h. Reaction progress was monitored by measuring the IR spectrum of the mixture after every 30 sec.

6.3 Results and Discussion

6.3.1 Oxidation of the Pre-catalyst

To study pre-catalyst oxidation, a solution of *ca.* 0.1 mmol of **5** in 0.4 mL dry $CDCl_3$ in an NMR tube was treated with 10 equiv. of TBHP. ^{1}H and ^{13}C NMR spectra were continuously obtained at intervals of 10 min for 4 h. NMR profiles are shown in Figure 6.2 and Figure 6.3.

Upon addition of TBHP to compound **5**, the signal of the Cp ligand (Cp-$(CO)_3$ in ^{1}H NMR spectrum shifts slightly upfield from 5.39 ppm to 5.36 ppm, possibly due to change in polarity. In the interval of 15–25 min after addition of the oxidant, a new peak at 6.47 ppm appears, and the peak at 5.36 ppm for **5** diminishes and disappears completely after 65 min. Subsequently, a peak at 6.45 ppm evolves and increases in intensity while the peak at 6.47 ppm disappears. The signal for the Cp ligand at 6.45 ppm persists for the entire duration of reaction progress monitoring and is also observed after 24 h.

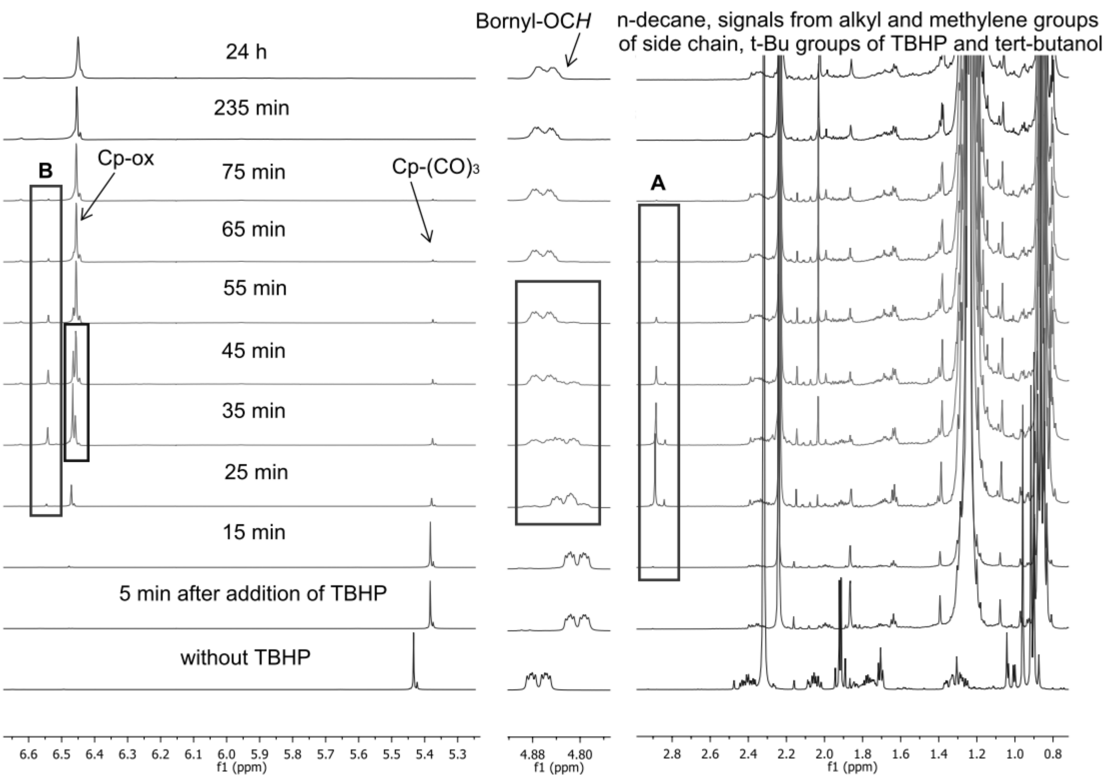

Figure 6.2. Kinetic ^{1}H NMR profile for the oxidation of 0.1 mmol of 5 with 10 equiv. of TBHP (in n-decane) in $CDCl_3$ at 22 °C.

In the period following oxidative decarbonylation, in the ^{13}C NMR spectrum (Figure 6.3) the Cp signal of **5** at 93.5 ppm decreases in intensity and two Cp signals at 111.9 and 113.5 ppm can be seen. The peak at 111.9 ppm rapidly decreases in intensity (at around 45 min) and a new signal at 112.3 ppm is seen that increases in intensity. The signals at 111.9 and 113.5 ppm disappear altogether after 65 min. ^{95}Mo NMR of the reaction mixture after 24 h shows a broad signal at -628 ppm and is identified as the oxo-peroxo complex since chemical shifts for similar complexes lie in the same range.[18,20] The persistent Cp signal at 6.45 ppm in ^{1}H NMR and 112.3 ppm in ^{13}C NMR are thus assigned to the oxo-peroxo complex. The short-lived signals at 6.47 ppm and 111.9 ppm correspond to the Cp ligand of the dioxo complex $[CpMo(O)_2R]$, **I** which is formed first and gives the oxo-peroxo species $[CpMo(O)(O_2)R]$, **II** on further oxidation with TBHP, as shown in Eq. (1).

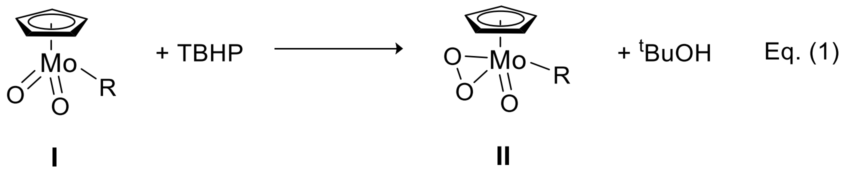

ΔH = -1.8 kcal/mol, ΔG = -0.9 kcal/mol (R = CH_2COOCH_3)

Scheme 6.1. Oxidation of dioxo complex I to oxo-peroxo species **II**.

The signal for the proton at the chiral carbon of the bornyl ester group C(=O)OC*H appearing as multiplet at 4.74–4.79 ppm in complex **5** also changes. In the interval of 25–55 min, the changes in this multiplet indicate that the species (dioxo *and* oxo-peroxo) formed on oxidation of **5** have hydrogen with similar chemical shift. After ~65 min, the multiplet is seen at 4.82–4.9 ppm. These changes coincide with the complete oxidative decarbonylation of the complex as observed by disappearance of Mo-CO signals (originally at 226.85, 227.0 and 240.58 ppm) in ^{13}C kinetic NMR profile after about 25 min of addition of TBHP (Figure 6.3).

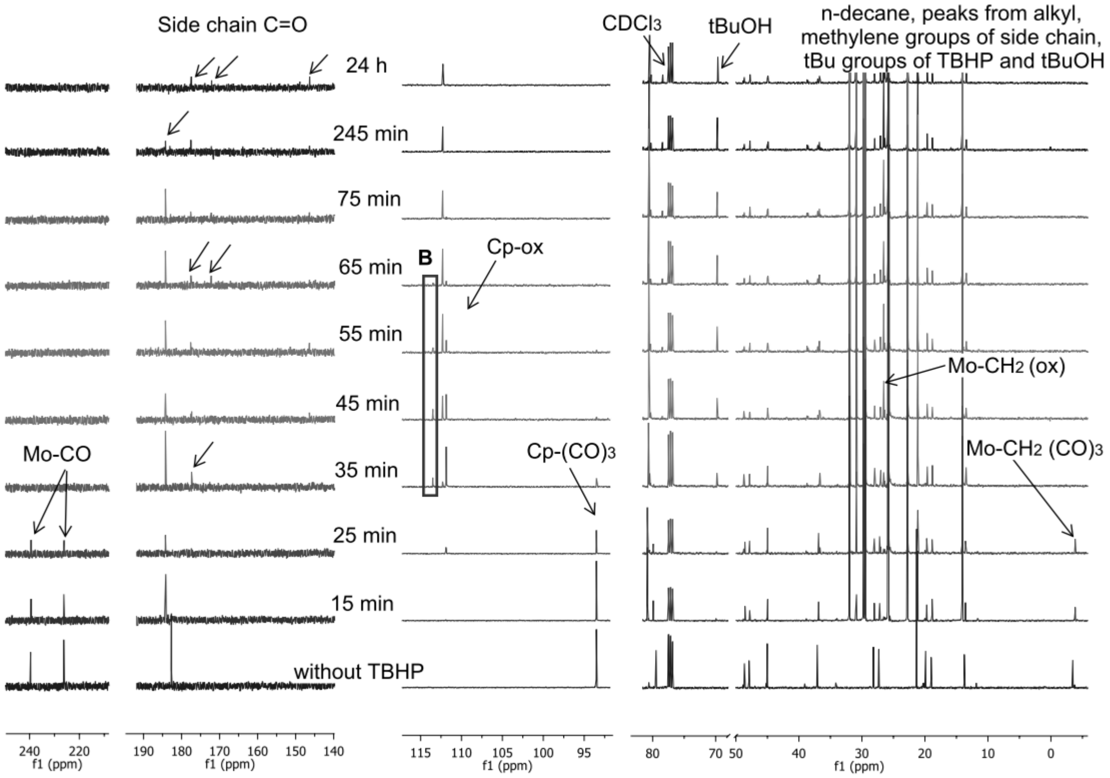

Figure 6.3. Kinetic ^{13}C NMR profile for reaction of 0.1 mmol of 5 with 10 equiv. of TBHP (n-decane) in $CDCl_3$ solvent at 22 °C.

The signal for α-C (Mo-CH_2) originally at -3.45 ppm in ^{13}C spectra of **5**, diminishes in intensity, and appears farther downfield at 26.5 ppm. Two signals are observed after oxidation at 177.4 and 172.2 ppm in the region of chemical shift for the side chain ester carbonyl group and disappearance of the signal at 184.1 ppm of the tricarbonyl pre-catalyst. At the end of 4 h of reaction monitoring, a light yellow precipitate and bright yellow supernatant are observed in the NMR tube. The complete assignment of the observed ^{1}H and ^{13}C NMR chemical shifts is summarized in Table 6.1.

Oxidation of **5** with 10 equiv. of TBHP in $CHCl_3$ was also studied by *in situ* FTIR spectroscopy. The stretching frequencies for terminal CO and ester –C=O groups at 2034 (a), 1952 cm^{-1} (b); and 1672 cm^{-1} (c) respectively disappear altogether after 4 h. Two new bands are observed for the ester group – 1717 cm^{-1} (c') and 1620 cm^{-1} (c'') which suggests that two oxidised CpMo species must be present that retain the side chain. Absorption at 775 cm^{-1} is similar to the v(Mo-O-Mo) reported for $[((C_5(CH_2Ph)_5)MoO)_2(\mu\text{-}O)]$ complex[10] and the strong stretching frequencies at 990, 957, 916 and 890 cm^{-1} lie in the range reported for v(Mo=O) in many CpMo dioxo and oxo-peroxo complexes.[1,10,15] Despite presence of several characteristic bands of metal-oxo species in the IR spectra, it is evident that more than one species is present which makes it difficult to assign them to either complexes **I**, **II** (Figure 6.1) or intermediates **B_1**, **B_2** (Scheme 6.3) or even *mono*- or *bis*-μ-oxo complexes (Scheme 6.6).

Table 6.1. Assignment of ^{1}H and ^{13}C NMR chemical shifts (in ppm) observed during oxidative decarbonylation of **5** with 10 equiv. of TBHP oxidant in $CDCl_3$ at 22 °C. R* = $CH_2COOBornyl$, Cp = C_5H_5, n.o. = not observed.

Complex	^{1}H NMR, δ (ppm)		^{13}C NMR, δ (ppm)		Time
5	Cp	5.39	Cp	93.52	0–65 min
	C(O)OCH	4.74-4.79	Mo-CH_2	-3.45	
			(O=C)OR*	182.9 → 183.9[a]	
			Mo-CO	226.85, 227.0, 240.58	
I (dioxo) $CpMoO_2R$*	Cp	6.47	Cp	111.9	25–65 min
			Mo-CH_2	n.o.	
			(O=C)OR*	177.2	
II (oxo-peroxo) $CpMoO(O_2)R$*	Cp	6.45	Cp	112.3	45 min–48 h
	C(O)OCH	4.82-4.90	Mo-CH_2	26.5	
			(O=C)OR*	172.4	
A	Cp	2.85	Cp	n.o.	15–65 min
B	Cp	6.52	Cp	113.5	25–65 min

[a] Changes in chemical shift due to change in polarity on addition of TBHP.

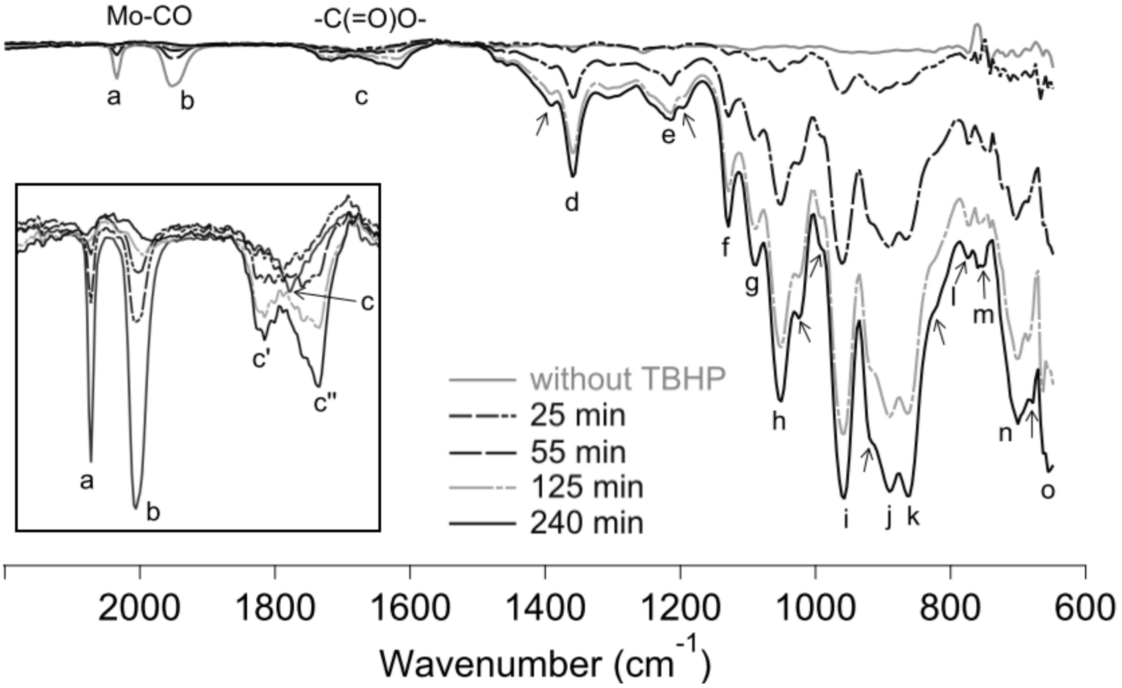

Figure 6.4. *In situ* IR profile for the oxidation of pre-catalyst 5 with 10 equiv. of TBHP at 25 °C in $CHCl_3$. Inset shows the carbonyl region. Baseline corrected spectrum at t = 0 min immediately after addition of TBHP is indicated in red). All other spectra show only evolving absorption bands.

Oxidation of the pre-catalyst is invariably accompanied by the formation of a precipitate. This is a limitation for quantitative kinetic studies by NMR since only homogeneous systems can be studied accurately.[40] Due to the heterogeneous nature of the reaction, an evaluation of its rate or rate constant by following reaction progress is difficult. Nevertheless, it is still possible to derive some qualitative information about this oxidative transformation as discussed in the following sections.

Table 6.2. Observed absorption bands during oxidation of pre-catalyst **5** with 10 equiv. of TBHP studied by *in situ* FTIR in $CHCl_3$ solvent.[a]

Label	Wavenumber (cm^{-1})		Assignment
	t = 0 min	t = 240 min	
a	2034	–	v_s(C≡O)
b	1952	–	v_a(C≡O)
c	1672	c' 1717	v(C=O)
		c'' 1620	v(C=O)
d	–	1389 *sh*, 1359	v_a(CC), Cp (?)
e	–	1214, 1195 *sh*	v (C-O) (^{t}BuOH) (?)
f	–	1128	v_s(CC), Cp (?)
g	–	1087	(?)
h	–	1050, (1024 *sh)*	β(CH), Cp (?)
i	–	(990 *sh*), 957	v_{sym}(Mo=O)
j	–	(916 *sh)*, 890	v_{asym}(Mo=O)
k	–	864, (827 *sh)*	v(O-O)
l	–	775	v(Mo-O-Mo)
m	–	760, 752	(?)
n	–	700, 678 *sh*	(?)
o	–	655	(?)

[a] Abbreviation sh refers to ‘shoulder’ peak indicated by an arrow in Figure 6.4. Due to broad, overlapping absorption bands and hints of formation of more than one Mo-oxo species, an accurate assignment of all observed stretching frequencies from 600-1300 cm^{-1} is tedious and thus not attempted here.

6.3.2 Pre-catalyst Oxidation under Varying Reaction Conditions

6.3.2.1 Effect of Oxidant Concentration

When complex **5** dissolved in $CDCl_3$ is treated with 20 equiv. and 50 equiv. of TBHP at room temperature, ^{1}H and ^{13}C NMR profiles (Figure 6.5). Similar to those illustrated in Section 6.3.1 are observed. Considering the chemical shift for Cp ligand in ^{1}H NMR profile, it is evident that at least three distinct species are formed following oxidative decarbonylation, indicated by signals at 6.46 ppm (oxo-peroxo), 6.48 ppm (dioxo) and 6.55 ppm (species **B**, see Table 6.1), that are shifted downfield from the Cp of tricarbonyl pre-catalyst **5** appearing at 5.39 ppm. Also, a signal at 2.91 ppm (species **A**) is seen which only exist in the time period of 15-45 min after addition of TBHP. In ^{13}C NMR profile (Figure 6.5(b)) three downfield shifted Cp signals are seen at 111.85 ppm (dioxo), 112.35 ppm (oxo-peroxo) and 113.4 ppm (intermediate **B**). The sum concentration of the oxidized complexes, i.e. [**I**] + [**II**], *vs.* time plot for oxidation of **5** with 50 equiv. TBHP is shown in Figure 6.5(c).

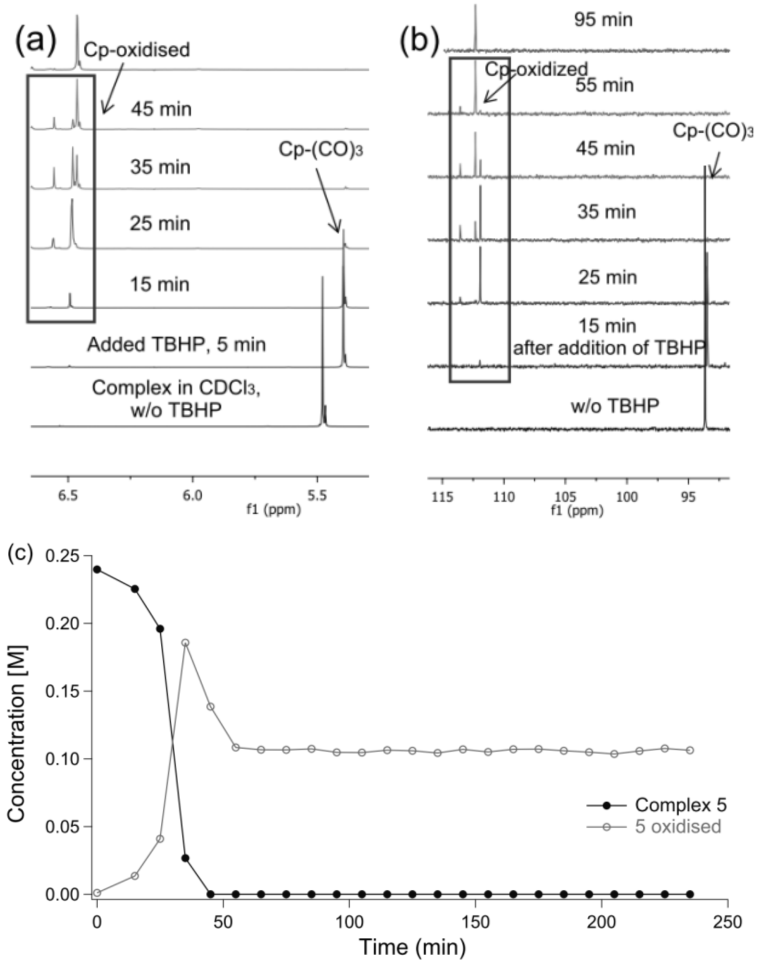

Figure 6.5. Kinetic (a) ^{1}H and (b) ^{13}C NMR profiles for the oxidation of complex **5** with 20 equiv. of TBHP, displaying changes in chemical shift for the Cp ligand. Concentration *vs*. time plots for oxidation of ca. 0.1 mmol pre-catalyst **5** with (c) 50 equiv. TBHP (5.5 M in n-decane) at 22 °C.

After treating **5** with 50 equiv. of TBHP (relative excess), the oxidized species, *vide supra* oxo-peroxo complex **II**, is stable and very little precipitate is observed in the NMR tube. NMR signals assigned as **A** and **B** are also observed during the period of decarbonylation and transformation of dioxo complex to oxo-peroxo species. This observation suggests that the species that precipitates must either be soluble in the polar reaction medium or, that the oxidative transformation that results in the formation of the precipitate is suppressed in presence of excess oxidant. Note however the proposal in Section 6.3.3, that the precipitate is a species formed on loss of Cp ligand, *via* an intermediate with σ-bonded or η^1-Cp, and that signal **A** corresponds to such a species. At high TBHP concentration (50 equiv.), ^{1}H NMR signal **A** is still observed and therefore the latter proposed alternative that formation of the precipitate is suppressed is not plausible.

6.3.2.2 Effect of Pre-catalyst Concentration

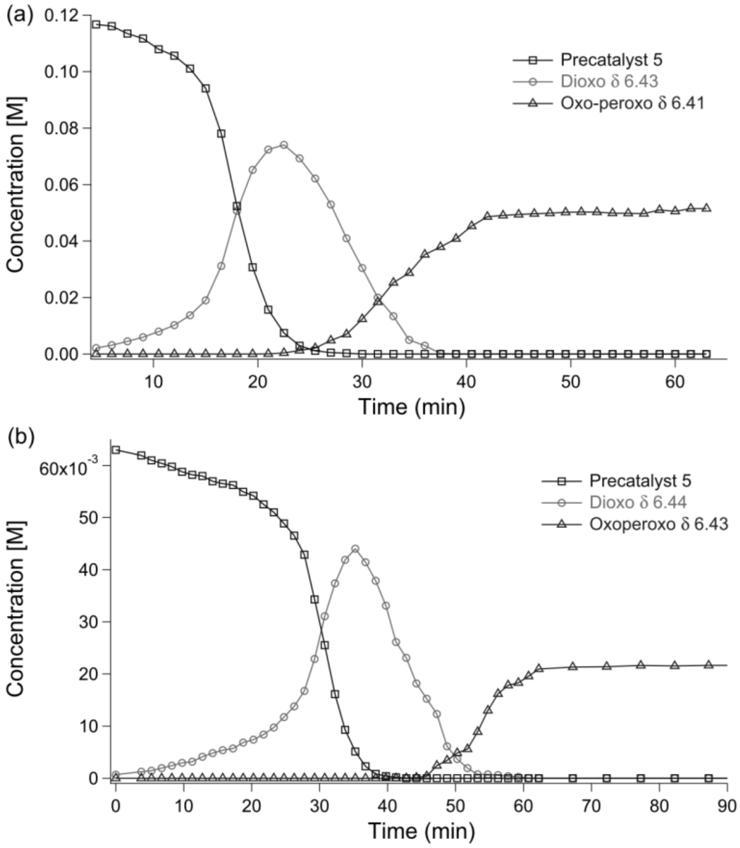

Figure 6.6. Oxidation of pre-catalyst 5 with 20 equiv. of TBHP oxidant, 0.4 mL $CDCl_3$, 22 °C. (a) $[cat]_{t=0}$ = 0.12 M (0.048 mmol), $[cat]_{t=60min}$ = 0.0515 M. (b) $[cat]_{t=0}$ = 0.061 M (0.0246 mmol), $[cat]_{t=80\ min}$ = 0.0216 M.

From a study of oxidation of different concentrations of **5** with TBHP (20 equiv. in all cases it is found that the yield of the oxidized complex **II** after 60 min is 43% from oxidation of 0.048 mmol of **5**, and 35% after 80 min when 0.246 mmol of **5** is treated with TBHP (relative excess). The determined yields reflect that oxidative decarbonylation of the tricarbonyl pre-catalyst is not very efficient. Nevertheless, since oxidation of the pre-catalyst is accompanied by the formation of a precipitate, it is reasonable to attribute the poor yields to the amount of **II** that is present in solution and thus measurable by solution NMR.A comparison of Figure 6.6(a) and (b) illustrate the effect of dilution on the rate of pre-catalyst oxidation. Even though a relatively larger excess of TBHP is available for oxidation of lesser amount of the pre-catalyst, oxidative decarbonylation takes longer – *ca.* 40 min for $[cat]_0$ = 0.061 M and 25 min for $[cat]_0$ = 0.12 M. This counterintuitive observation is easily explained. Oxidation of a smaller amount of the pre-catalyst in the same amount of solvent results in dissipated influence of temperature increase on the reaction rate. Effect of temperature on the oxidation reactions is discussed in the next section.

6.3.2.3 Effect of Temperature

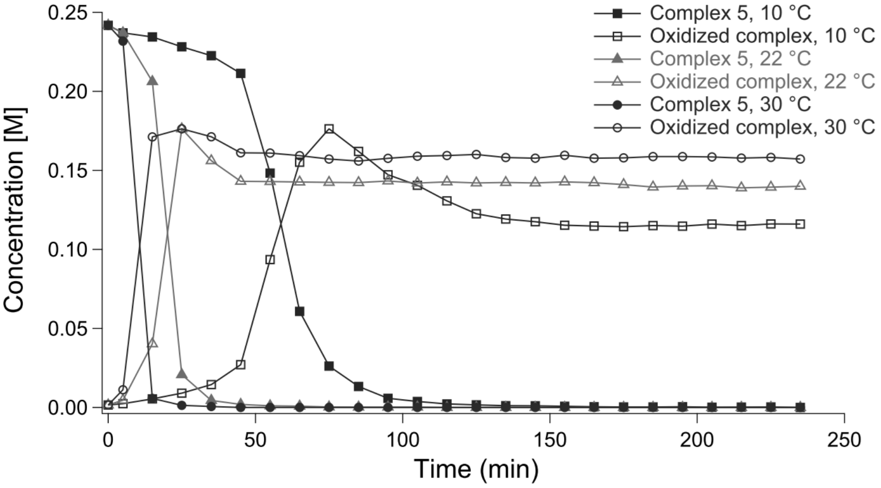

Figure 6.7. Plot of concentration *vs.* time of 5 and sum of dioxo and oxo-peroxo complexes (I + II) formed on oxidation of 5 at 10 (blue), 22 (green) and 30 °C (red) using 20 equiv. of TBHP in $CDCl_3$.

The changes in concentration of **5** and resulting oxidized complexes during its oxidation with 20 equiv. of TBHP (in n-decane) at different reaction temperatures are illustrated in Figure 6.7. It is evident that at 30 °C, the conversion of **5** to oxidized complexes **I** and **II** is faster and nearly complete by 15 min, compared to oxidation at 10 °C (75 min) or 22 °C (25 min). It is interesting to note that at different temperatures, oxidation of **5** ($[\mathbf{5}]_{t=0}$ = 0.241 M) forms the same amount of oxidized species, $[\mathbf{5_{ox}}]_{max}$ = 0.176 M in yield 73%. However, the concentrations of the oxidized complexes present in solution after 4 h differ – 0.157 M (yield 65%) at 30 °C; 0.139 M (yield 57.4%) at 22 °C and, 0.115 M (yield 47.5%) at 10 °C. It is possible that for reactions at 22 °C and 30 °C, the concentration of **I** and **II** together is quantified to be higher compared to reaction at 10 °C simply because of better solubility of these species at higher temperatures, which is actually measurable by NMR.

It is observed that pre-catalyst oxidation at 10 °C is incomplete even after 6 h, and no precipitate is formed. However, as the NMR sample gradually reaches room temperature, small amounts of the pale yellow precipitate can be observed. This implies that the precipitate is thermodynamically more stable than **I** and **II**. The formation of the precipitate can also be attributed to oxidation of the remaining amount of tricarbonyl precursor **5** with TBHP. At this stage, it is unclear whether the precipitate if formed from oxidation of **5** or a decomposition product of the oxidized complexes. A summary discussion of the nature of the precipitate is presented in the next section.

6.3.3 Nature of the Precipitate

As mentioned before, oxidation of the pre-catalyst with TBHP invariably leads to formation of a precipitate along with complexes **I** and **II** which are present in solution. Concluding from the study of pre-catalyst oxidation under varying reaction conditions, it can be summarized that the formation of the precipitate can be avoided by using a large excess of the oxidant (50 equiv. of TBHP excess, Section 6.3.2.1) or alternatively a low concentration of the catalyst (Section 6.3.2.2). In addition, when oxidation is done at low temperature (10 °C, Section 6.3.2.3) and until pre-catalyst is completely oxidized, formation of the precipitate can be successfully suppressed. Thus precipitate formation is a thermodynamically driven process. Furthermore, during catalytic epoxidation no precipitate formation occurs (Chapter 5).

Although formation of a precipitate has been previously reported for a number of similar complexes, the nature of the precipitate has remained elusive.[10,27,41–43] Large scale oxidation of **5** with 10 equiv. TBHP at reflux conditions in CH_2Cl_2 (at 45 °C) results in the formation of an insoluble precipitate **5a**, and a pale yellow supernatant that was quenched with MnO_2, dried with $MgSO_4$, filtered and concentrated to give a pale yellow oily residue **5b**. Analysis of precipitate **5a** suggests a composition of 24.59% C, 3.12 % H and 34.33% Mo, corresponding to the simplest molecular formula $C_6H_9MoO_7$, assuming that no other elements are present and a single species is formed. Molecular ion peak for **5a** (CI +ve MS) is observed at 288.8 which fits the molar mass for the calculated simplest ratio. The fingerprint region for **5a** shows absorptions at 949 and 885 cm^{-1} that correspond to v(Mo=O) and v(O-O) respectively. Additionally, $v_s(Mo(\eta^2-O_2))$ and $v_a(Mo(\eta^2-O_2))$ bands at 586 cm^{-1} and 561 cm^{-1} suggest the presence of dioxo and peroxo linkage in the precipitate, which is therefore a Mo-containing species. Instructively, both metal coordinated CO signals and carbonyl ester of the side chain are missing from the IR spectrum of **5a**. Thermogravimetric analysis of **5a** shows a decomposition temperature of 197 °C and concurrent loss of 15.22% of original mass. At this temperature, complete decomposition of the complex mixture is apparent from simultaneous loss of *m/z* 18 (H_2O), 56, 66 (Cp), 96 (Mo), 122, 138 and other smaller fragments.

Unfortunately, complete characterization of **5a** by NMR is hindered by its insolubility in non-coordinating NMR solvents. In addition, the experimental results (elemental analysis and mass spectrometry (MS)) could not be reproduced. A second attempt at characterization of the precipitate suggested a different molecular formula of $C_4H_{10}MoO_8$ which was inconsistent with its MS data. This suggests that **5a** is very likely to be a mixture of complex molybdenum oxides and/or peroxides. Although side chain ligand dissociation occurs at reflux temperature, as evidenced by formation of precipitate **5a** which does not show any characteristic absorption frequencies of the chiral ester carbonyl group, under the catalytic epoxidation conditions it is evident from kinetic NMR results (Chapter 5) that presence of the olefin stabilizes the oxidized complex or at least influences the oxidative decarbonylation process in a way that neither the chiral side chain dissociates nor decomposition to complex molybdenum oxides occurs. For these reasons, we are inclined to regard formation of precipitate **5a** as a consequence of partial complex decomposition instead of a distinct or reproducible product of oxidation of **5**.

^1H and ^{13}C NMR spectra of **5b** in $CDCl_3$ are similar to the spectra illustrated in Figure 6.2 and Figure 6.3, i.e. indicating primarily the presence of oxo-peroxo complex **II** along with ^tBuOH. The FTIR spectrum of **5b** obtained in C_6D_6 shows characteristic, but weak absorptions at 1735 and 1691 cm^{-1} for the ester linkage of the side chain. Additionally, absorption bands at 950 cm^{-1}, 884 cm^{-1}, 561 cm^{-1} can be assigned to v(Mo=O), v(O-O) and $v_s(Mo(\eta^2-O_2))$ respectively.

*6.3.4 Nature of the Intermediate Species **A** and **B***

In the time following oxidative decarbonylation of pre-catalyst **5**, two transient signals at 2.85 and 6.52 ppm (assigned arbitrarily to Cp ligand of unknown species **A** and **B** respectively) are observed in

^{1}H NMR. The corresponding transient signal in ^{13}C NMR for **A** could not be easily identified. The signal at 113.5 ppm can be assigned to Cp ligand in species **B**, by correlating with the ^{1}H NMR shifts for this unidentified species. These 'extra' signals exist for a brief time during and after oxidative decarbonylation of **5**.

NMR Signal **A**

In the previous section, we found that the precipitate is a Mo-based oxo species which is devoid of the cyclopentadienyl ligand. Colbran et al. have previously reported a similar observation in which a highly substituted Cp ligand is lost from the active [Cp'MoO_2Br] complex at the later stages of the epoxidation reaction.[44] In the case of reaction of the tricarbonyl pre-catalysts with a large excess of TBHP, overcrowding of the metal centre can be anticipated as this is an oxidative addition reaction. Haptotropic shifts of π-coordinated cyclopentadienyl and indenyl ligands has been well studied in literature, and usually take place to compensate for steric or electronic saturation at the metal centres.[45,46] In other words, it can be reasoned that the $\eta^5 \rightarrow \eta^1$ Cp haptotropic shift results in an electron deficient metal centre (Cp changes from $6e^- \rightarrow 2e^-$ donor ligand), which would explain its tendency to react with the oxidant TBHP. At this stage, the most plausible explanation for the appearance of signal **A** is that it indicates a σ-bonded Cp ligand, with a predicted chemical shift of 2.9 ppm for the hydrogen at σ-C. Instead of the expected multiplet (dd) for this H, the signal appears as a singlet (Figure 6.2), and we reason that it is due to the two fluxional processes (a) rotation of η^1 Cp along the Mo-C bond, and (b) metallotropic migration along the ring carbons of η^1 Cp.

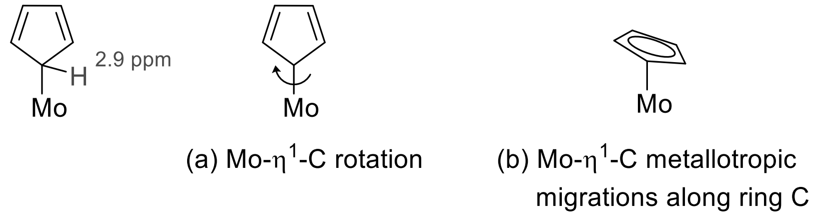

Figure 6.8. Proposed structures for assignment of the NMR signal A, assumed to refer to the Cp ligand.

As discussed in the previous section, analytical data suggests that the precipitate is a non-Cp containing Mo complex. Furthermore, during catalytic epoxidation NMR signal **A** is not observed and precipitate formation does not occur (Chapter 5). Considering these two observations together, we propose that the precipitate forms *via* an intermediate with a σ-bonded Cp ligand and this is observed in NMR as the ^{1}H NMR signal at 2.85 ppm in $CDCl_3$ during oxidation of **5** with TBHP.

NMR Signal **B**

When Mo(II) complex **5** is treated with excess TBHP, formation of several intermediate oxidized species having oxidation states of Mo as +III, +IV or +V is possible, before complexes dioxo and oxo-peroxo in the highest oxidation state +VI are obtained. Under such strong oxidizing conditions, Mo(VI) complexes are the stable end products that have been isolated and characterized, yet this does not exclude the possibility of formation as well as side reactions of aforementioned intermediate Mo oxo species.

Photochemical or thermal decarbonylation of [CpMo(CO)$_3$R] complexes is known to result in the formation of intermediates of the type [CpMo(CO)$_2$(L)R] and [CpMo(CO)(L)$_2$R] (where L = N-donor ligand).[47] In the presence of TBHP, the coordinatively unsaturated Mo species formed on loss of CO groups can be stabilized by the formation of Mo=O, Mo-OO^{t}Bu and Mo-OH species. The stoichiometry and mechanism of this oxidative transformation is currently unknown.

Similar to organometallic models for molybdenum oxotransferases[48] and Tp*Mo complexes,[49] one may anticipate the possible involvement of the reaction couple Mo^{IV}O/Mo^{VI}O$_2$, Eq. (2) in the initial stage of oxidative decarbonylation with TBHP. The under-coordinated Mo(IV) species may be stabilized through coordination of solvent (CH$_3$OH, H$_2$O), substrate olefin or O-donor TBHP.[11,50–54] However in all cases, its quick conversion to the Mo(VI) complex **I** is more likely since an excess of TBHP is present.

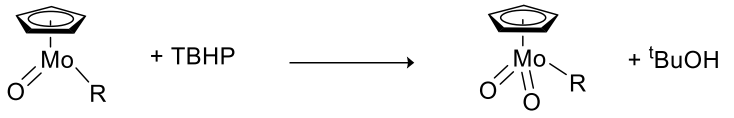

Eq. (2)

mono-oxo

I, di-oxo

$\Delta H = -99.3$ kcal/mol, $\Delta G = -98.6$ kcal/mol (R = CH_2COOCH_3)

Scheme 6.2. Oxidation of Mo(IV) mono oxo complex to Mo(VI) dioxo complex **I**.

The transformation shown in Eq. (2) is highly exothermic and thus a plausible explanation for the violently exothermic oxidative decarbonylation observed for several molybdenum carbonyl pre-catalysts (see Table 6.3 and Section 6.3.5).

Table 6.3. Calculated thermodynamic parameters (ΔH and ΔG in kcal mol^{-1})[a] for oxidative decarbonylation of [CpMo(CO)$_3$R] pre-catalyst with TBHP oxidant to give either Mo^{IV} or Mo^{VI} oxo species depending on the stoichiometry of the reaction and evolution of either CO or CO$_2$. R = -CH$_2$COOCH$_3$.

Reactants	Products	ΔH	ΔG
Mo(II)	**Mo(IV)**		
[CpMo(CO)$_3$R] + (CH$_3$)$_3$COOH	[CpMo(O)R] + (CH$_3$)$_3$COH + 3 CO	+18.5	-15.0
[CpMo(CO)$_3$R] + 2 (CH$_3$)$_3$COOH	[CpMo(O)R] + 2 (CH$_3$)$_3$COH + 2 CO + CO$_2$	-68.7	-101.8
[CpMo(CO)$_3$R] + 3 (CH$_3$)$_3$COOH	[CpMo(O)R] + 3 (CH$_3$)$_3$COH + CO + 2 CO$_2$	-156.0	-188.6
[CpMo(CO)$_3$R] + 4 (CH$_3$)$_3$COOH	[CpMo(O)R] + 4 (CH$_3$)$_3$COH + 3 CO$_2$	-243.2	-275.5
Mo(II)	**Mo(VI)**		
[CpMo(CO)$_3$R] + 2 (CH$_3$)$_3$COOH	[CpMo(O)$_2$R] + 2 (CH$_3$)$_3$COH + 3 CO	-80.8	-113.5
[CpMo(CO)$_3$R] + 3 (CH$_3$)$_3$COOH	[CpMo(O)$_2$R] + 3 (CH$_3$)$_3$COH + 2 CO + CO$_2$	-168.0	-200.4
[CpMo(CO)$_3$R] + 4 (CH$_3$)$_3$COOH	[CpMo(O)$_2$R] + 4 (CH$_3$)$_3$COH + CO + 2 CO$_2$	-255.3	-287.2
[CpMo(CO)$_3$R] + 5 (CH$_3$)$_3$COOH	[CpMo(O)$_2$R] + 5 (CH$_3$)$_3$COH + 3 CO$_2$	-342.5	-374.0

[a] See experimental section for calculation method details.

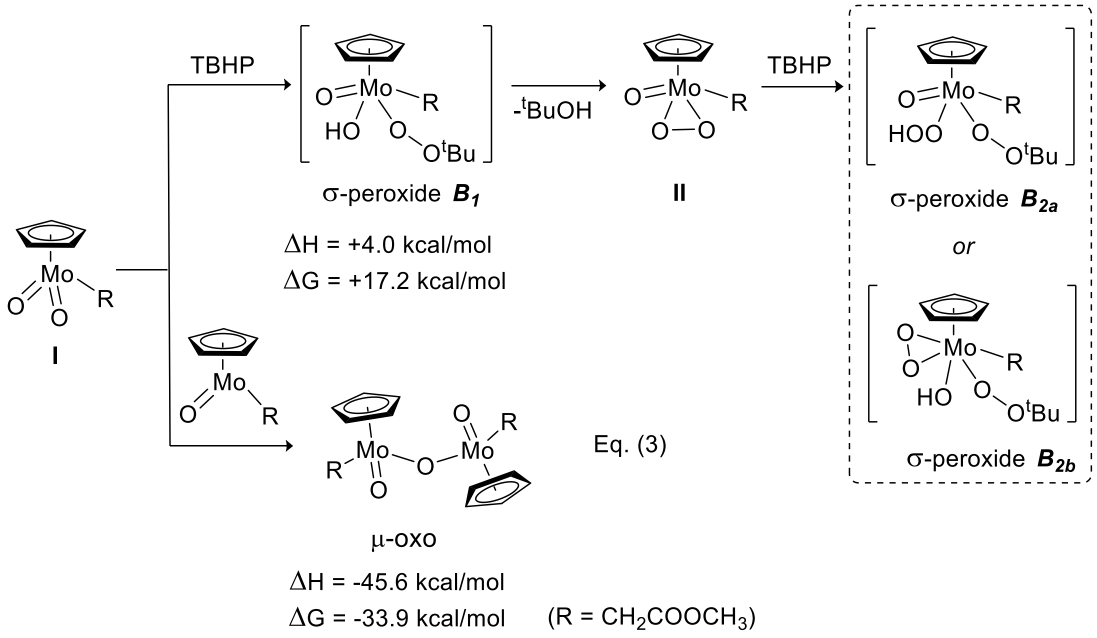

Scheme 6.3. Possible CpMo oxo species for transient NMR signal assigned **B**.

There are two plausible alternatives for the identity of species corresponding to NMR signal **B**. This signal appears during the transformation of dioxo complex **I** to oxo-peroxo species, **II** and can correspond to the Cp moiety either in an intermediate of the type [CpMo(O)(OH)(OO^{t}Bu)] or in *mono*- and *bis*-(μ-oxo) dimeric species [$(CpMoOR)_2(\mu\text{-}O)_{1,2}$], as discussed below.

Alternative 1

The formation of σ-peroxide intermediate complexes **B$_2$** from reaction of **II** with TBHP have been previously proposed for pre-catalysts [$CpMo(CO)_3(CH_3)$][18,19] and [$CpMo(CO)_3(CF_3)$].[20] Similar intermediates might be expected to form on reaction of **I** and **II** with TBHP. During catalysis, the alkene is expected to competitively react with the intermediate **B$_1$** for the formation of epoxide (ΔG = -57.7 kcal mol^{-1}) instead of further reaction to oxo-peroxo complex by loss of ^{t}BuOH (ΔG = -18.1 kcal mol^{-1}) (see Eq.s (A) and (B) in Scheme 6.4). This is confirmed from kinetic ^{1}H and ^{13}C NMR profiles of catalytic epoxidation of cyclooctene given in Chapter 5.

Note however that in the *absence* of the substrate both σ-peroxide intermediates **B$_1$** and **B$_2$** can exist. In the presence of excess TBHP, intermediate **B$_1$** is expected to quickly result in formation of **II** with loss of ^{t}BuOH instead of persisting in solution. Since signal **B** disappears soon after the Cp signals in the kinetic NMR profiles indicate the complete conversion of **I** to **II** (Table 6.1), there is a valid argument that ^{1}H and ^{13}C NMR signals 6.52 ppm and 113.5 ppm respectively correspond to Cp ligand in species **B$_1$**.

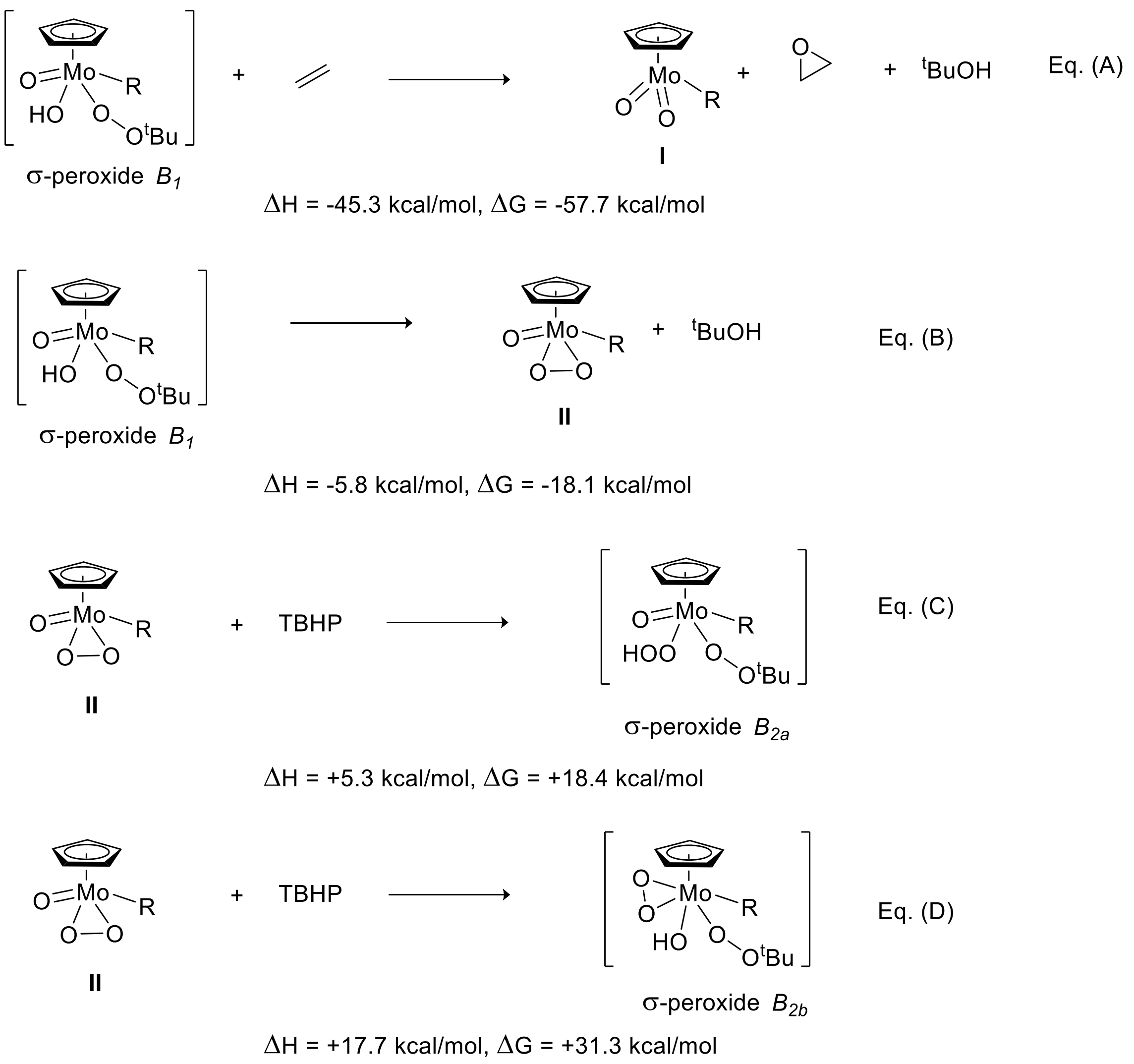
σ-peroxide B1
I
ΔH = -45.3 kcal/mol, ΔG = -57.7 kcal/mol
Eq. (A)
σ-peroxide B1
II
ΔH = -5.8 kcal/mol, ΔG = -18.1 kcal/mol
Eq. (B)
II
TBHP
σ-peroxide B2a
ΔH = +5.3 kcal/mol, ΔG = +18.4 kcal/mol
Eq. (C)
II
TBHP
σ-peroxide B2b
ΔH = +17.7 kcal/mol, ΔG = +31.3 kcal/mol
Eq. (D)

Scheme 6.4. Catalytic epoxidation involving intermediate $\mathbf{B_1}$ in competition with formation of oxo-peroxo complex **II** (Eq.s (A) and (B)). Formation of active intermediates $\mathbf{B_{2a}}$ and $\mathbf{B_{2b}}$ on reaction of **II** with TBHP (Eq.s (C) and (D)) R = CH_2COOCH_3 in all cases.

Similarly intermediates $\mathbf{B_{2a}}$ or $\mathbf{B_{2b}}$ should also form, exist in equilibrium with **II** indefinitely (in the absence of alkene) and also be observed in NMR – except unless the reaction of **II** with TBHP has a high activation barrier. Indeed, it is found that ΔG for these processes are +18.4 and +31.3 kcal mol^{-1} respectively. Instead the signal **B** disappears once the transformation of dioxo to oxo-peroxo is complete, which strongly argues against the possibility of this species being $\mathbf{B_2}$. This observation also questions the validity of assigning the ^{1}H and ^{13}C NMR signals to Cp ligand in $\mathbf{B_1}$ (as argued above). This is because calculated thermodynamic data suggests that a more suitable, second alternative is available − that signal **B** might correspond to a μ-oxo bridged complex (ΔG = +17.2 kcal mol^{-1} *vs.* ΔG = -33.9 kcal mol^{-1} (Eq.(3), Scheme 6.3).

Alternative 2

The existence of Mo(IV) species during oxidative decarbonylation has been rationalized above. As mentioned before, oxygen atom transfer processes involving $Mo^{IV}O/Mo^{VI}O_2$ couple are known for several organometallic models of molybdoenzymes.[48,49,55,56] An analogous transformation with hydroperoxide oxidant is proposed in Scheme 6.5.

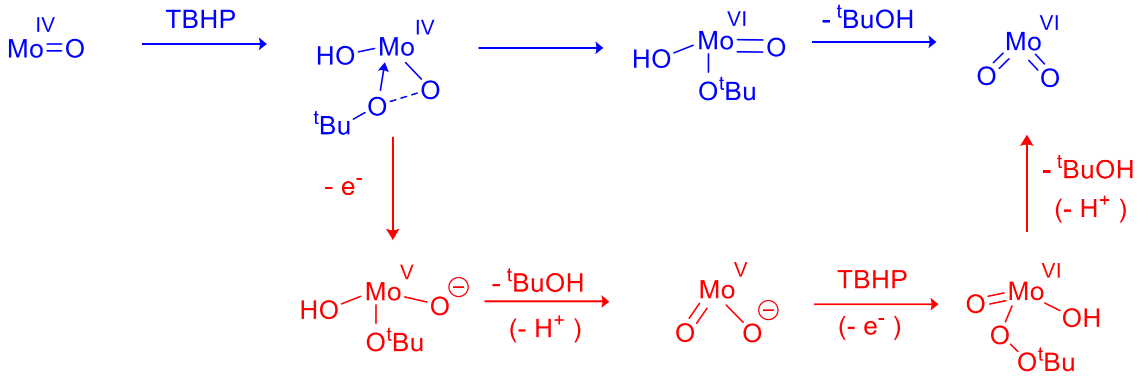

Scheme 6.5. Proposed two *one-electron* oxidation processes during the transformation of Mo(IV) to Mo(VI) *via* Mo(V) species with TBHP. Monoanionic ligands Cp and R have been omitted for clarity.

Formation of Mo(V) μ-oxo bridged species under oxidative conditions is also quite common[48,49,57] and their formation may either be irreversible or reversible.[57,58] In context of complexes studied here, the formation of the μ-oxo bridged complex [$(CpMoOR)_2(\mu\text{-}O)$] from the dioxo complex and the proposed mono-oxo species [CpMoOR] is also calculated to be thermodynamically feasible, ΔG = -33.9 kcal mol^{-1} (Eq. (3)). If NMR signal **B** is assigned to Cp ligand in such species, it would appear that the formation of the dimer is reversible, and occurs in the period of oxidative decarbonylation (25-45 min). The μ-oxo dimer thus formed may then react further with TBHP and undergo dissociation to give monomeric complexes. Transformation illustrated in Eq. (4), ΔG = +30.7 kcal mol^{-1} is not favoured, when compared to the more feasible and highly exothermic reaction pathway for the μ-oxo dimer to give two molecules of **I** (Eq. (5), ΔG = -66.9 kcal mol^{-1}) or even a *bis*-μ-oxo dimer, according to Eq.(6).

Note that the proposed dimeric molybdenum(V) oxo complexes are spin-paired and diamagnetic,[59] unlike paramagnetic monomeric Mo(V) species indicated in Scheme 6.5. Thus, if signal **B** in ^{1}H and ^{13}C NMR refers to the Cp ligand of such a species, its appearance in NMR is not unusual.

No significant changes in NMR spectra are seen near completion of the epoxidation reaction, except that the NMR signal of Cp ligand in oxo-peroxo complex can be observed. In the context of the study of pre-catalyst oxidation reaction, this may be interpreted as the stabilization of dioxo complex **I** in the presence of the reductant olefin substrate, epoxycyclooctane and the polarity of solvent or reaction medium which discourages its further oxidation to the oxo-peroxo complex. Additionally this observation may also imply that the reactions with respect to reversible (*μ*-oxo) dimer formation (Eq. (3)) and dissociation (Eq. (5)) (to give **I**) are suppressed as long as the dioxo complex is involved in the catalytic process.

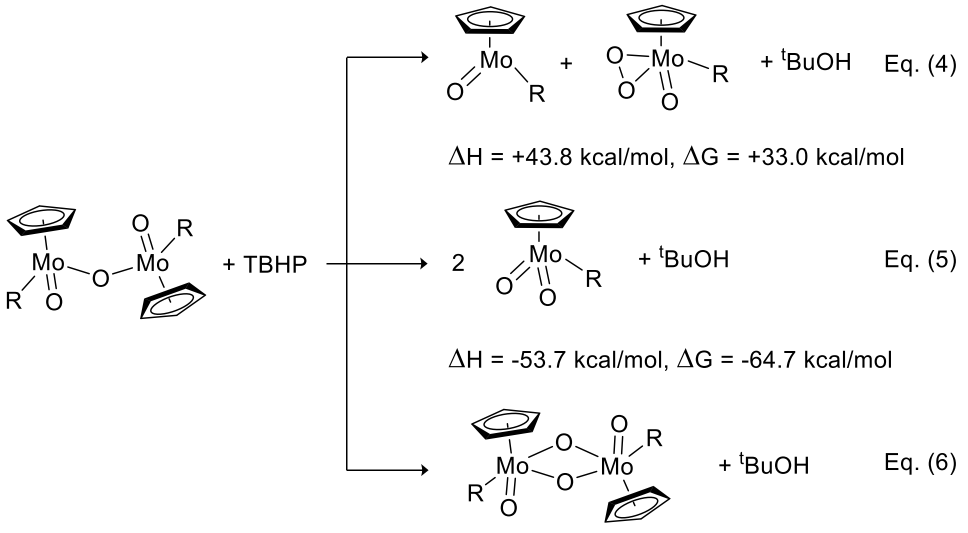

ΔH = +43.8 kcal/mol, ΔG = +33.0 kcal/mol

ΔH = -53.7 kcal/mol, ΔG = -64.7 kcal/mol

ΔH = -45.4 kcal/mol, ΔG = -42.1 kcal/mol

(R = CH_2COOCH_3 in all cases)

Scheme 6.6. Oxidative transformations possible with mono-µ-oxo Mo(V) intermediate complex.

Absence of NMR signals **A** and **B** during catalytic epoxidation of *cis*-cyclooctene suggests that due to the presence of the ‘reductant’ alkene substrate, the equilibria illustrated in Eq.s (2) and (3) are suppressed by ‘consuming’ the dioxo complex **I** or the σ-peroxide intermediate in the epoxidation reaction (Eq. (7)), so that the concentration of CpMoOR and $(CpMoOR)_2(\mu\text{-}O)$ does not sufficiently build up.

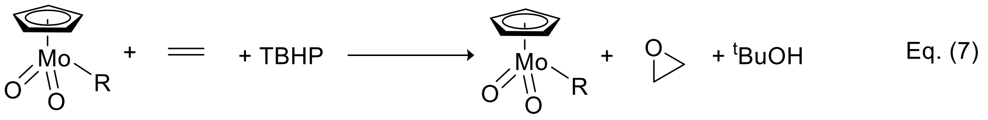

ΔH = -41.3 kcal/mol, ΔG = -40.6 kcal/mol (R = CH_2COOCH_3)

Scheme 6.7. Epoxidation of ethene with TBHP oxidant catalyzed by the dioxo complex $[CpMoO_2R]$.

The *bis*-µ-oxo species $[(CpMoOR)_2(\mu\text{-}O)_2]$ is very likely formed according to Eq. (6). Even though DFT calculations indicate that this species is thermodynamically quite stable, with a large excess of TBHP oxidant or at high reaction temperature, the *bis*-µ-oxo complex may participate in equilibria involving complexes **I** and **II**, according to Eq. (8). Disappearance of signal **B** in the presence of an excess of TBHP then indicates that the equilibrium involving proposed dimeric µ-oxo species and **I** and **II** is shifted favourably towards stabilization of these monomeric species.

If species identified from NMR signal **B** is indeed a µ-oxo bridged species, then it also follows that its catalytic activity in epoxidation of alkenes cannot be ruled out. Complexes of this type without Cp ligand[60,61] and even with the Cp ligand[10,11] have been reported to display good conversions of the alkene substrates to their epoxides, though as published before,[10] such complexes are less active than the mononuclear complexes. It is interesting to note that kinetic and mechanistic studies on epoxidation catalysis with µ-oxo complexes $[Cp_2M_2O_5]$ (M = Mo, W)[10,62,63] use the monomeric dioxo complex as a model for these studies, but do not address the dissociation of the μ-oxo bridged species to monomeric complexes with TBHP. Therefore, it is unclear whether such complexes are capable of oxygen atom transfer and/or catalytic activity as dimeric complexes or whether they simply contribute in catalysis by forming the active monomeric complexes in the presence of excess TBHP.

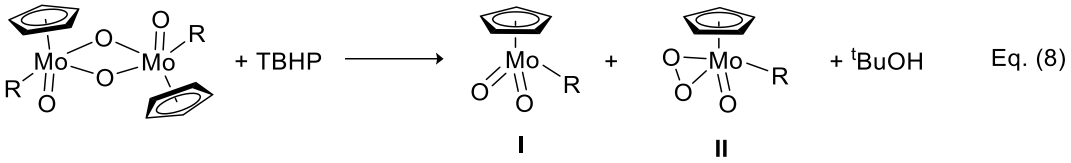

ΔH = -10.1 kcal/mol, ΔG = -23.5 kcal/mol (R = CH_2COOCH_3)

Scheme 6.8. Conversion of *bis*-μ-oxo Mo(V) dimer to monomeric complexes **I** and **II** with excess TBHP.

6.3.5 Scheme for Oxidative Transformations

Oxidation of the alkyl ester complex, R = $CH_2COOBornyl$ (**5**) and other pre-catalysts R = CH_3, $CH_2C_6H_5$, $CH_2C_6F_5$ and $CH_2COOC_2H_5$ with a relative excess of TBHP is invariably accompanied by the formation of a precipitate. However, at higher oxidant concentration and in the presence of the substrate, no precipitate is observed. Since two additional intermediates are observed during oxidation of **5**, oxidation of pre-catalysts having different side chains was also investigated. We have found that the appearance of NMR signals **A** and **B** is not unique to the alkylester complex **5**, and is also observed during the oxidation of complexes **1**, $[CpMo(CO)_3CH_3]$, $[CpMo(CO)_3(CH_2C_6H_5)]$ and $[CpMo(CO)_3(CH_2C_6F_5)]$ with TBHP (see Supporting Information). Oxidation reactions of the complexes **2**, **3** and $[CpMo(CO)_3Cl]$ are difficult to study since oxidative decarbonylation of these complexes is either quite exothermic or too fast to be followed on the time scale for NMR measurements. Oxidation of the complex R = CH_3 was studied at 5 °C for this reason and with complexes **1**, R = $CH_2C_6H_5$ and $CH_2C_6F_5$ the reactions could be studied at room temperature.

Since the oxidant TBHP is usually employed in a large excess for the *in situ* reaction, we also considered the possibility of further oxidation of **II** with TBHP. Calhorda et al. have previously calculated the likelihood of formation of the *bis*-peroxo complex $[CpMo(O_2)_2CH_3]$ from the oxo-peroxo analogue *via* an intermediate of the type $[CpMo(O_2)(OH)(OOCH_3)(CH_3)]$ (oxidant CH_3OOH).[19] This process is deemed unlikely due to a high activation energy barrier. This transformation illustrated in Eq. (9) has ΔG = +12 kcal mol^{-1} for R = CH_2COOCH_3.

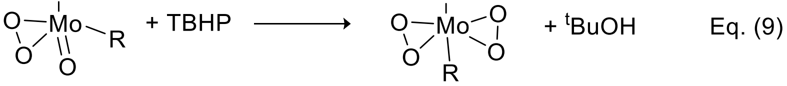

ΔH = +12.0 kcal/mol, ΔG = +12.0 kcal/mol (R = CH_2COOCH_3)

Scheme 6.9. Oxidation of oxo-peroxo species $[CpMo(O)(O_2)R]$ to bisperoxo complex with TBHP.

It is important to note that catalysis reactions are usually performed at 55 °C, and thus formation of any ‘unlikely’ species specified in Eq.s (1−9, A−D) cannot be entirely ruled out. It is also necessary to not overestimate the number of complex species present during catalysis since presence of the olefin substrate suppresses oxidation of **I** to **II**. Although formation of μ-oxo dimers is thermodynamically allowed and preferred, their contribution to catalytic activity may or may not be significant compared to mononuclear complexes.[10]

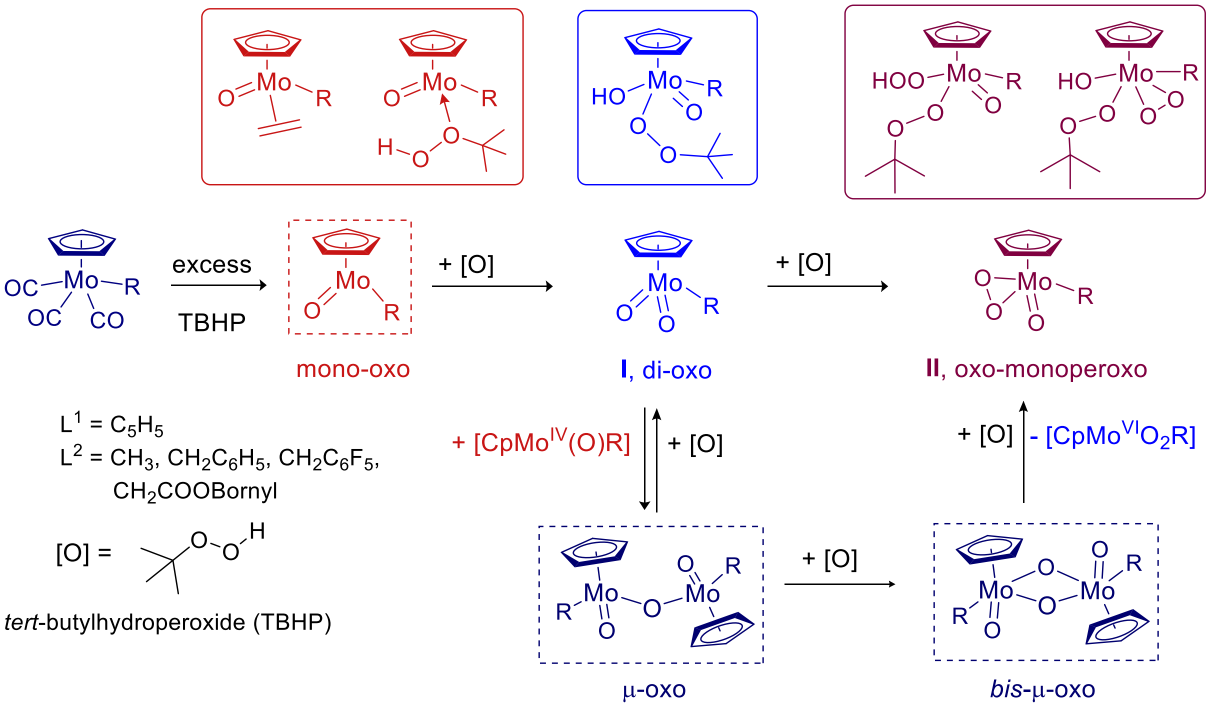

Scheme 6.10. Summary of kinetic equilibria involved in oxidation reactions with [CpMo(CO)$_3$(CH$_2$COOR)] pre-catalysts and excess TBHP (n-decane) oxidant.

The results discussed in previous sections illustrate that the oxidation of CpMo(II) pre-catalysts such as **5** follow a more detailed reaction pathway than a simple transformation of tricarbonyl species into the two Mo(VI) complexes **I** and **II**. The proposed oxidative pathways are illustrated in Scheme 6.10.

From spectroscopic data and DFT calculations, we have attempted to determine the outcome of oxidation of [CpMo(CO)$_3$R*] complexes with the hydroperoxide oxidant TBHP. We have argued that treating pre-catalyst **5** with a sufficient excess of TBHP converts the Mo^{II} complex into Mo^{VI} dioxo complex **I** either directly or stepwise *via* the Mo^{IV} monooxo species in a highly exothermic process. The coordinatively unsaturated Mo^{IV} complex can be stabilized by coordination with the substrate during catalytic epoxidation. However, further oxidation to give the dioxo complex is always thermodynamically preferred. In the absence of the substrate, complex **I** is further oxidized with TBHP to give the oxo-peroxo species **II** and can also react with the mono-oxo Mo^{IV} species in a highly exothermic, thermodynamically feasible process to give mono-μ-oxo dimeric species. In the presence of a reductant, i.e. olefin substrate, complex **I** is primarily involved in catalytic epoxidation and subsequent oxidative transformations to **II** and oxo-bridged dimer are suppressed.

DFT calculations to investigate the role of the proposed intermediates in oxidative transformations of the tricarbonyl pre-catalysts are the subject of current investigation and some results are discussed in Chapter 7. In addition, we are investigating the possibility that during epoxidation of alkenes, the Lewis acidic Mo(VI) metal centre is not the only oxo complex during the catalytic process.

6.4 Conclusion

In Section 6.3.1, the oxidation of [$CpMo(CO)_3(CH_2COOBornyl)$] pre-catalyst has been studied by kinetic NMR. It is found that in addition to the formation of oxidized Mo(VI) complexes **I** and **II**, there are at least two transient species (arbitrarily assigned **A** and **B**) that are present in the period following oxidative decarbonylation. A study of pre-catalyst oxidation in Section 6.3.2 under various reaction conditions is helpful in evaluating how oxidant and pre-catalyst concentration as well as reaction temperature affect the efficiency of this oxidative transformation. Formation of a precipitate on treating such pre-catalysts with TBHP is discussed in Section 6.3.3. In Section 6.3.4, the existence of the Mo(IV) mono-oxo complex, and μ-oxo bridged dimeric complexes or intermediate [$CpMo(O)(OH)(OO^tBu)$) is proposed to explain the signals seen in ^1H and ^{13}C NMR. Even though it is unclear yet whether these intermediate species are catalytically active or stoichiometric oxidants, it is logical to consider the possibility that the concentration of these species influences the concentration of the known dioxo and oxo-peroxo active species. Kinetic studies were conducted by treating similar pre-catalysts with TBHP and it is found that the formation of species **A** and **B** is not unique to the alkylester complex **5**. Subsequently, a scheme outlining the various oxidative transformations of the [$CpMo(CO)_3R$] pre-catalysts is discussed in Section 6.3.5.

6.5 References

[1] F.E. Kühn, A.M. Santos, M. Abrantes, Chem. Rev. 106 (2006) 2455–2475.

[2] F.E. Kühn, J. Zhao, W.A. Herrmann, Tetrahedron: Asymmetry. 16 (2005) 3469–3479.

[3] K.R. Jain, W.A. Herrmann, F.E. Kühn, Coord. Chem. Rev. 252 (2008) 556–568.

[4] M. Groarke, I.S. Gonçalves, W.A. Herrmann, F.E. Kühn, J. Organomet. Chem. 649 (2002) 108–112.

[5] A.M. Al-Ajlouni, A.A. Valente, C.D. Nunes, M. Pillinger, A.M. Santos, J. Zhao, C. C. Romão, I. S. Gonçalves, F. E. Kühn, Eur. J. Inorg. Chem. (2005) 1716–1723.

[6] W.R. Thiel, M. Angstl, N. Hansen, J. Mol. Catal. A Chem. 103 (1995) 5–10.

[7] S. Wolowiec, J.K. Kochi, Inorg. Chem. 30 (1991) 1215–1221.

[8] E. d.P. Carreiro, A.J. Burke, J. Mol. Catal. A Chem. 249 (2006) 123–128.

[9] J.M. Wallis, J.K. Kochi, Inorg. Chim. Acta 160 (1989) 217–221.

[10] A.M. Martins, C.C. Romão, M. Abrantes, M.C. Azevedo, J. Cui, A.R. Dias, M. T. Duarte, M. A. Lemos, T. Lourenço, R. Poli Organometallics 24 (2005) 2582–2589.

[11] C. Dinoi, M. Ciclosi, E. Manoury, L. Maron, L. Perrin, R. Poli, Chem. Eur. J. 16 (2010) 9572–9584.

[12] H. Mimoun, I.S. de Roch, L. Sajus, Tetrahedron. 26 (1970) 37–50.

[13] K.B. Sharpless, J.M. Townsend, D.R. Williams, J. Am. Chem. Soc. 94 (1972) 295–296.

[14] M.J. Calhorda, P. Jorge, Curr. Org. Chem. 16 (2012) 65–72.

[15] M. Abrantes, A.M. Santos, J. Mink, F.E. Kühn, C.C. Romão, Organometallics 22 (2003) 2112–2118.

[16] N. Grover, F.E. Kühn, Curr. Org. Chem. 16 (2012) 16–32.

[17] A.A. Valente, J.D. Seixas, I. S. Gonçalves, M. Abrantes, M. Pillinger, C.C. Romão Catal. Lett. 101 (2005) 127–130.

[18] A.M. Al-Ajlouni, D. Veljanovski, A. Capapé, J. Zhao, E. Herdtweck, M.J. Calhorda, F. E. Kühn Organometallics 28 (2009) 639–645.

[19] P.J. Costa, M. José Calhorda, F.E. Kühn, Organometallics 29 (2010) 303–311.

[20] S.A. Hauser, M. Cokoja, M. Drees, F.E. Kühn, J. Mol. Catal. A Chem. 363-364 (2012) 237–244.

[21] M. Drees, S.A. Hauser, M. Cokoja, F.E. Kühn, J. Organomet. Chem. (2013) DOI 10.1016/j.jorganchem.2013.05.004.

[22] J. Zhao, A.M. Santos, E. Herdtweck, F.E. Kühn, J. Mol. Catal. A Chem. 222 (2004) 265–271.

[23] A. Capapé, A. Raith, E. Herdtweck, M. Cokoja, F.E. Kühn, Adv. Synth. Catal. 352 (2010) 547–556.

[24] Chapter 4.

[25] J.C. Alonso, P. Neves, M.J.P. da Silva, S. Quintal, P.D. Vaz, C. Silva, A. A. Valente, P. Ferreira, M. J. Calhorda, V. Félix, M. G. B. Drew Organometallics. 26 (2007) 5548–5556.

[26] V.V.K.M. Kandepi, J.M.S. Cardoso, B. Royo, Catal. Lett. 136 (2010) 222–227.

[27] T.R. Amarante, P. Neves, A.C. Coelho, S. Gago, A.A. Valente, F.A.A. Paz, M: Pillinger; I. S: Gonçalves Organometallics 29 (2010) 883–892.

[28] P. Neves, C.C.L. Pereira, F.A.A. Paz, S. Gago, M. Pillinger, C.M. Silva, A. A. Valente, C. C. Romão, I. S. Gonçalves J. Organomet. Chem. 695 (2010) 2311–2319.

[29] H.B. Schlegel, J. Comp. Chem. 3 (1982) 214–218.

[30] S.H. Vosko, L. Wilk, M. Nusair, Can. J. Phys. 58 (1980) 1200–1211.

[31] C. Lee, W. Yang, R.G. Parr, Phys. Rev. B Condens. 37 (1988) 785–789.

[32] A.D. Becke, J. Chem. Phys. 98 (1993) 5648–5652.

[33] W.J. Hehre, J. Chem. Phys. 56 (1972) 2257–2261.

[34] R. Krishnan, J.S. Binkley, R. Seeger, J. A. Pople, J. Chem. Phys. 72 (1980) 650–654.

[35] P.J. Hay, W.R. Wadt, J. Chem. Phys. 82 (1985) 270–283.

[36] P.J. Hay, W.R. Wadt, J. Chem. Phys. 82 (1985) 299–310.

[37] T.S. Piper, G. Wilkinson, J. Inorg. Nucl. Chem. 3 (1956) 104–124.

[38] R.B. King, A. Fronzaglia, J. Am. Chem. Soc. 88 (1966) 709–712.

[39] E.R. Burkhardt, J.J. Doney, R.G. Bergman, C.H. Heathcock, J. Am. Chem. Soc. 109 (1987) 2022–2039.

[40] D.G. Blackmond, Angew. Chem. Int. Ed. 44 (2005) 4302–4320.

[41] M. Abrantes, T.R. Amarante, M.M. Antunes, S. Gago, F.A. Almeida Paz, I. Margiolaki, A. E. Rodrigues, M. Pillinger, A. A. Valente, I. S. Gonçalves Inorg. Chem. 49 (2010) 6865–6873.

[42] P.M. Reis, C.A. Gamelas, J.A. Brito, N. Saffon, M. Gómez, B. Royo, Eur. J. Inorg. Chem. (2011) 666–673.

[43] M. Abrantes, F.A.A. Paz, A.A. Valente, C.C.L. Pereira, S. Gago, A.E. Rodrigues, J. Klinowski, M. Pillinger, I. S. Gonçalves J. Organomet. Chem. 694 (2009) 1826–1833.

[44] M. Pratt, J.B. Harper, S.B. Colbran, Dalton Trans. (2007) 2746–2748.

[45] L.F. Veiros, Organometallics 19 (2000) 5549–5558.

[46] C.C. Romão, L.F. Veiros, Organometallics 26 (2007) 1777–1781.

[47] H.G. Alt, Angew. Chem. Int. Ed. English. 23 (1984) 766–782.

[48] J.H. Enemark, J.J.A. Cooney, J.-J. Wang, R.H. Holm, Chem. Rev. 104 (2004) 1175–1200.

[49] V.W.L. Ng, M.K. Taylor, C.G. Young, Inorg. Chem. 51 (2012) 3202–3211.

[50] H.G. Alt, J.A. Schwärzle, C.G. Kreiter, J. Organomet. Chem. 153 (1978) 7–10.

[51] C.G. Kreiter, K. Nist, H.G. Alt, Chem. Ber. 114 (1981) 1845–1852.

[52] W.M. Harrison, C. Saadeh, S.B. Colbran, D.C. Craig, J. Chem. Soc., Dalton Trans. (1997) 3785–3792.

[53] P. Chandra, S.L. Pandhare, S.B. Umbarkar, M.K. Dongare, K. Vanka, Chem. Eur. J. 19 (2013) 2030–2040.

[54] J. Morlot, N. Uyttebroeck, D. Agustin, R. Poli, ChemCatChem. 5 (2013) 601–611.

[55] Z. Xiao, C.G. Young, J.H. Enemark, A.G. Wedd, J. Am. Chem. Soc. 114 (1992) 9194–9195.

[56] J.A. Craig, E.W. Harlan, B.S. Snyder, M.A. Whitener, R.H. Holm, Inorg. Chem. 28 (1989) 2082–2091.

[57] R.H. Holm, Chem. Rev. 87 (1987) 1401–1449.

[58] M.S. Reynolds, J.M. Berg, R.H. Holm, Inorg. Chem. 23 (1984) 3057–3062.

[59] V.S. Joshi, M. Nandi, H. Zhang, B.S. Haggerty, A. Sarkar, Inorg. Chem. 32 (1993) 1301–1303.

[60] D.M. Baird, S. Falzone, J.E. Haky, Inorg. Chem. 28 (1989) 4561–4562.

[61] C.L. Pereira, S.S. Balula, F.A.A. Paz, A.A. Valente, M. Pillinger, J. Klinowski, I. S. Gonçalves, Inorg. Chem. 46 (2007) 8508–8510.

[62] P. Sözen-Aktaş, E. Manoury, F. Demirhan, R. Poli, Eur. J. Inorg. Chem. 2013 (2013) 2728–2735.

[63] A. Comas-Vives, A. Lledós, R. Poli, Chem. Eur. J. 16 (2010) 2147–2158.

6.6 Supporting Information

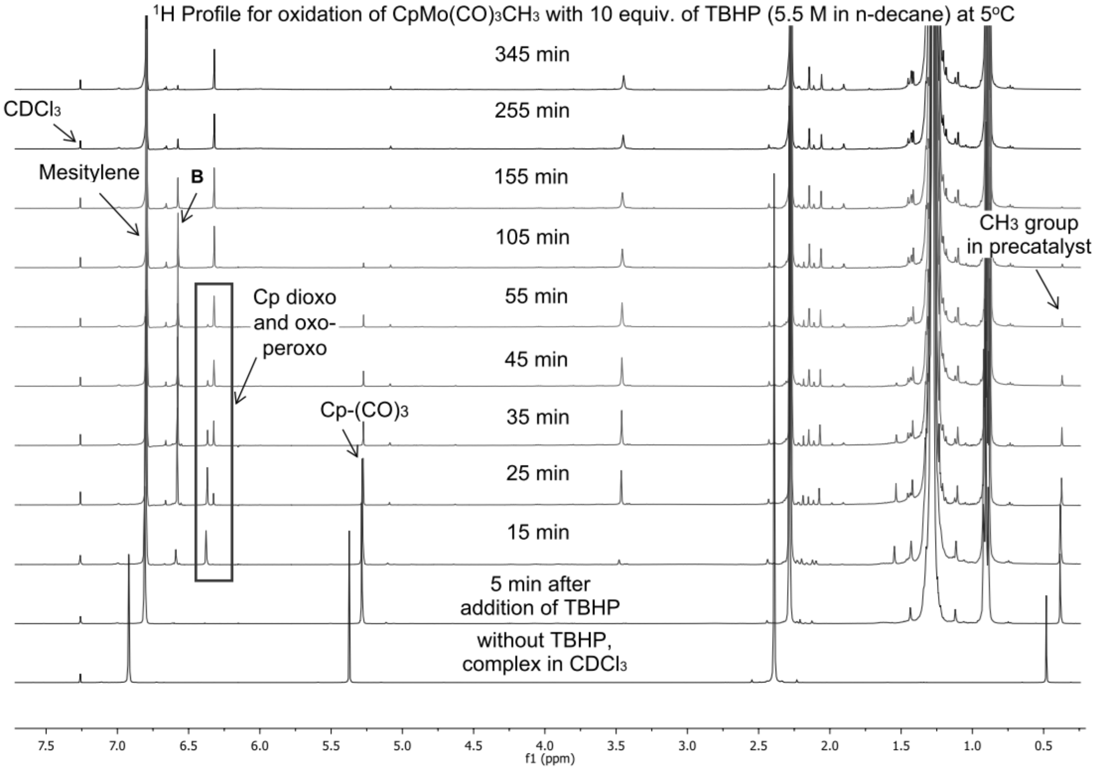

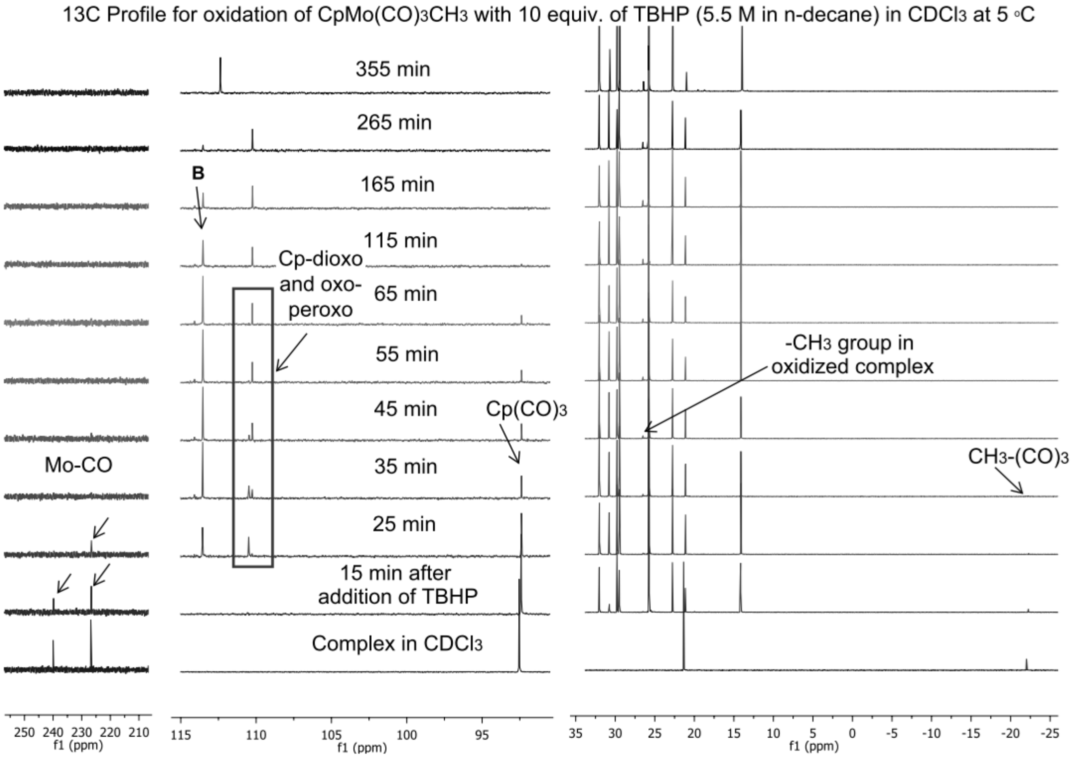

Figure 6.9. ^1H and ^{13}C NMR Profiles – Oxidation of $CpMo(CO)_3CH_3$ with 10 equiv. TBHP (5.5 M in n-decane) at 5 °C.

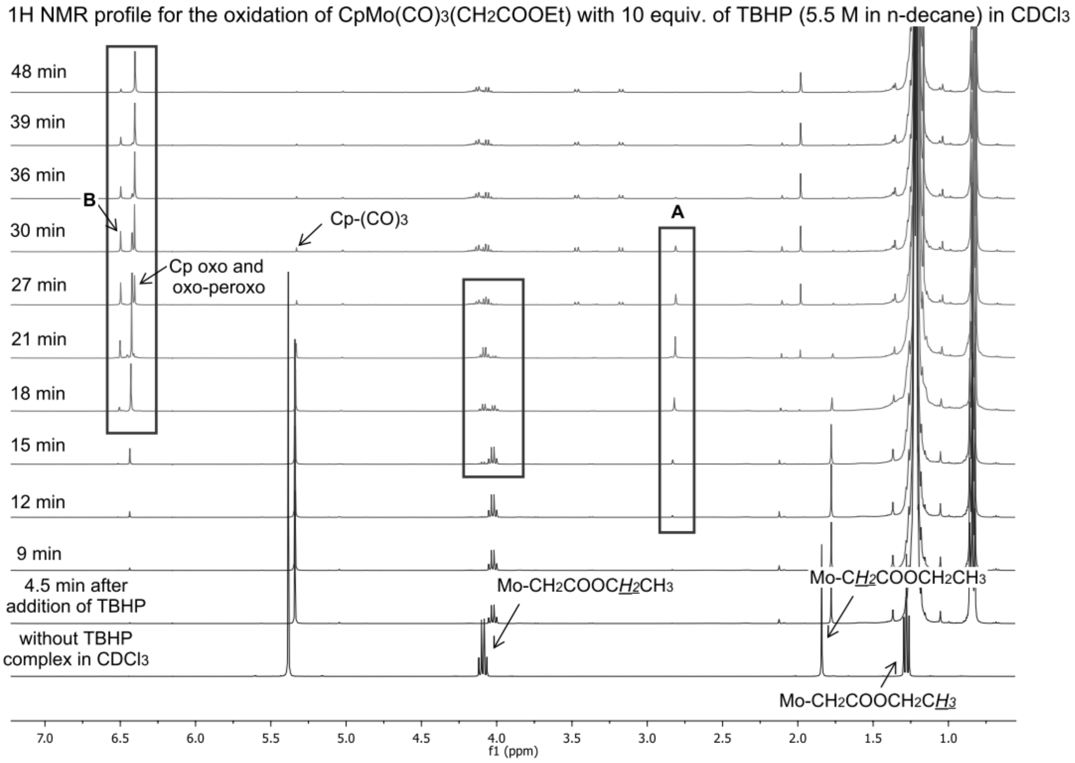
1H NMR profile for the oxidation of CpMo(CO)3(CH2COOEt) with 10 equiv. of TBHP (5.5 M in n-decane) in CDCl3

Figure 6.10. ^{1}H NMR Profile – Oxidation of **1** with 10 equiv. TBHP (5.5 M, n-decane) at 22 °C in $CDCl_3$.

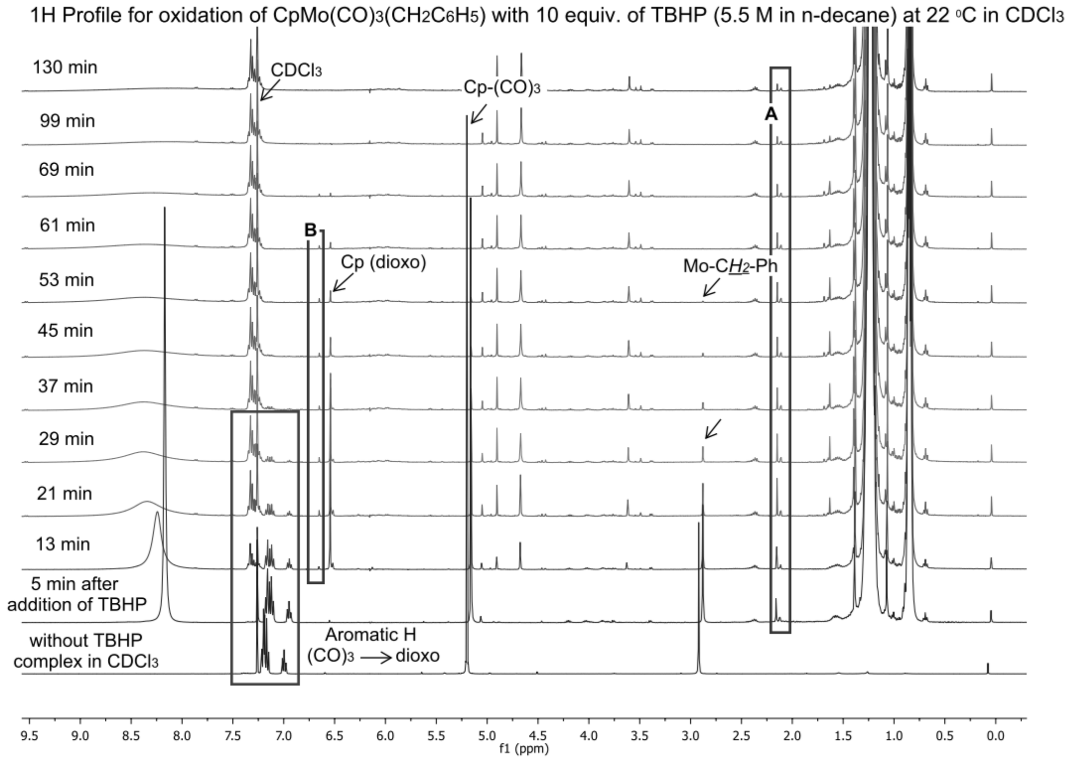
1H Profile for oxidation of CpMo(CO)3(CH2C6H5) with 10 equiv. of TBHP (5.5 M in n-decane) at 22 °C in CDCl3

Figure 6.11. Oxidation of $CpMo(CO)_3(CH_2C_6H_5)$ with 10 equiv. of TBHP at 22 °C in $CDCl_3$.

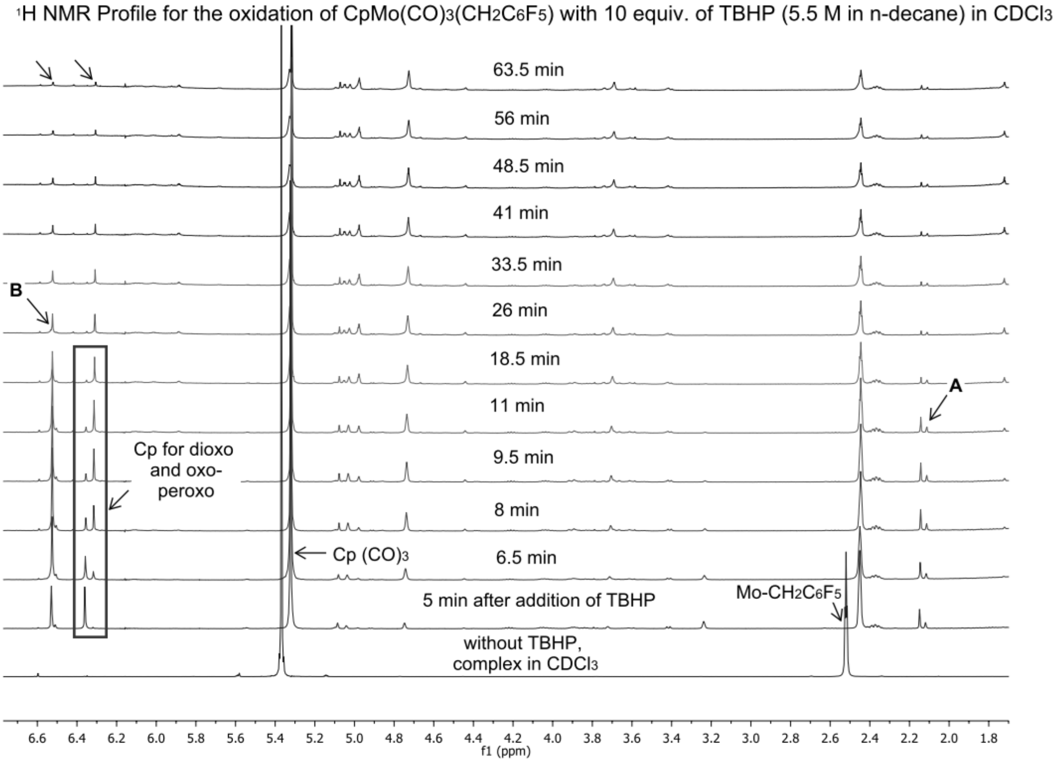

Figure 6.12. ^{1}H Profile – Oxidation of [CpMo(CO)$_3$(CH$_2$C$_6$F$_5$)] with 10 equiv. of TBHP (5.5 M, n-decane) at 22 °C in CDCl$_3$.

Analytical data for **5a** and **5b**

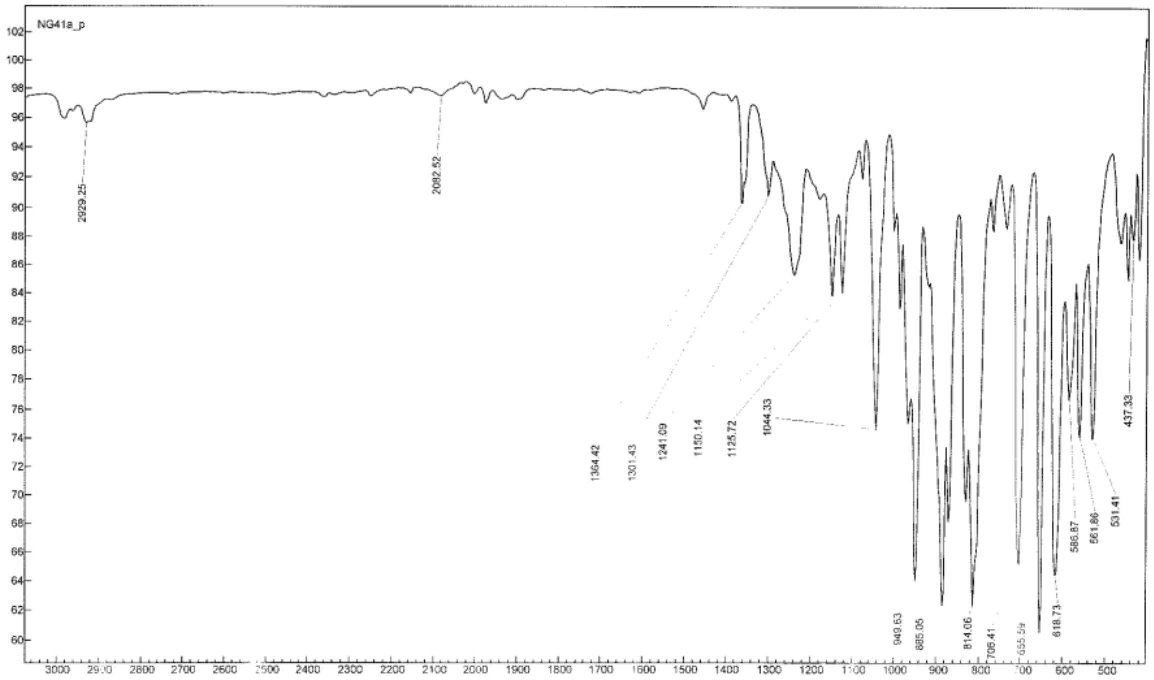

Figure 6.13. FTIR spectrum of the isolated precipitate **5a**.

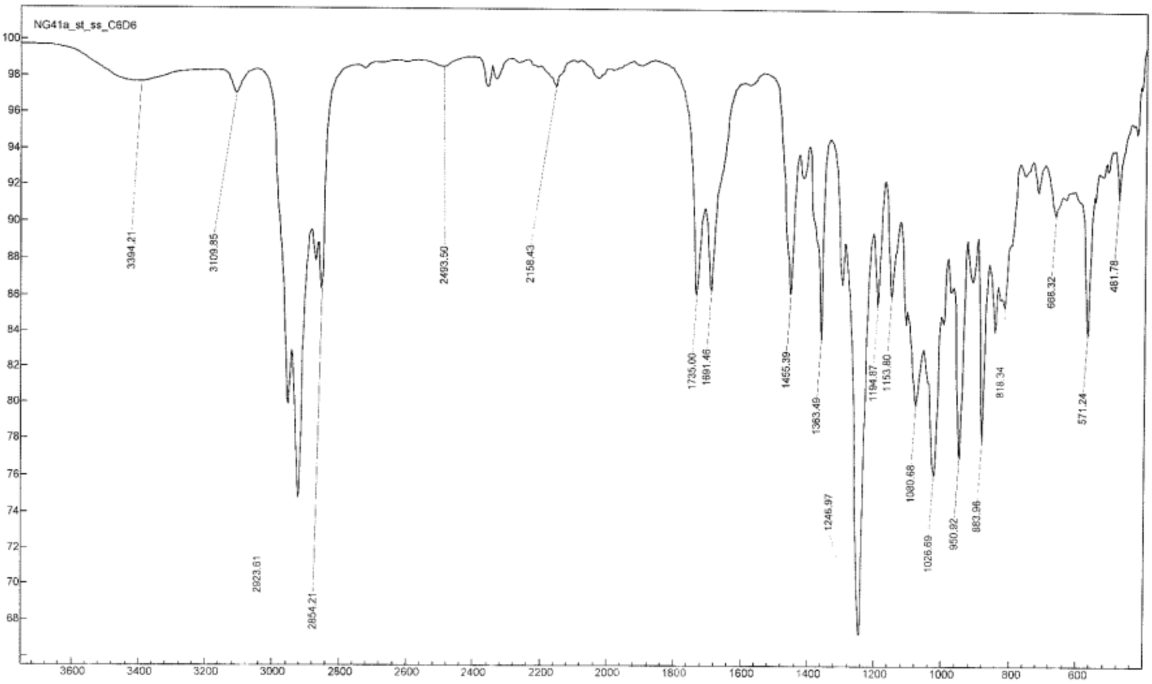

Figure 6.14. FTIR spectrum of the pale yellow supernatant **5b** (in C_6D_6).

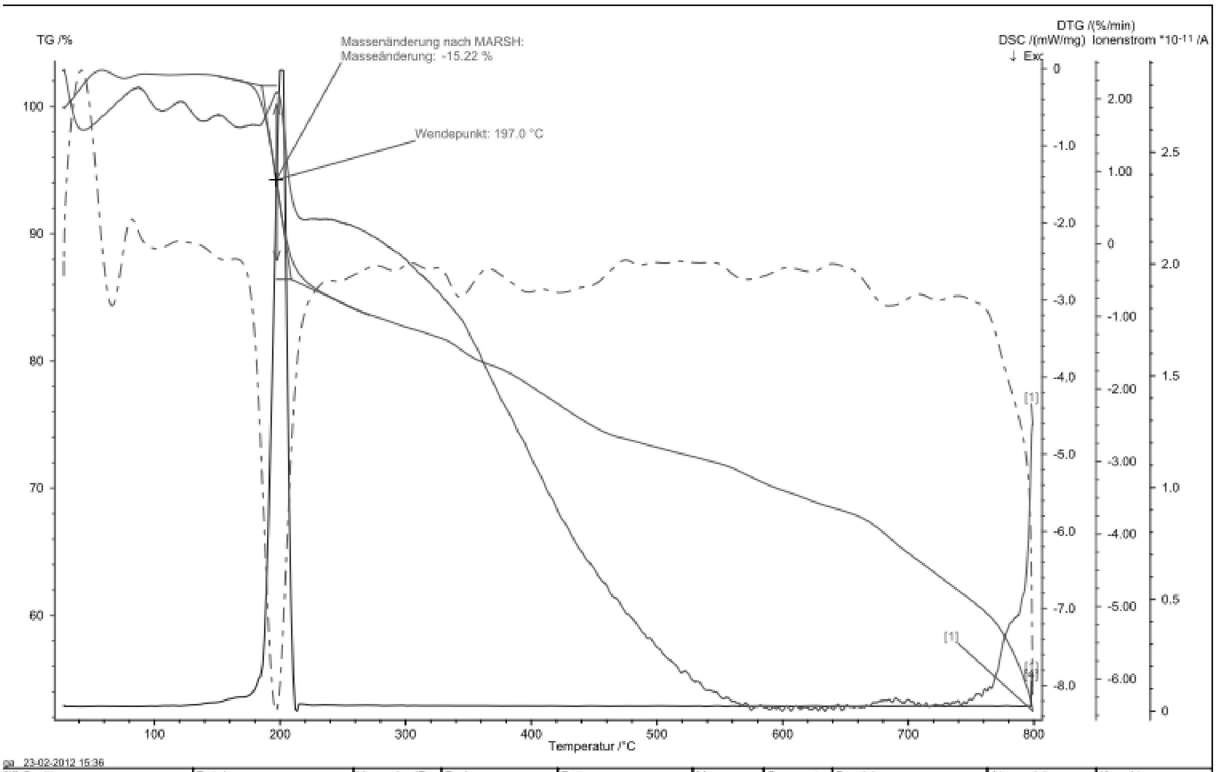

[#] Gerät	Datei	Versuchs-ID	Probe	Datum	Masse	Segment	Bereich	Atmosphäre	Korrektur
[1] NETZSCH STA 409 PC/PG	NG41ap MS2130.dsv	002130	NG41ap MS2130	23.02.2012 11:46:58	6.300 mg	1/1	30.0/10.00(K/min)/800.0	Argon/60 / ---/---	DSC:020/TG:820
[4] Balzers MID	002130_m56.00_s1.ASC	002130	Masse 56.00	23.02.2012 11:47:02		1/1	29.0/10.00(K/min)/799.0		0

Figure 6.15. TGA-DSC for **5a**, decomposition temperature 197 °C, curve showing *m/z* 55.

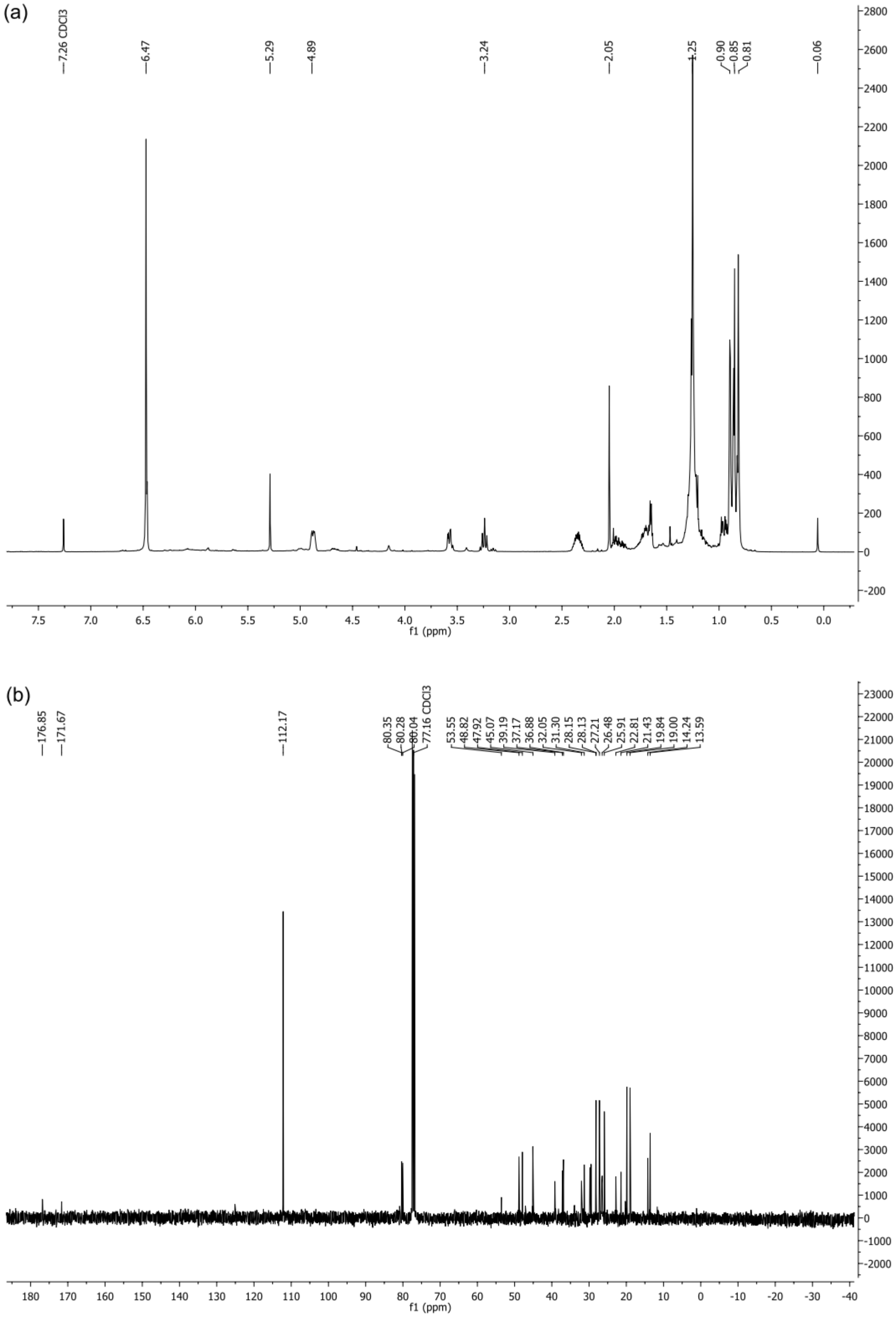

Figure 6.16. (a) ^{1}H and (b) ^{13}C NMR spectra of **5b** in $CDCl_3$.

```
Table S1 - Crystal Data and Details of the Structure Determination
                 for: GroNi6
                                Crystal Data

        Formula 2 Mo O5.36, C17 H22 Mo O5.23, C17 H22 Mo O5, C16 H20 Mo O5
        Formula Weight                                               1604.45
        Crystal System                                            Monoclinic
        Space group                            P21                (No.   4)
        a, b, c [Angstrom]          22.4707(5)    7.0620(2)    23.4265(5)
        alpha, beta, gamma [deg]            90    112.704(1)           90
        V [Ang**3]                                                3429.44(15)
        Z                                                                  2
        D(calc) [g/cm**3]                                              1.554
        Mu(MoKa) [ /mm ]                                               0.787
        F(000)                                                          1642
        Crystal Size [mm]                            0.12 x  0.16 x  0.20

                            Data Collection

        Temperature (K)                                                  296
        Radiation [Angstrom]                              MoKa       0.71073
        Theta Min-Max [Deg]                                       0.9,  25.5
        Dataset                                 -27: 27 ;  -8:  8 ; -28: 28
        Tot., Uniq. Data, R(int)                      76028,  12626,   0.055
        Observed data [I > 2.0 sigma(I)]                               10042

                              Refinement

        Nref, Npar                                              12626,   851
        R, wR2, S                                     0.0512, 0.1445, 1.04
        w = 1/[\s^2^(Fo^2^)+(0.0723P)^2^+9.7594P] where P=(Fo^2^+2Fc^2^)/3
        Max. and Av. Shift/Error                                  0.45, 0.01
        Flack x                                                      0.00(5)
        Min. and Max. Resd. Dens. [e/Ang^3]                      -0.84, 1.31
```

Due to disordered peroxo moieties at two of the four independent molecules in the asymmetric unit, the refinement could not proceed to a satisfying model. The structural proof of the oxo-peroxo species is valid.

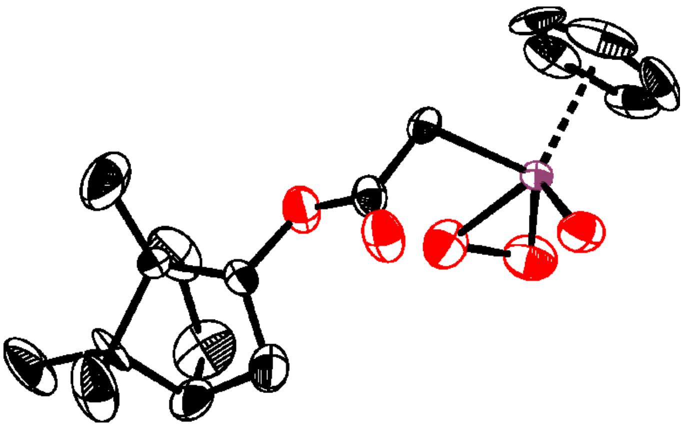

7 Theoretical Concepts and Experimental Insights − Catalysis with [CpMo(CO)$_3$R] Complexes

7.1 Introduction

In the previous chapters of this thesis, the presence of Mo(IV) and Mo(V) intermediates during the oxidative transformation of Mo(II) tricarbonyl pre-catalysts to catalytically active Mo(VI) oxo complexes with TBHP has been proposed. To reiterate, it is known that Mo(VI) complexes [CpMoO$_2$R] and [CpMo(O)(O$_2$)R] are both catalytically active. Although the existence of Mo(IV) and Mo(V) is proposed, it is not experimentally confirmed until now whether these species participate in the epoxidation reaction *as catalytically active species* or *as intermediates* that determine the concentration of the known (dioxo and oxo-peroxo) catalytically active species.

From the kinetic NMR and mechanistic studies in Chapters 5 and 6, explanations for the exothermicity of oxidative decarbonylation, formation of Mo-containing insoluble precipitate, and lack of effective asymmetric induction have been proposed. In this chapter, the most relevant results of recent theoretical work undertaken to investigate the stability and catalytic potential of Mo(IV) mono oxo complex [CpMoOR] (R = CH$_2$COOCH$_3$) are summarized. Similar to the kinetic ^{1}H and ^{13}C NMR experiments outlined before in the study of oxidation reactions of alkylester complex [CpMo(CO)$_3$(CH$_2$COOBornyl)] **5** with TBHP, the effect of deuterated oxidant and presence of additives was also investigated. The results of these experiments are presented in Section 7.3.2 and Section 7.3.3 respectively.

7.2 Experimental

All theoretical calculations were performed by Dr. Markus Drees, Lehrstuhl für Anorganische Chemie/Molekulare Katalyse, Catalysis Research Center, Technische Universität München (mailto: markus.drees@ch.tum.de), using software Gaussian09 C.02. and B3LYP/6-31G** basis set for all atoms except Mo (Stuttgart 1997 ECP). Free energy differences have been reported for gas phase at 298.15 K and 1.0 atm.

Complex [CpMo(CO)$_3$(CH$_2$COOBornyl)] was synthesized according to procedure outlined in Chapter 4. *tert*-butanol and HFIP were purchased from Sigma Aldrich and used as received.

Kinetic NMR experiments for studying the kinetic isotope effect – TBHP-d was obtained by treating TBHP (n-decane solution purchased from Sigma Aldrich, < 4% water) with D$_2$O (>99%) overnight and then drying organic phase with molecular sieves. For pre-catalyst oxidation, *ca.* 0.1 mmol of **5** and mesitylene (internal standard) dissolved in 0.4 mL CDCl$_3$ was treated with 10 equiv. of TBHP-d at 22 °C and the reaction progress was followed by kinetic ^{1}H and ^{13}C NMR as mentioned above. Catalytic epoxidation was studied for 0.1 mmol of **5**, mesitylene and 10 equiv. of *cis*-cyclooctene dissolved in 0.4 mL CDCl$_3$ with addition of 20 equiv. TBHP-d.

A study of the effect of additives *tert*-butanol and hexafluoroisopropanol (HFIP) – 0.05 mmol of complex [CpMo(CO)$_3$(CH$_2$COOBornyl)], naphthalene (internal standard), 0.5 mmol (10 equiv.) of *cis*-cyclooctene and 0.5 mmol of HFIP or *tert*-butanol were dissolved in 0.4 mL CDCl$_3$. The catalytic epoxidation reaction was initiated by the addition of 20 equiv. of TBHP at 22 °C. The reaction progress was followed by kinetic ^{1}H and ^{13}C NMR as mentioned above.

7.3 Results and Discussion

7.3.1 Theoretical Study: Mo(IV) Mono-oxo Complex, its Stability and Catalytic Potential

Note: Work discussed in this section is in preparation for publication.

In the various kinetic and mechanistic studies of [CpMo(CO)$_3$R]-based catalytic epoxidation published in literature, the starting point of DFT calculations is always the dioxo or oxo-peroxo oxidized complexes.[1–4] The transformation of Mo(II) to Mo(VI) with TBHP and any intermediates formed during this reaction are not taken into account. This is primarily because of lack of experimental evidence of possible intermediates, since decarbonylation is highly exothermic (for some pre-catalysts) and so far, only the stable end products – dioxo and oxo peroxo complexes have been isolated and characterized by various spectroscopic methods and X-ray crystallography.[5–9]

Photochemically induced decarbonylation of [CpMo(CO)$_3$R] pre-catalysts is known to occur *via* a sequential loss of CO groups and intermediates of the type [CpMo(CO)$_2$R] and [CpMo(CO)R] are known to exist.[10] It might be anticipated that decarbonylation in the presence of hydroperoxide oxidant TBHP would differ mechanistically from photochemical decarbonylation. Here, coordinative unsaturation and hence instability of intermediates formed during the Mo(II)→Mo(VI) transformation can be compensated by formation of terminal metal oxo ligand (Mo=O). Therefore it is not unreasonable to suggest the formation of a Mo(IV) intermediate [CpMoOR] during the course of conversion of Mo(II) to Mo(VI) complexes.

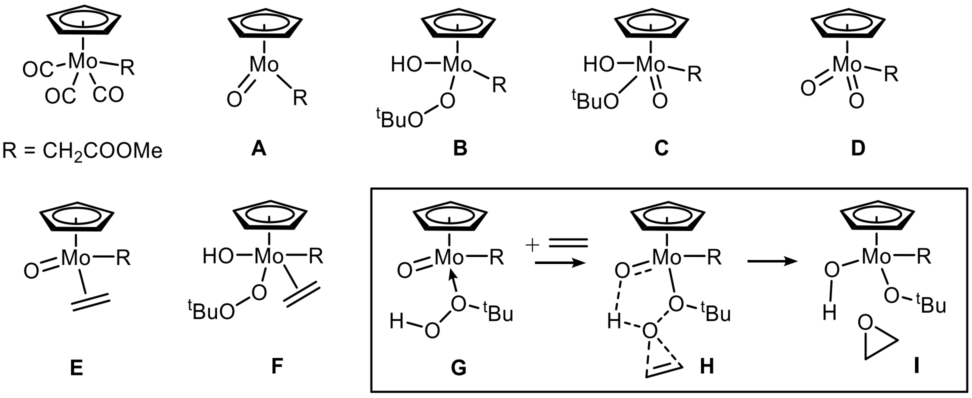

Figure 7.1. Complexes discussed in this section.

Hence, theoretical calculations were undertaken to follow the formation of a Mo(IV) mono oxo complex [CpMoOR] from the tricarbonyl Mo(II) pre-catalyst [CpMo(CO)$_3$R] (R = CH$_2$COOCH$_3$). Thermodynamic data suggests formation of this Mo(IV) complex from reaction of Mo(II) precursor and TBHP is highly exothermic, $\Delta H = -243.2$ kcal mol^{-1} and also a thermodynamically favoured process, $\Delta G = -275.5$ kcal mol^{-1}. The mono oxo complex **A** is easily converted to the dioxo complex

[$CpMoO_2R$] **D**, ΔG for this transformation is -98.5 kcal mol^{-1}. During this process, two intermediates **B** and **C** have been proposed to form (Figure 7.1). However, they are both shown to be unlikely candidates for epoxidation of ethylene on account of high activation energy barriers.

This theoretical work has also considered the possibility of stabilization of complex **A** on coordination of the olefin substrate as a η^2-ligand. Calculations propose the formation of a stable alkene adduct [$CpMoO(\eta^2\text{-}C_2H_4)R$], **E**. However, based on transition state activation barriers, formation of **E** requires a relative higher local concentration of the alkene compared to the oxidant because conversion of **A** to the dioxo complex **D** is more favourable.

In order to investigate the catalytic potential of the ethylene adduct **E**, activation of TBHP is shown to occur in a manner that results in formation of intermediate **F**. Next, insertion of the alkene in Mo-O bond and subsequent oxygen atom transfer (Calhorda mechanism[3]) are calculated. Although the barriers for olefin insertion with intermediate **F** are smaller than insertion into Mo-O in the corresponding dioxo complex [$CpMoO_2R$], a comparison of the relative activation energies shows that addition of TBHP to **E** in this fashion is rather unlikely and conversion of **A** to **D** is much more facile. Hence it is concluded that **A** is not catalytically active since Mo centre is essentially oxophilic and epoxidation is inferior to the further oxidation of Mo(IV) to Mo(VI) complexes.

Note that in this study, activation of TBHP upon coordination as a neutral molecule (**G**) is *not* considered.[4] For the unsaturated Mo(IV) complex, transformation of **G** → **H** (or **I**) is another possible pathway of olefin epoxidation. Olefin pre-coordination is not essential in this case. However, as before, it is calculated that since Mo(IV) species is coordinatively unsaturated, there is a lower activation barrier for process **G** → **B** compared to oxygen transfer to olefin substrate *via* process **G** → **H**. Nevertheless, stabilization of Mo metal centre by neutral donor molecules TBHP, ^{t}BuOH, H_2O_2, CH_3OH etc. cannot be ruled out.[4]

In this theoretical work, similar mechanistic calculations have been done for complex [$CpMo(CO)_3Cl$]. From a consideration of various transition state activation barriers, it is concluded that compared to the alkylester complex R = CH_2COOCH_3, the chloro complex would transform mono-oxo [CpMoOR] to dioxo [$CpMoO_2R$] in a slightly less facile manner; overall ΔG = -83.7 kcal mol^{-1} (R = Cl) < ΔG = -98.6 kcal mol^{-1} (R = CH_2COOCH_3). Similar to the mono-oxo alkylester complex, the chloro analogue has been shown to be unlikely to catalyse the epoxidation of ethene *via* both *outer-sphere* Sharpless mechanism and Calhorda olefin insertion mechanism (see Section 8.1.1) with transition state activation barriers of ~ 50 kcal mol^{-1} and ~ 22 kcal mol^{-1} respectively.

7.3.2 Kinetic Isotope Effect

When TBHP (in n-decane) is replaced with its deuterated analogue as the oxidant, it is observed that pre-catalyst oxidation is much faster with no discernable induction period. Similar to observations of experiments with TBHP (see Chapters 5 and 6), epoxidation of cyclooctene takes precedence over further oxidation of the dioxo complex **I** when TBHP-d is used. Thus, after quantitative conversion of cyclooctene to epoxycyclooctane takes place, the catalytically highly active dioxo complex **I** forms the oxo-peroxo complex **II**.

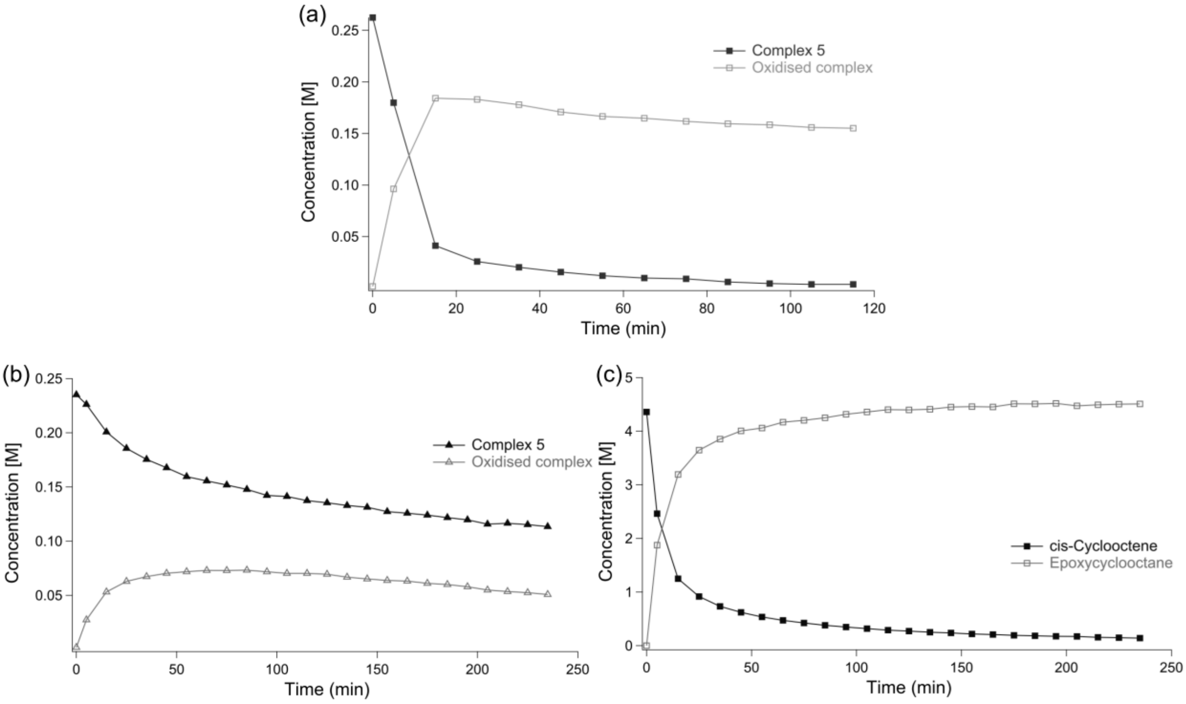

Figure 7.2. Concentration *vs.* time plots for (a) oxidation of *ca.* 0.1 mmol pre-catalyst [CpMo(CO)$_3$(CH$_2$COOBornyl)] (**5**) with 10 equiv. of TBHP-d, (b) **[5]** and sum concentration of oxidized complexes **[I + II]** during catalytic epoxidation, and (c) *cis*-cyclooctene and its epoxide, when catalytic epoxidation was performed at 22 °C in CDCl$_3$ (**5**:substrate:TBHP-d = 1:10:20).

Concluding from results of oxidation reactions with non-deuterated TBHP (discussed in Chapter 6) it is found that for the two oxidative transformations, i.e. pre-catalyst oxidation and catalytic epoxidation, $k_H/k_D < 1$. Here k_H and k_D represent the rate constants for the overall oxidative transformations with TBHP and TBHP-d respectively. This suggests that inverse, secondary kinetic isotope effect is operative. However, one must be cautious with interpreting these results since it is possible that during catalysis, some residual D$_2$O utilized for deuteration of the oxidant and adventitious H$_2$O (<4%) from TBHP may be present. Thus, according to the *“proton relay mechanism”* or extensive H-bonding network stabilization described in literature by various authors,[2,4,11,12] it is likely that the rates of the two oxidation reactions are faster but not necessarily due to kinetic isotope effect.

7.3.3 Effect of additives HFIP and ^{t}BuOH on catalytic epoxidation

Previously, a kinetic study of olefin epoxidation with MoO$_2$X$_2$L (X = halide, L = bidentate Lewis base) complexes has asserted that the side product *tert*-butanol acts as a possible competitor to TBHP or olefin substrate at the metal centre and thus has a deactivating influence on catalysis.[13] To evaluate the effect of *tert*-butanol additive on the progress of the epoxidation reaction, 10 equiv. of *tert*-butanol was added together with 10 equiv. of *cis*-cyclooctene in CDCl$_3$ prior to catalysis initiation by addition of TBHP. Unlike previous results, it is found that catalytic epoxidation is faster when *tert*-butanol is present than in the absence of this additive (Figure 7.3).

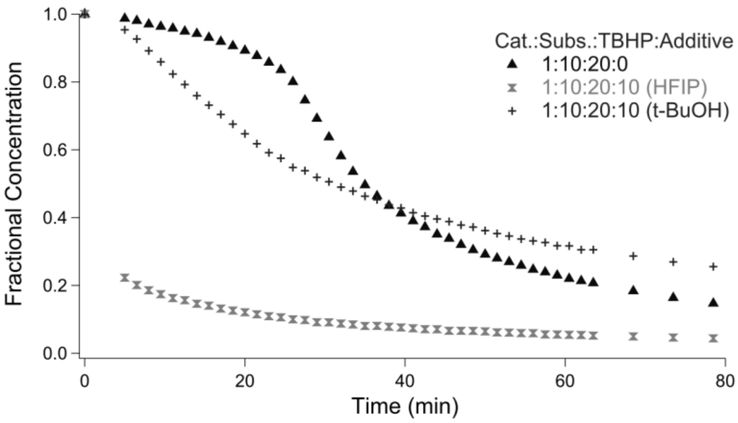

Figure 7.3. Fractional concentration of *cis*-cyclooctene *vs.* time during its epoxidation catalyzed by **5** (1 equiv.) with 20 equiv. of TBHP in the absence or presence of additives HFIP and t-BuOH (10 equiv.)

The key difference between catalysis with MoO_2X_2L and $[CpMo(CO)_3R]$ type complexes is the oxidative decarbonylation process that needs to occur with the CpMo complexes before catalytically active species is obtained. During this process of conversion of a Mo(II) pre-catalyst to Mo(VI) dioxo species, vacant coordination sites may become temporarily available.[10] The additive ^{t}BuOH can then coordinate to the metal centre to form an alkoxide complex[14] or as a neutral solvent molecule that stabilizes catalyst intermediates.[4] Whichever mechanism of interaction might be operative, it is quite curious that ^{t}BuOH solvent promotes catalytic epoxidation instead of the auto-retardation effect observed with MoO_2X_2L-based catalysis and an induction period (that lasts about 25 min in the absence of an additive) is not observed. Instead, the fractional concentration *vs.* time plot shows first-order behaviour.

With hexafluoroisopropanol (or HFIP) as an additive, the substrate *cis*-cyclooctene is converted into its epoxide even faster than in the absence of the fluorinated solvent. Previously, the higher rate of epoxidation reactions has been suggested to be consequence of activation of hydroperoxide/peroxide oxidants *via* hydrogen bond assistance.[15–19] In a similar manner, 78% of cyclooctene is converted to its epoxide within 5 min after addition of TBHP when HFIP is present in the reaction mixture, catalyst:substrate:TBHP:HFIP = 1:10:20:10 in $CDCl_3$ solvent at 22 °C. Since HFIP is also capable of coordinating as a neutral molecule similar to ^{t}BuOH,[4] or as an alkoxide by virtue of its Brønsted acidic nature,[20] the higher reaction rate may also be partly explained as discussed for ^{t}BuOH above.

7.4 Conclusion

A combination of theoretical and experimental work discussed in this chapter illustrates that altering the initial reaction conditions of '*in situ*' catalytic epoxidation involving $[CpMo(CO)_3R]$ complexes by either presence of deuterated oxidant and protic solvents has a clear effect on the reaction progress. While several possible sophisticated mechanistic scenarios can be envisioned for any particular reaction conditions employed, a simple hypothesis may yet explain the differences in catalytic behaviour. Thus it is proposed that during oxidative decarbonylation of Mo(II) pre-catalysts, coordinatively unsaturated complex species can exist for a short time before the Mo(VI) dioxo complexes [$CpMoO_2R$] are formed. Such an intermediate species, suggested to be a Mo(IV) complex, can and probably in good likelihood *does* interact with the substrate, protic solvents or reactants ^{t}BuOH, HFIP and TBHP, depending on the local concentration of such additives present in the reaction mixture at the initial stages of the reaction. It is shown that when equimolar concentrations of the alkene substrate and TBHP are present, formation of a η^2-alkene adduct with Mo(IV) centre is thermodynamically feasible and likely, although due to its highly oxophilic nature, further oxidation to Mo(VI) complex would prefer to take place. It is proposed that similar to ethene coordination, additives with donor capability such as ^{t}BuOH and HFIP may compete for coordination at the metal centre with TBHP. Hence modified versions of previously proposed mechanisms of catalytic epoxidation may be required to explain experimental observations.

7.5 References

[1] C. Dinoi, M. Ciclosi, E. Manoury, L. Maron, L. Perrin, R. Poli, Chem. Eur. J. 16 (2010) 9572–9584.

[2] A. Comas-Vives, A. Lledós, R. Poli, Chem. Eur. J. 16 (2010) 2147–2158.

[3] P. J. Costa, M. José Calhorda, F.E. Kühn, Organometallics 29 (2010) 303–311.

[4] J. Morlot, N. Uyttebroeck, D. Agustin, R. Poli, ChemCatChem 5 (2013) 601–611.

[5] A. M. Al-Ajlouni, D. Veljanovski, A. Capapé, J. Zhao, E. Herdtweck, M.J. Calhorda, F. E. Kühn, Organometallics 28 (2009) 639–645.

[6] A.M. Martins, C.C. Romão, M. Abrantes, M.C. Azevedo, J. Cui, A.R. Dias, M. T. Duarte, M. A. Lemos, T. Lourenco, R. Poli, Organometallics 24 (2005) 2582–2589.

[7] D. Saurenz, F. Demirhan, P. Richard, R. Poli, H. Sitzmann, Eur. J. Inorg. Chem. (2002) 1415–1424.

[8] M. V Galakhov, P. Gómez-Sal, T. Pedraz, M.A. Pellinghelli, P. Royo, A. Tiripicchio, A. V. de Miguel, J. Organomet. Chem. 579 (1999) 190–197.

[9] D. Chakraborty, M. Bhattacharjee, R. Krätzner, R. Siefken, H.W. Roesky, I. Uson, H.-G. Schmidt, Organometallics 18 (1999) 106–108.

[10] H.G. Alt, Angew. Chem. Int. Ed. English. 23 (1984) 766–782.

[11] J. Jee, A. Comas-vives, C. Dinoi, G. Ujaque, R. Van Eldik, Inorg. Chem. 46 (2007) 4103–4113.

[12] P. Chandra, S.L. Pandhare, S.B. Umbarkar, M.K. Dongare, K. Vanka, Chem. Eur. J. 19 (2013) 2030–2040.

[13] A.M. Al-Ajlouni, A.A. Valente, C.D. Nunes, M. Pillinger, A.M. Santos, J. Zhao, C. C. Romão, I. S. Gonçalves, F. E. Kühn, Eur. J. Inorg. Chem. (2005) 1716–1723.

[14] W.M. Harrison, C. Saadeh, S.B. Colbran, D.C. Craig, J. Chem. Soc. Dalton Trans. (1997) 3785–3792.

[15] A. Berkessel, J.A. Adrio, D. Hüttenhain, J.M. Neudörfl, J. Am. Chem. Soc. 128 (2006) 8421–8426.

[16] A. Berkessel, J.A. Adrio, J. Am. Chem. Soc. 128 (2006) 13412–13420.

[17] P. Altmann, M. Cokoja, F.E. Kühn, Eur. J. Inorg. Chem. 2012 (2012) 3235–3239.

[18] S.P. de Visser, J. Kaneti, R. Neumann, S. Shaik, J. Org. Chem. 68 (2003) 2903–2912.

[19] A. Berkessel, J.A. Adrio, Adv. Synth. Catal. 346 (2004) 275–280.

[20] C.J. Willis, Coord. Chem. Rev. 88 (1988) 133–202.

8 The Fluorinated Complex [$CpMo(CO)_3CF_3$] and its Unexpected Catalytic Activity

Note: Chapter 8 is an original work by the author of this thesis based on the following published literature:

a. *S.A. Hauser, M. Cokoja, M. Drees, F.E. Kühn, J. Mol. Catal. A: Chem. 363-364 (2012) 237–244.*
b. *S.A. Hauser, Organorhenium and Organomolybdenum Oxides : Synthesis and Application as Olefin Epoxidation Catalysts, 2012. http://d-nb.info/1031550240*
c. *M. Drees, S.A. Hauser, M. Cokoja, F.E. Kühn, J. Organomet. Chem. (2013) DOI 10.1016/j.jorganchem.2013.05.004.*

The author does not claim any credit regarding analytical data (NMR, IR, Raman and crystallographic data) utilized for discussion in this chapter. The above references have been appropriately cited in the text and any oversight in doing so is unintentional and regretted. Other analytical data has been collected from cited published literature.

8.1 Introduction

Cyclopentadienyl molybdenum(II) tricarbonyl complexes [$CpMo(CO)_3R$] (R = alkyl, halide etc.) undergo oxidative decarbonylation when treated with *tert*-butylhydroperoxide (TBHP) to give dioxo [$CpMoO_2R$] and oxo-peroxo [$CpMo(O)(O_2)R$] complexes.[1–4] These oxidized complexes are highly active catalysts for epoxidation of unfunctionalized olefins with TBHP (Scheme 8.1).[5] The synthesis and characterization of such '*in situ'* catalysts and the kinetics and mechanisms of their oxidative transformations have been addressed previously in this thesis. In this chapter, explanations for the curious reactivity of the fluorinated complex [$CpMo(CO)_3(CF_3)$] that has been recently reported in literature as an olefin epoxidation pre-catalyst with TBHP are sought.[6–8]

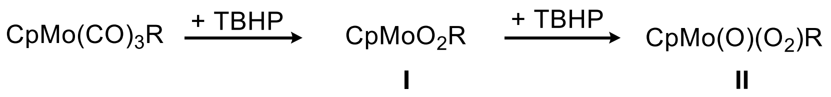

$$CpMo(CO)_3R \xrightarrow{+\text{ TBHP}} \underset{\textbf{I}}{CpMoO_2R} \xrightarrow{+\text{ TBHP}} \underset{\textbf{II}}{CpMo(O)(O_2)R}$$

Scheme 8.1. Oxidation of [$CpMo(CO)_3R$] pre-catalysts with TBHP gives dioxo and oxo-peroxo complexes **I** and **II** respectively.

8.1.1 Background

In a recent publication from Kühn and co-workers,[6] the electronic influence of the side chain group R on catalytic epoxidation activity in complexes [$CpMo(CO)_3R$] has been studied by comparing pre-catalysts R = CH_3 (**1**) and CF_3 (**2**) (Figure 8.1). It has been found that complex **2** undergoes slower oxidative decarbonylation with oxidant *tert*-butylhydroperoxide (TBHP) compared to **1**, and consequently performs poorly in the epoxidation of *cis*-cyclooctene at 25 °C in C_6D_6. Catalytic activity in the epoxidation of *cis*-cyclooctene with TBHP for pre-catalysts **1** and **2** is evaluated by considering their turnover frequencies (TOFs), which are 1139 h^{-1} and 240 h^{-1} respectively (see Table 8.2). The effect of various fluorinated solvents on catalytic activity of **1** and **2** has also been investigated. The catalytic performance of both complexes in hexafluoroisopropanol (HFIP) is reversed and higher than in C_6D_6 solvent. TOFs are 6339 h^{-1} for **2** and 1969 h^{-1} for **1** when using 0.125 mol% catalyst, ratio *cis*-cyclooctene:TBHP = 1:1.2 at 25 °C in HFIP. This observation has been attributed to the activation of TBHP by enhanced H-bonding in the fluorinated solvent[9–11] and faster oxidative decarbonylation of **2** by TBHP to give the active catalyst.

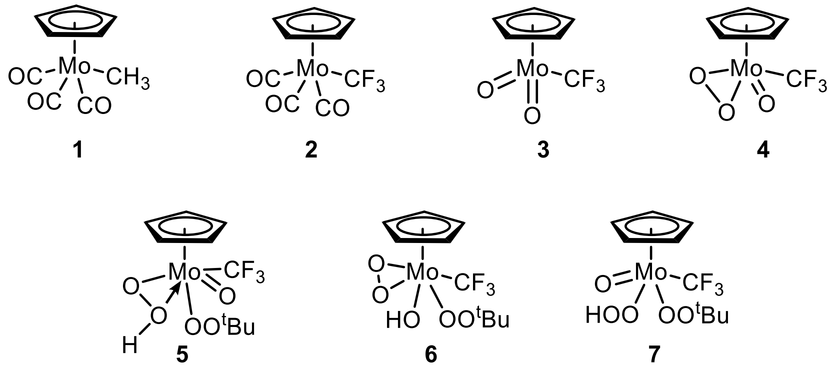

Figure 8.1. Complexes discussed in this chapter.

In a subsequent publication, the theoretical aspects of oxygen atom transfer from TBHP to ethylene, catalyzed by the oxidized complexes of **2**, namely dioxo complex $[CpMo(O)_2(CF_3)]$, **3** and oxo-peroxo analogue $[CpMo(O)(O_2)(CF_3)]$, **4** have been addressed.[8] From DFT calculations, the authors propose that complex **4** is more active than **3** and the formation of intermediates **5** and **6**, and **7** a possible product of reaction with excess TBHP has been suggested (see Figure 8.1).

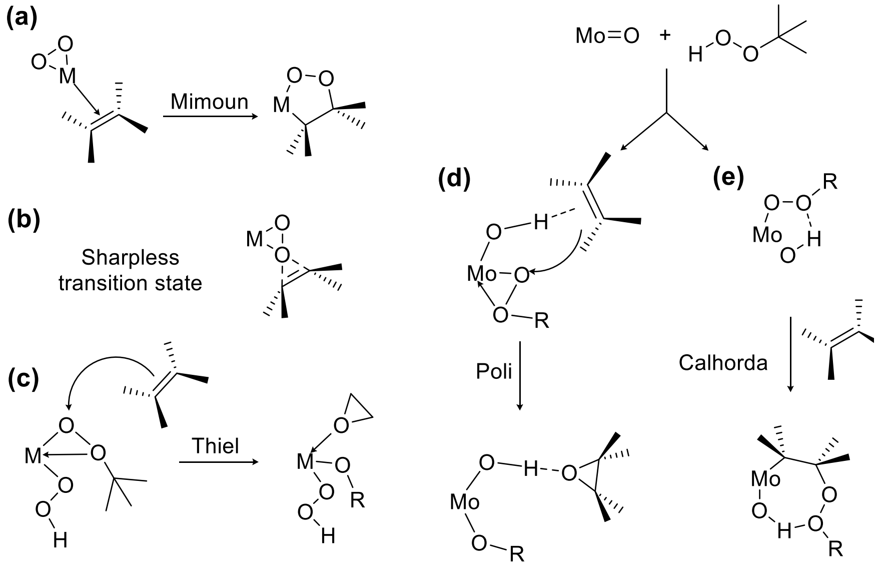

Scheme 8.2. Proposed mechanisms for oxygen atom transfer catalyzed by (a−c) molybdenum peroxo or (d,e) molybdenum oxo complex species. R = ${}^tBu$.

To briefly recapitulate, several mechanisms of oxygen atom transfer by metal peroxo species (Scheme 8.2(a–c)) are known. Transfer of an oxygen atom to a double bond may involve either the formation of a metallocycle (Mimoun)[12] or an *“exogenous attack”* i.e. Sharpless mechanism.[13] Thiel has proposed a similar mechanism for Mo-peroxo species applicable for TBHP as oxidant.[14–16] Mechanisms for metal-oxo complexes proposed by Poli[17–20] and Calhorda et al.[21,22] are shown in Scheme 8.2(d–e).

In this context, the theoretical calculations[8,21] for catalysis with oxo-peroxo complexes of **1** and **2** suggest that oxygen atom transfer in the case of [CpMo(O)(O_2)CH_3] takes place either without the involvement of the peroxo group (*via* 7-membered metallocycle) or by exogenous attack from the peroxo group in a competitive manner (Scheme 8.3(a)). For oxygen atom transfer in the case of [CpMo(O)(O_2)CF_3] (**4**) complex, the peroxo ligand is transformed into **7** and subsequently, oxygen atom transfer is more energetically favoured from the −OOH ligand and neither from the −OO^{t}Bu group nor from a η^2-peroxo ligand as in the Sharpless mechanism (Scheme 8.3(b)). Note that the activated complexes illustrated in Scheme 8.3 are formed on reaction of the oxo-peroxo CpMo complexes with TBHP, and these participate in epoxidation reaction. Hence complexes [CpMo(O)(O_2)R] (R = CH_3, CF_3) should not be considered as stoichiometric oxidants of olefin substrates in this text.

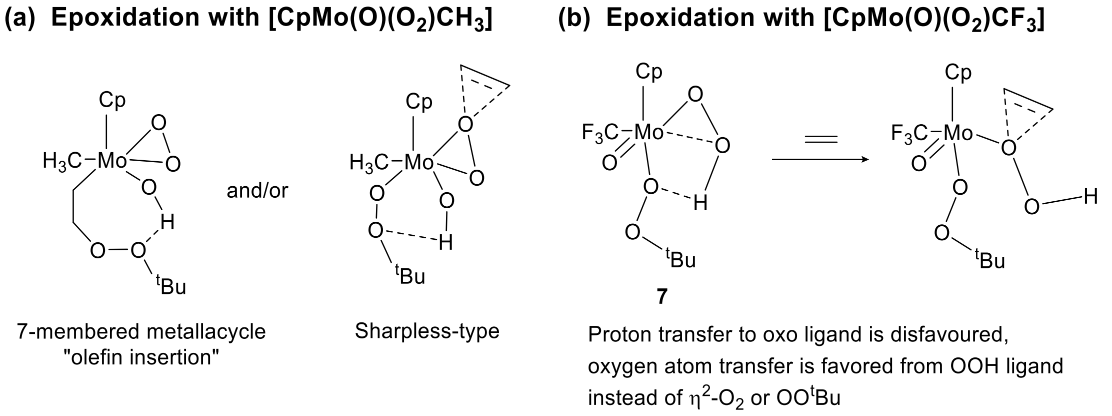

(a) Epoxidation with [CpMo(O)(O_2)CH_3] **(b) Epoxidation with [CpMo(O)(O_2)CF_3]**

Scheme 8.3. A comparison of mechanisms of oxygen transfer from complexes (a) [CpMo(O)(O_2)CH_3],[21] and (b) [CpMo(O)(O_2)CF_3].[8]

It is worthwhile to mention here a new mechanistic proposal by Augustin, Poli et al.[23] for a non-Cp, ONO-type tridentate Schiff base ligand (L) system [MoO_2L]$_2$ or its donor molecule octahedral adduct [MoO_2L(D)] and the interaction of these complexes with TBHP (Scheme 8.4). This mechanism differs slightly from the ones published before. The usual mechanisms of oxidant activation involve hydrogen transfer from TBHP to the electrophilic metal oxo or peroxo group, to form species such as [CpMo(O)(OH)(OO^{t}Bu)R] (from dioxo), and [CpMo(O_2)(OH)(OO^{t}Bu)R] or [CpMo(O)(OOH)(OO^{t}Bu)R] (from oxoperoxo).[17,21] In this publication however, coordination of TBHP as a *neutral molecule* to the metal centre has also been considered in calculations, with possible stabilizing contributions of H-bonding between the catalyst and water, *tert*-butanol (by product) and TBHP itself.[23]

The implications of this new mechanism relevant to our discussion with [$CpMoO_2R$] and [CpMo(O_2)(O)R] (R = CH_3, CF_3) catalysts are presented in Section 8.2.6.

Complexes studied by Agustin, Poli et al.

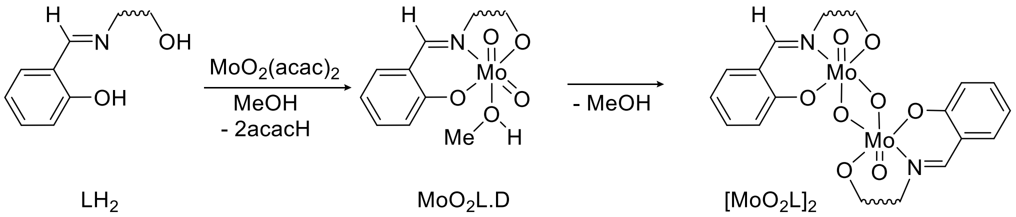

(a) Oxidant activation and oxygen transfer

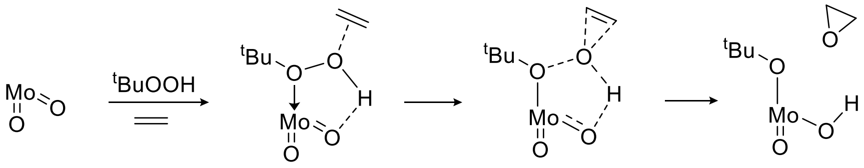

(b) Regeneration of the catalyst

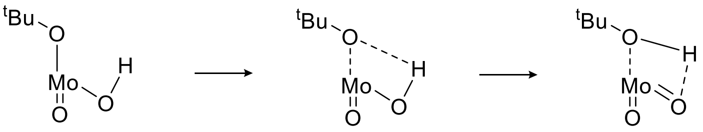

(c) 'Proton Shuttle effect', X = H, ^{t}Bu, O^{t}Bu

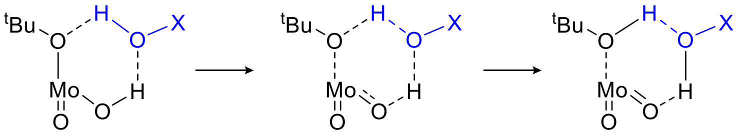

Scheme 8.4. Mechanisms proposed for interaction of the oxidant with the ONO tridentate Schiff base MoO_2 catalysts, (a) reaction of MoO_2 catalyst with TBHP and the olefin, (b) reactivation of the catalyst, and (c) the proton shuttle effect of water, tert-butanol or TBHP in catalyst regeneration.[23]

8.1.2 The Expected and Unexpected Catalytic Activity of Pre-catalyst ***2***

A difference in catalytic epoxidation activity of complexes **1** and **2** is unarguably expected to arise only from the electronic influence of the respective $-CH_3$ and $-CF_3$ substituents, since H and F atoms have been classically considered as isosteres. Indeed, Pauling electronegativity of the two groups differs significantly: $\chi = 2.28$ for CH_3 and $\chi = 3.49$ for CF_3.[24] However, the methyl and trifluoromethyl groups are not isosteric. The van der Waals radius and volume for CF_3 (2.7 Å and 42.5 Å^3) are larger than those for CH_3 (2.0 Å and 16.8 Å^3).[25] Hence a possible influence of steric differences on catalytic activity cannot be disregarded. The hydrophobicity parameter for CF_3 is 1.07 and for CH_3 group it has a value of 0.51.[26] This parameter might also be relevant for lower catalytic activity of **2**, considering the recent publications from Poli et al. on the lowering of relevant activation barriers in presence of H_2O [17,27] and the presence of adventitious water in TBHP oxidant (n-decane solution) sold commercially. A study of different perfluoroalkyl transition metal complexes has shown that the metal-R_f bond is usually stronger, less reactive and more thermally stable than metal-hydrocarbon alkyl linkage.[28] Thus, considering similar examples from literature, the lower activity of pre-catalyst **2** might be anticipated.

Nevertheless, it is also logical to assume that a more Lewis acidic or electrophilic metal centre would react faster with the nucleophilic oxidant TBHP and olefin substrate, resulting in a better catalytic performance. For this reason alone, and slower oxidative decarbonylation of **2** with TBHP notwithstanding, overall slower reactivity of pre-catalyst **2** compared to **1** is unusual.

It is necessary to mention forthwith that previous work[4,21] has unequivocally established that the dioxo complex of **1**, [CpMo(O)$_2$(CH$_3$)] is the primary catalytically active species for olefin epoxidation while in case of the fluorinated analogue **2**, the oxo-peroxo complex **4** has been considered to be the only species relevant for the catalytic reaction.[6,8] This has implications towards resolution of a similar issue, that of the inactivity of complex [Cp*Mo(O)(O$_2$)Cl] compared to [Cp*MoO$_2$Cl][1,29] (Cp* = C$_5$Me$_5$) which has only recently been re-addressed theoretically.[17] Therefore the question asked for complex **2** is, in fact, generic in nature − what causes the differences in reactivity of a dioxo and an oxo-peroxo derivative of [CpMo(CO)$_3$R] complex with TBHP and olefin?

When the oxo-peroxo complexes of **1** and **2** are isolated and applied for catalytic epoxidation, the trend is as expected, i.e. [CpMo(O)(O$_2$)(CF$_3$)] (**4**) performs better than [CpMo(O)(O$_2$)(CH$_3$)]. The TOF for epoxidation of *cis*-cyclooctene at 25 °C in C$_6$D$_6$ with 0.125 mol% of fluorinated oxo-peroxo complex **4** has been reported to be 2371 h^{-1} and with 0.250 mol% of methyl analogue, the TOF is 1268 h^{-1}.[6,7]

In the fluorinated solvent HFIP, higher catalytic activity of **2** (TOF = 6339 h^{-1}) compared to **1** (TOF = 1969 h^{-1}) for *cis*-cyclooctene epoxidation using 0.125 mol% catalyst and substrate:TBHP = 1:1.2, is again surprising. In the presence of HFIP, it is suggested that the solvent assists in oxidant activation by H-bonding and for this reason under these conditions, oxidative decarbonylation and catalytic epoxidation is faster with **2**. This is affirmed by catalysis in hexafluorobenzene (HFB, an aprotic fluorous solvent). In this case, pre-catalyst **2** (143 h^{-1}) is a poorer catalyst compared to **1** (677 h^{-1}), when applied for epoxidation of cyclooctene under reaction conditions mentioned before.

In the following sections, two lines of reasoning attempt to explain the unusual behaviour of the fluorinated complexes **2** and **4**. First, spectroscopic and structural evidence available for **1** and **2** and their oxo-peroxo complexes is compared in an attempt to find a correlation between analytical data and observed catalytic activity (TOF). Next, oxidative transformations of complexes **1** and **2** are discussed in context of the work presented in previous chapters of this thesis. This task is carried out in order to analyse whether proposed mechanisms for oxidative transformations of pre-catalysts [CpMo(CO)$_3$R] can be considered generic for various groups R .

8.2 The ‘Bottom-Up’ Approach

In consideration of the limited discussion in literature[6,8] and the objective to correlate catalytic activity and structural or spectroscopic parameters, complexes **1** and **2** (Section 8.2.2) and their oxidized complexes (Section 8.2.5) have been compared exhaustively. All available information regarding synthesis, stability, spectroscopic and structural data (^{1}H, ^{13}C, ^{95}Mo NMR, IR, crystallographic data) has been collected to explain the differences in catalytic activity. An attempt has been made to determine the reasons for, (a) slower oxidative decarbonylation of **2** compared to **1**, (b) differences in the mechanisms of oxidant activation and oxygen atom transfer, and (c) reversal of catalytic activity in fluorinated solvent HFIP for the two complexes.

8.2.1 Synthesis and Stability of the Pre-catalysts

Complex [$CpMo(CO)_3(CH_3)$] can be easily prepared from the reaction of Na[$CpMo(CO)_3$] and CH_3I in THF and is obtained pure after sublimation under vacuum at 25−50 °C.[30] Synthesis of the fluorinated analogue is not as straightforward and requires the synthesis of the acyl perfluoroalkyl molybdenum derivative [$CpMo(CO)_3(COCF_3)$], which gives complex **2** after pyrolysis (Scheme 8.5).[31,32]

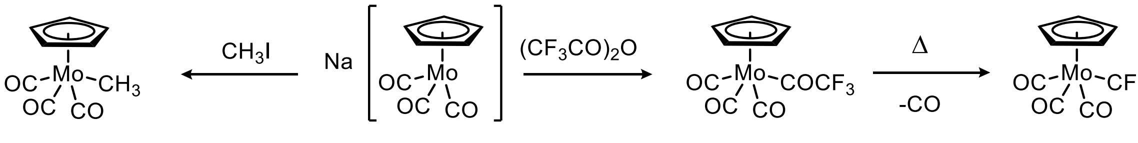

1 **2**

Scheme 8.5. Synthesis of complexes **1** and **2**.

With regard to stability of the pre-catalyst **2**, several fluorinated transition metal complexes are known to be susceptible to the α-elimination process illustrated in Figure 8.2(a), to produce a difluorocarbene species.[28,33-36] Such a species formed from **2** might be unstable and result in the formation of complex [$CpMo(CO)_3F$] by α-fluoride abstraction and CF_2. In presence of strong Lewis acids such as BF_3 and SbF_5, ionic complexes have been isolated.[34,37] Since no strong Lewis acids are present in the catalysis reactions and formation of [$CpMo(CO)_3F$] is unlikely for different reasons,[1] this line of argument might be disregarded.

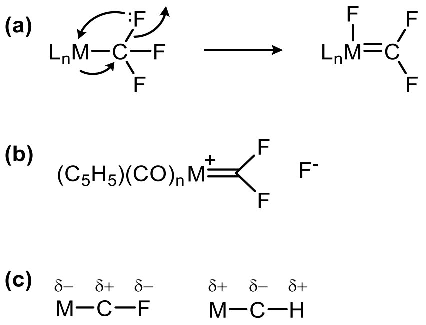

Figure 8.2. Illustration of (a) the formation of difluorocarbene species,[38] (b) hyperconjugation model proposed by King et al.,[31] and (c) the inductive effect of the α-fluoro or α-hydrogen atom on the metal.

Yet, King and Bisnette also proposed an ionic ‘no-bond resonance’, hyperconjugation model for the fluorinated complex **2** (Figure 8.2(b)) to explain the lower wavenumbers in IR for *v*(C-F) for **2** compared to the acyl complex [$CpMo(CO)_3(COCF_3)$].[31] Furthermore, the higher thermal stability (m.p.

---

[1] Outer *p* orbitals of F atom and *d* orbitals of Mo metal do not overlap sufficiently for covalent bond formation. Ionic complexes of the type [$CpMo(CO)_3$]FBF_3 and [$CpMo(CO)_3$]FPF_5 involving weak Mo···F interactions are known.[98,99]

of **2** = 153 °C; for acyl complex m.p. = 64-65 °C), stronger force constant for Mo-CF_3 bond (1.88 Ncm^{-1}), shorter M-CF_3 bond length (2.234 Å) − all indicate a partial double bond between Mo-CF_3 and one weak C-F bond. This discussion leads to a conclusion that CF_3 group is a good π acceptor due to availability of low lying σ^*(C-F) orbitals.[39] Therefore, backbonding between the metal and these acceptor orbitals might be responsible for the higher stability of **2** and for our purpose, the cause for its slower reactivity with TBHP. Although it has been asserted from molecular orbital calculations have shown that conclusions derived from only considering the back donation interaction M(dπ) → $CF_3(\sigma^*)$ might be erroneous and the electron-withdrawing character of CF_3 group is more important.[37,40,41]

In contrast, the possible decomposition processes for pre-catalyst **1** and similar Group VI complexes are mostly photoinduced[42] − (a) dealkylation *via* α-hydrogen abstraction,[43] (b) homolysis of the metal-carbon σ-bond,[44-46] and (c) 'trapping' of the $[CpM(CO)_2(CH_3)]$ complexes (M = Cr, W), with olefins.[47,48] In these processes, an initial thermally or photochemically induced loss of CO group initiates decomposition and finally dealkylation occurs. When the two pre-catalysts are treated with TBHP, it is likely that a similar process of CO loss occurs. This is however, more facile for **1** rather than pre-catalyst **2**.

Regardless of the debate on the *actual* reasons for higher stability of **2** compared to **1**, it is still possible to correlate pre-catalyst stability with slower oxidative decarbonylation of **2** with TBHP. It follows from logic that the presence of CF_3 group confers electron deficiency on the *whole* molecule and lowers the energy of all *d* orbitals of the metal. The presence of this perfluoro group makes the metal more negatively charged (Scheme 8.2(c)) compared to the alkyl analogue. This would make the complex less reactive towards oxidative addition type reactions, which primarily involve metal HOMO and reagent LUMO orbitals.[38] Hence the reaction of pre-catalyst **2** with TBHP to give intermediates and transition states of the type shown in Scheme 8.3 would be slower for this reason.

Table 8.1. A comparison of selected structural and spectroscopic parameters and TOFs of $[CpMo(CO)_3R]$ complexes, R = Cl, CH_3 (**1**), CF_3 (**2**).

Complex	$[CpMo(CO)_3Cl]$		**1**		**2**	
Parameter		Ref.		Ref.		Ref.
Mo-R Bond Length (Å)	2.5030(6)	49	2.326(3)	50	2.234(3)	7
Mo-C_t Bond Length (Å)	1.988	49	2.007	50	1.989	a
van der Waals Radius of R (Å)	1.75	25	2.0	25	2.7	26
Trans angle α_1 R-Mo-CO (°)	134.49(7)	49	129.60	50	131.42[a]	a
Trans angle θ C_t-Mo-R (°)	112.55	49	112.10	50	110.63	a
^{95}Mo NMR Shift (25 °C, C_6D_6)	-887	7	-1736	6	-1458	6
Melting Point (°C)	145	30	124	30	153	31
TOF (h^{-1})[b]	7930	7	1870	7	240	6

[a] Unpublished results by Hauser et. al. *Trans* angle for $[Cp^*Mo(CO)_3(CF_3)]$ is 130.2(2)°. [b] TOFs for the catalytic epoxidation of *cis*-cyclooctene with TBHP (substrate:TBHP = 1:1.2) at 25 °C in C_6D_6, with different catalyst mol% concentrations: $[CpMo(CO)_3Cl]$ = 0.063 mol%, [**1**] = 0.25 mol% and [**2**] = 0.5 mol%.

At this point, it may also be worthwhile to consider the steric effect of the side chain substituents and its influence on bond lengths (Table 8.1). This might be a starting point to explain the higher reactivity of the Cl complex in comparison to **1** and **2**. It is likely that since the Cl group is small, it exerts weaker steric hindrance at the metal centre and being located ‘at a distance’ (bond length is 2.5 Å), enables the approach of the oxidant and olefin in the coordination sphere in a more facile manner than relatively sterically encumbering CH_3 and CF_3 groups. See Section 8.2.2 for a discussion of the π-donor and π-acceptor ability of the ligands in relation to the *trans*-angle and reactivity.It is important to note that a ‘temporary’ dissociation of the side chain ligand CH_3, CF_3 or even Cl cannot be a proper explanation for the differences in catalytic activity. Either the Mo-R bond remains intact [51] (as it indeed does [4,52−54]) or it does not.[55,56] Here, examples where the Cp ligand is lost are not being considered.[2,57] An implication that after oxidative decarbonylation, the pre-catalysts are completely transformed into an undeterminable ‘decomposed’ species and not the dioxo and oxo-peroxo complexes − is also not entirely correct. Although a valid assertion, many such oxo complexes have been isolated, and structural proof that side chains are retained, is available.[4,29,58−60] Nevertheless, the possibility of a *part* of such pre-catalysts decomposing *via* Cp or R ligand loss into complex molybdenum oxides cannot be discounted. This refers to the observation of precipitate formation for several [CpMo(CO)$_3$R] pre-catalysts when they are treated with TBHP.[52,58,61]

*8.2.2 Comparison of Spectroscopic and Structural Data of **1** and **2***

The stereoelectronic effects of the methyl and trifluoromethyl groups are reflected in their structure and spectroscopic data. Table 8.2 is a summary of this data for pre-catalysts **1** and **2**.

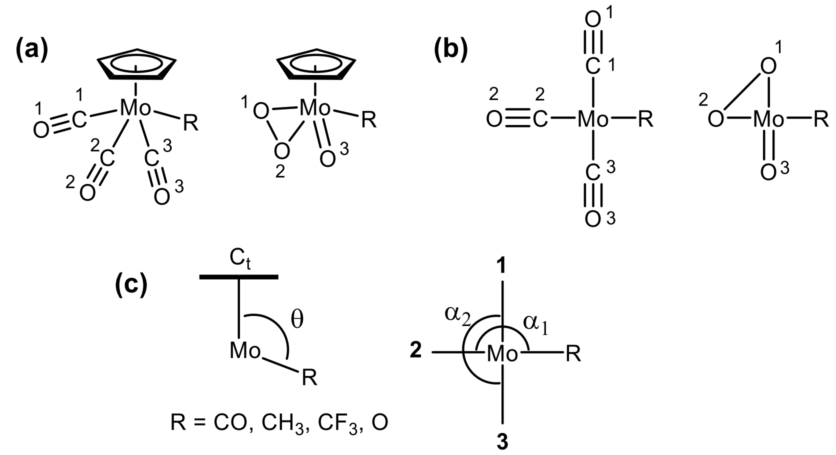

Figure 8.3. (a) Atom numbering scheme for 1 and 2 and their oxo-peroxo complexes. (b) The square planar analogy for basal ligands of the piano stool structures. (c) Bond angles θ and α, C_t refers to the centroid of pentahapto Cp ring.

In general, NMR data indicates that due to the –I effect of the CF_3 group, the complex as a whole becomes ‘deshielded’. The Cp ligand in **2** appears slightly downfield at 4.55 ppm (^{1}H NMR) and 93.1 ppm (^{13}C NMR). As expected, the α-C in **2** is strongly de-shielded (151.2 ppm) in comparison to α-C in **1** (-22.2 ppm). In fact, the chemical shift for α-C in **2** is close to that for known N-heterocyclic carbene CpMo complexes (difference of *ca.* 30 ppm from an average of 180 ppm).[55,62,63]

The appearance of three terminal CO signals for complex **2** in comparison to **1** is interesting. The small anisotropy of the two *cis*-CO (at 227 ppm) is most likely due to the steric bulk of the CF_3 group (see Section 8.1.2). The two *cis*-CO ligands in **1** however, are equivalent on account of the smaller volume of the CH_3 group and unrestricted rotation of the basal ligands in the piano stool structure (about the $Cp_{centroid}$-Mo axis). The slightly upfield shift in ^{13}C NMR for the *trans*-CO (from 240.5 ppm in **1** to 237.4 ppm in **2**) is most likely due to the structural *trans*-effect [2] of the trifluoromethyl group.[32,64,65] A comparison of ^{95}Mo NMR shifts also confirms the electronic deficiency of the metal in **2** with respect to **1**.[66] For a discussion of ^{95}Mo shifts for the oxidized complexes, see Section 8.2.5.

Table 8.2. Comparison of analytical, spectroscopic, structural and catalytic activity data for pre-catalysts $[CpMo(CO)_3CH_3]$ and $[CpMo(CO)_3CF_3]$. [6,7,31,50]

Parameter		$[CpMo(CO)_3CH_3]$, **1**	$[CpMo(CO)_3CF_3]$, **2**
Melting Point	°C	124[a]	153
^1H NMR[b]	$C_5\underline{H}_5$	4.42	4.55
^{13}C NMR[b]	$\underline{C}_5H_5$	92.4	93.1
	$\underline{C}(H/F)_3$	-22.2	151.2
	Mo–$\underline{C}$O	240.5, 227.4	237.4, 227.5, 227.4
^{95}Mo NMR[b]	Mo	-1736	-1458
IR	v_{CO}	2003, 1892, 1876	2045, 1961, 1937
	v_{CO}[c]	2012, 1920, 1903	2052, 1971, 1927
	v_s(Mo-C)	502w,sh	477w, 479s[d]
	v_a(Mo-C)	451s, 453m[d]	430vs, 432m[d]
	Mo-R stretch	406	250
	Mo-Cp stretch	335	351
Force constant[e]	K(Mo-R)	1.53	1.88
	K(Mo-Cp)	3.11	3.18
Bond Lengths (Å)	Mo-R	2.326(3)	2.232(5)
	Mo-C1	1.984(4)	2.003(3)
	Mo-C2	1.997(4)	2.018(5)
	Mo-C3	1.993(4)	2.001(3)
	C1-O1	1.144(4)	1.145(4)
	C2-O2	1.139(5)	1.137(3)
	C3-O3	1.131(4)	1.143(3)
	Mo-C_t	2.007	1.989
Bond Angles (°)	C1-Mo-C2	78.09(17)	76.80(11)
	C2-Mo-C3	78.87(15)	76.11(11)
	R-Mo-C1	72.39(13)	76.45(10)
	R-Mo-C3	72.41(17)	75.99(10)

---

[2] The terms *trans*-effect and *trans*-influence are distinguished in this text as kinetic *trans*-effect and structural *trans*-effect respectively, according to the nomenclature distinction in Ref. 100.

α_1	R-Mo-C2 (*trans*-CO)	129.61	131.42(17)
α_2	C1-Mo-C3 (*trans*-CO)	107.37	108.65(18)
θ_1	C_t-Mo-C1	127.48	126.86
θ_2	C_t-Mo-C2	118.28	117.95
θ_3	C_t-Mo-C3	124.21	124.34
θ_4	C_t-Mo-R	112.10	110.63
Catalytic Activity	TOF (h^{-1})	1139[f]	240[f]
		1969[g]	6339[g]

[a] Reference 30. [b] Measured in C_6D_6, reported in ppm. [c] After addition of *cis*-cyclooctene, shifting of absorption bands due to solvent effects. [d] Raman frequencies (cm^{-1}). [e] Calculated from IR frequencies, units Ncm^{-1}. [f] Catalysis in C_6D_6 with 0.5 mol% catalyst, *cis*-cyclooctene: TBHP = 1:2.
[g] Catalysis with hexafluoroisopropanol (HFIP) solvent, 0.125 mol% catalyst, *cis*-cyclooctene: TBHP = 1:1.2.

The rationale of angular *trans* influence [3] for 18 e^- [CpMo(CO)$_3$R] complexes has been previously invoked to explain unusual bond lengths, bond angles, spectroscopic data and even reactivity.[32,65,67,68] According to this concept,

(a) π-acceptor ligands have a larger θ value than π-donor or π-neutral ligands,
(b) CO ligands that are *trans* to π-donor or π-neutral ligands have a lower θ angle than those *trans* to other π-acidic ligands,
(c) strong, covalently σ-bonding ligands prefer to be coordinated to the metal centre with a small θ angle and,
(d) distortion from the ideal pseudo-square pyramidal geometry occurs in such a way that the two larger θ angles correspond to *trans* ligands, as do the two smaller ones.

Thus, as summarized in Table 8.2, the values of θ_1–θ_3 (all CO ligands) are larger than θ_4 (for π-neutral ligand R), angle θ_2 corresponding to the CO ligand *trans* to R is smaller than θ_1 and θ_3. Covalently bonding R ligand has the smallest θ_4 value and ligands (θ_1,θ_3) and (θ_2,θ_4) form the two set of *trans* ligands. Since the differences in *trans* angles for pre-catalysts **1** and **2** are small, a formalism where these groups are simply compared as σ-donors is more useful.[4] From this structural analysis, although possible, the implications for reactivity of **1** and **2** with oxidant TBHP are difficult to describe within the scope of present work.

The lower ν(CO) frequencies for the CO groups in **1** compared to **2** indicate increased d→π*-backbonding in **1**. The electron density at the metal in **2** is offset by the inductive effect of CF_3 group and consequently, the metal is relatively more electron deficient (evident in the 'less negative' ^{95}Mo shift at -1458 ppm). Thus, lesser back donation to CO groups results in ν(CO) at higher frequencies for **2**. The higher values for the force constants of bonds Mo-CF_3 (1.88 Ncm^{-1}) and Mo-Cp (3.18 Ncm^{-1}) in **2** are again reminiscent of the higher stability of the pre-catalyst.

---

[3] Angular *trans* influence is a thermodynamic effect, dependent on the nature of the *trans* ligand and different from the concept of *trans* influence in square-planar and octahedral coordination compounds since bond angles are considered here instead of bond lengths. Ref. 65

[4] The π-acceptor property of CF_3 ligand has been shown to be very weak, despite the experimental observations of King et al. (Ref. 31) An explanation for the observed elongation of C-F bond is instead proposed on the basis of Bent's rule. (Ref. 101)

8.2.3 Reaction of **1** and **2** with TBHP

Oxidative decarbonylation of the pre-catalysts $[CpMo(CO)_3R]$ with TBHP forms catalytically active oxo complexes (Scheme 8.1) but as mentioned before, this oxidative transformation for pre-catalyst **2** has been found to be quite slow in comparison to **1**. Apart from the discussion in Section 8.2.1 on higher stability and lesser reactivity of **2** with the oxidant, one must consider the various oxidative transformations that can take place with TBHP.

There are very few kinetic and mechanistic studies on the decarbonylation reaction of CpMo complexes.[3,4,69] However, studies with other tridentate ligands[69–73] can provide clues about the transformation of a Mo(II) pre-catalyst into Mo(VI) oxo complexes. Oxidative decarbonylation converts Mo(II) to Mo(VI) and can involve either a sequential or simultaneous loss of the three CO groups, although the latter process seems very drastic and unlikely. Subsequently, Mo=O bonds must form considering the high affinity of the metal towards oxygen, that are readily available from the active hydroperoxide oxidant. Therefore, coordinatively unsaturated and thus highly reactive intermediates of the type $[CpMo(CO)_2R]$ and [CpMo(CO)R] might be anticipated during oxidative decarbonylation. Such species can be stabilized with the help of a donor solvent molecule,[20,74] by coordination of the olefin,[47,48] or even TBHP coordinating as a neutral molecule;[23] before being converted into the dioxo and oxo-peroxo species. Indeed, coordination of TBHP might be a step in the loss of CO as CO_2 and conversion of Mo-CO into Mo=O, similar to examples of molybdenum oxidoreductases.[75,76]

Previous studies have established that the structural *trans*-effect of the CF_3 group is quite strong,[64] and in fact comparable to that of the CH_3 group.[28,36] In the case of pre-catalysts **1** and **2**, the structural differences due to this effect can be observed but are marginal in magnitude. Hence the contribution of kinetic *trans*-effect with respect to reactivity with TBHP is likely to be small as well. As argued before, the overall electron deficiency of pre-catalyst **2** is a much more plausible reason for the slower oxidative decarbonylation. Yet, as discussed in the next sections, the kinetic *trans*-effect will be of more relevance for the oxo-peroxo complexes (the *actual* catalytic species) and their reactivity with the oxidant.

8.2.4 Differences in Reactivity of Dioxo and Oxo-peroxo Complexes

Regardless of *how* Mo(VI) species form, once these complexes are present in solution, the reasons for the high reactivity of the dioxo complexes compared to oxo-peroxo complexes in olefin epoxidation must be outlined. Table 8.3 is a qualitative summary of experimental results regarding the relative activity of the oxidized complexes for various tricarbonyl pre-catalysts. Subsequently, the relevance of ‘spectator oxo ligand’ effect in its influence on catalytic activity for these oxidized complexes is presented.[77,78]

Table 8.3. Overview of the reactivity of dioxo and oxo-peroxo complexes derived from tricarbonyl pre-catalysts on treatment with TBHP (decane), as reported in literature.[a]

Pre-catalyst	$[CpMoO_2R]$	$[CpMo(O)(O_2)R]$	Reference
$[CpMo(CO)_3Cl]$	Active	Less active/Inactive (?)	[2,3]
$[Cp^*Mo(CO)_3Cl]$	Active	Inactive	[1,29]
$[CpMo(CO)_3(CH_3)]$	Active	Less active	[4]
$[CpMo(CO)_3(CF_3)]$	Inactive (?)	Active	[6,8]

[a] Availability of kinetic data, i.e. rate constants is limited and the data is primarily based on experimental observations. Catalytic inactivity proposed but not confirmed experimentally is referred to as 'inactive (?)'. Since catalysis experiments are often performed under slightly different conditions, quantitative data, i.e. TOFs are not compared here.

Evidently for most cases, the $[MoO_2]^{2+}$ complexes are better catalysts than the corresponding $[MoO(O_2)]^{2+}$ species. It has been suggested that steric and electronic factors influence the comparative reactivity (and activation barriers) for these two species during activation of TBHP and oxygen transfer to alkene.[17] According to our current understanding, the two oxo complexes perform differently because the oxo and η^2-(O−O) ligands have different electrophilicity. These ligands act as a temporary repository of the proton of the hydroperoxide oxidant in both Poli and Calhorda mechanisms (Scheme 8.2) as illustrated below.

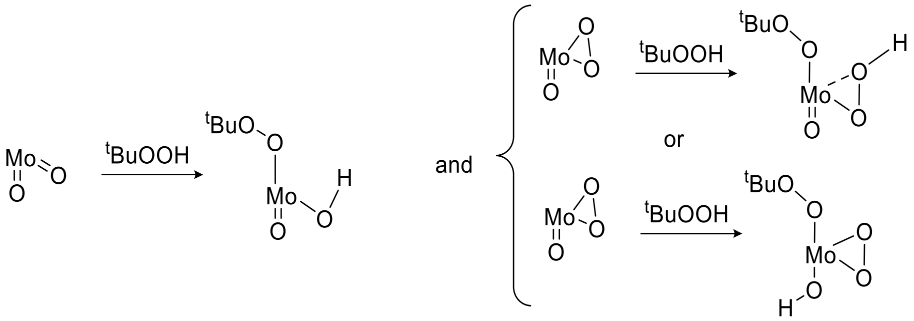

Figure 8.4. The oxo ligand and peroxo groups act as a proton depository. Cp ligand has been omitted for clarity.

In the case of complexes $[CpMo(O)(O_2)R]$, R = CH_3 and CF_3, the energy of the unoccupied antibonding σ* orbital for peroxo ligand is crucial in determining its reactivity, i.e. the ability of the peroxo group to accept additional electron density from the HOMO of the olefin (*via* Sharpless mechanism).[79] Additionally the relative preference of the oxo and peroxo ligands to form intermediates such as those shown in Figure 8.4, determines the pathway for oxidant activation and subsequent reaction with the alkene. Quite naturally, the stereoelectronic attributes of the ligand R in both $[CpMo(O)_2R]$ and $[CpMo(O)(O_2)R]$ complexes (specially a strong inductive influence of a group such as CF_3) would exert its effect on the relevant activation barriers in the Lewis acidic pathway shown in Figure 8.4. Therefore it is interesting to consider the effect of the spectator oxo ligand in dioxo complexes *vs.* oxo-peroxo complexes and also between the two dioxo species **A** and **B** and the two oxo-peroxo species **C** and **D**.

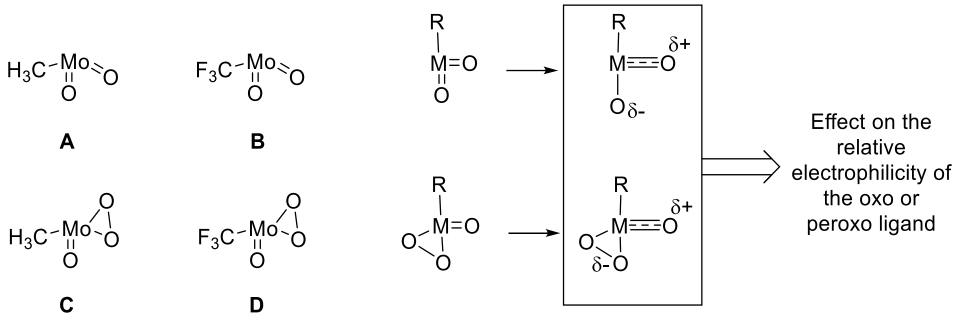
H3C-Mo(=O)=O
F3C-Mo(=O)=O
A
B
H3C-Mo(=O)(O2)
F3C-Mo(=O)(O2)
C
D
R
M=O
O
δ+
δ-
Effect on the relative electrophilicity of the oxo or peroxo ligand

Figure 8.5. Spectator oxo ligand effect for the oxidized complexes formed on treatment of pre-catalysts **1** and **2** with TBHP oxidant. R = CH_3 or CF_3. Cp ligand has been omitted for clarity.

In complexes with two or more such oxo donor ligands, the filled *p* orbitals of the heteroatoms compete for overlap with the same empty metal *d* orbitals. Obviously, the nature of the complex, i.e. the nature of ancillary ligands would determine which oxygen is able to donate electrons more easily to the metal (primarily by *trans* effect) and thus have a stronger interaction, almost akin to a Mo≡O triple bond.[77,78] This spectator ligand effect in turn would affect the reactivity of the second oxo group in case of **A** and **B** and the peroxo ligand in case of **C** and **D**. The dioxo complex derived from pre-catalyst **1** is more active than the oxo-peroxo complex[4] while the presence of the CF_3 group obviously has a detrimental effect on reactivity in species **B**. However in species **D**, this effect is alleviated by the conversion of one oxo ligand to oxo-peroxo. The remaining oxo ligand becomes more like a triple bond (shorter Mo=O bond length and elongation of Mo-η^2-O_2 and O-O bond lengths; see next section), and affects the electrophilicity of the peroxo ligand. This might be a reason for the stability of species such as **7** (Figure 8.1) and the higher reactivity of **4** compared to [CpMo(O)(O_2)(CH_3)]. The contribution of both '*trans*-effect' and 'spectator oxo effect' on catalytic activity in comparison to the inductive influence of the R groups may or may not be significant. Addressing this issue is not the focus of the present work but is helpful for explaining structural data.

Although the crystallographic data for dioxo complexes [CpMo$(O)_2$(CH_3)] and [CpMo$(O)_2$(CF_3)] is not available, it was possible to derive the various bond lengths and angles summarized in Table 8.4 from DFT calculated optimised geometries.

Table 8.4. Comparison of structural data for dioxo complexes [CpMo$(O)_2$(CH_3)] and [CpMo$(O)_2$(CF_3)] determined from their calculated ground state geometries.

Parameter	[CpMo$(O)_2$(CH_3)]	[CpMo$(O)_2$(CH_3)]
Bond Lengths (Å)		
Mo-C_t	2.187	2.159
Mo-O1	1.718	1.716
Mo-O2	1.718	1.716
Mo-R	2.167	2.198
C-H1	1.094	–
C-H2	1.094	–
C-H3	1.095	–

C-F1	–	1.361
C-F2	–	1.361
C-F3	–	1.350
Bond Angles (°)		
R-Mo-O1	99.92	98.24
R-Mo-O2	99.92	98.24
O1-Mo-O2	109.18	109.85
θ_1 (C_t-Mo-O1)	119.21	119.66
θ_2 (C_t-Mo-O2)	119.22	119.66
θ_3 (C_t-Mo-R)	105.31	106.11

The slightly shorter bond lengths Mo-C_t, Mo-O1 and Mo-O2 in the dioxo trifluoromethyl complex compared to [$CpMoO_2(CH_3)$] result from the overall lower electron density in this complex. The Mo-oxo bond lengths and bond angles R-Mo-oxo are equal for both complexes. Values of the *trans* angles θ_1 and θ_2 are identical, while a small difference exists for θ_3 – value of 106.11° for $-CF_3$ analogue is very slightly larger than 105.31° of $-CH_3$ complex. Curiously, one C-F bond length is shorter than the other two. Nevertheless, the differences in the ground state optimised structures of these complexes are too small to be of any major relevance. The higher reactivity of [$CpMoO_2(CH_3)$] with TBHP compared to [$CpMoO_2(CF_3)$] must therefore have an explanation that is not based on ground state geometry of these complexes.

The next section discusses the *trans*-effect of the ligand R and its influence on reactivity of oxo-peroxo complexes. The participation of the spectator oxo ligand is not discussed extensively, even though the significant shortening of the Mo=O bond and elongation of O−O bond of peroxo ligand in **4** compared to bond lengths in [$CpMo(O)(O_2)(CH_3)$] are obviously indicative parameters. To determine the extent to which the spectator oxo ligand plays a role in the stabilization of transition states for the oxidized complexes of **1** and **2**, and thus on their reactivity towards the olefin, is beyond the scope of the present work.

8.2.5 Comparison of Oxo-Peroxo Complexes

The structural and spectroscopic differences between complexes [$CpMo(O)(O_2)(CH_3)$] and [$CpMo(O)(O_2)(CF_3)$] are summarized in Table 8.5.

As discussed before for pre-catalysts **1** and **2**, ^1H and ^{13}C NMR chemical shifts of Cp ligand and α-C indicate that the fluorinated oxo-peroxo complex is overall 'deshielded' with respect to its non-fluorinated counterpart. Curiously, this similarity in trend does not extend to ^{95}Mo shifts, which indicate a reversed electronic situation: -609 ppm for [$CpMo(O)(O_2)(CH_3)$] is a more de-shielded metal centre when compared to that in **4**, which shows the ^{95}Mo signal at -709 ppm. ^{95}Mo chemical shifts are known to be sensitive to structural and electronic variations.[66] These shifts can be correlated with the *p* and *d* orbital population on Mo atom, the total electronic population on the metal and oxygen atom transfer capacity in Mo(VI)O_2 complexes.[80,81]

Table 8.5. Comparison of spectroscopic, structural and catalytic activity data for oxo-peroxo complexes complexes [$CpMo(O)(O_2)(CH_3)$] and [$CpMo(O)(O_2)(CF_3)$].[6,7]

Parameter		[$CpMo(O)(O_2)(CH_3)$]	[$CpMo(O)(O_2)(CF_3)$]
^1H NMR[a]	$C_5\underline{H}_5$	5.23	5.30
^{13}C NMR[a]	$\underline{C}_5H_5$	109.3	112.5
	$\underline{C}(H/F)_3$	24.8	148.0
^{95}Mo NMR[a]	Mo	-609	-709
IR	v(Mo=O)	951vs, 949vs[b]	953vs
	v(O-O)	850vw	870vw
	$v_s(Mo(\eta^2-O_2))$	575s, 576m[b]	571s
	$v_a(Mo(\eta^2-O_2))$	561vs, 559s[b]	525vs
	v(Mo-Cp)	368m, 368s[b]	376vs
	O=MoCp *def.*	–	302w
	O=Mo(η^2-O_2) *def.*	256s, 258vs[b]	243vs
	O=Mo(η^2-O_2) *def.*	219s, 218m[b]	204m
Bond Lengths (Å)	Mo-R	2.168(7)	2.197(3)
	Mo-O1	1.840(9)	1.922(2)
	Mo-O2	1.857(7)	1.933(2)
	Mo-O3	1.728(6)	1.689(2)
	O1-O2	1.271(14)	1.440(3)
	Mo-C_t	2.079	2.066
Bond Angle (°)	O1-Mo-O2	40.2(4)	43.88(9)
	O2-Mo-O3	104.9(4)	108.15(10)
	R-Mo-O1	80.1(4)	76.86(10)
	R-Mo-O3	97.4(3)	93.85(12)
α_1	R-Mo-O2 (*trans* angle)	120.3(3)	120.58(10)
α_2	O1-Mo-O3	111.34	110.22
θ_1	C_t-Mo-O1	130.02	131.97
θ_2	C_t-Mo-O2	111.75	110.75
θ_3	C_t-Mo-O3 (oxo ligand)	116.84	117.28
θ_4	C_t-Mo-R	105.41	105.81
Catalytic Activity	TOF (h^{-1})[c]	1265	2049
	Yield (%) after 4 h	*ca.* 70	*ca.* 90

[a] Measured in C_6D_6, reported in ppm. [b] Raman frequencies (cm^{-1}). [c] 0.25 mol% catalyst, *cis*-cyclooctene (400 equiv.), TBHP (480 equiv.), 25 °C in C_6D_6.

Even though the discussion here pertains to oxo-peroxo complexes and not dioxo species, a parallel from the studies of dioxo complexes by Teruel et al.[80,81] can be drawn to explain the unusual ^{95}Mo shifts and reactivity trend for [$CpMo(O)(O_2)(CH_3)$] and **4**. According to this concept, the metal oxo bond is polarized as $Mo^{\delta+}=O^{\delta-}$ and, normally, the charge on Mo reduces the basicity of the terminal oxo atom so that it is not readily attacked by nucleophiles. Therefore any electronic changes at the metal atom (chemical shift) will be reflected in the electrophilicity of the oxo ligands because of electronic population redistribution between Mo and oxygen. Since both Mo *p* and *d* orbital electron populations are involved in shielding the core, they are both responsible for influencing the ^{95}Mo chemical shift.

For Mo-alkyls, σ bonding is more relevant instead of π bonding.[80] Thus *p* orbital contribution to electronic situation at the metal would be of lesser significance in oxo-peroxo complexes compared to tricarbonyl complexes. Its magnitude is less sensitive to electronic changes and also has a lesser impact on ^{95}Mo chemical shifts. However, the *d* orbital contribution to Mo is larger and more sensitive to changes in the coordination sphere. Hence the effect of *d* orbital electronic populations on ^{95}Mo chemical shifts might be anticipated to be of more consequence. A larger *d* orbital electronic population at the metal results in more positive chemical shift (more electron rich, shielded metal centre, resonance at higher frequency) and thus the oxo (and oxoperoxo) ligand becomes less susceptible to nucleophilic attack.[80] The CH_3 group contributes more to the *d* electron density at Mo than CF_3, hence the order of ‘more positive’ ^{95}Mo shifts is -609 ppm (for CH_3) > -709 ppm (for CF_3). This fits the expected ‘inverse’ order of reactivity for these complexes with TBHP and olefin, i.e. methyl analogue is less active than trifluoromethyl complex **4** (see Table 8.5).

Note that this relationship does not apply to the tricarbonyl pre-catalysts and cannot be used to correlate with the rate of their oxidative decarbonylation with TBHP. For these complexes, terminal CO groups are capable of influencing the back donation capability (*p* orbital contribution more) and therefore trends in ^{95}Mo shifts and reactivity differ. In addition, the differences in the *magnitude* of relative contributions of *p* and *d* orbital electron populations is apparent in ^{95}Mo NMR – while the difference in chemical shift between oxo-peroxo complexes is 100 ppm, it is about three times larger ~278 ppm for the tricarbonyl pre-catalysts. Teruel et al. have also correlated the propensity of intramolecular *vs.* intermolecular oxygen transfer of molybdenum dioxo complexes with ^{95}Mo shifts.[80]

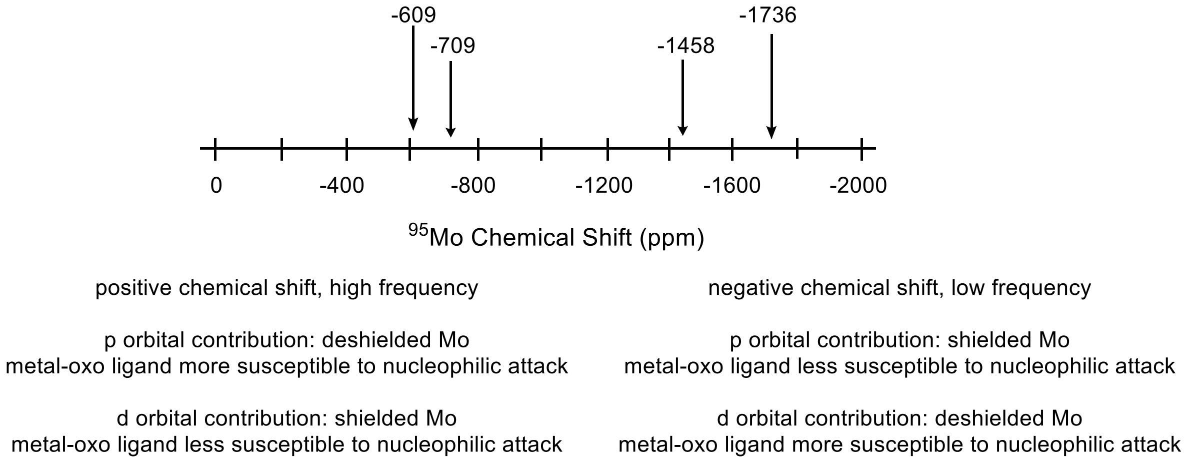
-609
-709
-1458
-1736
0
-400
-800
-1200
-1600
-2000
95Mo Chemical Shift (ppm)
positive chemical shift, high frequency
negative chemical shift, low frequency
p orbital contribution: deshielded Mo
metal-oxo ligand more susceptible to nucleophilic attack
p orbital contribution: shielded Mo
metal-oxo ligand less susceptible to nucleophilic attack
d orbital contribution: shielded Mo
metal-oxo ligand less susceptible to nucleophilic attack
d orbital contribution: deshielded Mo
metal-oxo ligand more susceptible to nucleophilic attack

Figure 8.6. ^{95}Mo shifts for pre-catalysts **1** (-1736 ppm), **2** (-1458) and their oxo-peroxo complexes [$CpMo(O)(O_2)(CH_3)$] (-609 ppm) and [$CpMo(O)(O_2)(CF_3)$] (-709 ppm).[6,7,80,81]

The IR stretching frequencies for the oxo-peroxo complexes are also instructive. Only a marginal increase in stretching frequency ν(Mo=O) is observed for species **4** compared to the analogous CH_3 complex and the decrease in Mo=O bond length is also small. Thus the spectator oxo effect is probably insignificant (see previous section). However, the trends in ν(O-O) and bond length O1-O2 are curiously, at odds. Complexes that exhibit higher ν(O-O) vibrational frequencies should exhibit shorter O-O bond lengths.[82] However while ν(O-O) of 870 cm^{-1} for $[CpMo(O)(O_2)(CF_3)]$ is 20 cm^{-1} higher than for $[CpMo(O)(O_2)(CH_3)]$, the bond length is longer in the fluorinated complex – 1.440(3) Å in comparison to 1.271(14) Å.

The bonding between metal and η^2-O_2 ligand can be described as a result of σ-interaction between the metal d_{xy} orbital and the in-plane peroxo π* orbital.[82] Because of the relatively higher electron density at Mo in the oxo peroxo fluorinated complex (see Figure 8.2(c)), there is less effective overlap of metal and peroxo orbitals which results in more delocalization of the electron density in the antibonding π* orbital of peroxo ligand. Hence a decrease in O-O bonding interactions leads to an increase in the O1-O2 bond length.

Thus the shorter Mo(=O) bond for complex **4** and the elongation of O1-O2 peroxo bond are a consequence of the *trans*-structural effect discussed in Section 8.2.2. Considering that the oxygen transfer to alkene involves the peroxo ligand with complex **4** and not the oxo group,[8] as in the case of oxo-peroxo derived from pre-catalyst **1**,[4,21] the shortening of Mo=O bond is reminiscent of the 'spectator oxo effect' in metathesis catalysts (Section 8.2.4).[77,78] Perhaps this also explains the higher reactivity of complex **4**, since reaction with the olefin or TBHP would be more facilitated for **4** than the oxoperoxo CH_3 analogue, for which epoxidation proceeds 3-5 times slower than its corresponding dioxo complex.[4]

8.2.6 Activity in Fluorinated Solvents

Fluorinated solvents have been shown to activate the oxidant H_2O_2 by an extensive H-bonding network.[9,11] In the absence of a catalyst, the fluorinated solvent−H_2O_2 system may even be utilized for the epoxidation of unfunctionalized olefins.[10,83] Epoxidation with methyltrioxorhenium (MTO)-H_2O_2 in fluorinated solvents has also been studied.[84,85] Similar to H_2O_2, activation of the organic hydroperoxide by HFIP may also occur. Indeed, Hauser et al. observed 10% epoxide yield after 4 h, when a mixture of *cis*-cyclooctene and TBHP was dissolved in HFIP without the pre-catalyst **2**.[6] It has also been observed that oxidative decarbonylation of **2** is faster in HFIP and therefore the two effects are perhaps cumulative – oxidant activation and presence of larger concentration of active catalyst – that result in higher conversion%. When hexafluorobenzene (HFB) was used as a solvent, no significant increase in catalytic activity was observed compared to catalysis in C_6D_6. Since HFB is an aprotic solvent, it is incapable of participating in oxidant activation as suggested for HFIP.[6]

It is known that the Lewis acidity of the metal centre primarily dictates the reactivity of high oxidation state Re(VII) and Mo(VI) complexes in these oxidative transformations.[86] Furthermore, selectivity to the epoxide is largely determined by the suppression of acid-catalyzed ring opening pathways, usually by addition of tertiary N-donor bases for CH_3ReO_3/H_2O_2 system.[87] Then, the higher rate of epoxidation in 'acidic' fluorinated alcohols (pKa = 9.3 for HFIP[88]) cannot simply be attributed to activation of the oxidant.[9] It is likely that these fluorinated additives influence the reaction mechanism as well,[10] perhaps in a similar manner to stabilization from the solvent CH_3OH.[23]

When we consider the reversal in catalytic activity of pre-catalysts **1** and **2** in HFIP with TBHP oxidant, an obvious query is *how* do the fluorinated solvents help with stabilization of transition states during oxygen transfer. Considering the high acidity of HFIP, perhaps the role is similar to the ‘proton shuttle effect’ illustrated in Scheme 8.4 for protic solvents. Several possibilities are proposed in Scheme 8.6. An answer to this issue is however, at present, beyond the scope of this work.

(a) TBHP Oxidant activation by HFIP

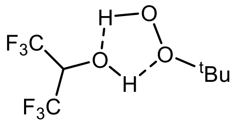
H—O
F3C
O
O
tBu
H
F3C

(b) Involvement of HFIP in oxidative transformations

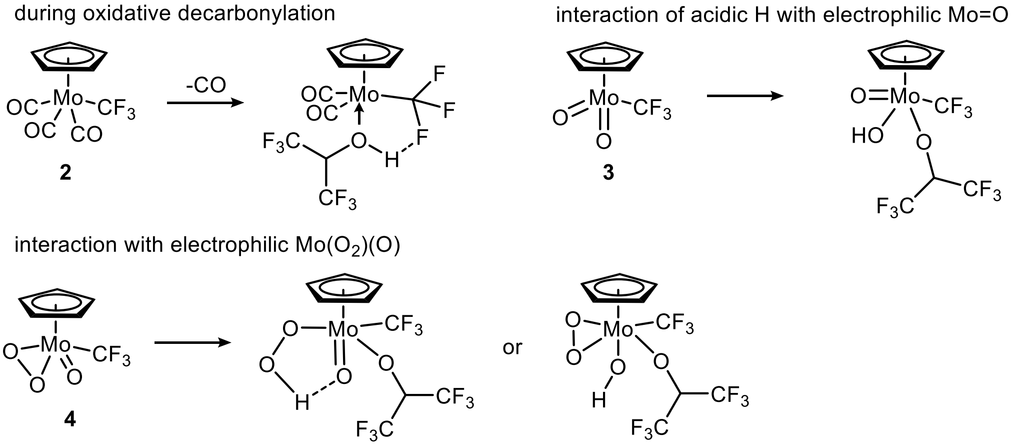
during oxidative decarbonylation
interaction of acidic H with electrophilic Mo=O
OC
Mo
CF3
OC
CO
2
-CO
OC—Mo
OC
F
F
F
F3C
O
H
CF3
Mo
CF3
O
O
3
O=Mo
CF3
HO
O
F3C
CF3
interaction with electrophilic Mo(O2)(O)
O—Mo
CF3
O
O
4
O—Mo—CF3
O
O
H
O
CF3
F3C
or
O
Mo
CF3
O
O
H
O
CF3
F3C

(c) Proton shuttle effect, X = H, ^{t}Bu, O^{t}Bu

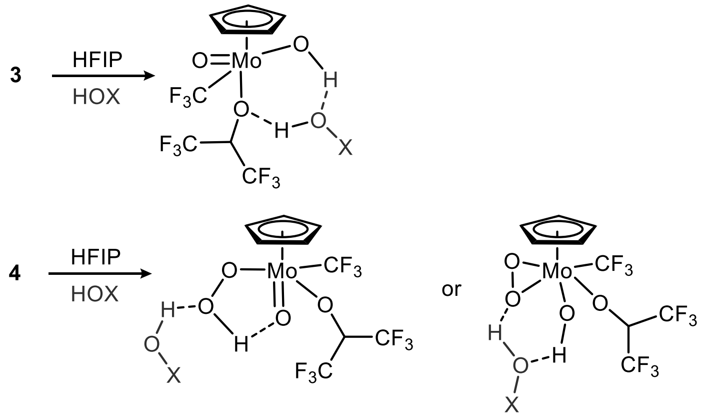
3
HFIP
HOX
O=Mo
O
H
F3C
O
H
O
X
F3C
CF3
4
HFIP
HOX
O—Mo—CF3
H
O
O
X
H
O
O
CF3
F3C
or
O
Mo
CF3
O
H
O
H
O
X
O
CF3
CF3

Scheme 8.6. The various possibilities of H-bonding with HFIP solvent. (a) In activation of TBHP, (b) interaction with pre-catalyst **2** after CO loss and interaction with oxidized complexes, (c) the effect of presence of water, *tert*-butanol or *tert*-butylhydroperoxide as neutral molecules.

8.3 The ‘Top-Down’ Approach

While the recent theoretical work by Drees et al. provides valuable information about the oxidized complexes derived from **2** and their relative reactivity towards TBHP,[8] it does not address the fundamental cause for the differences between pre-catalysts **1** and **2**. In this section, we address the unusual performance of pre-catalyst **2** in context of our understanding of reaction kinetics and mechanisms for oxidation reactions of [CpMo(CO)$_3$R] complexes with TBHP.

In the previous chapters, we have established that the two oxidative transformations – pre-catalyst oxidation and olefin epoxidation are intricately linked. From a kinetic NMR study of the oxidation reactions of complexes [CpMo(CO)$_3$R] (R = CH$_3$, CH$_2$COOR*, CH$_2$C$_6$H$_5$, CH$_2$C$_6$F$_5$), we have gained valuable information about the ‘*in situ* oxidation’ processes (Chapters 5 and 6) To summarize, the presence of an olefin suppresses the further conversion of the Mo-dioxo complex (**I**) to the Mo-oxo-peroxo complex (**II**) until epoxidation is complete (Scheme 8.1 and Scheme 8.7). The rate of conversion of *cis*-cyclooctene to its epoxide is quite high with the respective dioxo complex. The oxo-peroxo complex is catalytically active for epoxidation, but nearly always performs poorly in comparison to the dioxo catalyst (pre-catalyst **2** is an exception, see Section 8.2.4). Furthermore, existence of a coordinatively unsaturated Cp containing Mo(IV) species in the earliest stage of oxidation of the pre-catalyst has been proposed. Such a species is required to explain both – the highly exothermic decarbonylation process and, the formation of Mo(V) µ-oxo dimer(s). Experimental observations and thermodynamic data for complex [CpMo(CO)$_3$R], R = CH$_2$COOCH$_3$ (Chapter 6) also indicate that the oxo bridged species may be involved in the transformation of the dioxo complex to oxo-peroxo complex.

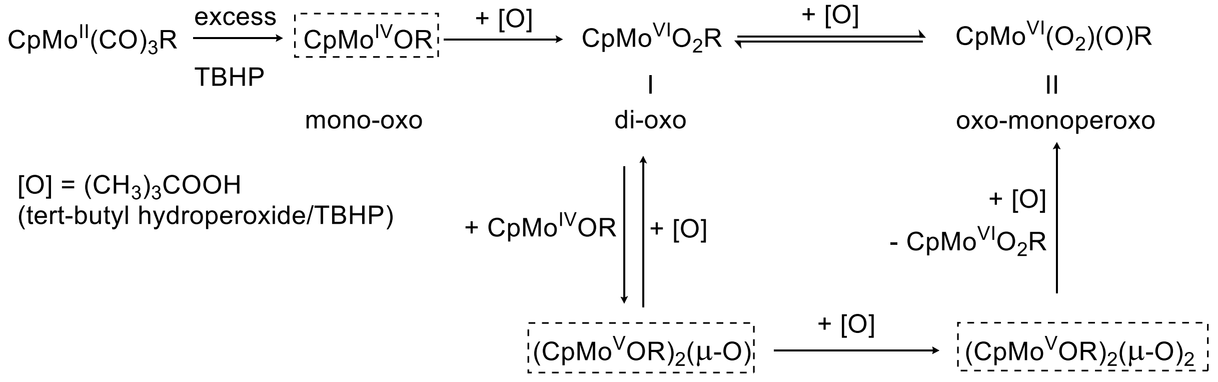

Scheme 8.7. Oxidative transformations of the tricarbonyl pre-catalysts [CpMo(CO)$_3$R] on treatment with excess TBHP oxidant.

8.3.1 *An Explanation from Reaction Kinetics*

The catalytically active oxo-peroxo species **4** is formed from further oxidation of the dioxo complex **3** with TBHP. Since it has been experimentally observed that oxidative decarbonylation of the tricarbonyl pre-catalyst **2** is quite slow in C$_6$D$_6$, the concentration of dioxo complex **3** is quite small (and of **4** even less), when the catalytic reaction is initiated by the addition of TBHP. If both dioxo and oxo-peroxo complexes derived from the fluorinated tricarbonyl complex are considered to be catalytically active, it follows that initial conversion of the substrate to its epoxide could not be fast and consequently TOFs would be lower. Since it has been shown from DFT calculations that epoxidation with dioxo complex **3** is energetically unfavourable,[8] the reaction rate is further reduced as only very small concentration of the active oxo-peroxo complex must be available for catalysis.

As a simple conclusion, we may reason for the ‘unexpected’ reactivity of **2** as follows: TOF with pre-catalyst **2** is less than that for **1** because only *in situ* catalysis reaction initiated by the addition of TBHP is being considered. In the initial period of the catalytic reaction, oxidative decarbonylation for **2** results in a small concentration of nearly inactive dioxo complex and consequently smaller substrate conversion% is observed. However, for pre-catalyst **1** the highly active dioxo catalyst [CpMo(O)$_2$(CH$_3$)] is quickly formed and thus participates in catalytic epoxidation, giving near quantitative cyclooctene conversion in a short time.

8.3.2 A Consideration of Reaction Mechanisms

The main *in situ* oxidative transformations that take place on treatment of [CpMo(CO)$_3$R] pre-catalysts with TBHP are: (i) pre-catalyst oxidation (or oxidative decarbonylation), (ii) hydroperoxide activation (with either dioxo or oxo-peroxo species, or even both) and, (iii) oxygen transfer to olefin (or catalytic epoxidation). Either of these processes may be affected in different ways due to the presence of ‘additives’, namely – H_2O,[17,20] *tert*-butanol[4,23] substrate olefin (Chapter 5) and solvent.

A comparison of DFT calculations for epoxidation with pre-catalysts **1**[21] and **2**[8] shows that their oxidized complexes, both dioxo and oxo-peroxo, prefer slightly different pathways of oxidant activation and oxygen transfer to the olefin. In these studies, activation barriers have been evaluated for the different mechanisms shown in Scheme 8.2. However, participation of Mo(IV) and Mo(V) species during catalyst oxidation and the possibility of their catalytic potential for epoxidation reaction has not been investigated. As illustrated in Scheme 8.7, we have proposed that the oxidative transformation of the Cp tricarbonyl Mo(II) pre-catalysts to the catalytically active Mo(VI) species involves the participation of Mo(IV) and Mo(V) species. In the case of pre-catalysts **1** and **2**, similar species can form. The oxo-peroxo complex **4** can be obtained either from oxidation of the dioxo complex **3** with TBHP or from μ-oxo dimers **A** or **B** (Scheme 8.8).[70,89–92]

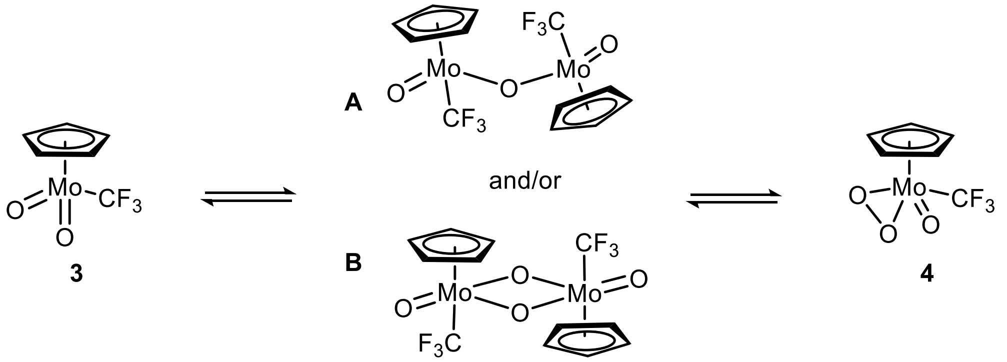

Scheme 8.8. Formation of oxo-bridged dimer species from the dioxo complexes of both pre-catalysts **1** and **2** is possible.

Such μ-oxo dimers are known for both Cr and W trifluoromethyl complexes, with Cp and Cp* ligands.[93] It is possible that the μ-oxo dimer formed from **2** is quite stable, so that predominantly the thermodynamic equilibrium prefers to keep **A** and **B** in solution than conversion to the active oxo-peroxo complex **4**. Perhaps **A** and **B** are only slowly converted to **4**. On the other hand, it is also possible that normally formation of species like **A** and **B** facilitates conversion of the dioxo to oxo-peroxo species, but in case of the CF_3 complex, occurrence of this transformation has inhibitory effect on the formation of catalytically active species **4**. This is however conjecture and answer to these questions are beyond the scope of the present work. Nevertheless, should these bridged dimers for pre-catalysts **1** and **2** exist, their contribution to catalytic performance cannot be ruled out.[58,94–97]

8.4 Conclusion

The difference in catalytic activity of complexes **1** and **2** has been previously explained as follows – slower oxidative decarbonylation of pre-catalyst **2** leads to a lower concentration of its active oxidized complex and consequently lower catalytic activity. Although this explanation is plausible, it is inadequate for the purpose of explaining analytical data and also understanding principles determining catalytic activity. In this work the fundamental explanations for the differences in activity have been sought using complex **2** as an example, so that we may understand and improve on the performance of similar pre-catalysts. This study is motivated from the broader perspective of rational structural and functional catalyst design instead of 'hit-and-trial' synthesis and application methodology.

To summarize, we find that Lewis acidity of the metal centre in tricarbonyl pre-catalysts [$CpMo(CO)_3R$] and catalytic performance are not necessarily related with each other. The reasons for lower catalytic activity of **2** compared to **1** are as follows:

1. Complex **2** reacts slowly with TBHP (slower oxidative decarbonylation) because it is more stable than **1**. Overall, the CF_3 complex is electron-deficient and the metal *d* orbitals are low-lying. There is more negative charge on the metal according to inductive effect $Mo^{\delta-}–C^{\delta+}–F^{\delta-}$ which results in stronger π*-backbonding to carbonyl groups. For these reasons, the tendency of **2** towards oxidative transformations with TBHP (which requires frontier orbital interactions) decreases.
2. CF_3 group being more hydrophobic than CH_3, complex **2** foregoes any possible advantages of H-bond assisted lowering of activation barriers during oxidative processes compared to **1**.
3. While we disagree with the notion that Mo-R linkage dissociates during catalysis, it can be argued that **2** has a lower activity since M-CF_3 bond is stronger (partial double bond character, shorter bond length) and thus unreactive compared to Mo-CH_3 bond. Additionally, the larger volume of the CF_3 group is sterically encumbering for reactions that take place at the metal centre in **2** compared to **1**.
4. Higher catalytic activity for the non-fluorinated pre-catalyst **1** is not in spite of its lesser Lewis acidity than **2**. It is because **1** quickly forms the dioxo complex [$CpMo(O)_2(CH_3)$] that is quite active. On the other hand, once highly active oxo-peroxo CF_3 species **4** is formed, it is more

susceptible to electrophilic attack from TBHP compared to analogous oxo-peroxo complex of pre-catalyst **1**.

5. From reaction kinetics, it is unreasonable to compare pre-catalysts **1** and **2** since they form both dioxo and oxo-peroxo species which differ in their catalytic activity. On treatment with TBHP, **1** quickly forms the highly active dioxo complex while **2** must first undergo decarbonylation to give **3**, which then reacts further with TBHP to give **4**, the latter being the more active species as expected from inductive effect of CF_3 group. Hence, *in situ* catalysis with **2** proceeds slower compared to **1**.
6. The active species **4** might be more susceptible to (irreversible?) deactivation processes such as *tert*-butanol coordination or μ-oxo dimer formation on account of the overall electron deficiency because of CF_3 group.
7. The structural and kinetic *trans*- effect of the CF_3 group is larger than that of CH_3 in the oxidized complexes. The spectator oxo ligand effect perhaps also assists in olefin epoxidation. This explains the expected high catalytic activity of the isolated oxo-peroxo complex **4**.

Therefore, superficially it is difficult to predict catalytic activity when such tricarbonyl complexes are employed *in situ* as pre-catalysts for olefin epoxidation. While it is true that the pre-catalysts are oxidized to the Mo(VI) complexes, presence of Mo(IV) and Mo(V) species is strongly suggested during this drastic change in oxidation state. Finally, assuming that neither Mo(IV) nor Mo(V) play a main role in olefin epoxidation, to predict catalytic activity it is important to consider the following factors:

(a) regarding the side chain ligand R in $[CpMo(CO)_3R]$ pre-catalysts: *steric influence (van der Waals volume), inductive effect (Hammett and Taft parameters, Pauling electronegativity), trans-directing influence;*

(b) in relation to the catalysis reaction: *the nature of the active species (dioxo vs. oxo-peroxo), presence of protic reagents or additives, temperature, solvent polarity, concentration of pre-catalyst, oxidant and nature of the olefin (internal or terminal).*

8.5 References

[1] M.K. Trost, R.G. Bergman, Organometallics. 10 (1991) 1172–1178.

[2] M. Abrantes, A.M. Santos, J. Mink, F.E. Kühn, C.C. Romão, Organometallics. 22 (2003) 2112–2118.

[3] A.A. Valente, J.D. Seixas, I.S. Gonçalves, M. Abrantes, M. Pillinger, C.C. Romão, Catal. Lett. 101 (2005) 127–130.

[4] A.M. Al-Ajlouni, D. Veljanovski, A. Capapé, J. Zhao, E. Herdtweck, M.J. Calhorda, F. E. Kühn, Organometallics. 28 (2009) 639–645.

[5] N. Grover, F.E. Kühn, Curr. Org. Chem. 16 (2012) 16–32.

[6] S.A. Hauser, M. Cokoja, M. Drees, F.E. Kühn, J. Mol. Catal. A Chem. 363-364 (2012) 237–244.

[7] S.A. Hauser, Organorhenium and Organomolybdenum Oxides : Synthesis and Application as Olefin Epoxidation Catalysts, 2012. http://d-nb.info/1031550240

[8] M. Drees, S.A. Hauser, M. Cokoja, F.E. Kühn, J. Organomet. Chem. (2013) DOI 10.1016/j.jorganchem.2013.05.004.

[9] A. Berkessel, J.A. Adrio, D. Hüttenhain, J.M. Neudörfl, J. Am. Chem. Soc. 128 (2006) 8421–8426.

[10] S.P. de Visser, J. Kaneti, R. Neumann, S. Shaik, J. Org. Chem. 68 (2003) 2903–2912.

[11] A. Berkessel, J.A. Adrio, J. Am. Chem. Soc. 128 (2006) 13412–13420.

[12] H. Mimoun, I.S. de Roch, L. Sajus, Tetrahedron. 26 (1970) 37–50.

[13] K.B. Sharpless, J.M. Townsend, D.R. Williams, J. Am. Chem. Soc. 94 (1972) 295–296.

[14] W.R. Thiel, T. Priermeier, Angew. Chem. Int. Ed. Engl. 34 (1995) 1737–1738.

[15] W.R. Thiel, J. Eppinger, Chem. Eur. J. 3 (1997) 696–705.

[16] W.R. Thiel, J. Mol. Catal. A Chem. 117 (1997) 449–454.

[17] A. Comas-Vives, A. Lledós, R. Poli, Chem. Eur. J. 16 (2010) 2147–2158.

[18] P. Sözen-Aktaş, E. Manoury, F. Demirhan, R. Poli, Eur. J. Inorg. Chem. 2013 (2013) 2728–2735.

[19] C. Dinoi, R. Poli, L. Perrin, L. Maron, Dalton Trans. 41 (2012) 1131–1133.

[20] C. Dinoi, M. Ciclosi, E. Manoury, L. Maron, L. Perrin, R. Poli, Chem. Eur. J. 16 (2010) 9572–9584.

[21] P.J. Costa, M. José Calhorda, F.E. Kühn, Organometallics. 29 (2010) 303–311.

[22] M.J. Calhorda, P. Jorge, Curr. Org. Chem. 16 (2012) 65–72.

[23] J. Morlot, N. Uyttebroeck, D. Agustin, R. Poli, ChemCatChem. 5 (2013) 601–611.

[24] S.G. Bratsch, J. Chem. Ed. 62 (1965) 101–103.

[25] D. Seebach, Angew. Chem. Int. Ed. Engl. 29 (1990) 1320–1367.

[26] M.A. McClinton, D.A. McClinton, Tetrahedron. 48 (1992) 6555–6666.

[27] J. Jee, A. Comas-vives, C. Dinoi, G. Ujaque, R. Van Eldik, Inorg. Chem. 46 (2007) 4103–4113.

[28] R.P. Hughes, Organo-Transition Metal Compounds Containing Perfluorinated Ligands, in: Adv. Organomet. Chem. Vol. 31, 1990: pp. 183–267.

[29] D. Chakraborty, M. Bhattacharjee, R. Krätzner, R. Siefken, H.W. Roesky, I. Uson, H.-G. Schmidt Organometallics. 18 (1999) 106–108.

[30] T.S. Piper, G. Wilkinson, J. Inorg. Nucl. Chem. 3 (1956) 104–124.

[31] R.B. King, M.B. Bisnette, J. Organomet. Chem. 2 (1964) 15–37.

[32] H. Huang, R.P. Hughes, A.L. Rheingold, Organometallics. 29 (2010) 1948–1955.

[33] R.P. Hughes, Eur. J. Inorg. Chem. 2009 (2009) 4591–4606.

[34] P.J. Brothers, W.R. Roper, Chem. Rev. 88 (1988) 1293–1326.

[35] J.D. Koola, D.M. Roddick, Organometallics. 10 (1991) 591–597.

[36] J.A. Morrison, Trifluoromethyl-Containing Transition Metal Complexes, in: Adv. Organomet. Chem. Vol. 35, 1993: pp. 211–239.

[37] D.L. Reger, M.D. Dukes, J. Organomet. Chem. 153 (1978) 67–72.

[38] O.A. Tomashenko, V. V Grushin, Chem. Rev. 111 (2011) 4475–4521.

[39] C. Hall, R.N. Perutz, Chem. Rev. 96 (1996) 3125–3146.

[40] T.G. Richmond, D.F. Shriver, Organometallics. 3 (1984) 305–314.

[41] M.B. Hall, R.F. Fenske, Inorg. Chem. 11 (1972) 768–775.

[42] H.G. Alt, Angew. Chem. Int. Ed. Engl. 23 (1984) 766–782.

[43] K.A. Mahmoud, A.J. Rest, H.G. Alt, J. Chem. Soc. Chem. Commun. (1983) 1011–1013.

[44] R.B. Hitam, R.H. Hooker, K.A. Mahmoud, R. Narayanaswamy, A.J. Rest, J. Organomet. Chem. 222 (1981) 9–13.

[45] R.H. Hooker, A.J. Rest, J. Chem. Soc. Dalton Trans. (1984) 761–770.

[46] E. Samuel, J. Organomet. Chem. 172 (1979) 309–315.

[47] H.G. Alt, J.A. Schwärzle, C.G. Kreiter, J. Organomet. Chem. 153 (1978) 7–10.

[48] C.G. Kreiter, K. Nist, H.G. Alt, Chem. Ber. 114 (1981) 1845–1852.

[49] A.O. Ogweno, M.O. Onani, Acta Crystallogr. Sect. E. Struct. Rep. Online. 68 (2012) m364.

[50] M. Abrantes, P. Neves, M.M. Antunes, S. Gago, F.A. Almeida Paz, A.E. Rodrigues, M. Pillinger, I. S. Gonçalves, C M. Silva, A. A. Valente, J. Mol. Catal. A Chem. 320 (2010) 19–26.

[51] P. Legzdins, E.C. Phillips, S.J. Rettig, L. Sanchez, J. Trotter, V.C. Yee, Organometallics. 7 (1988) 1877–1878.

[52] M. Abrantes, F.A.A. Paz, A.A. Valente, C.C.L. Pereira, S. Gago, A.E. Rodrigues, J. Klinowski, M. Pillinger, I. S. Gonçalves, J. Organomet. Chem. 694 (2009) 1826–1833.

[53] S. Li, Z. Wang, T.S.A. Hor, J. Zhao, Dalton Trans. 41 (2012) 1454–1456.

[54] J. Zhao, A.M. Santos, E. Herdtweck, F.E. Kühn, J. Mol. Catal. A Chem. 222 (2004) 265–271.

[55] S. Li, C.W. Kee, K. Huang, T.S.A. Hor, J. Zhao, Organometallics. 29 (2010) 1924–1933.

[56] R.B. King, A. Fronzaglia, J. Am. Chem. Soc. 88 (1966) 709–712.

[57] M. Pratt, J.B. Harper, S.B. Colbran, Dalton Trans. (2007) 2746–2748.

[58] A.M. Martins, C.C. Romão, M. Abrantes, M.C. Azevedo, J. Cui, A.R. Dias, M. T. Duarte, M. A. Lemos, T. Lourenço, R. Poli, Organometallics. 24 (2005) 2582–2589.

[59] D. Saurenz, F. Demirhan, P. Richard, R. Poli, H. Sitzmann, Eur. J. Inorg. Chem. (2002) 1415–1424.

[60] M. V. Galakhov, P. Gómez-Sal, T. Pedraz, M.A. Pellinghelli, P. Royo, A. Tiripicchio, A. V. de Miguel, J. Organomet. Chem. 579 (1999) 190–197.

[61] P.M. Reis, C.A. Gamelas, J.A. Brito, N. Saffon, M. Gómez, B. Royo, Eur. J. Inorg. Chem. (2011) 666–673.

[62] V.V.K.M. Kandepi, A.P. da Costa, E. Peris, B. Royo, Organometallics. (2009) 4544–4549.

[63] L. Schaper, L. Graser, X. Wei, R. Zhong, K. Öfele, A. Pöthig, M. Cokoja, B. Bechlars, W. A. Herrmann, F. E. Kühn, Inorg. Chem. 52 (2013) 6142–6152.

[64] T.G. Appleton, H.C. Clark, L.E. Manzer, Coord. Chem. Rev. 10 (1973) 335–422.

[65] R. Poli, Organometallics. 9 (1990) 1892–1900.

[66] M. Minelli, J. Enemark, R.T.C. Brownlee, M.J. O'Connor, A.G. Wedd, Coord. Chem. Rev. 68 (1985) 169–278.

[67] Z. Lin, M.B. Hall, Organometallics. 12 (1993) 19–23.

[68] P. Kubacek, R. Hoffmann, Z. Havlas, Organometallics. 1 (1982) 180–188.

[69] S.S. Balula, A.C. Coelho, S.S. Braga, A. Hazell, A.A. Valente, M. Pillinger, J. Seixas, C. C. Romão, I. S. Gonçalves, Organometallics. 26 (2007) 6857–6863.

[70] K. Wieghardt, M. Guttmann, P. Chaudhuri, W. Gebert, M. Minelli, C.G. Young, J. H. Enemark, Inorg. Chem. 24 (1985) 3151–3155.

[71] S. Wolowiec, J.K. Kochi, Inorg. Chem. 30 (1991) 1215–1221.

[72] J.M. Wallis, J.K. Kochi, Inorganica Chim. Acta. 160 (1989) 217–221.

[73] M. V Baker, M.R. North, B.W. Skelton, A.H. White, Inorg. Chem. 38 (1999) 4515–4521.

[74] P. Chandra, S.L. Pandhare, S.B. Umbarkar, M.K. Dongare, K. Vanka, Chem. Eur. J. 19 (2013) 2030–2040.

[75] J.H. Enemark, J.J.A. Cooney, J.-J. Wang, R.H. Holm, Chem. Rev. 104 (2004) 1175–1200.

[76] R. Hille, Dalton Trans. 42 (2013) 3029–3042.

[77] A.K. Rappe, W.A. Goddard III, J. Am. Chem. Soc. 104 (1982) 3287–3294.

[78] A.K. Rappe, W.A. Goddard III, J. Am. Chem. Soc. 104 (1982) 448–456.

[79] C. Di Valentin, P. Gisdakis, I. V Yudanov, N. Rösch, J. Org. Chem. 65 (2000) 2996–3004.

[80] H. Teruel, A. Sierralta, J. Mol. Catal. A Chem. 107 (1996) 379–383.

[81] H. Teruel, A. Sierralta, Polyhedron. 15 (1996) 2215–2221.

[82] M.S. Reynolds, A. Butler, Inorg. Chem. 35 (1996) 2378–2383.

[83] J. Legros, B. Crousse, D. Bonnet-Delpon, J.-P. Begue, Eur. J. Org. Chem. (2002) 3290–3293.

[84] M.C.A. van Vliet, I.W.C.E. Arends, R.A. Sheldon, Chem. Comm. (1999) 821–822.

[85] P. Altmann, M. Cokoja, F.E. Kühn, Eur. J. Inorg. Chem. 2012 (2012) 3235–3239.

[86] S. Köstlmeier, V.A. Nasluzov, W.A. Herrmann, N. Rösch, Organometallics. 16 (1997) 1786–1792.

[87] J. Rudolph, K.L. Reddy, J.P. Chiang, K.B. Sharpless, J. Am. Chem. Soc. 119 (1997) 6189–6190.

[88] J.-P. Begue, D. Bonnet-Delpon, B. Crousse, Synlett. 1 (2004) 18–29.

[89] R.H. Holm, Chem. Rev. 87 (1987) 1401–1449.

[90] J.A. Craig, E.W. Harlan, B.S. Snyder, M.A. Whitener, R.H. Holm, Inorg. Chem. 28 (1989) 2082–2091.

[91] M.S. Reynolds, J.M. Berg, R.H. Holm, Inorg. Chem. 23 (1984) 3057–3062.

[92] J. McMaster, J.H. Enemark, Curr. Opin. Chem. Biol. 2 (1998) 201–207.

[93] H. Huang, A.L. Rheingold, R.P. Hughes, Organometallics. 29 (2010) 3672–3675.

[94] D.M. Baird, C. Aburri, L.S. Barton, S.A. Rodriguez, Inorg. Chim. Acta. 237 (1995) 117–122.

[95] C.L. Pereira, S.S. Balula, F.A.A. Paz, A.A. Valente, M. Pillinger, J. Klinowski, I. S. Gonçalves, Inorg. Chem. 46 (2007) 8508–8510.

[96] M.E. Judmaier, C.H. Sala, F. Belaj, M. Volpe, N.C. Mösch-Zanetti, New J. Chem. 37 (2013) 2139–2149.

[97] V.S. Joshi, M. Nandi, H. Zhang, B.S. Haggerty, A. Sarkar, Inorg. Chem. 32 (1993) 1301–1303.

[98] W. Beck, K. Schloter, Z. Naturforsch. B. 33 (1978) 1214–1222.

[99] W. Beck, K. Sünkel, Chem. Rev. 88 (1988) 1405–1421.

[100] B.J. Coe, S.J. Glenwright, Coord. Chem. Rev. 203 (2000) 5–80.

[101] H.A. Bent, J. Chem. Phys. 33 (1960) 304–305.

9 Summary

In this thesis the synthesis and characterization of several different types of cyclopentadienyl molybdenum carbonyl complexes is described. These complexes have been applied as pre-catalysts for achiral and chiral epoxidation of unfunctionalized olefins. Within the broader objective of identifying either structural or spectroscopic parameters that can be correlated with observed catalytic activity, an attempt to outline design principles for such molecular catalysts has been made. The accepted notion of Lewis acidity and electrophilicity of Mo (for the metal centred olefin epoxidation reaction) being related to each other is challenged using several examples. Issues of process development and catalyst robustness of these complexes have also been addressed by studying the kinetic progress of catalytic epoxidation and pre-catalyst oxidation in detail. Subsequently, a mechanistic model has been developed for these *in situ* oxidation reactions.

In **Chapter 3**, synthesis and characterization of two novel imidazo-[1,5-*a*]pyridyl-3-ylidine carbene CpMo dicarbonyl complexes has been described. Since NHC ligands are strong σ-donors, it is expected that the complexes should be poor catalysts for epoxidation as Lewis acidity of the metal centre is reduced. Contrary to expectations, it is observed that these complexes undergo fast oxidative decarbonylation to form the catalytically active species. Subsequently, these complexes exhibit the highest TOFs of known CpMo pre-catalysts in the epoxidation of *cis*-cyclooctene in $CHCl_3$ at 55 °C with TBHP oxidant. A comprehensive discussion of ^{95}Mo chemical shifts, FTIR absorption frequencies, π*-acceptor ability of NHC ligands, X-ray crystallographic data and a thorough comparison with literature known examples is presented. It is reasoned that the unique stereoelectronic features of these complexes possibly explain the unusually high catalytic activity. It is also realized that other factors such as faster kinetics, easy availability of a vacant coordination site and fluxionality of the organometallic complex – are likely contributors towards the high catalytic activity as well.

In **Chapter 4**, alkylester complexes $[CpMo(CO)_3(CHR^2COOR^1)]$ that are either substituted or unsubstituted at the α-carbon have been synthesized. A chiral alkylester moiety as the side chain imparts chirality to the pre-catalyst and it is expected that enantioselective epoxidation might be feasible. Unfortunately however no asymmetric induction occurs during epoxidation of prochiral substrate *trans*-β-methylstyrene. Instructively, it is found that ^{95}Mo NMR shifts can be correlated with TOFs of epoxidation reaction with other tricarbonyl pre-catalysts, but only if the induction period of epoxidation is not considered, i.e. by evaluating TOFs for catalysis carried out at 55 °C. Such a relation is found valid only for very closely related complexes, since ^{95}Mo chemical shifts are very sensitive to stereoelectronic influence of the ligand environment. Additionally, catalytic activity may be affected by the kinetics and mechanism of the oxidation reactions, which makes it difficult to assess catalytic performance without identifying the nature of the active species.

Chapter 5 attempts to address the lack of information about kinetics of the catalyzed epoxidation reaction. From kinetic NMR study, the progress of epoxidation reaction under varying reaction conditions catalyzed by complex $[CpMo(CO)_3(CH_2COOBornyl)]$ with TBHP oxidant is discussed. It is found that the dioxo species [$CpMoO_2(CH_2COOBornyl)$] is the primary species for epoxidation. The initial period of catalysis is strongly influenced by relative substrate, oxidant and catalyst concentrations. Although conversion of the alkene substrate to its epoxide is faster at a higher temperature (and hence higher TOFs), efficiency w.r.t. catalyst robustness is not necessarily implied. Lack of kinetic and thermodynamic control originates from the exothermic nature of the decarbonylation reaction of the pre-catalyst. Furthermore, since the initial phase is strongly affected by reaction conditions employed, asymmetric transition states required for induction of chirality are unlikely to persist throughout the reaction. This results in formation of racemic mixtures of epoxides with prochiral substrate. It is also shown that the dioxo and oxo-peroxo CpMo complexes not only differ in their reactivity, but in a manner of speaking, their formation during epoxidation is influenced by substrate concentration. Since the oxo-peroxo complex begins to form at the concluding stages of the epoxidation reaction, it might as well be anticipated that epoxidation for second or third runs would be primarily catalyzed by the oxo peroxo species. When substrate:oxidant concentration ≥ 1, saturation kinetics is observed for epoxidation of *cis*-cyclooctene which implies a Michaelis-Menten type kinetic model and that the alkene might coordinate as a η^2-ligand. A brief critical review of published literature on kinetics of Mo-catalyzed olefin epoxidation reaction suggests that depending on the substitution on Cp, nature of the side chain ligand R and the reaction conditions employed, the pre-catalysts can exhibit variability in the stability of their oxo complexes and thus also reactivity towards alkenes.

Since it is evident that catalytic epoxidation and oxidative decarbonylation of tricarbonyl pre-catalysts are closely interlinked with each other, the study of the latter oxidative process is also warranted. Therefore in **Chapter 6** the transformation of Mo(II) pre-catalysts to Mo(VI) oxo complexes with TBHP oxidant has been addressed in more detail using kinetic NMR and *in situ* FTIR techniques. These experiments suggest the presence of two Mo species in addition to known Mo(VI) complexes dioxo [$CpMo(O)_2R$] and oxo-peroxo [$CpMo(O)(O_2)R$]. It is shown that in the absence of the olefin substrate and in presence of excess TBHP, the [$CpMo(CO)_3R$] pre-catalysts can transform into intermediate complexes having Mo oxidation states +IV and +V, while aforementioned Mo(VI) complexes are the end products. Thus the existence of a mono-oxo complex [$CpMo^{IV}(O)R$] and μ-oxo bridged complexes [$(CpMo^{V}(O)R)_2(\mu\text{-}O)_{1,2}$] is proposed and theoretically evaluated. To assess the efficiency of this process w.r.t. exothermicity of decarbonylation reaction and formation of precipitate, pre-catalyst oxidation has been studied under different reaction conditions (varying oxidant and catalyst concentrations, and reaction temperature).

Chapter 7 discusses additional mechanistic aspects of the two simultaneous oxidative transformations. Theoretical work on the stability and reactivity of the mono oxo Mo(IV) complex has been summarized. It is found that formation of such a complex is thermodynamically feasible and although a η^2-alkene adduct would stabilize the coordinatively unsaturated Mo(IV) centre, in the presence of excess TBHP, further oxidation of the complex is always favoured. Various mechanistic pathways of epoxidation were calculated and it is shown that the Mo(IV) complex is not catalytically active as its reaction with TBHP to give [$CpMo(O)_2R$] is energetically preferred. Kinetic isotope effect using deuterated oxidant TBHP-d and the effect of additives hexafluoroisopropanol (HFIP) and *tert*-butanol on catalytic epoxidation has also been studied.

From an understanding of the results of previous chapters, in **Chapter 8** the problem of unexpected lower catalytic activity (from expected higher reactivity due to highly Lewis acidic Mo centre) of literature-known [CpMo(CO)$_3$(CF$_3$)] complex is addressed. To explain the slower rate of oxidative decarbonylation and difference in mechanisms of catalytic epoxidation between the fluorinated complex and its non-fluorinated counterpart [CpMo(CO)$_3$(CH$_3$)] (in conventional organic solvents and fluorinated solvents), a detailed compilation of the analytical data of these pre-catalysts, their dioxo complexes and respective oxo-peroxo complexes has been done (using cited published and unpublished data). This data has been explained in detail invoking concepts of *trans* effect, spectator oxo ligand effect, angular *trans* influence (from distortions in *trans* bond angles), *p*- and *d*-orbital contributions towards shielding of Mo metal centre and observed ^{95}Mo chemical shifts, and Brønsted acidity and H-bond assisted activation of the hydroperoxide oxidant TBHP by fluorinated solvent HFIP. In a top-down approach, the kinetic and mechanistic model developed in the previous chapters has also been applied to explain the observed data. It is concluded yet again that Lewis acidity of the metal centre in the pre-catalyst is not sufficient to predict the catalytic activity of the complex in the epoxidation reaction. This is because electrophilicity is a kinetic term while Lewis acidity is relevant from a thermodynamic point of view and these concepts need not necessarily be related to each other. Instead, the reason for lower activity of the fluorinated complex is due to the cumulative effect of unique attributes of the trifluoromethyl group in an organometallic complex.

IV. Index

List of Figures

Figure 1.1. Illustration of different structural classes of molybdenum oxo complexes studied for epoxidation catalysis. 3
Figure 1.2 A literature compilation of CpMo complexes applied for homogeneous olefin epoxidation till date. See additional references. 6
Figure 1.3. The kinetic stages of a typical olefin epoxidation reaction using [CpMo(CO)$_3$R] precatalyst with TBHP. 13
Figure 1.4. Mechanisms proposed for olefin epoxidation with Mo-peroxo compounds. 15
Figure 1.5. Mechanisms proposed in literature for olefin epoxidation with Mo-oxo compounds. 16
Figure 3.1. Literature known CpMo(NHC)-complexes **A**,[27] **B** and **C**,[28] **D**,[29] **E** and **F**.[27] 32
Figure 3.2. ^{95}Mo NMR chemical shifts for CpMo(NHC) complexes discussed in this chapter. 37
Figure 3.3. ORTEP view of the single crystal X-ray structure of compound **2**. Thermal ellipsoids are drawn at the 50 % probability level. Hydrogen atoms are omitted for clarity. 38
Figure 3.4. ORTEP view of the single crystal X-ray structure of compound **3**. Thermal ellipsoids are drawn at the 50 % probability level. Hydrogen atoms are omitted for clarity. 39
Figure 3.5. Atom renumbering scheme in the distorted square planar analogy for basal ligands of the piano stool X-ray crystal structures for comparison of precatalysts **2**, **3**, **B**, **C** and **D**. *Trans* angles θ refer to C_t-Mo-R, where C_t = Cp centroid. 39
Figure 3.6. Kinetic profile of *cis*-cyclooctene epoxidation with precatalysts **2** and **3** (0.1 mol%) in $CHCl_3$ at 25 °C and 55 °C using TBHP (catalyst:substrate:oxidant = 1:1000:2000). 42
Figure 3.7. Conversions of *cis*-cyclooctene epoxidation with **2** (0.1 mol%) using TBHP (in *n*-decane) as oxidant at 55 °C in different solvents (catalyst:substrate:oxidant = 1:1000:2000). 43
Figure 3.8. Kinetic profile of *cis*-cyclooctene epoxidation with different concentrations of precatalyst **2** at 55 °C using TBHP (substrate:oxidant = 1:2) (a) in $CHCl_3$ solvent, (b) without additional co-solvent. 44
Figure 3.9. Kinetic profile of *cis*-cyclooctene epoxidation with different concentrations of precatalyst **3** in $CHCl_3$ at 55 °C using TBHP (substrate:oxidant = 1:2). 45
Figure 4.1. ORTEP view of the single crystal X-ray structure of compound **1**. 66
Figure 4.2. ORTEP view of the single crystal X-ray structure of compound **2**. 66
Figure 4.3. ORTEP view of the single crystal X-ray structure of compound **5**. 67
Figure 4.4. Conversion *vs.* time plot for different substrates with 1 mol% complexes 1-5 and TBHP oxidant at room temperature in dichloromethane unless stated otherwise. (a) *cis*-cyclooctene, (b) *cis*-cyclooctene + 0.1 mol% catalyst, (c) *cis*-cyclooctene, no co-solvent, (d) *cis*-cyclooctene, 55 °C, $CHCl_3$ solvent, (e) *cis*-stilbene, (f) *trans*-stilbene, (g) 1-octene, (h) *trans*-β-methylstyrene; ratio catalyst:substrate:oxidant = 1:100:200. 69
Figure 4.5. Variable temperature ^{13}C NMR (C_6D_6) of 5 in the *cis*-CO region, showing electronic inequivalence or asymmetry of the carbonyl ligands even at 70°C. 87
Figure 4.6. (a) ^{1}H-MAS and (b) ^{13}C-CPMAS spectra for complex CpMo(CO)$_3$(CH$_3$); (c) ^{1}H-MAS and (d) ^{13}C-CPMAS for complex 5. 89
Figure 4.7. ORTEP drawing with 50% ellipsoids for complex **1**. 90
Figure 4.8. ORTEP drawing with 50% ellipsoids for complex **2**. 91
Figure 4.9. ORTEP drawing with 50% ellipsoids for complex **5**. 92
Figure 5.1. Cyclopentadienyl molybdenum tricarbonyl alkylester precatalysts 1-5.[27] 98
Figure 5.2. ^{1}H kinetic NMR profile for reaction of 5 with 10 equiv. of *cis*-cyclooctene and 20 equiv. of TBHP (in decane) in $CDCl_3$ at 22 °C (with mesitylene as internal standard). 101

Figure 5.3. ^{13}C kinetic NMR profile for reaction of 5 with 10 equiv. of *cis*-cyclooctene and 20 equiv. of TBHP (in *n*-decane) in $CDCl_3$ at 22 °C (using mesitylene as internal standard). 102

Figure 5.4. Concentration *vs.* time plots for (a) catalytic epoxidation of *cis*-cyclooctene with TBHP and, (b) concentration of precatalyst 5 and the catalytically active oxidized complex I during epoxidation. 103

Figure 5.5. Concentration *vs.* time profiles for catalytic epoxidation of *cis*-cyclooctene with catalyst:substrate:TBHP = 1:10:20; at 10 °C (blue), 22 °C (green) and 30 °C (red) in $CDCl_3$. (a) Concentration of 5 and sum concentration of oxidized species I and II *vs.* time, (b) fractional concentration of *cis*-cyclooctene and epoxycyclooctane *vs.* time. 105

Figure 5.6. (a) Fractional concentration of *cis*-cyclooctene (in all cases, [S] = 10 equivalents with respect to 5) *vs.* time (min) during the epoxidation reaction using *ca.* 0.05 mmol of 5 with different concentrations of TBHP oxidant. Note: The fractional concentration of cyclooctene epoxide has been omitted for clarity. In all cases, mole fraction $n_{epoxide}$ = [1-(n_{CyOc})] within experimental error. (b) Induction phase behaviour differs on varying oxidant concentration. 106

Figure 5.7. Plot of fractional concentration of *cis*-cyclooctene *vs.* time during its epoxidation with TBHP (substrate:TBHP = 1:2) as dependent on varying concentrations of precatalyst 5. Reactions performed in 0.4 mL $CDCl_3$ at 22 °C. 107

Figure 5.8. (a) Plot of fractional concentration of *cis*-cyclooctene *vs*. time during epoxidation with 20 equiv. of TBHP (in n-decane) using 0.05 mmol of 5 (1 equiv.) in 0.4 mL of $CDCl_3$ at 22 °C. (b) Induction period behaviour on varying substrate concentrations for catalytic epoxidation. 108

Figure 5.9. ^{95}Mo NMR measured after 24 h of oxidation of precatalyst 5 with 10 equiv. of TBHP (n-decane) in CDCl3. 113

Figure 5.10. Kinetic plot of epoxidation of *cis*-cyclooctene with TBHP and oxo-peroxo complex obtained after oxidation of **5**. 113

Figure 6.1. Complexes discussed in this chapter. 116

Figure 6.2. Kinetic ^{1}H NMR profile for the oxidation of 0.1 mmol of 5 with 10 equiv. of TBHP (in n-decane) in $CDCl_3$ at 22 °C. 119

Figure 6.3. Kinetic ^{13}C NMR profile for reaction of 0.1 mmol of 5 with 10 equiv. of TBHP (n-decane) in $CDCl_3$ solvent at 22 °C. 120

Figure 6.4. *In situ* IR profile for the oxidation of pre-catalyst 5 with 10 equiv. of TBHP at 25 °C in $CHCl_3$. Inset shows the carbonyl region. Baseline corrected spectrum at t = 0 min immediately after addition of TBHP is indicated in red). All other spectra show only evolving absorption bands. 121

Figure 6.5. Kinetic (a) ^{1}H and (b) ^{13}C NMR profiles for the oxidation of complex **5** with 20 equiv. of TBHP, displaying changes in chemical shift for the Cp ligand. Concentration *vs*. time plots for oxidation of ca. 0.1 mmol pre-catalyst **5** with (c) 50 equiv. TBHP (5.5 M in n-decane) at 22 °C. 123

Figure 6.6. Oxidation of pre-catalyst 5 with 20 equiv. of TBHP oxidant, 0.4 mL $CDCl_3$, 22 °C. (a) $[cat]_{t=0}$ = 0.12 M (0.048 mmol), $[cat]_{t=60min}$ = 0.0515 M. (b) $[cat]_{t=0}$ = 0.061 M (0.0246 mmol), $[cat]_{t=80\ min}$ = 0.0216 M. 124

Figure 6.7. Plot of concentration *vs.* time of 5 and sum of dioxo and oxo-peroxo complexes (I + II) formed on oxidation of 5 at 10 (blue), 22 (green) and 30 °C (red) using 20 equiv. of TBHP in $CDCl_3$. 125

Figure 6.8. Proposed structures for assignment of the NMR signal A, assumed to refer to the Cp ligand. 127

Figure 6.9. ^{1}H and ^{13}C NMR Profiles – Oxidation of $CpMo(CO)_3CH_3$ with 10 equiv. TBHP (5.5 M in n-decane) at 5 °C. 138

Figure 6.10. ^{1}H NMR Profile – Oxidation of **1** with 10 equiv. TBHP (5.5 M, n-decane) at 22 °C in $CDCl_3$. 139

Figure 6.11. Oxidation of $CpMo(CO)_3(CH_2C_6H_5)$ with 10 equiv. of TBHP at 22 °C in $CDCl_3$. 139

Figure 6.12. ^{1}H Profile – Oxidation of [CpMo(CO)$_3$(CH$_2$C$_6$F$_5$)] with 10 equiv. of TBHP (5.5 M, n-decane) at 22 °C in CDCl$_3$. 140
Figure 6.13. FTIR spectrum of the isolated precipitate **5a**. 140
Figure 6.14. FTIR spectrum of the pale yellow supernatant **5b** (in C_6D_6). 141
Figure 6.15. TGA-DSC for **5a**, decomposition temperature 197 °C, curve showing *m/z* 55. 141
Figure 6.16. (a) ^{1}H and (b) ^{13}C NMR spectra of **5b** in CDCl$_3$. 142
Figure 7.1. Complexes discussed in this section. 146
Figure 7.2. Concentration *vs.* time plots for (a) oxidation of *ca.* 0.1 mmol pre-catalyst [CpMo(CO)$_3$(CH$_2$COOBornyl)] (**5**) with 10 equiv. of TBHP-d, (b) **[5]** and sum concentration of oxidized complexes **[I + II]** during catalytic epoxidation, and (c) *cis*-cyclooctene and its epoxide, when catalytic epoxidation was performed at 22 °C in CDCl$_3$ (**5**:substrate:TBHP-d = 1:10:20). 148
Figure 7.3. Fractional concentration of *cis*-cyclooctene *vs.* time during its epoxidation catalyzed by **5** (1 equiv.) with 20 equiv. of TBHP in the absence or presence of additives HFIP and t-BuOH (10 equiv.) 149
Figure 8.1. Complexes discussed in this chapter. 154
Figure 8.2. Illustration of (a) the formation of difluorocarbene species,[38] (b) hyperconjugation model proposed by King et al.,[31] and (c) the inductive effect of the α-fluoro or α-hydrogen atom on the metal. 158
Figure 8.3. (a) Atom numbering scheme for 1 and 2 and their oxo-peroxo complexes. (b) The square planar analogy for basal ligands of the piano stool structures. (c) Bond angles θ and α, C_t refers to the centroid of pentahapto Cp ring. 160
Figure 8.4. The oxo ligand and peroxo groups act as a proton depository. Cp ligand has been omitted for clarity. 164
Figure 8.5. Spectator oxo ligand effect for the oxidized complexes formed on treatment of pre-catalysts **1** and **2** with TBHP oxidant. R = CH$_3$ or CF$_3$. Cp ligand has been omitted for clarity. 165
Figure 8.6. ^{95}Mo shifts for pre-catalysts **1** (-1736 ppm), **2** (-1458) and their oxo-peroxo complexes [CpMo(O)(O$_2$)(CH$_3$)] (-609 ppm) and [CpMo(O)(O$_2$)(CF$_3$)] (-709 ppm).[6,7,80,81] 168

List of Schemes

Scheme 3.1. Synthesis of cyclopentadienyl molybdenum imidazo[1,5-*a*]pyridine-3-ylidene N-heterocyclic carbene containing complexes **2** and **3**. 35
Scheme 4.1. Synthesis of cyclopentadienyl molybdenum tricarbonyl alkylester complexes **1-5**. 62
Scheme 5.1. Oxidation of tricarbonyl precatalyst 5 with 10 equiv. TBHP (in n-decane) results in the formation of both dioxo (I) and oxo-peroxo (II) species at room temperature in CDCl$_3$. 100
Scheme 5.2. Oxidation of 5 with TBHP to give complexes I and II. In the absence of olefin *cis*-cyclooctene, k_2 is large. In the presence of olefin, k_1, $k_3 >> k_2$ and k_4 is small but positive. k_1, k_2, k_3 and k_4 refer to rate constants for the oxidative transformations. 104
Scheme 6.1. Oxidation of dioxo complex I to oxo-peroxo species **II**. 119
Scheme 6.2. Oxidation of Mo(IV) mono oxo complex to Mo(VI) dioxo complex **I**. 128
Scheme 6.3. Possible CpMo oxo species for transient NMR signal assigned **B**. 129
Scheme 6.4. Catalytic epoxidation involving intermediate $\mathbf{B_1}$ in competition with formation of oxo-peroxo complex **II** (Eq.s (A) and (B)). Formation of active intermediates $\mathbf{B_{2a}}$ and $\mathbf{B_{2b}}$ on reaction of **II** with TBHP (Eq.s (C) and (D)) R = CH$_2$COOCH$_3$ in all cases. 130
Scheme 6.5. Proposed two *one-electron* oxidation processes during the transformation of Mo(IV) to Mo(VI) *via* Mo(V) species with TBHP. Monoanionic ligands Cp and R have been omitted for clarity. 131

Scheme 6.6. Oxidative transformations possible with mono-μ-oxo Mo(V) intermediate complex...... 132
Scheme 6.7. Epoxidation of ethene with TBHP oxidant catalyzed by the dioxo complex [$CpMoO_2R$]. 132
Scheme 6.8. Conversion of *bis*-μ-oxo Mo(V) dimer to monomeric complexes **I** and **II** with excess TBHP. 133
Scheme 6.9. Oxidation of oxo-peroxo species [$CpMo(O)(O_2)R$] to bisperoxo complex with TBHP... 133
Scheme 6.10. Summary of kinetic equilibria involved in oxidation reactions with [$CpMo(CO)_3(CH_2COOR)$] pre-catalysts and excess TBHP (n-decane) oxidant. 134
Scheme 8.1. Oxidation of [$CpMo(CO)_3R$] pre-catalysts with TBHP gives dioxo and oxo-peroxo complexes **I** and **II** respectively. 153
Scheme 8.2. Proposed mechanisms for oxygen atom transfer catalyzed by (a−c) molybdenum peroxo or (d,e) molybdenum oxo complex species. 154
Scheme 8.3. A comparison of mechanisms of oxygen transfer from complexes (a) [$CpMo(O)(O_2)CH_3$],[21] and (b) [$CpMo(O)(O_2)CF_3$].[8] 155
Scheme 8.4. Mechanisms proposed for interaction of the oxidant with the ONO tridentate Schiff base MoO_2 catalysts, (a) reaction of MoO_2 catalyst with TBHP and the olefin, (b) reactivation of the catalyst, and (c) the proton shuttle effect of water, tert-butanol or TBHP in catalyst regeneration.[23] 156
Scheme 8.5. Synthesis of complexes **1** and **2**. 158
Scheme 8.6. The various possibilities of H-bonding with HFIP solvent. (a) In activation of TBHP, (b) interaction with pre-catalyst **2** after CO loss and interaction with oxidized complexes, (c) the effect of presence of water, *tert*-butanol or *tert*-butylhydroperoxide as neutral molecules. 170
Scheme 8.7. Oxidative transformations of the tricarbonyl pre-catalysts [$CpMo(CO)_3R$] on treatment with excess TBHP oxidant. 171
Scheme 8.8. Formation of oxo-bridged dimer species from the dioxo complexes of both pre-catalysts **1** and **2** is possible. 172

List of Tables

Table 1.1. Catalytic olefin epoxidation with complexes $Cp^{\neq}MO_2X$ and $Cp^{\neq}M(CO)_3X$ (M = Mo, W) at 55 °C with TBHP (5.5 M in *n*-decane). 7
Table 1.2. Catalytic olefin epoxidation with **17** and TBHP oxidant (catalyst:substrate:oxidant = 0.01:1:2) at 55 °C in $CHCl_3$ solvent. Ref. 33 8
Table 1.3. Catalytic epoxidation of various substrates with *ansa* complexes with TBHP in the ratio catalyst:substrate:oxidant = 0.01:1:2. 8
Table 1.4. Catalytic olefin epoxidation with complexes [$Cp^{\neq}MO_2]_2O$ (M = Mo, W) at 55 °C with TBHP (5.5 M in *n*-decane). Ref. 30. 10
Table 1.5. Catalytic epoxidation of *cis*-cyclooctene with *N*-heterocyclic carbene ligated cyclopentadienyl molybdenum complexes **30**-**39** at 55 °C with TBHP oxidant. 10
Table 1.6. Catalytic epoxidation of various substrates with complexes **41**-**43** at 55 °C. TBHP (in *n*-decane) employed as the oxidant unless stated otherwise. Catalyst:substrate:oxidant = 0.01:1:2. Ref. 39. 11
Table 1.7. Olefin epoxidation catalyzed by **44** and **45** with catalyst:substrate:oxidant ratio 1:100:200. Ref. 40 12
Table 1.8. *Cis*-cyclooctene epoxidation with complex **46** at 55 °C with different oxidants in different solvents using catalyst:substrate:oxidant = 1:100:150. Ref. 41. 12
Table 1.9. Oxidation of cyclohexene using [$CpMo(CO)_3(C\equiv CPh)$] catalyst (precursor for **47**).[a] Ref. 46. 13
Table 3.1. Selected spectral data for complexes discussed in this work.[a] 36

Table 3.2. Selected bond lengths [Å] and bond angles (°) of complexes [CpMo(CO)$_3$Cl] (abbreviated as CpCl),[50] **2**, **3**, **B**,[28] **C**,[28] **D**[29] and [Cp'Mo(CO)$_3$(CH$_3$CN)]BF$_4$ (abbreviated as [Cp']$^+$) where Cp' = C$_5$H$_4$Me.[45] X = Cl, Br or N. C1 is *trans* to carbene carbon C3, C2 is *trans* to the heteroatom X. 40

Table 3.3. Catalytic activities in terms of TOFs [h^{-1}] and conversions [%] (after 24 h) of *cis*-cyclooctene epoxidation with different concentrations [mol%] of **2** and **3** using TBHP (in *n*-decane) as oxidant at 55 °C, neat or in CHCl$_3$ (substrate:oxidant = 1:2). 44

Table 3.4. Conversions of different olefin substrates with **2** (0.1 mol%) to their epoxides using TBHP as oxidant at 55 °C in CDCl$_3$ (catalyst:substrate:oxidant = 1:1000:2000). 45

Table 3.5. Recycling for precatalyst 2 for epoxidation of cis-cyclooctene in RTIL [OMIM]NTf$_2$ with TBHP (n-decane) 54

Table 3.6. Comparison of structural data of ligand and complexes **2** and **3**. N2 refers to the nitrogen of fused pyridine moiety in imidazo[1,5-*a*]-3-pyridine ligand. 55

Table 4.1. Selected NMR Spectroscopic data for complexes **1-5** and comparison with [CpMo(CO)$_3$Cl] and [CpMo(CO)$_3$CH$_3$]. 63

Table 4.2. Mass spectrometry data and decomposition points for complexes **1-5**. 65

Table 4.3. Yield%[a] and TOF[b] range observed for epoxidation of olefin substrates with complexes **1-5**; 1 mol% catalyst, CH$_2$Cl$_2$ solvent at 22 °C unless stated otherwise. 68

Table 4.4. ^{95}Mo NMR shifts[a] and TOFs of epoxidation of *cis*-cyclooctene at 55 °C with TBHP (catalyst:substrate:TBHP = 1:100:200) for complexes **1−5**, [CpMo(CO)$_3$Cl] and [CpMo(CO)$_3$CH$_3$] in CHCl$_3$. 71

Table 4.5. TOFs[a] for complexes 1-5 (in mol mol$_{\text{Mo}}^{-1}$ h^{-1}) utilized for olefin epoxidation in DCM at 22 °C using TBHP with catalyst:substrate:oxidant = 1:100:200 unless stated otherwise. 93

Table 5.1. Assignment of ^{1}H and ^{13}C NMR chemical shifts (in ppm) observed during catalytic epoxidation of *cis*-cyclooctene with 5 and TBHP oxidant in CDCl$_3$ at 22 °C (5:CyOc:TBHP = 1:10:20). R* = CH$_2$COOBornyl, CyOc = *cis*-cyclooctene, EpCy = Epoxycyclooctane. 102

Table 6.1. Assignment of ^{1}H and ^{13}C NMR chemical shifts (in ppm) observed during oxidative decarbonylation of **5** with 10 equiv. of TBHP oxidant in CDCl$_3$ at 22 °C. R* = CH$_2$COOBornyl, Cp = C$_5$H$_5$, n.o. = not observed. 121

Table 6.2. Observed absorption bands during oxidation of pre-catalyst **5** with 10 equiv. of TBHP studied by *in situ* FTIR in CHCl$_3$ solvent.[a] 122

Table 6.3. Calculated thermodynamic parameters (ΔH and ΔG in kcal mol^{-1})[a] for oxidative decarbonylation of [CpMo(CO)$_3$R] pre-catalyst with TBHP oxidant to give either Mo^{IV} or Mo^{VI} oxo species depending on the stoichiometry of the reaction and evolution of either CO or CO$_2$. R = -CH$_2$COOCH$_3$. 128

Table 8.1. A comparison of selected structural and spectroscopic parameters and TOFs of [CpMo(CO)$_3$R] complexes, R = Cl, CH$_3$ (1), CF$_3$ (2). 159

Table 8.2. Comparison of analytical, spectroscopic, structural and catalytic activity data for pre-catalysts [CpMo(CO)$_3$CH$_3$] and [CpMo(CO)$_3$CF$_3$]. [6,7,31,50] 161

Table 8.3. Overview of the reactivity of dioxo and oxo-peroxo complexes derived from tricarbonyl pre-catalysts on treatment with TBHP (decane), as reported in literature.[a] 164

Table 8.4. Comparison of structural data for dioxo complexes [CpMo(O)$_2$(CH$_3$)] and [CpMo(O)$_2$(CF$_3$)] determined from their calculated ground state geometries. 165

Table 8.5. Comparison of spectroscopic, structural and catalytic activity data for oxo-peroxo complexes complexes [CpMo(O)(O$_2$)(CH$_3$)] and [CpMo(O)(O$_2$)(CF$_3$)].[6,7] 167

List of Publications

1. *Catalytic Olefin Epoxidation with η^5-Cyclopentadienyl Molybdenum Complexes.* N. Grover, F. E. Kühn, *Curr. Org. Chem.*16 (2012) 16–32.
2. *Homogeneous Catalytic Olefin Epoxidation with Molybdenum Complexes.* C. Müller, N. Grover, M. Cokoja, F. E. Kühn, *Adv. Inorg. Chem.* 65 (2013) 33–83.
3. *Cyclopentadienyl Molybdenum Alkylester Complexes as Catalyst Precursors for Olefin Epoxidation.* N. Grover, A. Pöthig, M. Cokoja, F. E. Kühn, *J. Mol. Catal. A. Chem.* (2013) (Manuscript in Preparation)
4. *On the way from $CpMoR(CO)_3$ to $CpMoR(O)_2$ – a DFT study about the pathways arising from the intermediate mono-oxo complex.* M. Drees, N. Grover, M. Cokoja, F. E. Kühn. (Manuscript in Preparation)
5. *Cyclopentadienyl Imidazo[1,5-a]pyridine-3-ylidene Complexes of Molybdenum and their Application as Olefin Epoxidation Pre-catalysts*. N. Grover, A. Schmidt, A. Pöthig, M. Cokoja, F. E. Kühn. (Manuscript in Preparation)
6. *Oxidation of $[CpMo(CO)_3R]$ pre-catalysts with tert-Butylhydroperoxide.* N. Grover, M. Drees, F. E. Kühn. (Manuscript in Preparation)

Conferences, Workshops, Poster Contributions and Presentations

1. *"Energy and Sustainability: Process and Materials"* May 13-14, 2011, Munich, Germany
   Joint Symposium of Northwestern University (Evanston, IL, USA) and Technische Universität München (Germany)
2. *"15th International Congress on Catalysis"* July 1-6, 2012, Munich, Germany
   Poster Title: Catalytic Achiral and Chiral Epoxidation of Unfunctionalized Olefins: Cyclopentadienyl Molybdenum η^1-Oxoalkyl (Enolate) Complexes
3. *"XXV International Conference on Organometallic Chemistry*" September 2-7, 2012, Lisbon, Portugal
   Poster Title: Cyclopentadienyl Molybdenum η^1-oxoalkyl Complexes for Catalytic Asymmetric Epoxidation of Unfunctionalized Olefins
4. *"Exploratory Workshop Bio-inorganic Chemistry"* May 3, 2013, Garching, Germany
   Institute of Advanced Study, Technische Universität München
5. *"4th INDIGO PhD Research Conference and Intensive Course"* October 6-10, 2013, Ludwigshafen-Regensburg, Germany
   Presentation Title: Cyclopentadienyl Molybdenum(II) Tricarbonyl Alkene Epoxidation Pre-catalysts: Synthesis, Catalysis, Kinetics and Mechanisms

Nidhi Grover

Date of Birth	23 May, 1986
Nationality	Indian
Contact	***nidhigrover.chem@gmail.com***

EDUCATION

Ph.D. in Chemistry (Dr. rer. nat) 2010 - 2013

Thesis Supervisor: Prof. Dr. Fritz E. Kühn, Chair of Inorganic Chemistry, Fachgebiet Molecular Catalysis, Technische Universität München, Germany

Dissertation Title: Cyclopentadienyl Molybdenum(II) Tricarbonyl Alkene Epoxidation Precatalysts: Synthesis, Catalysis, Kinetics and Mechanisms

M.Sc. Chemistry (Specialization: Organic Chemistry) 2007 - 2009

Department of Chemistry, University of Delhi, Delhi, India

Meritorious, First Division

B.Sc. (Hons.) Chemistry 2004 - 2007

Sri Venkateswara College, University of Delhi, New Delhi, India

Meritorious, First Division

All India Senior Secondary Certificate Examination, Central Board of Secondary Education (AISSCE-CBSE) Graduation with ‘Proficiency’ 2004

New Era Public School, Mayapuri, New Delhi, India

AWARDS/ MERIT ACCREDITATIONS

Postgraduate Science Meritorious Award (M.Sc. Final), University of Delhi	2010
Nanosystems Initiative Münich Student Research Award and Grant	2009
Shri Jugal Kishore Jain and Smt. Kalawati Jain Memorial Book Grant	2009
Postgraduate Science Meritorious Award (M.Sc. Previous), University of Delhi	2008
Graduate Science Meritorious Award, University of Delhi	2007
Award for University Examination-2006	2006
Science Meritorious Award, University of Delhi	2006
Scholarship in All India Senior School Certificate Examination	2004

RESEARCH EXPERIENCE

Doctoral study at the Chair of Molecular Catalysis, Fakultät Chemie, TUM	2010 - 2013
Summer Research Programme at Nanosystems Initiative Munich (NIM) Prof. Dr. Ernst Wagner, Chair of Pharmaceutical Biotechnology Ludwig-Maximilians Universität, Münich, Germany	2009
Summer Research Internship Prof. J. M. Khurana, Department of Chemistry, University of Delhi	2008

LANGUAGES

Hindi, English, German